Yassine Charabi (Ed.)
with Salim Al-Hatrushi

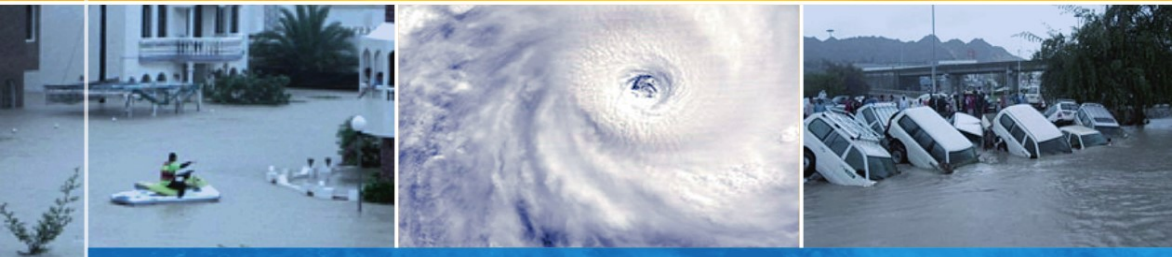

Indian Ocean Tropical Cyclones and Climate Change

Springer

Indian Ocean Tropical Cyclones and Climate Change

Yassine Charabi
Editor

Indian Ocean Tropical Cyclones and Climate Change

With
Salim Al-Hatrushi

Springer

Editor
Yassine Charabi
Department of Geography
Sultan Qaboos University
Muscat, Oman
yassine@squ.edu.om

ISBN 978-90-481-3108-2 e-ISBN 978-90-481-3109-9
DOI 10.1007/978-90-481-3109-9
Springer Dordrecht Heidelberg London New York

Library of Congress Control Number: 2009942532

Cover Images: Tropical Cyclone Kalunde, photo courtesy of NASA/GSFC, MODIS Land Rapid Response Team. Photos of damages caused by Cyclone Gonu (2007) in Muskat (left) and Oman (right), pages 178 and 227 of this volume.

Printed on acid-free paper

Springer is part of Springer Science+Business Media (www.springer.com)

Acknowledgments

We would like to express our sincere thanks to Professor Amer Bin Ali Al-Rawas, Vice Deputy Chancellor of Postgraduate Studies and Scientific Research (Sultan Qaboos University, Oman) for his exceptional support throughout many phases of the project. Thanks to the authors who have generously contributed to the chapters of this volume.

Preface

Tropical cyclones are topic that is not appropriately known to the public at large, but climate change has been on the public's mind since the last decade and a concern that has peaked in the new millennium. Like the television programs of Jean Yves Cousteau the 'plight of the oceans', have recent documentaries nurtured a consciousness that major climatological changes are in the offing, even have started to develop. The retreat of glaciers on mountain tops and in Polar Regions is 'being seen' on 'the small screen' and has favored an environmental awareness in all populations that are enjoying an average well-being on Planet Earth. The vivid images on screen of storms, floods, and tsunamis share the fear provoking landscapes of deforestation, desertification and the like. Watching such as this one is seen are voices warning of what over is 'in store' if the causative problems are not remedied. Talking and discussing are useful, but action must follow. Understanding the full ramifications of climate change on tropical cyclones is a task that will takes several decades.

In *Climate Change 2007*, the Fourth Assessment Report of the United Nations Intergovernmental Panel on Climate Change (IPCC) a high probability of major changes in tropical cyclone activity across the various ocean basins is highlighted. The Indian Ocean including the Arabian Sea and the Bay of Bengal are of particular concern because of the high population density along their coastlines. These coastal populations are vulnerable to the negative impact of these projected extreme events. The tropical Indian Ocean is characterized by surface warming trends that are more statistically significant, compared to model-simulated internal variability, than those in many other tropical basins including in the Northeast Pacific and North Atlantic. This raises the possibility that tropical cyclone trends resulting from global warming could emerge in the Indian Ocean prior to other basins.

The 2007 North Indian Ocean cyclone season was exceptional in the annual cycle of tropical cyclone formation. The north Indian Ocean basin witnesses the genesis of four tropical cyclones (Akash, Gonu, Yemyein and Gonu). Cyclone Gonu was the strongest tropical cyclone on record in the Arabian Sea, and tied for the strongest tropical cyclone on record in the northern Indian Ocean and was the strongest *named* cyclone in this basin. Intense cyclones like Gonu have been extremely rare over the Arabian Sea, as most storms in this area tend to be small and dissipate quickly. The cyclone caused about $4 billion in damage and nearly 50 deaths in Oman, where the cyclone was considered the nation's worst natural disaster.

To improve our understanding of tropical cyclones and changes of their activity in the Indian Ocean, an International Conference on Indian Ocean Tropical Cyclones and Climate Change was held in Muscat, Sultanate of Oman on 8–11 March 2009. The conference was organized by Sultan Qaboos University (SQU), in collaboration with the Ministry of Transportation and Communication (Directorate General of Meteorology and Air Navigation), the Ministry of Environment and Climate Affairs, The Ministry of Regional Municipalities and Water Resources, The Research Council (Oman), World Climate Research Programme and the World Meteorological Organization. At this scientific forum, attended by a large number of experts in tropical cyclone research, various aspects of cyclone activity in the Indian Ocean were discussed. The conference was the first step towards an ongoing international focus on potential impact of climate change in the Indian Ocean.

We asked several scientists who participate in the conference for their interest in developing a volume devoted entirely to the Indian Ocean Basin in which tropical cyclones form and develop. The response was universally positive, and these authors have generously contributed to the chapters that compromise this volume.

This volume is relevant to managers, policymakers, researchers, graduates and undergraduates students in Geography, Climatology, Meteorology, Environmental and Planetary Sciences. Moreover, the insights offered are not meant to exhaust the topic, but rather are intend to stimulate thinking and awareness. We have attempted to offer the recent progress on tropical cyclonegenisis, operational Tropical Cyclone forecasting and warning systems and Climate Change and Tropical Cyclone Activity and new syntheses in other areas, such as Assessment of Risk and Vulnerability from tropical Cyclones, including construction, archival and retrieval of best-track and historic data sets, Disaster Preparedness, Management and Reduction and Recent high impact tropical cyclone events in the Indian Ocean: Nargis, SIDR, Gonu and other events.

We invite you to explore the following chapters with an eye to developing a greater sense of the possible range in which climate change can influence tropical cyclones activity. The awareness of managers, policymakers, and research-more than any modeling exercise- will ultimately determine how well we constrain and respond to the challenge of climate change.

Muscat, Oman Yassine Charabi

Contents

Part I
Climate Change and Tropical Cyclone Activity

A Climatology of Intense Tropical Cyclones in the North Indian Ocean Over the Past Three Decades (1980–2008)

Karl Hoarau and Ludovic Chalonge

Keywords Decadal distribution • interannual and intraseaonal activity

Introduction

The North Indian Ocean (NIO) is not considered as one of the more active tropical cyclone basins. On average each year, only five or six systems reach at least the tropical storm stage, 35 knots or more (Singh et al. 2001). In the current debate on global warming and the evolution of the intense cyclones number, studies have given different results for the NIO. Webster et al. (2005) found an extreme increase of the Cat 4 and 5 cyclones number (Saffir and Simpson 1974) from 1975 to 2004. Landsea et al. (2006) have shown that the databases were not reliable enough as reanalysed Cat 4 and 5 cyclones have been estimated at Cat 2 and/or 3 in the previous best track. And this could change the trend reported by Webster et al. (2005). Kossin et al. (2007) did not highlight any trend from 1983 to 2005 for the same intensities. In order to bring new features, this paper provides a climatology of intense tropical cyclones in the NIO from 1980 to 2008 based on the reanalyses of the satellite pictures. This study has been inspired from Landsea (1993) who published a paper on a climatology of intense Atlantic hurricanes. The intense cyclones are those with maximum sustained winds of 100 knots or more.

Data and Methodology

The Indian geostationary satellites have been launched from April 1982. All of the meteorological community did not get an access to these satellites' data. Moreover, INSAT had a spatial resolution of 11 km, then 8 km in the infrared spectrum.

K. Hoarau (✉) and L. Chalonge
University of Cergy-Pontoise, 33 Boulevard du Port, 95011 Cergy Cedex, France
e-mail: KHoarau@aol.com

Y. Charabi (ed.), *Indian Ocean Tropical Cyclones and Climate Change*,
DOI 10.1007/978-90-481-3109-9_1,

Before the arrival of the European satellite Meteosat 5 (1998), the North Indian Ocean was at the edge of the GMS and Meteosat area. Despite a resolution of 4 km in infrared, these latter satellites could not catch the true eye temperature of the cyclones. And this parameter is an important one to estimate the cyclones' intensity from the infrared pictures. Therefore, we also used the Noaa polar orbiting satellites with a resolution of 4 km. In fact, the intensity is derived from the Dvorak's analysis (1984). The required data are the eye temperature and the clouds top temperature surrounding the center. The technique is based on rules which allow getting an estimated intensity. Kossin et al. (2007) did a global reanalysis with satellite pictures, including the North Indian Ocean. But the authors of this paper were warned of the fact that with the 8 km resolution used, and the angle viewing problem in the Indian Ocean until 1998, they could not catch the absolute intensity of cyclones. And they did not use the Noaa satellites. Therefore, this research is the first reanalysis of the major cyclones' intensity with the satellite data at the resolution of 4 km. All the cyclones of the 1980–2008 period have been reanalyzed with the same technique.

The Interannual and Intraseaonal Activity of the Intense NIO Cyclones

In almost 30 years, 21 cyclones reached the category 3 or more. Only five intense cyclones formed in the Arabian Sea. The decadal distribution has been the following: five cyclones in the 1980s, 11 cyclones in the 1990s, and five cyclones in the 2000s (Fig. 1).

The Cat 4 and 5 cyclones (115 knots or more) did not display any upward trend since 1980, even if the 1990s has been by far the more active decade. These data do

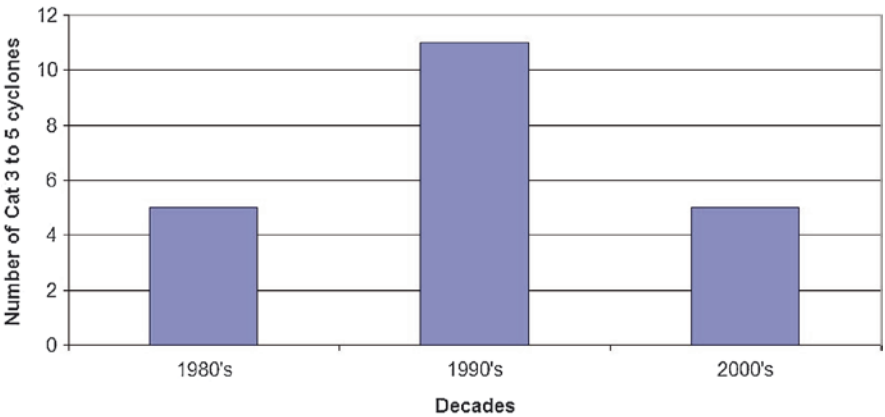

Fig. 1 The decadal distribution of the intense cyclones number

not confirm the conclusions of Webster et al. (2005) for the NIO. Moreover, for each decade, the figures did not show a continuous increase of the intense cyclones' rate related to all the categories (1–5): 38.5% in the 1980s, 44% in the 1990s, and 33.3% in the 2000s (Fig. 2).

The monthly distribution indicates two peaks with seven cyclones in May and eight in November (Fig. 3). From 1980 to 2008, no intense cyclone has been observed from July to September; the monsoon season is accompanied by a strong vertical wind shear. Four of the five cyclones in the Arabian Sea developed in May and June. Then, the monsoon winds induce an upwelling in the northwest part of this sub-basin. To reach an intense stage, 17 of the 21 intense cyclones have undergone a rapid intensification in 24 h. This supposed a wind's increase of 35 knots from 65 knots (T4.0) to at least 100 knots (T5.5). In the Dvorak's Technique (1984), an increase of 1.5 T-number is considered as a rapid intensification.

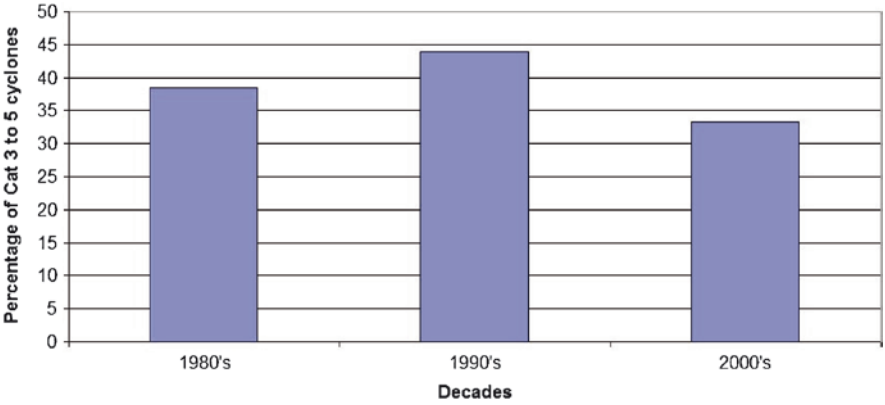

Fig. 2 The rate of intense cyclones related to all the categories (1–5)

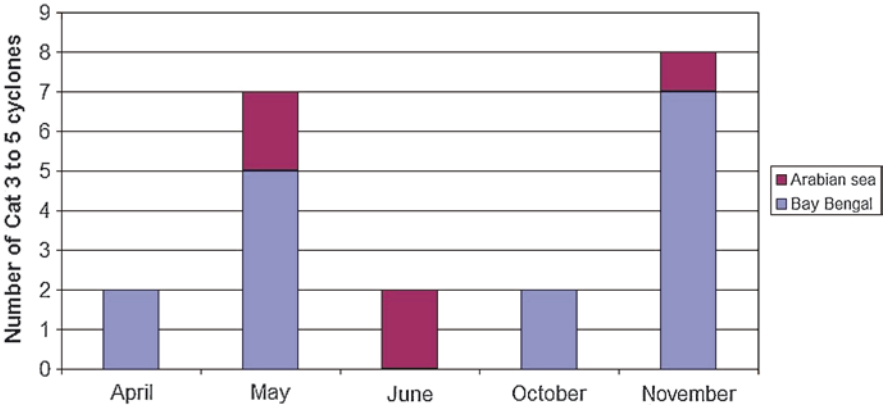

Fig. 3 The monthly distribution of intense cyclones

We preferred to use the wind increase rather than the pressure decrease used by Kaplan and DeMaria (1999) and Holliday and Thompson (1979) on the north Atlantic and the western North Pacific cyclones, respectively. Cyclone Gonu (2A in June 2007) intensified from 70 to 145 knots, displaying a remarkable intensification of 75 knots in 24 h in the Arabian Sea. Despite a weaker activity than the other basins, the NIO has extreme intensities which arevery comparable. In fact, we reanalyzed tropical cyclone 5B at 155 knots in October 1999 in the Bay of Bengal. This latter sub-basin has very warm waters and gets stronger cyclones. Amongst the 21 cyclones having reached the Cat 3 or more, 16 made landfall with an intensity at least of 100 knots. This could be an indication that the NIO is a small basin and that the frequent interaction with the lands and the landfalls prevent the cyclones to reach a greater intensity. India, Bangladesh, Birmania, and Pakistan have already been hit by intense cyclones over the 1980–2008 period. This is not an impossible event for countries like Oman, Somalia, or Yemen, specially for small-size tropical cyclones.

Summary

This research highlighted the characteristics of the intense tropical cyclones with sustained winds over 1 min of 100 knots and more (Categories 3, 4, 5) in the NIO over the last 3 decades (1980–2008). The cyclones' intensity has been reanalyzed from the polar and geostationary satellites pictures with the Dvorak's Technique (1984) which uses the enhanced infrared. The extreme intensity by decade did not change a lot: 140 knots for Gay (coming from the western North Pacific) in November 1989, 155 knots for 05B in October 1999, and 145 knots for Gonu in June 2007. However, the NIO has the potential in terms of sea temperature to intensify the cyclones around 160–170 knots. Over the last 29 years, 21 cyclones reached an intense stage of at least 100 knots: five cyclones have been observed in the 1980s, 11 cyclones in the 1990s, and five cyclones in the 2000s. If the 1990s has been by far the more active decade, there is no upward trend since 1980. The reliable dataset is too short to highlight natural decadal variations. The Categories 4 and 5 cyclones (115 knots and more) have a comparable distribution mode: four cyclones in the 1980s, eight cyclones in the 1990s, and five cyclones in the 2000s. These results show that there is no direct relation between the cyclones' intensity and the sea temperature. In fact, this latter continued to increase in the 2000s whereas the number of intense cyclones has decreased. Amongst the 21 intense cyclones, only five cyclones, including Gonu at 145 knot in 2007, formed in the Arabian Sea. The monthly distribution indicates two peaks with seven cyclones in May and eight in November. To reach an intense stage, 17 cyclones have undergone a rapid intensification which matches at least with a wind increase of 35 knots for a period of 24 h. A remarkable feature is that 16 cyclones made landfall with an intensity of at least 100 knots: eight cyclones in India, five cyclones in Bangladesh,

two cyclones in Birmania, and one cyclone in Pakistan. It is not impossible that countries like Oman, Somalia, or Yemen could be hit by small-size intense cyclones despite a dry air intrusion in these areas.

References

Dvorak VF (1984) Tropical cyclone intensity analysis using satellite data. NOAA Tech. Rep. NESDIS 11, National Oceanic and Atmospheric Administration, 47p

Holliday CR, Thompson AH (1979) Climatological characteristics of rapidly intensifying typhoons. Mon Wea Rev 107:1022–1034

Kaplan J, DeMaria M (1999) Climatological and synoptic characteristics of rapidly intensifying tropical cyclones in the North Atlantic Basin, 23rd Conference on Hurricanes and Tropical Meteorology, Miami, FL, Am Meteor Soc 592–595

Kossin JP, Knapp KR, Vimont DJ, Murname RJ, Harper BA (2007) A globally consistent reanalysis of hurricane variability and trends. Geophys Res Lett 34:L.04815

Landsea CW (1993) A climatology of intense (or major) Atlantic hurricanes. Am Meteor Soc 121:1703–1713

Landsea CW, Harper BC, Hoarau K, Knaff JA (2006) Can we detect trends in extreme tropical cyclones? Science 313:452–454

Saffir RH, Simpson B (1974) The hurricane disaster potential scale. Weatherwise 27:169–186

Singh OP, Ali Kahn TM, Rahman (2001) Has the frequency of intense tropical cyclones increased in the North Indian Ocean? Curr Sci 80:575–580

Webster PJ, Holland GJ, Curry JA, Chang HR (2005) Changes in tropical cyclone number, duration, and intensity in a warming environment. Science 309:1844–1846

Tropical Cyclones in a Hiearchy of Climate Models of Increasing Resolution

P.L. Vidale, M. Roberts, K. Hodges, J. Strachan, M.E. Demory, and J. Slingo

Keywords Resolution model • storm track density

Introduction

Tropical Cyclone (TC) is normally not studied at the individual level with Global Climate Models (GCMs), because the coarse grid spacing is often deemed insufficient for a realistic representation of the basic underlying processes. GCMs are indeed routinely deployed at low resolution, in order to enable sufficiently long integrations, which means that only large-scale TC proxies are diagnosed. A new class of GCMs is emerging, however, which is capable of simulating TC-type vortexes by retaining a horizontal resolution similar to that of operational NWP GCMs; their integration on the latest supercomputers enables the completion of long-term integrations. The UK–Japan Climate Collaboration and the UK-HiGEM projects have developed climate GCMs which can be run routinely for decades (with grid spacing of 60 km) or centuries (with grid spacing of 90 km); when coupled to the ocean GCM, a mesh of 1/3 degrees provides eddy-permitting resolution. The 90 km resolution model has been developed entirely by the UK-HiGEM consortium (together with its 1/3 degree ocean component); the 60 km atmospheric GCM has been developed by UJCC, in collaboration with the Met Office Hadley Centre.

Data and Methodology

We initially present results from a 3-model, atmosphere-only multi-resolution intercomparison including the UKMO-HC HadGEM1, ECHAM5, and MIROC models, integrated for the entirety of the AMIP2 period (25 years), using a hierarchy

P.L. Vidale (✉), M. Roberts, K. Hodges, J. Strachan, M.E. Demory, and J. Slingo
NCAS Climate, University of Reading, UK and UKMO Hadley Centre, UK

Y. Charabi (ed.), *Indian Ocean Tropical Cyclones and Climate Change*,
DOI 10.1007/978-90-481-3109-9_2,

of mesh sizes that provide increasing resolution, from ~150 to ~60 km. These GCMs have not been built a priori with the specific purpose of simulating TCs; on the contrary, these climate models are general-purpose, aiming to represent spatial scales normally only addressed by "weather resolving" NWP models operated at major international weather forecasting centers. Our feature tracking methodology, normally used to track cyclones and anti-cyclones, targets vorticity as the main variable, and has been extended in three-dimensional space to specifically scan for TCs, using the property that these storms have a warm core and thus display a marked vertical vorticity gradient. We apply dynamically identical and globally consistent TC diagnostic criteria to 6-hourly simulation fields over each model integration analyzed in our inter-comparison. Our simulation results indicate that all the GCMs in our model matrix are capable of credibly representing storm climatologies, e.g., TC storm tracks in all basins, as well as the preferential location of their genesis and lysis. An example is given in Fig. 1, which shows a climatology of northern hemisphere storm track density for the TC season, from May to November. We compare the simulated climatologies with three observational data sets, two of them re-analyses (for the latter we applied a tracking methodology identical to that used for the climate models we considered).

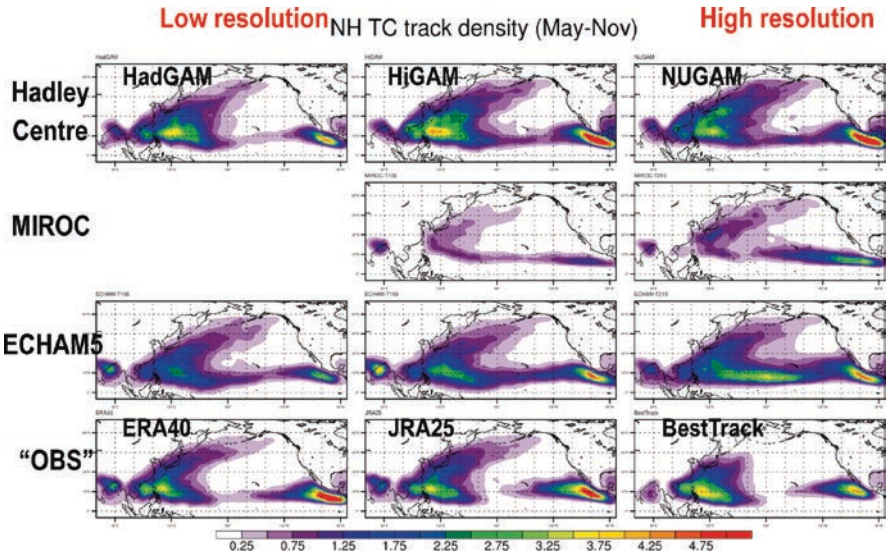

Fig. 1 Statistics of Tropical Cyclones in AMIP2 integrations (25 years) in the Pacific basin: the role resolution and of model formulation

Results

These results indicate that model resolution is not a crucial factor in representing the spatial distribution of Tropical Cyclone storm track densities; on the contrary, model formulation seems to be a more important factor in the spatial distribution of the storms. Storm intensity appears to be sensitive to resolution, with more violent storms emerging at the higher-resolution end of the GCM resolution hierarchy spectrum. Figure 2 provides an indication of storm intensity distribution, by presenting a histogram of storm count versus central relative vorticity (a proxy for storm intensity). By comparing with the typical vorticities found in the re-analyses, it is possible to say that the lowest-resolution GCMs produce too many storms in the weaker categories, while the highest-resolution GCMs produce a larger number of the very intense storms.

A more intuitive way to assess the same resolution dependence is to stratify the storm counts into operational categories. An example is shown in Fig. 3.

Interannual variability provides another good test for the value of GCM resolution. The AMIP2 Sea Surface Temperatures, used to force the atmospheric models, are potentially able to provide a signal sufficient to control the spawning of storms, which can be then assessed in each basin, for each simulated year. An example of this type of analysis is provided in Fig. 4.

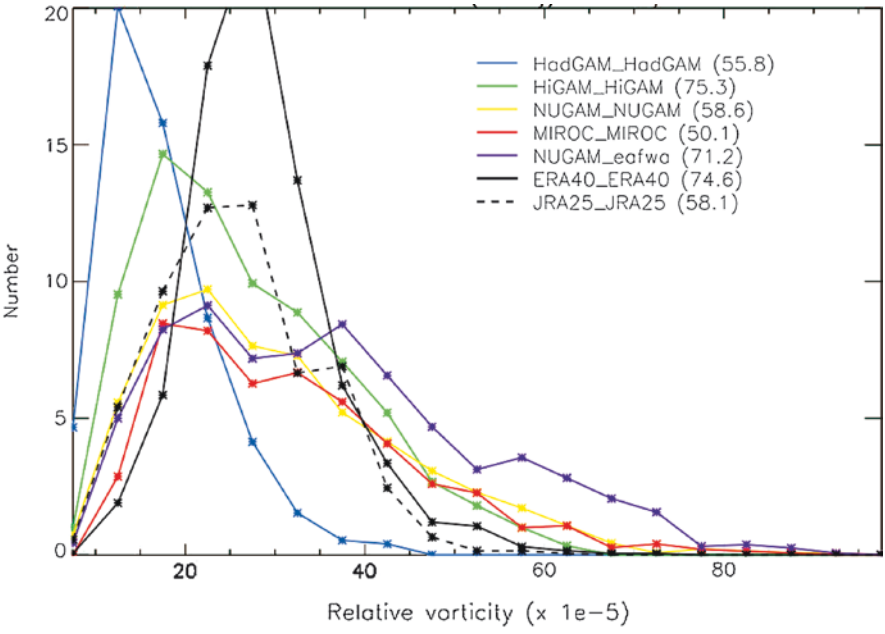

Fig. 2 A histogram of storm count versus storm relative vorticity in AMIP2 integrations (25 years). The HadGAM model has a grid spacing of 135 km; HiGAM corresponds to 90 km, while NUGAM has a grid spacing of 60 km. The two observational products are shown in black

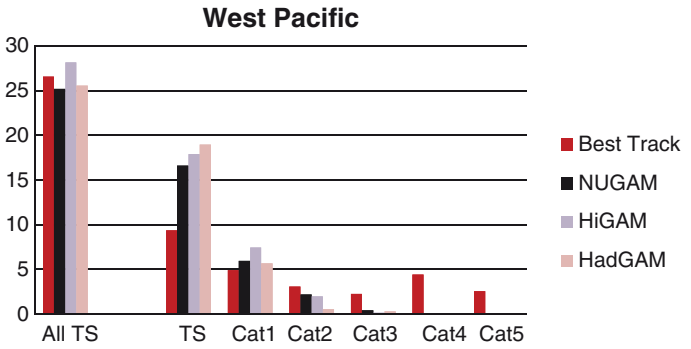

Fig. 3 A histogram of storm count versus TS-TC categories in AMIP2 integrations (25 years). The HadGAM model has a grid spacing of 135 km; HiGAM corresponds to 90 km, while NUGAM has a grid spacing of 60 km. The Best Track observational product is shown in red

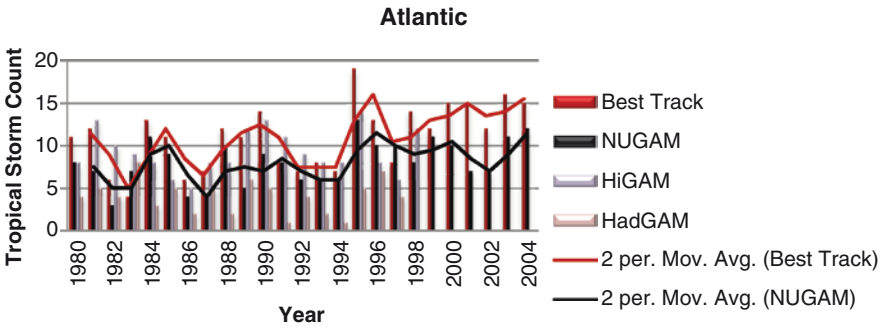

Fig. 4 Interannual variability of TC count in the Atlantic basin for AMIP2 integrations (25 years). The HadGAM model has a grid spacing of 135 km; HiGAM corresponds to 90 km, while NUGAM has a grid spacing of 60 km. The Best Track observational product is shown in red

Interannual variability time series correlations for the lowest-resolution model are 0.16; for the mid-resolution model 0.54; the highest-resolution model has a correlation of 0.74. These results indicate that the highest-resolution model has better skill at representing interannual variability of TC counts at the basin scale, with the proviso that a realistic SST forcing can be applied. This prompted us to apply our methodology to the centennial-scale simulations with the coupled HiGEM AO-GCM, targeting a wide range of variability, from interannual to decadal. HiGEM produces a very realistic ENSO, so that an analysis of the TC response to different ENSO phases can give further insight into model skills and TC predictability potential (e.g., if HiGEM should be used for seasonal prediction). Figure 5 shows the modeled TC response to Niño and Niña anomalies in the ocean, for the Pacific basin.

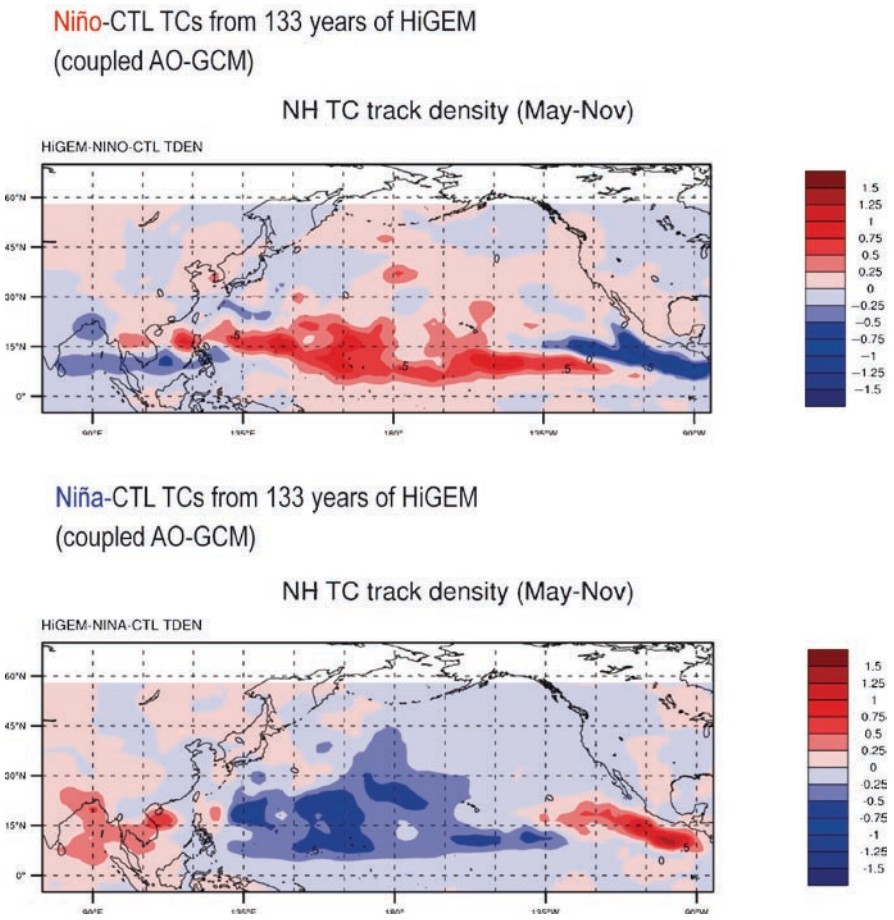

Fig. 5 TC track density: response to Niño and Niña anomalies in the ocean, derived from a centennial-scale AOGCM simulation with HiGEM

These results are in good agreement with observations and provide a further test of model reliability, also verifiable in terms of the chain of processes that lead from the appearance of the anomaly in the Pacific basin, all the way to subsequent anomalies, appearing in other basins, e.g., in the Central West Atlantic.

Summary

We have assessed the skills of a new generation of GCMs, capable of resolving weather scales, for the simulation of the geographical and temporal distribution of Tropical Cyclones. A systematic intercomparison of three state-of-the-art GCMs

indicates that model resolution is not crucial in the representation of the climatology of storm track density, but plays an important role in the determination of storm intensities. Analysis of interannual variability of storm counts also indicates that model resolution in excess of ~50–60 km is needed in order to be able to represent the highest-intensity TCs (Cat 4, 5), which are completely absent in the lower-resolution GCMs; this analysis also indicates that there is no convergence at 50–60 km and that much higher resolution is needed in order to realistically represent the full spectrum of TC intensities. The centennial-scale coupled model response to ENSO variability reinforces our confidence in the chain of mechanisms involved in TC generation within our atmospheric model. While the resolution that we can currently afford to run climate models for long-term simulations is still clearly insufficient, the large sample of simulated TCs provides good value, in particular because it is globally consistent; moreover, our operational framework allows us to test multiple ideas regarding the role of controlling mechanisms. Future work will revolve around a systematic analysis of the large-scale environment at each model resolution, with the objective of reconciling our findings with the diagnostic methodologies normally applied to much coarser GCMs.

Modeling Climate Change: Perspective and Applications in the Context of Bangladesh

M.J.B. Alam and F. Ahmed

Keywords Climate parameters • Global mean temperature

Introduction

During the past few decades, climate scientists have been warning about changes in global climate with intense impacts on agriculture, livelihood, water resources, ecosystem, energy, and other socioeconomic affairs. Meteorological information and observations of vulnerable entities such as glacier melting unequivocally substantiate the projections. The recent forecast of IPCC reveals that global mean temperature is expected to increase by 2.4°C by the end of this century resulting in consequential effects on sea-level rise, volume and pattern of precipitation and, magnitude and frequency of extreme events such as cyclones (IPCC 2007a). Studies also suggest that the rate of change of climate parameters observed during the past few decades is unprecedented which may result in irreversible changes in the global ecosystem. Bangladesh is one of the most vulnerable countries with respect to the impacts of climate change. The country's vulnerability stems from its exposure to a wide range of climate change parameters, geographical setup, and socioeconomic conditions. Germanwatch identified Bangladesh as the most vulnerable country on the basis of Climate Risk Index score (Germanwatch 2008). Government of Bangladesh has identified climate change as a priority issue and initiated formulating strategies. In this connection, assessing the potential risk and comparison among alternate options are the prime requirements. For this purpose, climate change impact models are widely used. This paper summarizes the findings of application of such models in Bangladesh.

M. Alam (✉) and F. Ahmed
Department of Civil Engineering, Bangladesh University of Engineering and Technology (BUET), Dhaka-1000, Bangladesh
e-mail: jobair@ce.buet.ac.bd; jobair@yahoo.com

Y. Charabi (ed.), *Indian Ocean Tropical Cyclones and Climate Change*,
DOI 10.1007/978-90-481-3109-9_3,

Physiography of Bangladesh

This section provides a brief overview of biophysical, social, and economic characteristics of Bangladesh.

Biophysical

Bangladesh has an area of 147,570 km^2 and lies in between 20°34′ and 26°38′ North latitude and 88°01′ and 92°41′ East longitude and consists of flat fertile alluvial land. Bangladesh straddles the Tropic of Cancer between Myanmar and India, and extends 390 miles (625 km) in the North to the South and by 190 miles (305 km) in the East to the West. Over 90% of the land is flat with many rivers that flow into the Bay of Bengal through a huge delta that is mostly less than 9 m above sea level. Low altitude results in regular inundation of hundreds of square miles during the monsoon (June–October) when 75% of the annual rain falls. Over 66% of the land is arable, 20% is irrigated, and 17% is forest. With about half of its surface below the 10 m contour line, Bangladesh is located at the lowermost reaches of three mighty river systems – the Ganges–Padma river system, the Brahmaputra–Yamuna river system, and the Surma–Meghna river system.

Social

Bangladesh is a country of over 145 million people with a population density of 928/km^2. Though the country is making good progress in the socioeconomic field in increasing the literacy rate, higher life expectancy, increasing food production, and decreasing infant mortality and total fertility, progress in poverty reduction is very slow. The population growth rate has been reduced from 2.5% in the mid-1970s to 1.48% in 2005.

Economic

Bangladesh is an agriculture-based country. Agriculture contributes about 20% to the national economy which is followed by industry and trade services. In recent years, there is a trend of decreasing agricultural contribution in the total GDP and increasing contribution of industry and trade services. At present, industry and service sectors contribute about 15.2% and 13.7%, respectively. Dhaka, the capital of Bangladesh, contributes about 13% of national income which is followed by Chittagong, the major industrial and port area of the country.

Key Environmental Stresses

This section presents key environmental stresses that Bangladesh is facing and their relation with economic growth and social development.

Land and Soil

Water erosion is the most widespread form of degradation affecting 25% of agricultural land of Bangladesh. Various kinds of soil erosion such as sheet, rill and gully erosion, landslide, riverbank erosion, and coastal erosion occur in Bangladesh. Accelerated soil erosion has been encountered in the hilly regions of the country, which occupy about 1.7 million hectares. In a study at the Rangamati station of the Bangladesh Agricultural Research Institute (BARI), total soil loss of 2.0–4.7 t/ha per year was observed. In addition, the country is losing its forest area at the rate of about 3% annually due to deforestation. The deforested area is also becoming susceptible to severe water erosion which is about 102 t/ha/year (NAPA 2005). In Bangladesh, bank erosion is caused mainly due to strong river currents during the rainy season. About 1.7 million hectares of floodplain areas are prone to riverbank erosion. North-western part of Bangladesh is also affected by wind erosion during the dry periods of the year.

Water

With its growing population, Bangladesh faces worsening difficulty in managing its limited water resources. Increasing population and decreasing availability of irrigation pose serious concern for the country. The growing population causes increase in demand for food leading to irrigation of more crops which in turn creates demand for more water. One of the other major concerns in water resource management related to increasing population is the problem faced by the poor in gaining access to water. The problem is further aggravated by pollution of existing water bodies by industries, runoff from the indiscriminate use of fertilizer and pesticides, and poor drainage. Widespread arsenic contamination of groundwater is a relatively recent threat to domestic water supply as well as irrigation. In terms of income generation, water has been found to be the second most important resource after land. The role of women and children in supplementing household incomes is affected largely by difficulties in accessing water sources, particularly during the dry season.

Forestry and Biodiversity

Bangladesh possesses a rich biological heritage of flowering plants, mammals, birds, reptiles, amphibians, fishes, etc. and it is a zone of wide-ranging biodiversity. It has an area of 2.46 million hectares of forests distributed all over the country. The

natural forests of Bangladesh were considered as one of the richest and biologically diverse forest resources due to its unique geophysical location. These forests consist of three major vegetation types occurring on the three distinctly different land types. An estimated 5,700 species of angiosperms are available in the forests of Bangladesh, of which some 2,260 species are reported from the Chittagong region which falls between two major floristic regions of Asia. It is reported that there are about 86 species of timber plants, 130 species of fiber plants, and 29 species of medicinal plants available in the country. Besides domesticated species, a total of about 932 species of amphibians and amniotes have so far been recorded, which include 23 species of amphibians,154 species of reptiles, 632 species of birds (358 non-passerine and 274 passerine), and 132 species of mammals.

Natural Disasters of Bangladesh

Bangladesh is a disaster-prone country. Every year, natural disasters such as cyclones and floods cause enormous damage to the people of the country. Since independence in 1971, cyclonic storm surges and floods killed more than 460,000 and 41,000 people, respectively. They also affected another 45 million and 356 million peoples, respectively [3]. This section provides a brief overview of natural disasters affecting the country.

Floods in Bangladesh

Floods occur almost every year in Bangladesh. Flood in a limited scale is a blessing for the country but beyond that scale it is a havoc causing loss of human lives, livestock, shelters, and crops. Bangladesh experienced eight severe floods in four decades. Catastrophic floods cause significant damage to crops and properties in addition to colossal human suffering. In 2007 two devastating spells of flood hit the country causing damage to crop, livestock, fisheries, and forestry sectors.

Cyclones in Bangladesh

The coastal area of Bangladesh is hit by cyclone storms and associated storm surges regularly causing loss of human lives and livestock and severe damage to crop, property, and coastal environment. About one-tenth of the global total of tropical cyclones forming in different regions of the tropics occurs in the Bay of Bengal (Alam et al. 1999). Approximately, one-sixth of the tropical storms, born in the Bay of Bengal, moves toward the coast of Bangladesh. In 2007 the country was hit by "SIDR" causing death to more than 4,000 people and damage of about US$8

billion. The cyclone of April 29, 1991 was the most catastrophic since 1970, with wind speed of 240 km/h and tidal waves surging to 6 m in height. The storm took an immense toll of human lives (140,000 deaths) and caused severe suffering and inflicted substantial damage to social and physical infrastructures. In 1985, a cyclone caused a tidal wave to smash through the islands, killing 10,000 people. In 1970, the second most powerful storm to hit Bangladesh ravaged the country with wind speed of 220 km/h and claimed half a million lives.

Droughts

Droughts affect in different intensities in Kharif, Rabi, and pre-Kharif seasons causing damage to Aman and Rabi crops of 2.3 and 1.2 million hectares, respectively. Drought tends to affect western districts more severely, especially when the monsoon is curtailed. It is estimated that in 1981/82 drought affected 10 million people. The drought of 1979 was one of the severest in recent times affecting about 42% area of the country.

River Erosion

Riverbank erosion is a serious problem in Bangladesh. It is a process largely controlled by river dynamics which has been aggravated by climate-change-related issues. The disruption in the life of many local communities is almost a continuous process due to riverbank erosion and the changing course of rivers. During floods, riverbank erosion becomes very acute and leads to loss of valuable land.

Effect of Climate Change

IPCC predictions suggest that there will be significant change in temperature and rainfall caused by climate change which is summarized in Table 1 (Agrawala et al. 2003; IPCC 2007b). Observed meteorological data also demonstrate trends commensurate with the prediction. This section summarizes the actual and potential adverse impacts of climate change on socioeconomic indicators. Meteorological data reveals that maximum and minimum monsoon time temperatures show an increasing trend annually at the rate of 0.05°C and 0.03°C, respectively. Considerable increasing trend in cyclone frequency over the Bay of Bengal during November and May has been observed in recent study. Significant sea level rise has been observed during the last 22 years (7.8 mm/year at Cox's Bazar) which is much higher than the mean rate of global sea level rise (SMRC 2003). There also exist clear evidences of saline intrusion in coastal areas. Alteration in climate is severely affecting agricul-

Table 1 Expected climate change scenarios for Bangladesh

	Temperature change (°C) mean			Precipitation change (%) mean			Sea-level rise (cm)		
	Annual	DJF	JJA	Annual	DJF	JJA	IPCC	SMRC	NAPA
2030	1.0	1.1	0.8	5	−2	6	14	18	14
2050	1.4	1.6	1.1	6	−5	8	32	30	32
2100	2.4	2.7	1.9	10	−10	12	88	60	88

DJF: December–January–February; JJA: June–July–August; NAPA: National Adaptation Programme of Action; SMRC: SAARC Meteorological Research Center

ture, livelihood and economy of the country. Impacts on poor and vulnerable groups are more severe. Natural disasters in 2007 caused a total loss of 1.8 million ton of rice which is annual requirement of 10 million people of the country. During the last ten years the country lost more that 3 percent of its GDP due to natural disasters.

The following section presents an analysis of implications of climate change on specific economic parameters with an objective of achieving better understanding of the issue.

Climate Change Models with Application in Bangladesh

Climate change is a gradual and complex process which requires a significant amount of time to identify the alterations through observation. Consequent impacts on environmental and socioeconomic parameters are even slower. Reversing the course and adapting to conditions are also a time-consuming process. Models play a very important role in this connection by facilitating means to visualize future conditions under different assumptions and scenarios of input parameters. Models can assist in understanding climate risks, impact prediction, assessment of cost of impact, analysis of investment needs for adaptation, and framework for adaptation. In this context climate change models, which include PRECIS, RegCM, and MM5, have been customized and applied for Bangladesh. Different types of models have been used to overcome the uncertainties and compare the outputs. Also, the models have been calibrated using observed meteorological data during the period of 1961–2007. As shown in Fig. 1, model output may differ from observation Islam (Islam and Uyeda 2007).

Climate change is expected to affect the ecosystem, food, coastal area, industry, settlement, health, and water. This section presents the model-based outputs of the impacts of climate change on agriculture, economy, health, and energy sector of Bangladesh. Based on the outputs of regional climate models, models for each of the sectors are being developed.

Analysis of agricultural implication is based on the impact of climate change on rice production as rice is the most important food grain for the country. Analysis is conducted using DSSAT 4 model system (utilizing CERES-Rice). Figure 2 reveals

that rice production may reduce by 40% by 2070 resulting in serious food shortage. There exists regional variability in impacts on production of rice.

Economy of Bangladesh is expected to suffer severely due to climate change impacts. As shown in Fig. 3, by the end of this century climate-change-induced damage to industry and infrastructure sector will amount to more than US$300 billion and result in loss of employment/livelihood to more than 70 million people.

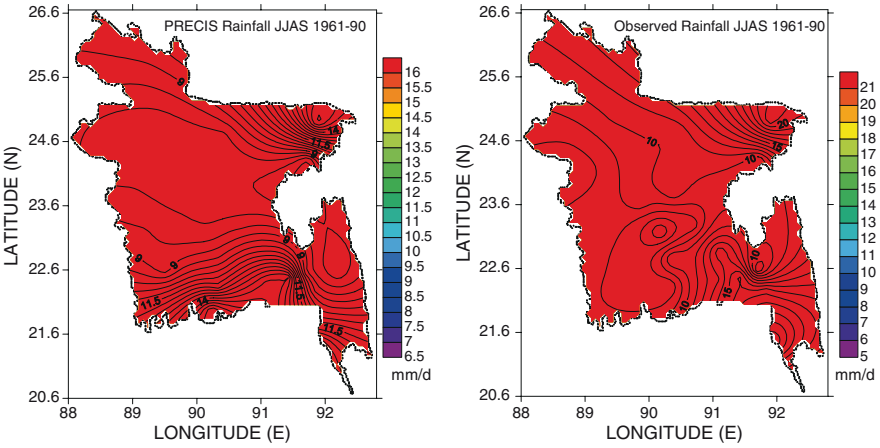

Fig. 1 Differences between model prediction and observation in rainfall forecasts. Projected impact of climate change on Bangladesh

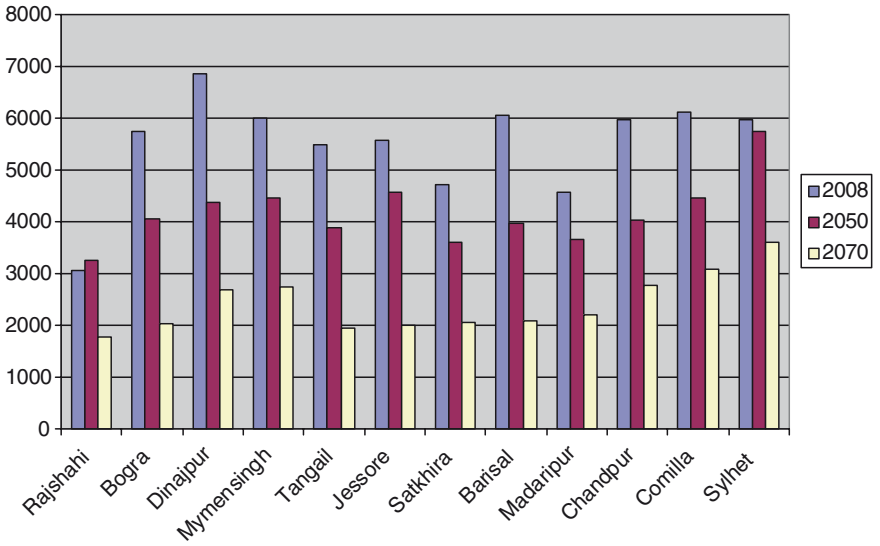

Fig. 2 Impact of climate change on rice production in Bangladesh

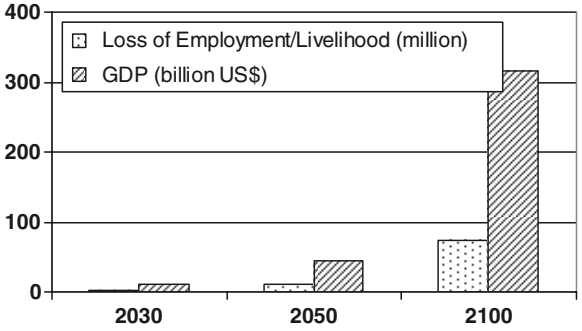

Fig. 3 Impact of climate change on GDP and employment/livelihood

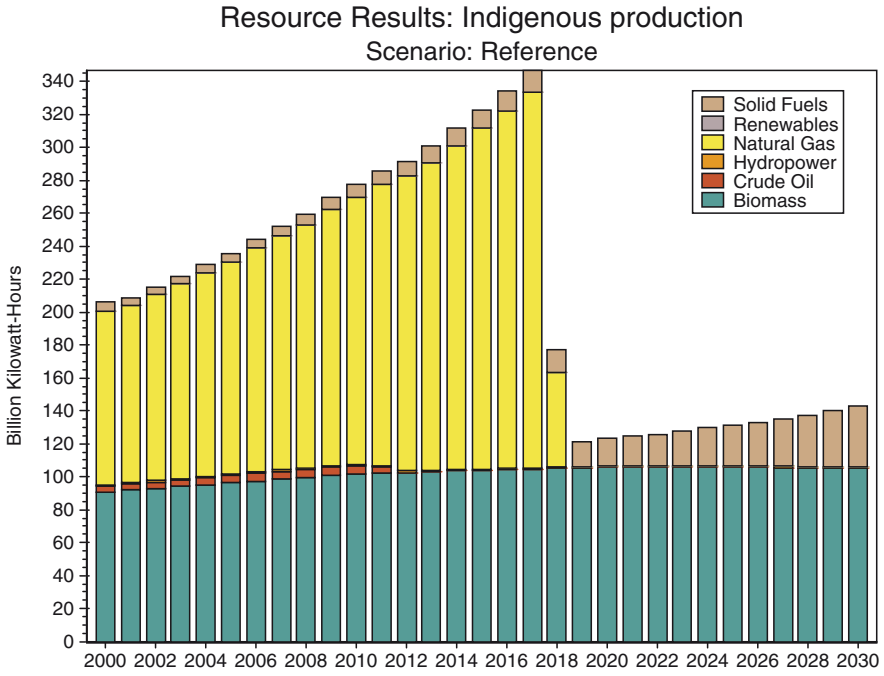

Fig. 4 Energy supply scenario in Bangladesh

Due to increase of average temperature it is expected that energy demand for cooling and preservation of perishable goods will increase. It will adversely affect already depleted energy supply scenario. As shown in Fig. 4, the main source of energy in the country is natural gas which is expected to be exhausted by 2018. Changes in temperature, rainfall, and salinity level are expected to affect the health sector severely. Mosquito-borne diseases like malaria and dengue will increase.

Because of reduction in the availability of fresh water diseases like diarrhea and cholera will spread further. Besides, increased frequency of natural disasters and incidences of bushfire will also result in increased deaths and damages.

Conclusion

Bangladesh is expected to be a major victim of global warming and climate change. Climate change induced by global warming is jeopardizing the country's development and risking sustainability. The government identified climate change as a major development concern and committed to take urgent and long-term actions to reduce risk and vulnerability. Analyses suggest that climate change may result in the reduction in agricultural output and employment, increased demand for energy and aggravated health problems. Besides preventive measures, government should also emphasize on Climate Insurance Pool (CIP). Further research is deemed necessary on risk management resulting from uncertainties and variability of climate parameters.

References

Agrawala S, Ota T, Ahmed AU, Smith J, Aalst MV (2003) Development and climate change in Bangladesh: focus on coastal flooding and the sundarbans, OECD

Alam M, Nishat A, Siddique SM (1999) Water resources vulnerability to climate change with special references to inundation. In: Huq S, Karim Z, Asaduzzaman M, Mahtab F (eds) Vulnerability and adaptation to climate change for Bangladesh. Kluwer, Dordrecht, The Netherlands

IPCC (2007a) Climate change 2007: Synthesis Report, IPCC Plenary XXVII, Valencia, Spain, November 2007

IPCC (2007b) Climate Change 2007: impacts, adaptation and vulnerability. Cambridge University Press, Cambridge

Islam MN, Uyeda H (2007) Use of TRMM in determining the climate characteristics of rainfall over Bangladesh, Remote Sensing of Environment, vol. 108. Elsevier, pp. 264–276. doi:10.1016/j.rse.2006.11.011

Germanwatch (2008) Global Climate Risk 2009: weather related loss events and their impacts on countries in and in a long-term comparison. Germanwatch e.V., Bonn, Germany

NAPA (2005) National Adaptation Programme of Action, Ministry of Environment and Forest, Government of the People's Republic of Bangladesh

SMRC (2003) The vulnerability assessment of the SAARC Coastal Region due to sea level rise: Bangladesh case, SMRC-No.3, SMRC Publication, Dhaka, Bangladesh

Changes in Tropical Cyclone Precipitation Over China

Fumin Ren, Guoxiong Wu, Xiaoling Wang, and Yongmei Wang

Keywords Precipitation • the Objective Synoptic Analysis Technique

In this paper, an objective technique for estimating the tropical cyclone precipitation (TCP) from station observations for China, which is called the Objective Synoptic Analysis Technique (OSAT), is proposed. As the OSAT technique is to imitate the process whereby a weather forecaster manually analyzes a synoptic map, OSAT shows a good ability to distinguish TC precipitation. To analyze the TC precipitation, OSAT takes two steps: separating independent rainbelts and distinguishing TC's rainbelt (Fig. 1). First, based on the structure of precipitation distribution, the daily precipitation field can be separated into several independent rainbelts and some scattered precipitation stations. In this step, there are five substeps: computing raining rate of neighborhood station, selecting the most potential rainbelt centers, defining the main characteristics of a rainbelt, roughly defining edges of the L rainbelts, and carefully defining edges of the L rainbelts. Second, according to the relationships between the TC center and independent rainbelts and the scattered precipitation stations, the rainbelts associated with a TC can be determined. In this step, there are two substeps: selecting potential TC rainbelts and defining the whole TC rainbelt.

There are two important parameters in OSAT: thresholds for distance of absolute TC precipitation (D_0) and for TC's size (D_1). Values of D_0 and D_1 according to TC's intensity are showed in Table 1.

Using OSAT, the tropical cyclone precipitation is partitioned in China. The TCP spatial distribution, its ratio to total annual rainfall, the changes in the TCP volume,

F. Ren and X. Wang
Beijing Climate Center, China Meteorological Administration, Beijing, China

G. Wu (✉)
National Climate Center, China Meteorological Administration
46 Zhongguancun Nandajie, Beijing 100081, China
e-mail: guoji@cma.gov.cn

Y. Wang
Yuncheng Weather Bureau, Yuncheng, China

Y. Charabi (ed.), *Indian Ocean Tropical Cyclones and Climate Change*,
DOI 10.1007/978-90-481-3109-9_4,

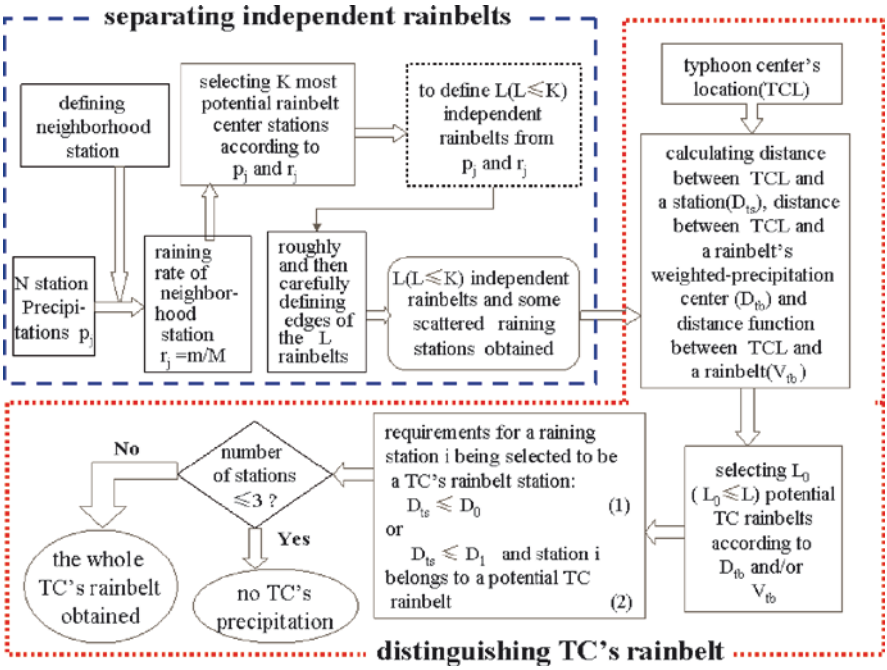

Fig. 1 Flowchart of Objective Synoptic Analysis for partitioning tropical cyclone (TC) precipitation for China

Table 1 values of D_0 and D_1 according to tropical cyclone (TC) maximum wind speed

	TC's maximum sustained wind speed (m/s)	D_0 (km)	D_1 (km)
TCs far away from China	$u < 17.2$ (tropical depression)	200	600
($D_{min} > 300$ km)	$17.2 \leq u < 24.4$ (tropical storm)	300	800
	$24.4 \leq u < 32.6$ (strong tropical storm)	400	1,000
	$u \geq 32.6$ (typhoon and above)	500	1,100
TCs close to China	$u < 17.2$ (tropical depression)	300	800
($D_{min} \leq 300$ km)	$u \geq 17.2$ (tropical storm and above)	500	1,100

and the annual frequency of the torrential TCP events during the period 1957–2004 are examined with a focus on their long-term trends in this study. Tropical cyclones significantly contribute to the annual rainfall in southern, southeastern, and eastern China, including Taiwan and Hainan islands. The annual TCP exceeds 500 mm in central-eastern Taiwan, central-eastern Hainan, and along the eastern coastline in South China. Some Taiwan stations received 1,000–1,350mm annual TCP. The TCP decreased northwestward quickly, with values less than 10mm in northern and western parts of the TC influenced region, while the annual TCP was 50–200mm in the lower valley of the Yangtze River, most regions south of the middle and lower

valleys of the Yangtze River (Fig. 2a). Figure 1b showed that in Taiwan, Hainan, the southeastern coastal regions, and the easternmost Shandong Peninsula, TCP contributes more than 10% precipitation, with 20–30% in most of Taiwan, the coastline south of 25°N, and 30–40% in most of Hainan and locations of Taiwan and the coastline. In southern-most Taiwan and western-most Hainan, TCP accounts for 40–45% of the total precipitation. Meanwhile, the ratios decrease northwestward quickly, with values less than 1% in northern and western parts of the TC-influenced region.

Together with interdecadal and interannual variations, significant downward trends are found in the TCP volume, the annual frequency of torrential TCP events, and the contribution of TCP to the annual precipitation, over the last 48 years. Figure 3a displays time series of the total annual TCP volume for China. First, a downward linear trend can be found during 1957–2004, with a rate of −3.0 km^3/year. A Kendall test indicates that the trend is statistically significant at 0.01 significance level. Second, the TCP includes interdecadal variation and prominent year-to-year

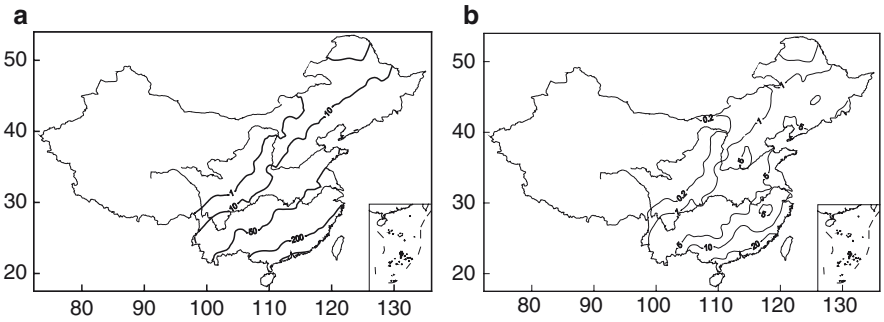

Fig. 2 Climatology of station tropical cyclone (TC) precipitation during 1971–2000. (**a**) Spatial distribution of average annual TC precipitation (in mm). (**b**) Spatial distribution of ratio of average annual TC precipitation to average total rainfall

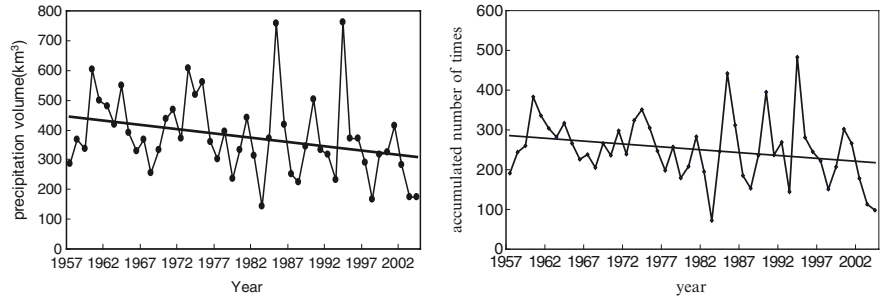

Fig. 3 Variations of tropical cyclone (TC) precipitation. (**a**) Variations of total annual volume of TC precipitation for China (in km^3). (**b**) Variations of accumulated number of times with torrential TCP (≥50 mm/day) of individual station

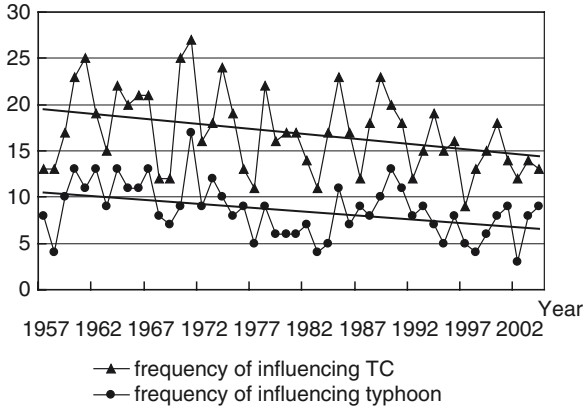

Fig. 4 Variations of frequency of influencing tropical cyclone (TC) and influencing typhoon (MSWS ≥ 32.7m/s) for China

fluctuations. In the early 1960s, early 1970s, 1985, and 1994, China received much above-normal TCP, with maximums of 761.3 and 759.2 km^3 in 1994 and 1985, respectively. Meanwhile, in the late 1960s, 1983, and 1998, much below-normal TCPs were observed in China, with minimum of 141.8 km^3 in 1983.

Figure 3b presents variations of the total annual frequency of the torrential TCP events (≥50 mm/day) for individual stations. A significant (at 0.05 level) decreasing trend can be clearly seen with similar interdecadal variations and year-to-year fluctuations as shown in Fig. 2a for the annual TCP volume. The most frequency of the torrential TCP events occurred in 1994 and 1985, with least frequency in 1983. Further examination shows that the total annual frequency of the torrential TCP events is well-correlated with the annual TCP, with a correlation coefficient of 0.94. Figure 4 shows time series of the frequency of TCs and typhoons that affected China from 1957 to 2004. The frequencies of the influencing TCs and typhoons also display significant decreasing trends during the period, with 0.05 and 0.01 significant levels, respectively. Both of them also show obvious year-to-year fluctuations, with maximums of 27 and 17, both in 1971.The variations in frequency of influencing TCs and TCP imply that, during the last 48 years, China experienced decreasing typhoon influence.

The downward trends in TCP were accompanied with decreases in the numbers of TCs and typhoons that affected China during the period 1957–2004. These changes strongly suggest that China has experienced decreasing TC influence over the last 48 years, especially in terms of TCP.

Toward Improved Projection of the Future Tropical Cyclone Changes

Masato Sugi

Keywords Projection experiments • The Earth Simulator

Introduction

We have been conducting a series of climate change projection experiments with a high-resolution AGCM using the Earth Simulator. We used a 20-km mesh AGCM for climate change projection experiments in the KYO-SEI project (FY2002–2006). The 20-km mesh AGCM is essentially the same as the current operational NWP model at JMA, although some physical processes are updated for the NWP model. The experiment is a time-slice type AGCM experiment with the SST projected by low resolution MRI CGCM.

Projection of Future Tropical Cyclone Activity

One of the greatest advantages of the 20-km mesh AGCM is that the model is able to simulate tropical cyclones much more realistically than lower resolution models. By this experiment, we could clearly show that the future tropical cyclones would intensify, but the global number of tropical cyclones would decrease (Fig. 1) (Oouchi et al., 2006).

The intensification of tropical cyclones in the future warmer and wetter climate is rather an expected result. On the other hand, the decrease in the number of tropical cyclones is a little surprising and is not a readily acceptable result without a

M. Sugi (✉)
Meteorological Research Institute, Nagamine Tsukuba, Ibaraki, 305-0052, Japan
e-mail: msugi@mri-jma.go.jp

Y. Charabi (ed.), *Indian Ocean Tropical Cyclones and Climate Change*,
DOI 10.1007/978-90-481-3109-9_5,

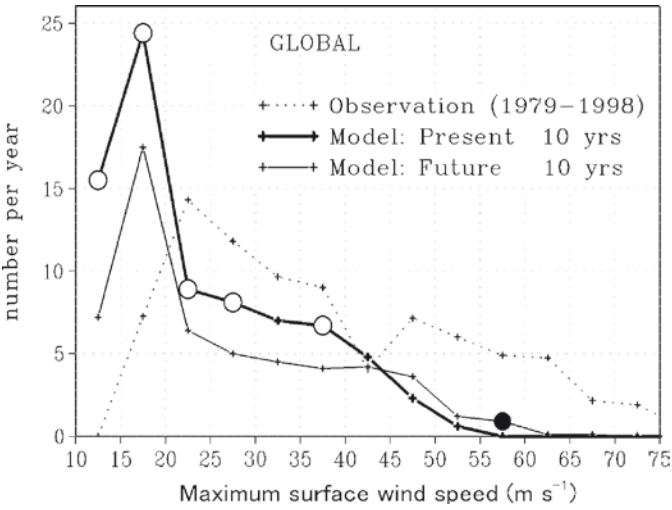

Fig. 1 Global frequency distribution of tropical cyclones as a function of life-time maximum wind speed of each tropical cyclone (Oouchi et al., 2006)

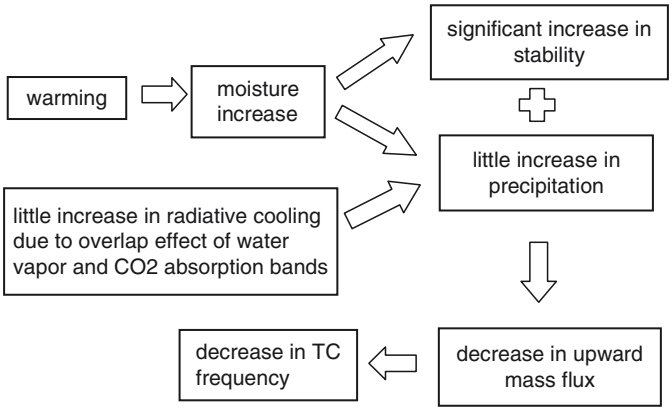

Fig. 2 Schematic diagram showing the mechanism of the reduction of global tropical cyclone frequency in the future warm climate

good explanation. We have shown that the decrease in the number of tropical cyclones could be explained by a weakening of the tropical circulation (upward mass flux) due to the increased stability in the future warmer climate (Fig. 2) (Sugi et al., 2002; Sugi and Yoshimura, 2004). The important point is that, when the atmospheric moisture significantly increases due to warming, the stability significantly increases, while the precipitation (heating) increases not as much. This is because the precipitation (heating) is not controlled by the availability of moisture, but by the atmospheric radiative cooling. It is interesting to note that the radiative

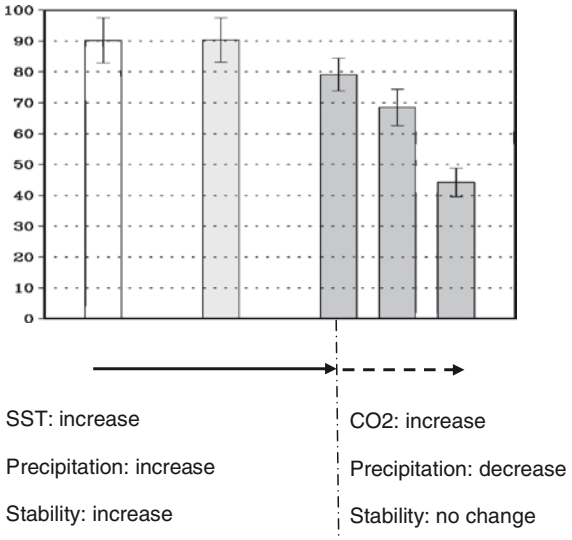

Fig. 3 Changes in tropical cyclone frequency when the SST is increased without changing CO_2 (left three bars), and when the CO_2 is increased without changing SST (right three bars) (Yoshimura and Sugi, 2005)

cooling does not increase so much as moisture, due to the overlap effect of water vapor and CO_2 long wave radiation absorption bands. It has been shown that, due to the overlap effect, number of tropical cyclones decreases if the CO_2 is increased without increasing SST (Fig. 3) (Yoshimura and Sugi, 2005).

IPCC Conclusions and Remaining Issues

On the basis of the results from our very high-resolution model and other models, IPCC (2007) concluded regarding the future changes in tropical cyclone activities as "Based on a range of models, it is *likely* that future tropical cyclones (typhoons and hurricanes) will become more intense, with larger peak wind speeds and more heavy precipitation associated with ongoing increases of tropical sea surface temperatures. There is *less confidence* in projections of a global decrease in numbers of tropical cyclones." We should note that there are large uncertainties in these projections of future changes in tropical cyclone activities, particularly in the regional changes. Remaining major issue is how we can improve the models and reduce the uncertainties. Although the 20-km mesh AGCM is able to simulate tropical cyclones much more realistically than lower resolution models, the intensity is still considerably weaker than reality. Is that because the resolution is still not sufficient? Can we simulate more intense tropical cyclones by improving cumulus parameterization scheme? We have noted that there is a considerable disagreement

among the models regarding the regional changes in the future tropical cyclone frequency. Is this because simulation of the tropical cyclogenesis process is very sensitive to the cumulus parameterization schemes in the models? Are the models not able to simulate the tropical cyclogenesis process properly?

Tropical Cyclogenesis Process

We examined the role of convection in the tropical cyclogenesis process. There is no doubt that the genesis and development of tropical cyclones are a cooperative process between the cumulus convection and tropical cyclone scale vortex. Examination of high-resolution reanalysis data JRA-25 and geostationary satellite GMS IR data indicate that a large-scale low-level convergence of absolute vorticity is the most essential process in tropical cyclogenesis (Fig. 4). It should be noted that the large-scale low-level convergence is caused by an ensemble of convective clouds scattering around the prestorm vortex. This suggests that tropical cyclogenesis can be simulated by a GCM if the effects of an ensemble of convective clouds are properly parameterized.

We also examined the role of convection-scale vortices in the tropical cyclogenesis process. Figure 5 shows the simulations of tropical cyclogenesis with 20-km-, 5-km-, and 2-km-mesh nonhydrostatic model JMA/MRI NHM. In 20-km NHM and 5-km NHM, Kain-Fritch scheme is used for cumulus convection parameterization, while in the 2-km NHM cumulus convection is computed explicitly. We can see many convection-scale vortices in the 5-km NHM and 2-km NHM. There are many anticyclonic vortices as well as cyclonic vortices associated with convective clouds. And if we take area average over an active convection area of 100-km scale, the averaged positive vorticity is not so large. This suggests that these convection-scale vortices do not play an essential role in the development of positive vorticity associated with the tropical cyclone scale rotation.

Conclusions

In a new 5-year project KAKUSHIN program (FY2007–2011), we are aiming at improving the climate change projection, particularly reducing the uncertainty in the projections of regional climate change and extreme events. In order to improve a GCM projection of future tropical cyclone activity, improvement of the cumulus convection in the model is vitally important. Improving cumulus convection parameterization is also a key to the improvement of GCM projection of regional scale climate changes. There is an argument that further improvement of cumulus parameterization is not possible, since many efforts already have been made but only little progress has been achieved recently, and therefore cloud resolving GCM is necessary for further improvement. However, for a statistically reliable projection of

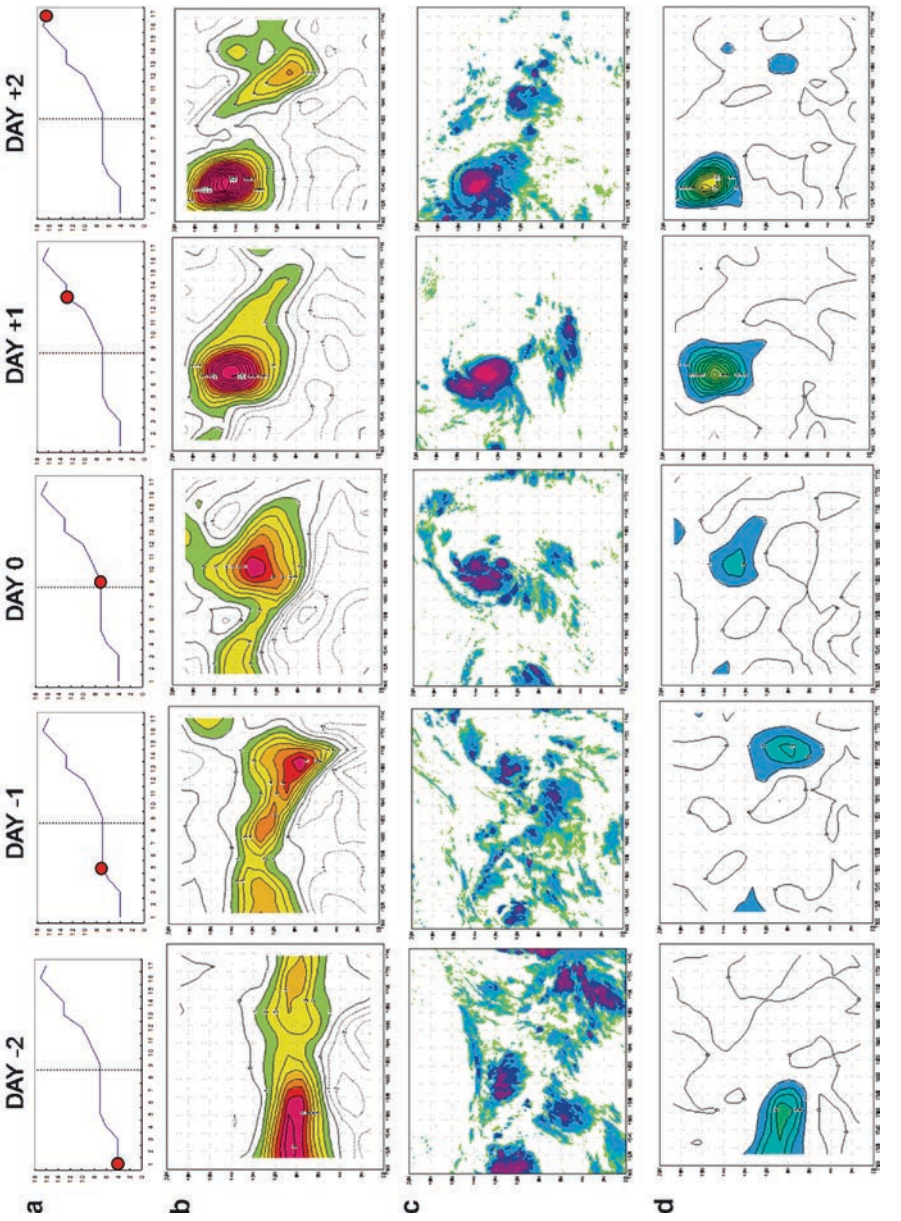

Fig. 4 Geneis process of typhoon T0416 (CHABA) during 18UTC 16 August - 18UTC 18 August 2004. (**a**) Voticity at 925 hPa vortex center (**b**) Vorticity at 925 hPa (**c**) GMS IR image (TBB) (**d**) Convergence of absolute vorticity at 925 hPa ($-(\zeta + f)$ D)

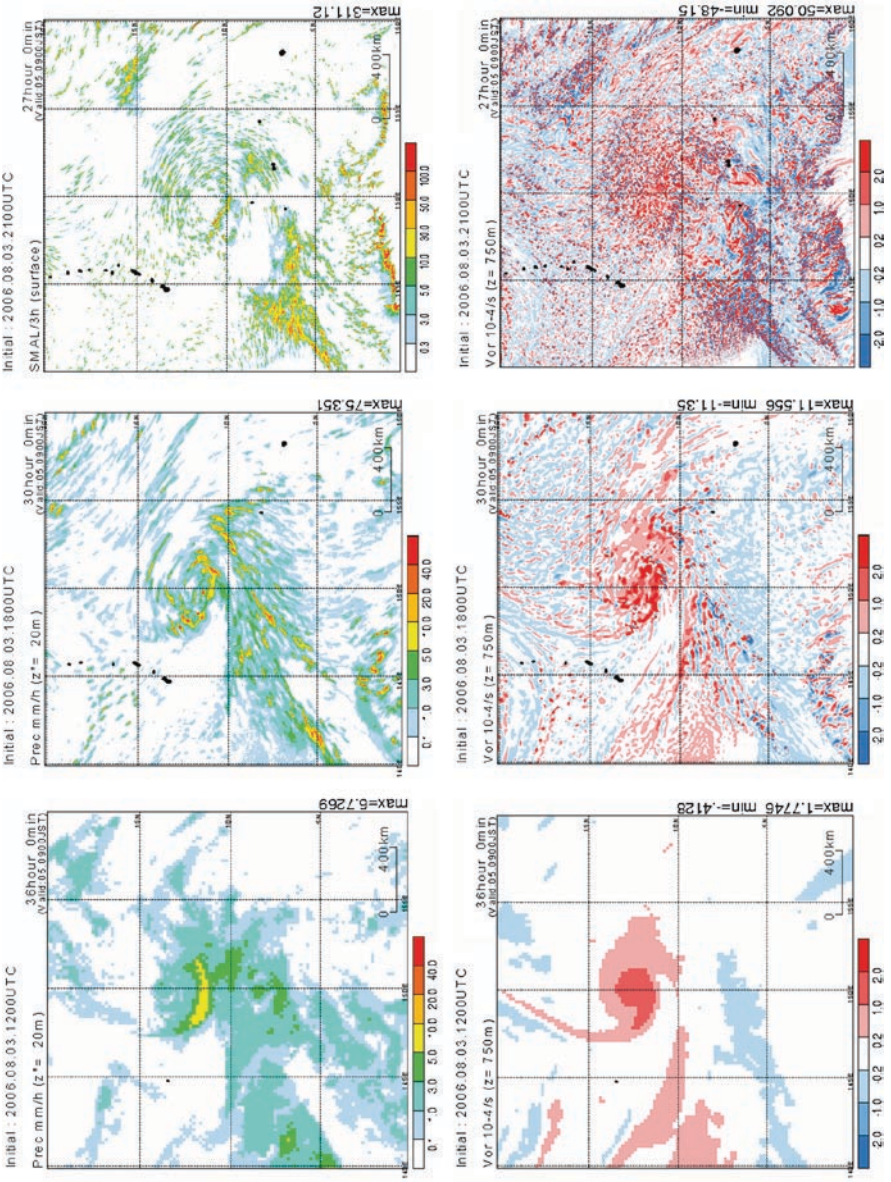

Fig. 5 Simulation of genesis process of typhoon T0608 (SAOMAI) at 00UTC 5 August 2006 with 20-km NHM, 5-km NHM, and 2-km NHM (from left to right). Top panels show 3-h precipitation. Bottom panels show vorticity at 750 m altitude

regional climate change and extreme events, we need a large number of ensemble experiments, which are not possible with cloud resolving GCM. Improvement of cumulus parameterization scheme is no doubt a difficult task, but difficult is not the same as impossible. We believe it is possible and it is a very challenging task for modelers. We are now working on this challenging task of developing a new cumulus parameterization scheme based on simulations of cumulus convection with a cloud resolving NHM.

Acknowledgment The Earth Simulator has been used for the climate change projection experiments with high-resolution AGCM in the KYO-SEI Project and KAKUSHIN Program. Both these projects are supported by MEXT (Ministry of Education, Culture Sports, Science, and Technology).

References

IPCC (2007) The physical science basis of climate change: A report of Working Group I. Fourth Assessment Report of Intergovernmental Pannel on Climate Change. Cambridge University Press.

Oouchi K, Yoshimura J, Yoshimura H, Mizuta R, Kusunoki S, Noda A (2006) Tropical cyclone climatology in a global-warming climate as simulated in a 20km-mesh global atmospheric model: frequency and wind intensity analysis. J Meteorol Soc Japan 84:259–276

Sugi M, Yoshimura J (2004) A mechanism of tropical precipitation change due to CO2 increase. J Climate 17:238–243

Sugi M, Noda A, Sato N (2002) Influence of global warming on tropical cyclone climatology: an experiment with the JMA global model. J Meteorol Soc Japan 80:249–272. doi:10.2151/jmsj.80.249

Yoshimura J, Sugi M (2005) Tropical cyclone climatology in a high-resolution AGCM - impacts of SST warming and CO2 increase. SOLA 1:133–136. doi:10.2151/sola.2005-035

Global Warming and Tropical Cyclone Activity in the Western North Pacific

Johnny C.L. Chan

Keywords Annual TC numbers • Tropospheric relative vorticity

Introduction

This paper provides a summary of some of the recent studies of the climate of tropical cyclone (TC) activity in the Western North Pacific (WNP) region, and its possible relation with global warming. Because two recent review articles (Chan 2004, 2005) have summarized most of the research on this topic up to around 2002, this paper will only discuss the studies that came after this time. Readers interested in the earlier works can consult these two articles. Section 2 discusses the variations of TC numbers and number of intense TCs and how they might or might not be related to global warming. Variations of TC tracks and landfall locations are presented in Section 3. A summary is then given in Section 4.

Variations in TC Activity

Annual TC Numbers

The annual number of TCs in the WNP shows large interannual as well as interdecadal variations, with peaks in the 1960s and 1990s (Fig. 1). Regardless of data uncertainties in the presatellite era it is obvious from Fig. 1, that the annual number

J.C. Chan (✉)
Guy Carpenter Asia-Pacific Climate Impact Centre,
City University of Hong Kong, Hong Kong, China
e-mail: Johnny.chan@cityu.edu.hk

Y. Charabi (ed.), *Indian Ocean Tropical Cyclones and Climate Change*,
DOI 10.1007/978-90-481-3109-9_6,

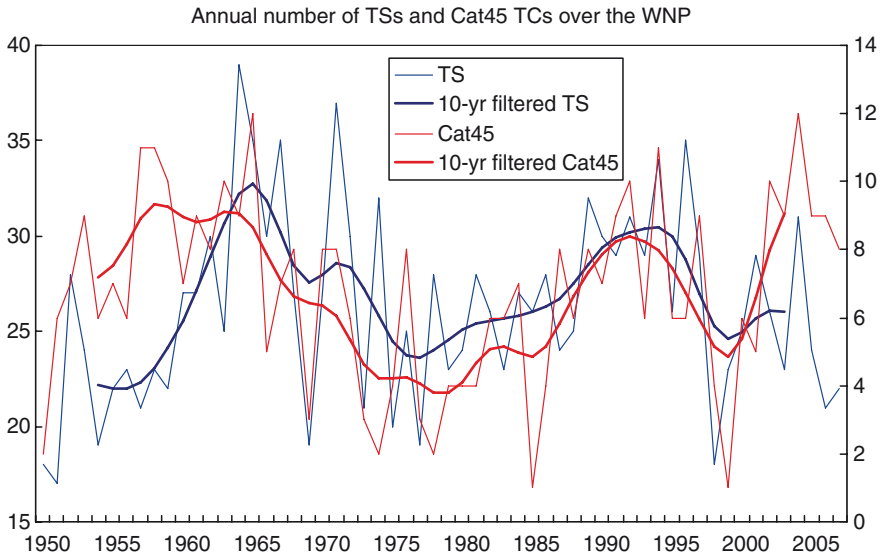

Fig. 1 Annual number of tropical cyclones with tropical storm intensity or above (TS, blue, left axis) and in the Saffir–Simpson categories 4 and 5 (Cat45, red, right axis) in the Western North Pacific. Heavy line is the 10-year Gaussian-filtered and light line is the annual number

of TCs in the WNP does not show any linear trend. Instead, large interannual and interdecadal, or even multidecadal, variations exist. This result, therefore, suggests that global warming cannot be related to the variation in the annual number of TCs in the WNP. The interannual variations are apparently contributed largely by the El Niño/Southern Oscillation (ENSO) and the quasi-biennial oscillation in the stratosphere (see review in Chan 2004, 2005) through modifications of the dynamic conditions for genesis (Gray 1979). The causes of the decadal or multidecadal variations have not been studied in detail, but they are likely to be similar to the causes of similar variations in the number of intense TCs, which will be discussed in the next subsection.

Annual Number of Intense TCs

Chan (2006) examined the annual accumulated cyclone energy (ACE, which has a correlation of 0.82 with the number of Category 4 and 5 TCs (NCat45) – see Chan 2008) variations from the 1960s and found that the values of the ACE in the 1960s were nearly as high as those in the 1990s (see NCat45 curve in Fig. 1). Because some TCs are likely missed in the presatellite era and techniques for estimating TC intensity were not as good then, it is likely that the ACE value in the earlier era should be higher than that calculated from the best-track dataset. To quantify this

further, Chan (2006) found the value of NCat45 during the period 1960–1974 to be 105, which is similar to that during the 1990–2004 period of 115, while that during the 1975–1989 is 75. On the basis of the earlier argument, the NCat45 during the earlier period should likely be >105, and hence even closer to that during the latter period. In other words, the increase in the number of intense TCs from 1975 to 2004 is simply the rising branch of the multidecadal variation, rather than a long-term trend.

On the basis of the results of Chan and Liu (2004), Chan (2006, 2007) further showed that the annual variation of ACE can be explained by similar variations in the relative vorticity, vertical wind shear, and the moist static energy over the WNP. However, the correlation between ACE and SST is not significant, and in fact negative. Such a negative correlation was discussed by Chan and Liu (2004) as not being a causal relationship, but rather a reflection of the relationship between TC activity and ENSO. Thus, the increase in SST, which is likely a result of global warming, cannot be attributed to the variation of the frequency of intense TCs in the WNP. To understand the multidecadal variations of intense TC activity in the WNP further, Chan (2008) performed a wavelet analysis of the annual NCat45 and found two distinct periods: 2–7 years and 16–32 years. Reconstructing the time series using the 16–32-period component gives two above-normal (A: 1960–1970 and 1987–1997) and one below-normal (B: 1971–1986) periods (Fig. 2). Various thermodynamic and dynamic parameters over the entire WNP were then composited for each of these three periods. For the thermodynamic parameters, the most significant difference between the A and B periods appears to be the moist static energy (MSE, Fig. 3)[1] in the south-eastern part of the WNP (the boxed area in

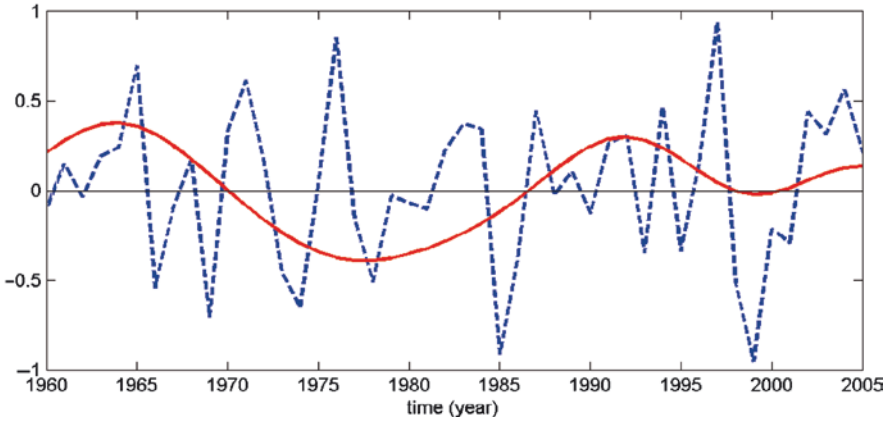

Fig. 2 Normalized reconstructed time series of NCat45 at 2–7-year (blue dashed) and 16–32-year (red) periods (Redrawn from Chan 2008)

[1]Note that the second principal component is shown because the coefficients of the first component shows a continuous increase, which is to be expected as the moist static energy is related to the air temperature that has been on the increase due to global warming.

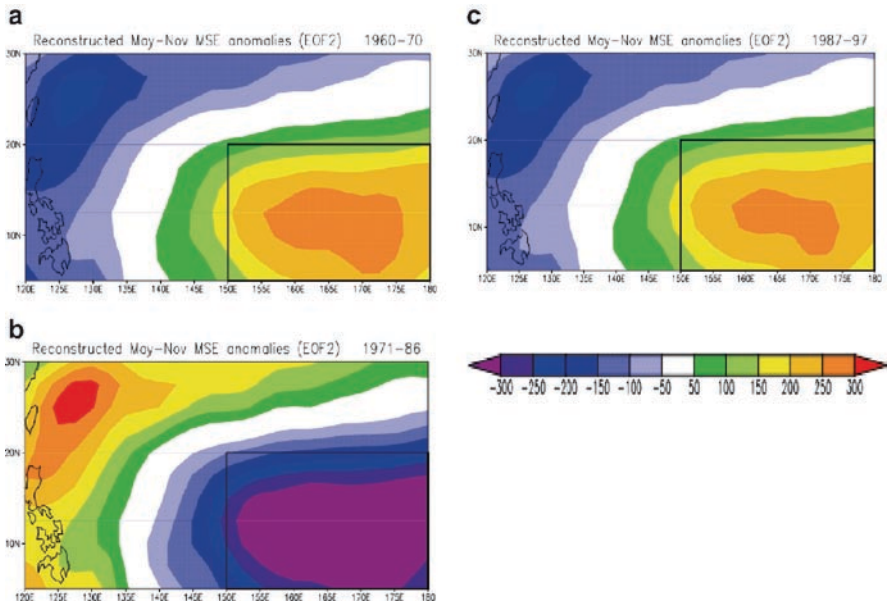

Fig. 3 1,000–500 hPa mean MSE anomalies over the WNP averaged between May and Nov reconstructed from the second principal components for each of the three periods: (**a**) 1960–1970, (**b**) 1971–1986, and (**c**) 1987–1997. Unit: J kg^{-1}. The thick rectangle indicates the "boxed" area discussed in the text (Redrawn from Chan 2008)

Fig. 3) where the MSE is higher during the A periods and lower during the B period. In addition, the atmosphere within the boxed area is more unstable during the A periods (not shown, please refer to Chan 2008). Thus, within this boxed area, the atmosphere is more conducive to intense convection, which was verified based on precipitation anomalies (not shown, please refer to Chan 2008). As all TCs form from well-developed cloud clusters, this result suggests that it is likely that more TCs form in this boxed area during the A years. While the SST in this boxed area is also slightly higher during the A years, the difference between the A and B years is only about 0.1°C.

Although more TCs form in the boxed area during the A years, for them to intensify to category 4 and 5 requires dynamic conditions favorable to the continuous intensification of these TCs. Chan (2008) found that this is indeed the case as the lower tropospheric relative vorticity over the entire WNP is stronger during the A years (not shown). The vertical wind shear is also smaller (Fig. 4). The TCs also tend to stay over water for a longer period of time in the A years (Fig. 5). In other words, during the A years, more TCs form in the south-eastern part of the WNP, traverse across the WNP under more favorable dynamic conditions for intensification, and remain over the open ocean for a long time. These TCs, therefore, have a

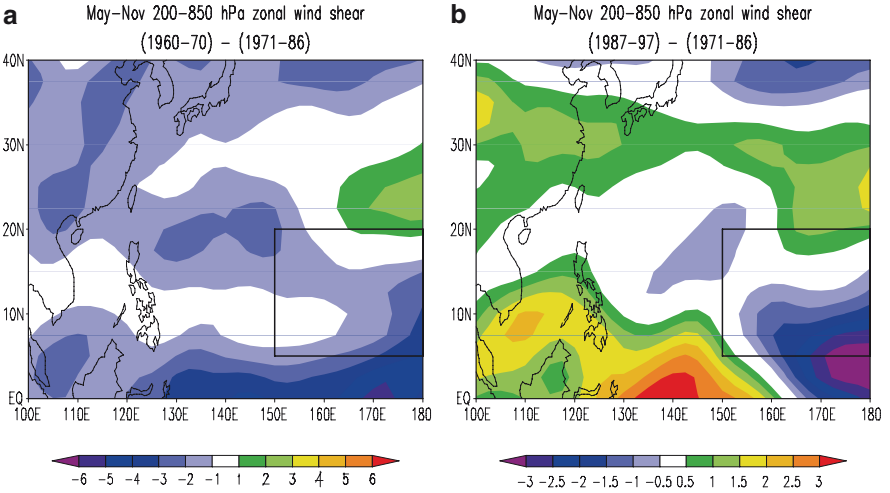

Fig. 4 Differences in May–Nov averaged vertical (200 hPa minus 850 hPa) zonal wind shear between 1971–1986 and (**a**) 1960–1970, and (**b**) 1987–1997. Unit: m s^{-1}. The thick rectangle indicates the "boxed" area discussed in the text (Redrawn from Chan 2008)

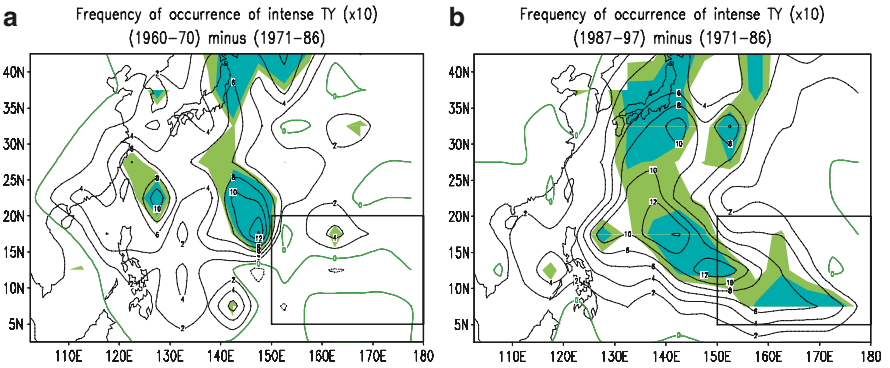

Fig. 5 Difference in the occurrence of category 4 and 5 typhoons per 10 years occurring in each 5°latitude × 5°longitude box between (**a**) 1960–1970 and 1971–1986 and between (**b**) 1987–1997 and 1971–1986. Positive numbers indicate less in the period 1971–1986. Light and dark shadings indicate the difference is significant at the 90% and 95% significance level respectively. The thick rectangle indicates the "boxed" area discussed in the text (Redrawn from Chan 2008)

larger potential to become intense TCs. The reason for the increased frequency of intense TCs is thus *not* due to an increase in SST, but a change in the planetary atmospheric (thermodynamic *and* dynamic) conditions that favor both the formation and intensification of TCs. That is, global warming cannot explain the variation in the frequency of occurrence of intense TCs in the WNP.

Summary

Two conclusions may be drawn from these observational analyses. First, based on the data for the period 1950 to the present, it is apparent that neither the number of TCs nor the number of intense TCs shows a monotonic increase, even if data uncertainties in the presatellite or early-satellite eras are taken into consideration. Second, the numbers of TCs and of intense TCs go through large interannual and interdecadal variations, both of which can be explained by similar variations in the planetary-scale atmospheric (thermodynamic and dynamic) conditions over the Pacific. These two conclusions suggest that the increase in SST as a result of global warming cannot be used to explain the observed variations in TC activity.

Variations in Tracks and Landfall Locations

It has been documented that TCs move generally with their surrounding flow, known as the steering flow (George and Gray 1976; Chan and Gray 1982). Therefore, any changes in the atmospheric flow would lead to changes in the track, and hence the places where TCs will land. Such variations in the track have been documented, both on interannual and interdecadal time scales. In this section, these variations are described together with possible reasons for such variations.

Interannual Variations

To study the frequency of landfall in greater detail, Chan and Xu (2009) divided the Asian coast into three sections: south (Philippines, Vietnam, and South China), middle (Taiwan and East China), and north (Korea and Japan) and counted the number of landfalling TCs each year. They found that in each of the regions, the annual number of landfalling TCs goes through large interannual as well as interdecadal variations. The interannual variations have periods of 2–8 years while those in the interdecadal time scale have a period between 16 and 32 years (Fig. 6). The interdecadal variations will be discussed further in section 3b. For the interannual variations, the number in one region does not correlate well with that in the other two regions. However, the number in each region correlates significantly with the sum of all the landfall numbers as well as the total number of WNP TCs, which suggests that if the WNP is active, it is likely to bring about more landfalls in each of the regions. This result is in contrast with that found by Holland (2007) in the Atlantic.

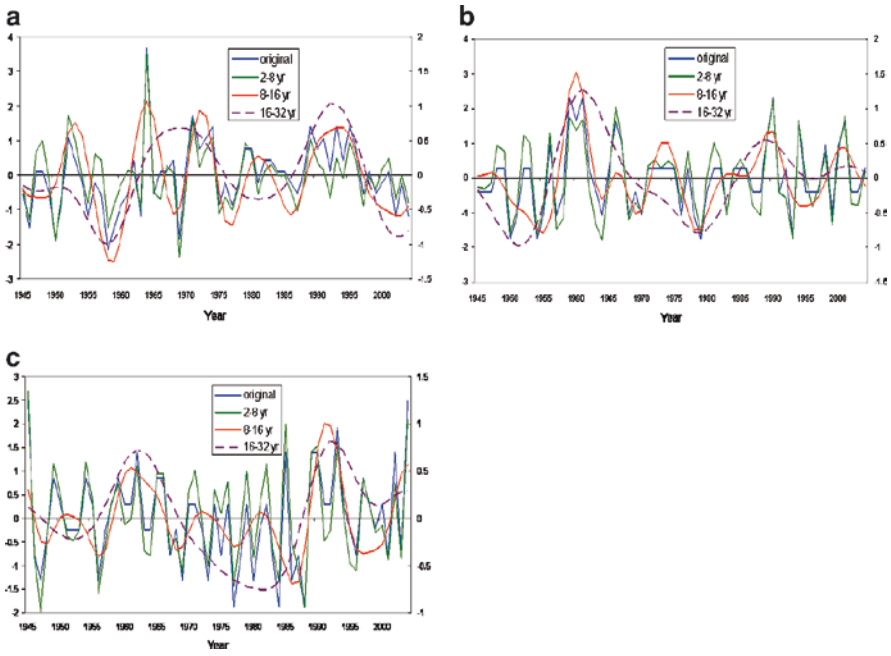

Fig. 6 Reconstruction of the time series of the standardized number of landfalling TCs in the (**a**) south, (**b**) middle, (**c**) north Asian coast region (see text for the definition of the regions) for periods 2–8 years (green), 8–16 years (red, values multiplied by 5), and 16–32 years (purple dashed, values multiplied by 10), all using scale on the right axis

Interdecadal Variations

Liu and Chan (2008) performed a principal component analysis of the 10-year-filtered number of TCs occurring within each 5°latitude × 5°longitude box and found that patterns of first three principal components almost reproduce completely the track distributions in three different eras, each spanning about 10–15 years (Fig. 7). The pattern of the first principal component is very similar to the track distribution during the 1977–1988 period (cf. Figs. 7a and b), that of the second to 1964–1976 (cf. Figs. 7c and d) and that of the third to 1989–1997 (cf. Figs. 7e and f). They found that the coefficients associated with these principal components are correlated with those of the zonal winds and geopotential heights at 500 hPa, which suggests that variations of these tracks are due to those in the steering flow caused by changes in the planetary-scale atmospheric circulation.

The original series is also plotted (blue, scale on left axis) (redrawn from Chan and Xu 2009). As mentioned in section 4.1, Chan and Xu (2009) found multidecadal

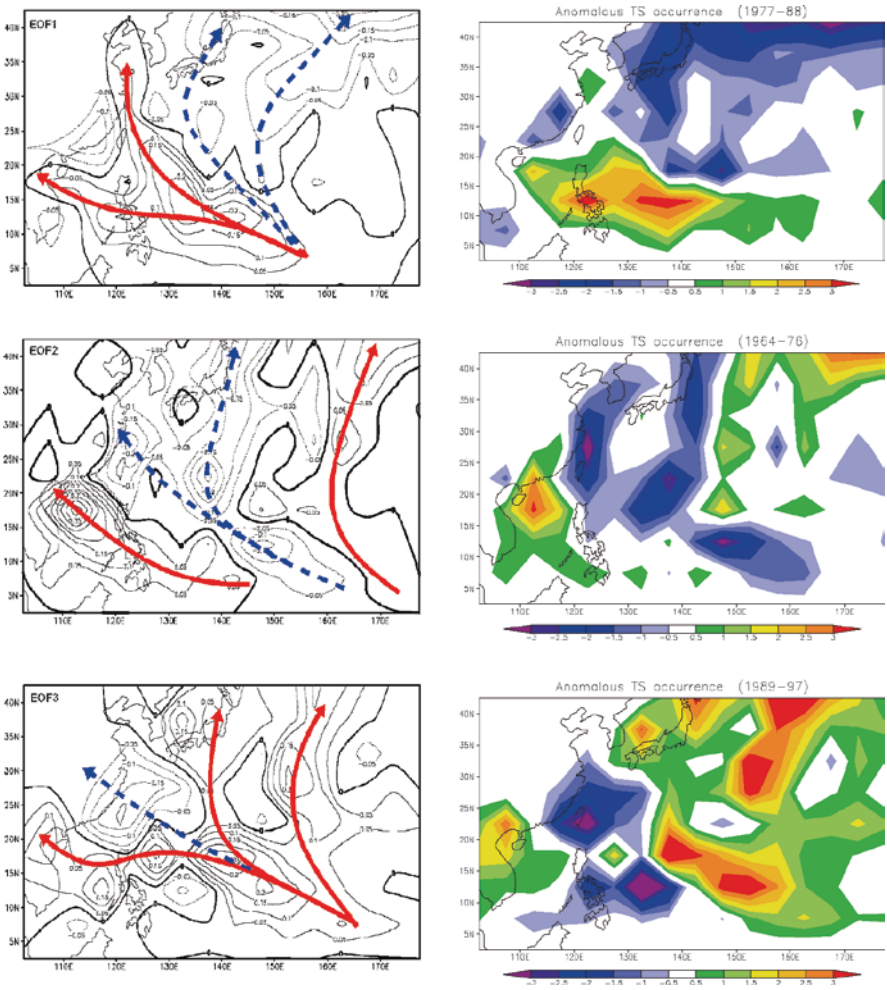

Fig. 7 Loading patterns of the annual TC occurrence pattern for the (a) first, (c) second, and (e) third EOFs. The red solid and blue dashed arrows indicate the prevailing tracks with increased and decreased frequency, respectively. (b) 1977–1988, (d) 1964–1976, and (c) 1989–1997 are the corresponding anomalous TC frequency of occurrence during each of the periods (Redrawn from Liu and Chan 2008)

variations in the frequency of landfalling TCs along the Asian coast (see Fig. 6). At multidecadal time scales, the annual number of landfalling TCs varies in unison among all regions of Asia during some periods but in others, one region would have an above-normal number of landfalling events while the other regions would have below-normal numbers (Fig. 8). In general, the number of in each region correlates very well with that of the total number of WNP tropical cyclones.

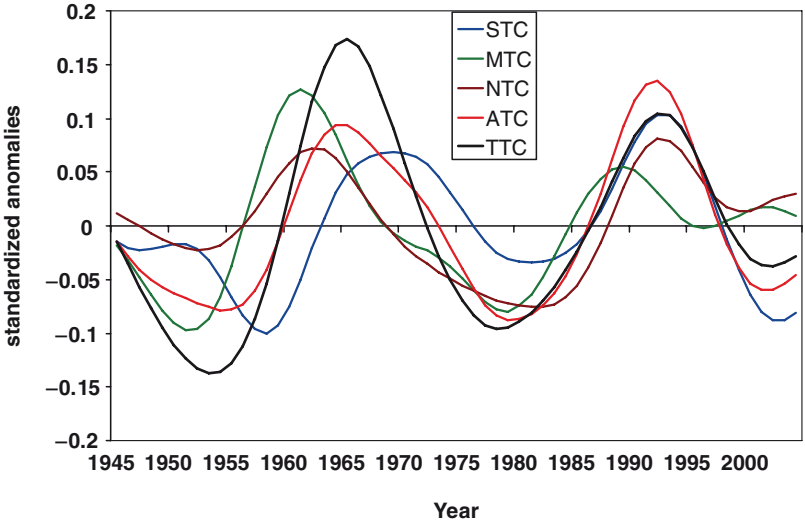

Fig. 8 16–32-year reconstructed time series of the standardized anomalies of the number of landfalling TCs in the south (STC), middle (MTC), north (NTC) Asian coast region (see text for the definition of the regions). The time series of the total number of landfalling TCs in the Asian region (ATC) and the total number of TCs occurring in the WNP (TTC) are also shown (Redrawn from Chan and Xu 2009)

Summary

The results on the track and landfall variations of TCs in the WNP appear to be very similar to those on the total activity in that no single region has seen a continuous decrease or increase in TC activity during the last half a century. Instead, the frequency of TCs passing through any given location, either over the ocean or land, goes through large interannual and interdecadal variations caused by similar variations in the large-scale atmospheric and oceanographic conditions.

Summary and Discussion

Given the observed increase in global temperature and the concomitant increase in SST, it appears to be intuitive to assume that TC activity, which depends on the energy from the ocean, would also increase as a result. However, it has been shown that such an assumption is not valid, at least for the WNP. None of the parameters related to TC activity (total number, number of intense TCs, tracks, and landfall locations) shows a linear trend during the past 50 years, but all of them show large variations on interannual and interdecadal time scales. Most of the interannual

variations appear to be correlated with those in the planetary-scale atmospheric and oceanographic conditions associated with ENSO. Variations on interdecadal time scales are also related to similar variations in the atmospheric flow patterns as well as ocean temperatures over the Pacific. The reason for these apparently counterintuitive results is that TC activity is not simply governed by the thermodynamic conditions in the atmosphere and ocean. Dynamic conditions are also necessary. In other words, even if the thermodynamic conditions have become more favorable under a global-warming scenario (higher temperatures and larger amount of water vapor available), the dynamic conditions have yet to be shown to have changed in such a way as to be more conducive for TC formation and development. It might actually be interpreted that the thermodynamic conditions are the necessary ones but the dynamic conditions are the sufficient ones. In other words, without the support of more favorable dynamic conditions, only more cloud clusters will form over the tropical ocean (due to more favorable thermodynamic conditions, and may result in more overall rainfall) but the overall number of clusters that can develop into TCs or intense TCs remain largely the same as that in the era prior to any significant global warming. Flow patterns that govern TC movement have also not been found to possess a linear trend and hence it is not possible to draw the conclusion that any region is likely to see a continuous increase or decrease in the frequency of TC occurrence.

References

Chan JCL (2004) Variations in tropical cyclone activity over the western North Pacific: from interdecadal to intraseasonal. In: Murnane RJ, Liu K-B (eds) Hurricanes and typhoons past, present and future. Columbia University Press, New York, pp 269–296

Chan JCL (2005) Interannual and interdecadal variations of tropical cyclone activity over the western North Pacific. Meteor Atmos Phys 89:143–152

Chan JCL (2006) Comment on “Changes in tropical cyclone number, duration, and intensity in a warming environment”. Science 311:1713b

Chan JCL (2007) Interannual variations of intense typhoon activity. Tellus 59A:455–460

Chan JCL (2008) Decadal variations of intense typhoon occurrence in the western North Pacific. Proc Royal Soc A 464:249–272

Chan JCL, Gray WM (1982) Tropical cyclone movement and surrounding flow relationships. Mon Wea Rev 110:1354–1374

Chan JCL, Liu KS (2004) Global warming and western North Pacific typhoon activity from an observational perspective. J Climate 17(23):4590–4602

Chan JCL, Xu M (2009) Interannual and interdecadal variations of landfalling tropical cyclones in East Asia. Part I: Time series analysis. Int J Climatol (in press)

George JE, Gray WM (1976) Tropical cyclone motion and surrounding parameter relationships. J Appl Meteor 15:1252–1264

Gray WM (1979) Hurricanes: their formation, structure, and likely role in the tropical circulation. In: Shaw DB (ed) Meteorology over the tropical oceans. Roy Meteor Soc, pp 155–218

Holland GJ (2007) Misuse of landfall as a proxy for Atlantic tropical cyclone activity. EOS Trans AGU 88(36):349–350

Tropical Cyclones and Climate Change: An Indian Ocean Perspective

Thomas R. Knutson

Keywords TC frequencies • TC intensities

Introduction

The tropical Indian Ocean is characterized by surface-warming trends that are more statistically significant, compared with model-simulated internal variability, than those in many other tropical basins including in the Northeast Pacific and North Atlantic (e.g., Knutson et al., 2006, see Figs. 5, 7, 9). This raises the possibility that tropical cyclone (TC) trends resulting from global warming could emerge in the Indian Ocean prior to other basins. Here, some studies of climate-warming impacts on tropical cyclone behavior relevant to this issue are reviewed.

Tropical Cyclone Intensities

Elsner et al. (2008) have noted recent (1981–2006) upward trends in the upper quantiles of TC intensities aggregated over the globe. The upward trends in the Indian Ocean basins appear second only to the Atlantic basin in terms of their overall statistical significance. However, some questions remain about the homogeneity of the satellite-derived historical intensity estimates for the Indian Ocean in particular (Chris Landsea, personal communication), as Elsner et al.'s estimates required a substantial adjustment for changes in the satellite view angle over time during the record. This issue remains a topic of active research. In terms of the expected (modeled) response of Indian Ocean TC activity to greenhouse warming, fewer studies with

T.R. Knutson(✉)
Geophysical Fluid Dynamics Laboratory/NOAA, Princeton, NJ, USA

Y. Charabi (ed.), *Indian Ocean Tropical Cyclones and Climate Change*,
DOI 10.1007/978-90-481-3109-9_7,

high-resolution hurricane-climate models have been reported to date for the Indian Ocean basin than for the Atlantic. However, some existing idealized modeling experiments with a version of the GFDL hurricane model (Knutson et al., 2001, Fig. 3) suggest that greenhouse warming in the Indian Ocean (as well as other tropical storm basins) may lead to higher intensities (a few percent per °C of ocean warming) and higher near-storm rainfall rates. Similarly, in the North Indian Ocean basin, theoretical potential intensity analyses based on CMIP3 climate model ensembles (Vecchi and Soden, 2007, Fig. 4) show projected increases for potential intensity of a few percent per degree of global warming.

Tropical Cyclone Frequencies

Existing global modeling studies exploring the response of TC frequency in the Indian Ocean to greenhouse warming have not shown agreement even on the sign of projected change. For example, in a recent review of such studies, three global models project an increase and three models a decrease in the frequency in response to a greenhouse-gas-dominated climate-warming signal. Our recent regional modeling study on TC frequency and greenhouse warming (Knutson et al., 2008), although focused on the Atlantic basin, may also have some relevance for the Indian Ocean. The dynamic model used in this study simulates the interannual variability and decadal trend in Atlantic TC counts (1980–2006) remarkably well when forced with past large-scale conditions from NCEP reanalyses. In subsequent experiments, we use this model, driven by the NCEP large-scale conditions modified by a multimodel ensemble climate-change signal. These simulations show a decrease in tropical storm and hurricane frequency in the Atlantic basin for projected late twenty-first century conditions, despite the strong SST warming projected there by the IPCC AR4 models. Additional experiments (Garner et al., 2009) suggest that the decrease in storm frequency in the model is likely due in large part to an increase in vertical shear over parts of the Atlantic basin, as projected by a multimodel composite for the twenty-first century (Vecchi and Soden, 2007). However, in contrast to the Atlantic, Vecchi and Soden's IPCC AR4 model late twenty-first century composite shows a substantial *decrease* in vertical wind shear over much of the low-latitude Indian Ocean with global warming, as well as an even more pronounced increase of potential intensity than in the Atlantic. These findings suggest that late twenty-first-century model projections of reduced tropical storm and hurricane frequency in the Atlantic may not apply for Indian Ocean TC frequency. Further quantitative studies to explore these issues with a variety of models are strongly recommended, and further global modeling studies are ongoing at GFDL and other climate modeling centers. Data homogeneity has been an important issue for TC/climate change studies in the Atlantic basin, and will undoubtedly also be important for future Indian Ocean basin studies. To illustrate its importance, we will review some recent studies on possible TC trends in Atlantic-basin TC activity. In particular, Vecchi and Knutson (2008) and others

suggest that the relatively scarcity of reporting ship tracks in the Atlantic basin, especially in the late 1800s and early 1900s, likely leads to a spurious or inflated positive trend in tropical-storm counts from the late 1800s to present. In this study, Vecchi and Knutson estimated the year-by-year rate of missing storm occurrence using an analysis of historical ship-track records combined with known satellite-era storm tracks to infer potential missing storm rates in the presatellite era. Similar methodologies could be applied to TC observations in the Indian Ocean. In any case, future studies of past trends in Indian Ocean TCs should consider limited ship-track density as a possible source of spurious trends in the TC record.

Conclusions

In summary, results presented here suggest that the Indian Ocean may be a crucial region to study from the viewpoint of climate change detection and attribution of both SST and its relation to tropical cyclone activity. Specifically, the findings suggest that the signal of a warming-induced change in TC activity could emerge sooner in the Indian Ocean than in other basins. However, detection of an anthropogenic signal will depend crucially on having homogeneous long-term records of key variables, such as TC frequency, duration, intensity, and rainfall.

References

Elsner JB, Kossin JP, Jagger TH (2008) The increasing intensity of the strongest tropical cyclones. Nature 455:92–95. doi:10.1038/nature07234. http://myweb.fsu.edu/jelsner/PDF/Research/ElsnerKossinJagger2008.pdf

Garner ST, Held I, Knutson TR, Sirutis JJ, (2009) The roles of wind shear and thermal stratification in past and projected changes of Atlantic tropical cyclone activity. J. Climate, 22(17), doi:10.1175/2009JCLI2930.1

Knutson TR, Tuleya RE, Shen W, Ginis I (2001) Impact of CO_2-induced warming on hurricane intensities as simulated in a hurricane model with ocean coupling. J Climate 14:2458–2468. http://www.gfdl.noaa.gov/reference/bibliography/2001/tk0101.pdf

Knutson TR, Delworth TL, Dixon KW, Held IM, Lu J, Ramaswamy V, Schwarzkopf D, Stenchikov G, Stouffer RJ (2006) Assessment of twentieth-century regional surface temperature trends using the GFDL CM2 coupled models. J Climate 19(9):1624–1651. http://www.gfdl.noaa.gov/reference/bibliography/2006/tk0601.pdf

Knutson TR, Sirutis JJ, Garner ST, Vecchi GA, Held IM (2008) Simulated reduction in Atlantic hurricane frequency under 21st century warming conditions. Nature Geoscience 1:359–364. http://www.gfdl.noaa.gov/~gav/REPRINTS/KSGVH_08_HURR.pdf

Vecchi GA, Knutson TR (2008) On estimates of historical North Atlantic tropical cyclone activity. J Climate 21:3580–3600. http://www.gfdl.noaa.gov/reference/bibliography/2008/gav0802.pdf

Vecchi GA, Soden BJ (2007) Increased tropical Atlantic wind shear in model projections of global warming. Geophys Res Lett 34:L08702. doi:10.1029/2006GL028905. http://www.gfdl.noaa.gov/~gav/REPRINTS/VS_07_SHEARS.final.pdf

Recent Trends in Tropical Cyclone Activity in the North Indian Ocean

O.P. Singh

Keywords Simulation of intensity • TC frequency

Introduction

The North Indian Ocean (NIO) which accounts for about 5% of total global tropical cyclones produces about four TCs per year out of which three form in the Bay of Bengal (BOB) and one forms in the Arabian Sea (AS). Because of various socioeconomic factors, these cyclones inflict heavy loss of life and property in the NIO rim countries. Utilizing reliable dataset of satellite era, it has been shown that the stronger TCs with maximum sustained winds (MSW) exceeding 95 nautical miles per hour (knots) and above have become more frequent in the NIO during the past 3 decades. When the frequency of all TCs with MSW exceeding 63 knots is considered, the uptrend reduces. Thus, an increase in the frequency of stronger TCs in NIO during the past few decades is a reality. Extensive work has been done on the changes in the frequency and intensity of TCs of North Indian Ocean (Bay of Bengal and Arabian Sea) by Indian meteorologists (Mooley 1980, 1981; Singh et al. 2000, 2001; Singh 2007; Srivastav et al. 2000). There has been certain amount of ambiguity about the reliability of TC data before the satellite detection of TCs which commenced in the 1970s. For the NIO, the satellite detection of TCs started in 1972 by the Joint Typhoon Warning Centre (JTWC), Guam (now shifted to Pearl Harbor, Hawaii), USA. The India Meteorological Department (IMD) started the satellite detection of TCs from the early 1980s onward when the Indian geostationary satellite, INSAT was launched. The JTWC data on TCs of NIO for 1972–2006 have been used in the present work. Utilizing IMDs existing dataset, a few earlier works (Singh et al. 2001; Singh 2007; Srivastav et al. 2000) have shown that there

O.P. Singh(✉)
India Meteorological Department, New Delhi, INDIA

Y. Charabi (ed.), *Indian Ocean Tropical Cyclones and Climate Change*,
DOI 10.1007/978-90-481-3109-9_8,

is an uptrend in the frequency of intense TCs in NIO during the months of high TC activity, i.e., November and May. In the present study, an attempt has been made to derive firm conclusions on recent trends in the annual number of stronger TCs in NIO removing the ambiguity of data of presatellite era.

Results and Discussion

Trends in the Frequency of Stronger TCs (Maximum Sustained Wind [MSW] 96 knots and Above)

In Fig. 1, the frequency of stronger TCs in NIO for the 3 decades; 1972–81, 1982–91, and 1992–2001 has been shown. Only two stronger TCs formed in the NIO (Bay of Bengal and Arabian Sea) during 1972–1981. The frequency increased to 4 and 9 stronger TCs in the next 2 decades, respectively. The implications of this increase in stronger TC number in the NIO may be enormous for the NIO rim countries like Bangladesh, India, Myanmar, Sri Lanka, and even Pakistan and Oman. The observed trend in the frequency of stronger TCs with NIO during past decades shows that on an average the rim countries have to face about one TC of category 3 and above every year. The situation 3 decades ago was one TC of category 3 and above every 5 years. Thus, there is a fivefold increase in the occurrence of a stronger TC in NIO. Table 1 summarizes all 15 cases of stronger TCs that occurred in the NIO during the 3 decades period from 1972 to 2001.

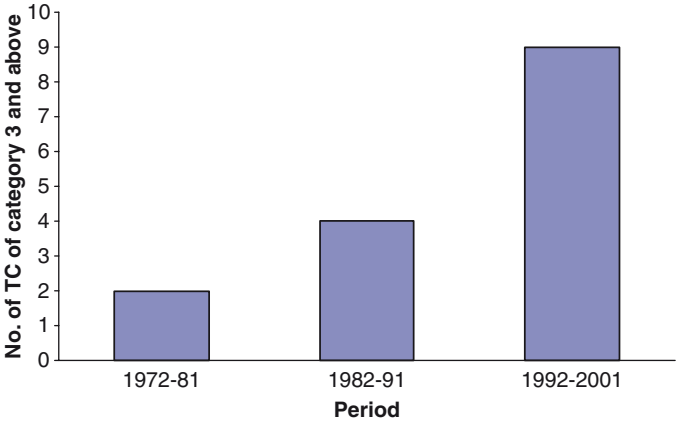

Fig. 1 Decadal frequency of stronger TCs (of category 3 and above) in the NIO basin (Bay of Bengal and Arabian Sea) during the satellite era

Table 1 Summary of all TCs of category 3 and above in the NIO during 1972–2001

S. No.	Period	TC category	MSW (knots)	Sea area
1.	9–23 Nov 1977	3	110	BOB
2.	14–20 Nov 1977	3	111	BOB
3.	30 April–5 May 1982	4	120	BOB
4.	21–30 Nov 1988	3	110	BOB
5.	3–11 May 1990	4	125	BOB
6.	22–30 April 1991	5	140	BOB
7.	26 April–3 May 1994	4	125	BOB
8.	18–25 Nov 1995	3	105	BOB
9.	1–7 Nov 1996	4	115	BOB
10.	13–20 May 1997	4	115	BOB
11.	1–9 June 1998	3	105	AS
12.	15–21 May 1999	3	110	AS
13.	15–18 Oct 1999	4	120	BOB
14.	25 Oct–3 Nov 1999	5	140	BOB
15.	21–29 May 2001	3	110	AS

Simulation Experiments

In order to simulate the impacts of global climate change (due to increased anthropogenic emissions) on the cyclogenesis in the Bay of Bengal, two experiments, namely one with fixed amount of greenhouse-gas concentration corresponding to 1990 levels called the "control" (CTL), and the other with annual compound increase of 1% in the greenhouse-gas concentration for 2041–2060 from 1990 onward called the "greenhouse gas" (GHG) were conducted. The annual compound increment of 1% in the greenhouse-gas concentration has been adopted from the projections of Intergovernmental Panel for Climate Change (IPCC). The model used was HadRM2 of Hadley Centre for Climate Prediction and Research, UK. The horizontal resolution of the model is 0.44° × 0.44°, i.e., minimum resolution of 50 × 50 km at the equator. The criteria adopted for the identification of storms, in addition to a local minimum in sea-level pressure, was as follows: (i) Sea-level pressure departure <-5 hPa, (ii) Maximum wind speed >15 m/s, and (iii) Duration of the storm of at least 2 days. It may be pointed out that all storms (vortices) could be easily identified in the simulations.

Simulation of Intensity

The results on intensity simulations for May, October, and November are presented in Fig. 2. During all the 3 months the model has simulated an enhancement in the average maximum wind speed of the storms. In October the average wind speed has

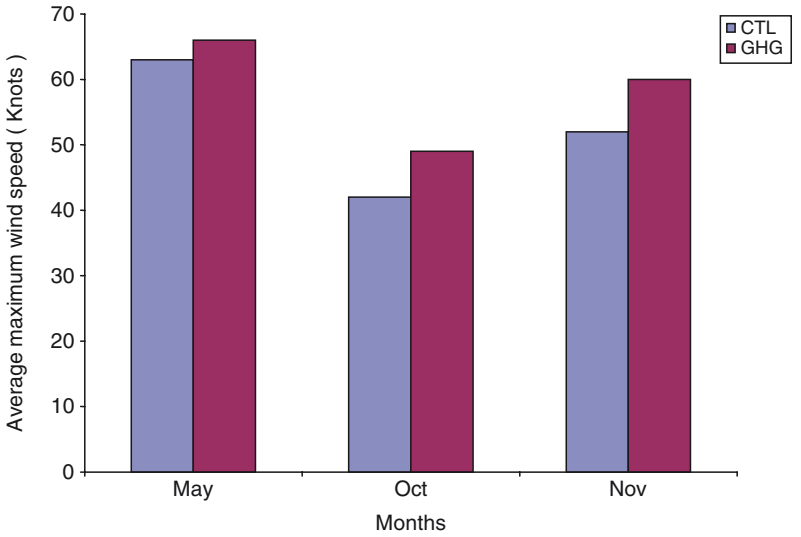

Fig. 2 Simulated intensities (in terms of maximum winds) during May, October, and November. CTL and GHG refer to "control" and "Greenhouse Gas" experiments, respectively

gone up from 42 kts in CTL to 48 knots in GHG and in November it has gone up from 52 knots in CTL to 60 kts in GHG. Thus during both intense cyclone months the intensity has increased and the average cyclone during these months will be a severe cyclone (maximum wind speed more or equal to 48 knots), which is not the case at present during October. Similarly, during May also the average intensity has increased slightly in GHG as compared to CTL. Thus the model has simulated an increase in the average maximum wind speed of cyclones forming during May, October, and November.

References

Mooley DA (1980) Severe cyclonic storms in the Bay of Bengal, 1877–1977. Mon Wea Rev 108:1647–1655

Mooley DA (1981) Increase in the frequency of the severe cyclonic storms of the Bay after 1964 - Possible causes. Mausam 32:35–40

Singh OP (2007) Long-term trends in the frequency of severe cyclones of Bay of Bengal: observations and simulations. Mausam 58:59–66

Singh OP, Khan TMA, Rahman S (2000) Changes in the frequency of tropical cyclones over the North Indian Ocean. Meteorol Atmos Phys 75:11–20

Singh OP, Khan TMA, Rahman S (2001) Has the frequency of intense tropical cyclones increased in the North Indian Ocean? Curr Sci 80:575–580

Srivastav AK, Sinha Ray KC, De US (2000) Trends in the frequency of cyclonic disturbances and their intensification over Indian Seas. Mausam 51:113–118

Part II
Progress on Tropical Cyclogenesis

Generating Synthetic Tropical Cyclone Databases for Input to Modeling of Extreme Winds, Waves, and Storm Surges

T.A. Hardy, L.B. Mason, and J.D. McConochie

Keywords Track and pressure model • *SynCyc*

Introduction

The attack of a severe tropical cyclone at any location is a rare event; therefore, a long data record is necessary in order to determine the characteristics of the population of storms that can affect a location. Unfortunately, reliable and complete data of tropical cyclone tracks and central pressures are not nearly long enough to define the severe end of the distributions. To mitigate this problem of the lack of data in the two Australian tropical cyclone regions a state-of-the-art modeling system has been developed and deployed in three projects, two in the Coral Sea (Hardy et al., 2003, 2004) and one in the Northwestern Australia waters. The Coral Sea studies produced a set of 3,000 years of synthetic tropical cyclones and then simulated the winds, waves, and storm tides. Three climate change scenarios were also modeled. The Northwestern study was much more ambitious, modeling 100,000 years of tropical cyclones to obtain robust measures of the 100–10,000 year return periods of wind and wave conditions. The modeling system required development and/or adaptation of a series of models: (a) synthetic tropical cyclone model, (b) parametric wind field model, (c) wave model, and (d) storm surge and current model. This modeling technique could be applied to any tropical cyclone region to provide input to wind, wave, storm surge, erosion, rainfall, and flood routing models.

T.A.Hardy (✉) and L.B. Mason
Marine Modelling Unit, Australian Maritime College, Launceston, TAS 7250
e-mail: t.hardy@amc.edu.au

J.D. McConochie
Metocean Group, Woodside Energy Ltd., Perth, WA 6000

Y. Charabi (ed.), *Indian Ocean Tropical Cyclones and Climate Change*,
DOI 10.1007/978-90-481-3109-9_9,

Track and Pressure Model, *SynCyc*

The model *SynCyc* (James and Mason, 2005), which generates a time series of parameter values that define the track and strength of a tropical cyclone (i.e. position and central pressure), was used to generate a very large number of synthetic tropical cyclones. This modeling is needed to define (frequency and magnitude) the severe end of the tropical cyclone population which cannot be determined using the very short historical data record. *SynCyc* has undergone continuous development throughout this series of projects.

James and Mason (2005) discuss an empirical approach to the modeling of the time series of positions and pressures of tropical cyclones affecting the Great Barrier Reef Marine Park (GBRMP) and the east coast of Queensland. Their approach is similar to that of Vickery et al. (2000). An important feature of the model is the random interpolation (Scheffner et al., 1996) of the historical initial conditions to provide a large database from which to initiate the simulations. Each tropical cyclone is assumed to be an independent realization of the following autoregressive stochastic process:

$$s^{t+1} = f(s^t, s^{t-1}, ..., s^{t-q}) + \varepsilon^t, \tag{1}$$

where the vector $\boldsymbol{s}$ contains variables describing the change in time of position and central pressure of the cyclone; $f(.)$ is a deterministic function; t is the time step; q is the order of the model; and $\{\varepsilon^t\}$ is a sequence of identically distributed independent random variables. The modeling process involves (a) choosing the elements of $\boldsymbol{s}$; (b) choosing an appropriate form for f; (c) estimating the values of the coefficients in f; and (d) calculating an ensemble of residuals (ε).

The northwestern region has a larger and more refined data set and the population of tropical cyclones exhibits much more complexity as compared to the Coral Sea. Unlike the Coral Sea projects for which one set of relatively simple equations sufficed for generating synthetic tropical cyclones throughout that region, the equations for the northwestern project are more complex and eight regions (see Fig. 1) each with its unique set of coefficients was required.

The governing equations for the changes in time, longitude (λ), latitude (ϕ) of the storm's center, and central pressure deficit (Δp_0) in the implementation of *SynCyc* for the northwestern project are given by:

$$\dot{\lambda}^{t+1} = a_0 + a_1\dot{\lambda}^{t} + a_2\lambda^t + a_3\ddot{\lambda}^{t} + a_4\phi^t + a_5\dot{\phi}^{t} + a_6U_\lambda + a_7U_\phi + \varepsilon_\lambda \tag{2}$$

$$\begin{aligned}\dot{\phi}^{t+1} = {} & b_0 + b_1\dot{\phi}^{t} + b_2\phi^t + b_3\ddot{\phi}^{t} + b_4\dot{\lambda}^{t} + b_5U_\phi + b_6\dot{\phi}^{t}U_\phi \\ & + b_7\dot{\lambda}^{t}U_\lambda + b_8\dot{\lambda}^{t}U_\phi + b_9\Delta p_0^t + \varepsilon_\phi\end{aligned} \tag{3}$$

$$\Delta\dot{p}_0^{t+1} = c_0 + c_1\Delta\dot{p}_0^{t} + c_2\Delta p_0^t + c_3e^{-c_4\left(\Delta p_0^t - \Delta p_{MPI}\right)} + c_5U_\lambda + c_6U_\phi + c_7h + \varepsilon_p \tag{4}$$

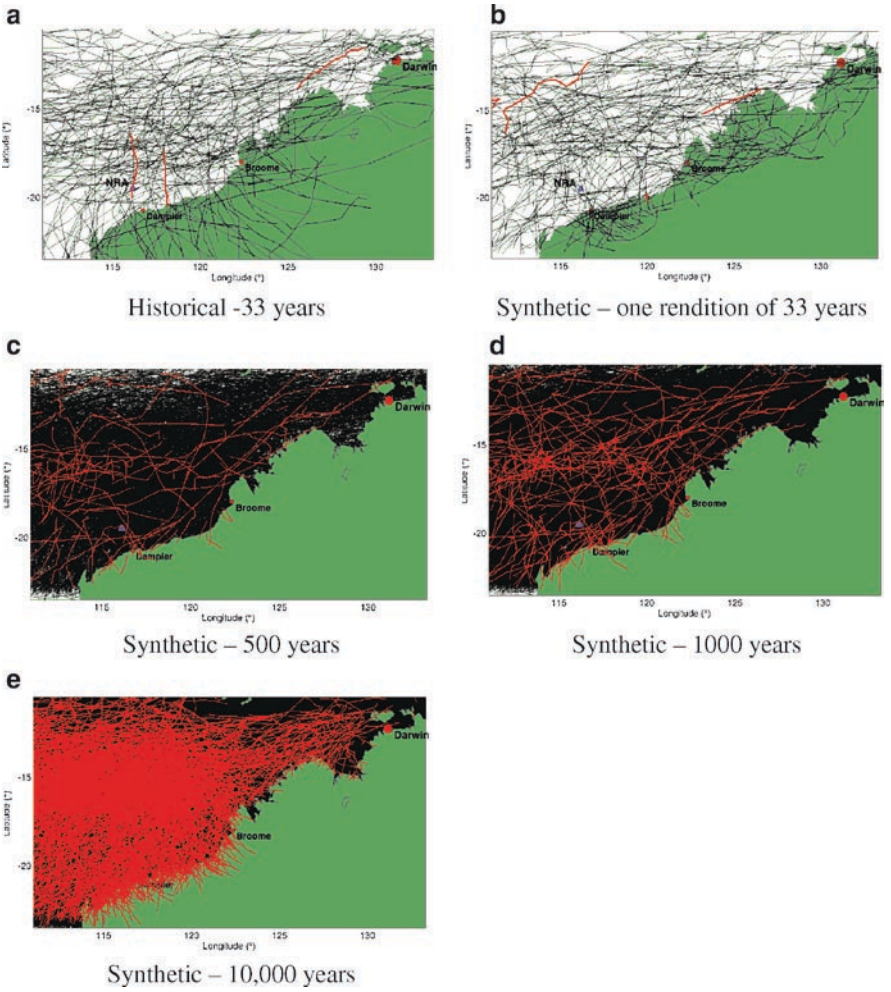

Fig. 1 Tropical cyclone tracks for labeled sets. Portion of the tracks are in red where the central pressure is less than 920 hPa. (**a**) Historical – 33 years. (**b**) Synthetic – one rendition of 33 years. (**c**) Synthetic – 500 years. (**d**) Synthetic – 1,000 years. (**e**) Synthetic – 10,000 years

A single over dot (e.g., $\dot{\phi}$) indicates the change of the variable with respect to time (velocity). A double over dot indicates acceleration. The superscripts indicate the time step. The time and spatial varying zonal and meridional components of the synoptic wind are U_λ and U_ϕ, respectively; h is the local water depth and MPI is the maximum potential intensity, given as a central pressure, that had spatial and seasonal variability. The model coefficient vectors a, b, and c were estimated by minimizing the root mean square error in the multiple linear regression fitting of the deterministic (minus the residual terms: ε_λ, ε_ϕ, and ε_p) model equations to

historical cyclone data. After the best fit was obtained, a large set of residuals (ε_λ, ε_ϕ and ε_p) was created by the difference between the model and the measurements at each time step of the historical storm ensemble.

The first two terms on the right hand side (RHS) Eqs. 5, 6 and 7 indicate a linear relationship between the values of the variables at successive time steps. Thus, the model assumes persistence from one time step to the next in changes in longitude, latitude and central pressure. Tests determined that including higher-order terms (data at $t - 1$ and earlier) was not as effective.

Many possible additional terms were tested, based on experience and judgment. Those that improved the comparison between model and measurements for a variety of measures (see Fig. 1 below) were selected for inclusion. Those that offered little improvement were discarded. Linear terms composed of a coefficient times the values of latitude, longitude, and central pressure deficit, as well as their velocities and accelerations, were considered. Nonlinear terms, multiplying two or more parameters, were also considered and although the physical significance may be less apparent, several were included, such as terms 7, 8, and 9 in Eq. (3). Water depth (h) was found to be useful, perhaps as an indicator of the capability of a storm to lose intensity by mixing up cooler waters in deeper regions, as opposed to its tendency to maintain intensity in the more well-mixed, shallower shelf regions. Not all of the above components are included in each of the three equations and, of those included, not all have a nonzero value of the coefficient in each of the model subregions. For instance water depth was included in only one of the eight subregions in the northwestern project.

Some attempt was made to include physical reasoning with the empiricism. The third term on the RHS of Eq. (3) creates an increasing tendency for changes in latitude to be directed poleward, if the tropical cyclone approaches the equator. The fourth term on the RHS of Eq. (4) creates an increasing tendency for changes in central pressure deficit to be negative as the value of the central pressure deficit approaches theΔp_{MPI}, which is a concept based on thermodynamic principles, and is associated with the physical limitation on tropical cyclone intensity (Emanuel, 1988; Bister and Emanuel, 2003). Equation (4) provides an elastic barrier at these low (more severe) central pressures. This is important because it ensures that storms more intense than the *mean* MPI can occur in the simulations. A latitudinal dependence of the mean MPI in the northwestern project allows for cyclones to lose intensity more rapidly at higher latitudes (where the mean MPI is weaker). Note that it is the spatial variation of MPI that is important, not the spatial mean (which could be subsumed in the coefficient c_2). Maps depicting the geographical variation of computed MPI data have been posted on the web by Bister and Emanuel (2003).

The process of determining the formulation of the equations, the number and size of subregions and values of coefficients was not a single series of steps. Rather it involved a heuristic iterative process that was repeated and refined over many trials. For each combination of equation formulation, subregion definition, and coefficient value set, comparisons were calculated at a number of locations throughout the study area. The accuracy of the model was evaluated and changes in

equation formulation and/or model subregions were considered in an effort to improve model performance.

Without the inclusion of the residual terms (ε_λ, ε_ϕ and ε_p) in Eqs. (2, 3, and 4) the model is deterministic, but at each model time step an important realistic variation was incorporated by randomly selecting with replacement from the set of residuals for each equation. One could think of this random variable as accounting for the unknown influences on tropical cyclone movement and intensity that are not included in the deterministic portion of the model.

The final model configuration (number of subregions and the components to include in each equation) was determined after an exhaustive iterative process comparing model performance to historical data.

Simulation of Synthetic Ensemble

The simulation of each synthetic storm begins with initial values of position (latitude and longitude) and central pressure deficit, as well as the change with respect to time of these three parameters. The seventh initial parameter is the time of year. These seven initial values for each synthetic storm are obtained from the random selection within a seven dimensional "sphere" with a multidimensional "radius" determined from standardized (de-meaned) and normalized (by standard deviation) values of nearest-neighbor "distances" in these seven parameters. For the creation of each synthetic storm an historical storm was randomly selected with replacement and its initial values for these seven parameters defined the "center" of the hyper-sphere. For storms which are crossing the boundary at initialization, the dimension of the hypersphere is reduced to six, as the latitude and longitude of a boundary point are related. After the initialization, at each time step during the simulation the values of latitude and longitude of the storm's center and its central pressure deficit are determined using Eqs. (2), (3) and (4). These synthetic data are the prime inputs into the modeling of the spatial and temporally varying windfield of a tropical cyclone, which then form the force for the wave and storm surge and current models.

For the Coral Sea projects the time series of approximately 10,000 synthetic storms were created representing 3,000 years of data. For the northwestern project, over 450,000 synthetic tropical cyclones were generated representing 100,000 years of record in order to be able to create a robust estimate of the 10,000 year values of waves and winds required in the study. It is important to emphasize that the these projects do not predict the next 3,000 or 100,000 years of storm activity, rather they define the population of tropical cyclones that threaten the study areas under existing conditions.

An example of the *SynCyc* outputs for the Northwestern project is given in Fig. 2, in which tracks are shown for the historical tropical cyclones and several subsets of the synthetic tropical cyclone ensemble. Very severe portions of tracks, defined as central pressures less than 920 hPa, are shown in red. The sparse

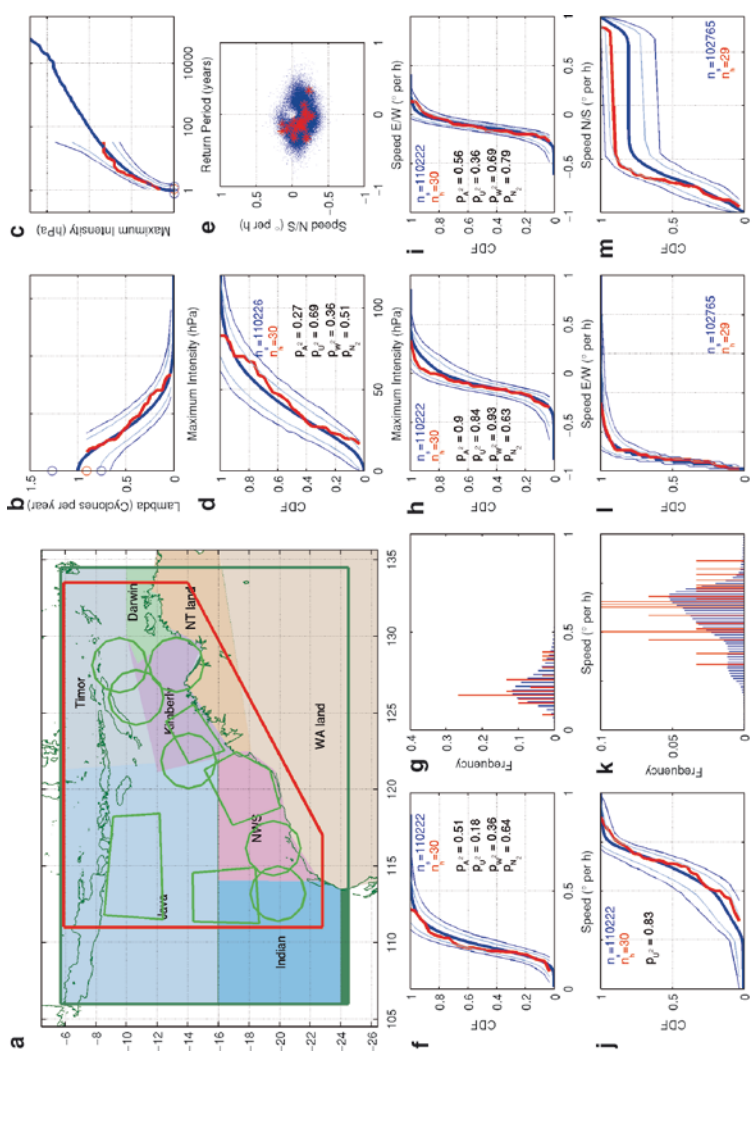

Fig. 2 Example comparison between historical data (red) and model results (blue) collected while the storms were inside a comparison area (one of the green circles or polygons). Multiple such comparison areas are shown. Because of the commercial-in-confidence nature of the project, the results in this figure are from a single unidentified comparison area and the scale of central pressure has been removed from (**b**) and (**c**). Thin blue curves in graphs are 90% confidence bands about individual ordinates. The medium blue curves bound 90% of a set of 5,000 curves, each with the same number of points as the historical set, which were obtained from a bootstrap-like analysis of the synthetic results. Goodness of fit statistics (P value) for W^2 (Cramer-von Mises), A^2 (Anderson-Darling), U^2 (Watson), and N_2 (Neyman) are included on the CDF figures

nature of the data in the historical record is obvious (Fig. 2a). Each subset of 33 years (Fig. 2b) shows variation. The increasing coverage shown in Fig. 2c and d shows it is necessary to have much more than 1,000 years of simulations (Fig. 2d) in order to get good estimates of the spatial variability of intensity and frequency. It is important to realize that the effects of a tropical cyclone are multidimensional and do not solely depend on intensity (i.e., central pressure deficit). For example, severe wave heights are determined by size, location, speed, direction of motion, and straightness of track, as well as by intensity. Although the most commonly cited, central pressure deficit often is not the most important parameter. *SynCyc* provides the synthetic data to define (frequency and intensity) the population of storms and then the windfield, wave, and storm surge models calculate the magnitude of the winds, waves, water levels, and currents so that the magnitude versus frequency curves can be created for each of these storm effects.

An exhaustive set of data comparisons was conducted in the development of model and some of these are included in Fig. 1, in which a CDF for each of the maximum intensity, speed, heading, total time, and mean annual time is included, as well as a plot of frequency of maximum intensity. Multiple statistics and comparisons were calculated for each of the several outlined regions "comparison areas" shown as green circles and polygons on the map in Fig. 1. The data shown in Fig. 1 are for one of these comparison areas. The identity of the area has been suppressed due to the confidential nature of the data. These storms entering a comparison area have a wide variety of initialization locations and many would have traversed through several model subregions, each with its separate set of model coefficients before arriving at the location where the data were collected and analyzed.

It is important to note that the process does not slavishly reproduce the historical data during the relatively short 33 years of accurate data collection, but allows variations that would occur in a longer historical data series of multiple sets of 33 year periods. Thus, multiple renditions of 33 years of synthetic data result in some sets that are very much more severe and some that are very much less severe, but most that are close to the values of the historical data. This is reflected in the spread of the confidence intervals in Fig. 1.

References

Bister M, Emanuel KA (2003) Hurricane climatological potential intensity maps and tables. Program in Atmospheres Oceans and Climate, Massachusetts Institute of Technology. http://wind.mit.edu/~emanuel/pcmin/climo.html

Emanuel KA (1988) The maximum intensity of hurricanes. J Atmos Sci 45:1143–1155

Hardy TA, McConochie JD, Mason LB (2003) Modeling tropical cyclone wave population of the Great Barrier Reef. J Waterway, Port, Coastal and Ocean Eng, ASCE 129:104–113

Hardy TA, Mason LB, Astorquia A, Harper BA (2004) Tropical cyclone-induced water levels and waves: Hervey Bay and Sunshine Coast. Queensland climate change and community vulnerability

to tropical cyclones: Ocean Hazards Assessment Stage 2. http://www.longpaddock.qld.gov.au/ClimateChanges/pub/OceanHazardsMenu.html

James MK, Mason LB (2005) Synthetic tropical cyclone database. J Waterway, Port, Coastal and Ocean Eng, ASCE 131:181–192

Scheffner NW, Borgman LE, Mark DJ (1996) Empirical simulation technique based storm surge frequency analyses. J Waterway, Port, Coastal and Ocean Eng, ASCE 122:93–101

Vickery PJ, Skerlj PF, Twisdale LA (2000) Simulation of hurricane risk in the US using empirical track model. J Struct Eng, ASCE 126:1222–1237

Numerical Simulation of the Genesis of Cyclone Nargis Using a Global Cloud-System Resolving Model, NICAM

Wataru Yanase, Hiroshi Taniguchi, and Masaki Satoh

Keywords Simulation of TC genesis • tropical waves

Introduction

We have been challenging the simulation of tropical cyclone (TC) geneses using a global/regional cloud-system resolving model (GCSRM), non-hydrostatic ICosahedral-grid atmospheric model (NICAM) (Satoh et al. 2008). A GCSRM has the advantages that it can deal with the organization of meso-scale cloud systems into a tropical cyclone during the cyclogenesis process, and that it can cover the long-distance movement of TC sources such as tropical waves. Using a GCSRM, our goal is to reveal the relation between predictabilities and mechanisms of TC geneses. In the previous studies, two important perspectives have been suggested related to TC geneses: environments and sources. The large-scale environments explain probability distribution of TC geneses including climatological seasonal change, interannual variability like ENSO, and intraseasonal oscillation such as Madden-Julian Oscillation. On the other hand, the precise timings of TC geneses seem to be triggered by synoptic-scale sources such as tropical waves, extratropical disturbances, and energy dispersions from neighboring TCs. Recently we have demonstrated that the 14-km-grid GCSRM can predict the timing of Typhoon 21st in 2006 with the lead time of more than 3 days, which was controlled by the westward propagating wave over the North Pacific. In 2008, Cyclone Nargis caused terrible disaster in Myanmar; we examined the predictability of Nargis genesis using the NICAM model.

W. Yanase (✉) and M. Satoh
Center for Climate System Research, The University of Tokyo, Japan
e-mail: yanase@ccsr.u-tokyo.ac.jp

H. Taniguchi and M. Satoh
Frontier Research Center for Global Change, Japan Agency for Marine-Earth Science and Tech, Japan

Y. Charabi (ed.), *Indian Ocean Tropical Cyclones and Climate Change*,
DOI 10.1007/978-90-481-3109-9_10,

Methodology

We used the NICAM (Non-hydrostatic ICosahedral-grid Atmospheric Model) with and without the stretched grid system. In the stretched grid system, the grids were concentrated on the Bay of Bengal with the center point at (90°E, 5°N), which saves the computational costs, and therefore, makes it possible to perform a number of simulations. We adopted the stretched grid system in the simulations, because we did not find any distinct sources that moved long-distance during the simulation period. Just to be safe, we validated the stretched grid simulation by comparing with quasi-uniform grid simulations for a few cases. The finest grid intervals were 14 or 7 km to marginally resolve the organization of meso-scale cloud systems. We used a cloud microphysics scheme, NSW6, with six water categories (water vapor, cloud, rain, cloud ice, snow, and graupel) and no cumulus parameterization schemes.

For the initial condition, we used two global atmospheric datasets. One is the analysis data used for the operational forecast of Japan Meteorological Agency (JMA), and the other is final analysis data of National Center for Environmental Prediction (NCEP). Since we are interested in the genesis of Nargis, which occurred at 12 UTC on 27 April in 2008 according to the best-track data, the initial times earlier than this time were used for the simulations. The sea-surface temperature (SST) was prescribed using the NOAA's weekly OISST dataset with temporal and spatial interpolations.

Simulation Results

First, we will show the results of simulations using different grid systems and datasets with the initial time at 12 UTC on 25 April, 2 days before the genesis. Figure 1 shows the daily locations of simulated cyclones (circles) and the sea-level pressures (SLP) at 12 UTC on 2 May. Figure 1a shows the actually observed track and SLP. The Nargis was generated over the western Bay of Bengal, moved eastward, and made a landfall on Myanmar on 2 May. Figure 1b shows the result of the simulation using a stretched 14-km grid system and initial dataset of NCEP. The model simulated the cyclogenesis over the western Bay of Bengal. However, the northward movement in the simulation was different from the observed track. On the other hand, Fig. 1e shows the result of the simulation also using a stretched 14-km grid system but initial dataset of JMA. The model simulated the cyclogenesis over the eastern Bay of Bengal, which is different from the observation, although it reproduced the landfall of a cyclone on Myanmar. Thus, the model failed to simulate the actual track of Nargis. In order to confirm the stretched grid system worked appropriately, we performed a simulation using a quasi-uniform 14-km grid system and initial dataset of JMA (Fig. 1d). By comparing Figs. 1d and e, it seems that the stretched grid system could qualitatively produce the same genesis location and the

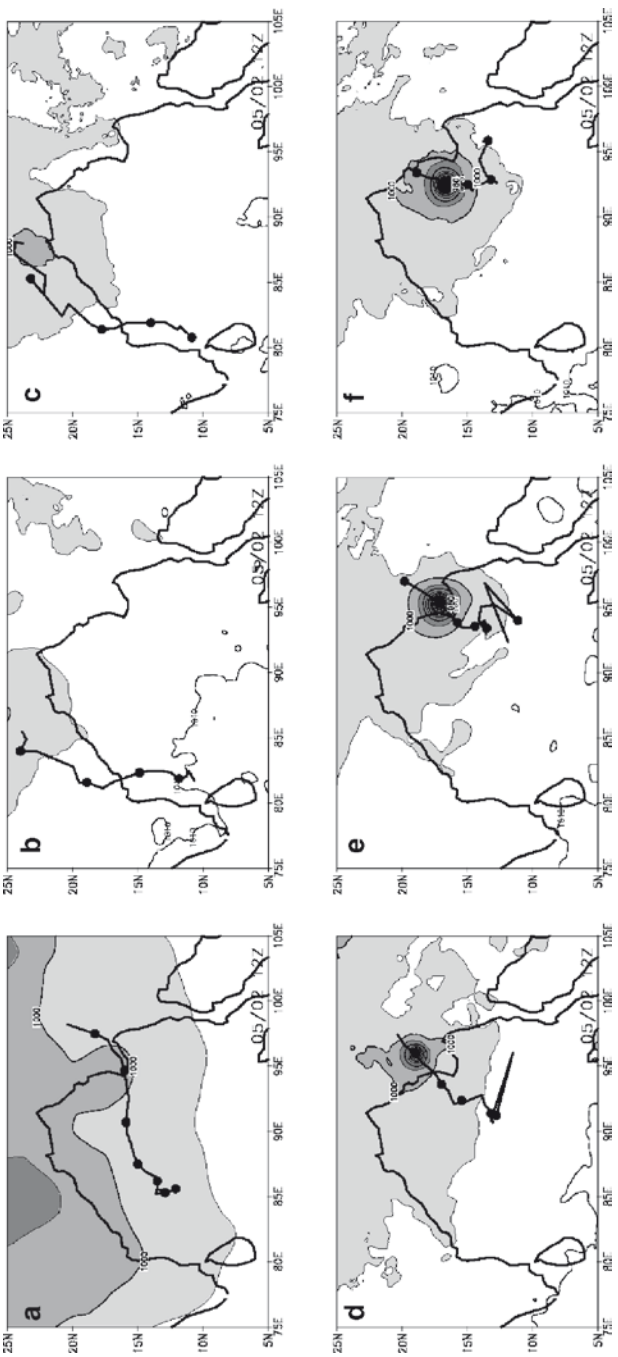

Fig. 1 SLPs (shade) at 12 UTC 2 May and tracks of Cyclone Nargis (black curves) in observation and simulation started at 12 UTC 25 April. (**a**) Observation (best track of the University of Hawaii and SLP of JCDAS reanalysis data); (**b**) stretched 14-km grid with NCEP initial data; (**c**) stretched 7-km grid with NCEP data; (**d**) quasi-uniform 14-km grid with JMA data; (**e**) stretched 14-km grid with JMA data; and (**f**) stretched 7-km grid with JMA data. The contour interval of SLP is 5 hPa, and dark, medium, and light gray shades indicate SLP less than 995, 1,000, and 1,005 hPa, respectively

subsequent track as the quasi-uniform grid system did, although there is a little quantitative difference. We also performed simulations using stretched 7-km grid systems for both NCEP and JMA datasets (Figs. 1c and f). The results suggest that the qualitative characteristics of cyclogenesis locations and tracks are almost the same as in the corresponding simulations using a stretched 14-km grid system. Thus, the result of the simulation depends more on the initial datasets (NCEP or JMA) than on the grid systems. Therefore, we performed the other simulations using a stretched 14-km grid system to save computational costs.

We examined different initial times using NCEP and JMA dataset (not shown). The simulated tracks varied depending on the initial times and datasets. Only a few cases simulated the track similar to the actually observed. However, all the simulations with the initial times of 12 UTC 24th, 00 UTC 25th, 12 UTC 25th, 00 UTC 26th, 12 UTC 26th, and 00 UTC 27th showed cyclogeneses over the Bay of Bengal. This might mean that the model simulated the high probability of cyclogenesis around the actually observed time, late April. To confirm this, we have examined the probability of cyclogeneses during the other periods. Figure 2 shows whether 8-day simulations with initial times every 2 days between 2 April and 20 May (the lines on the left) produced cyclones over the Bay of Bengal (large circles on each line). Apparently, the simulated probability was higher around late April than in the other period, although a few simulations with initial times after the actual cyclogenesis include the circulation of Nargis in the initial condition, which should be

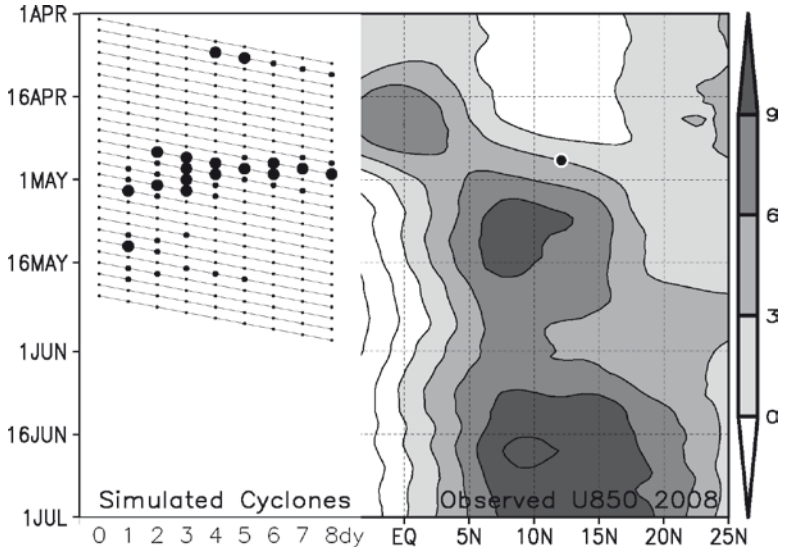

Fig. 2 Simulated probability of cyclone formations (*left*: circles) and observed timing and zonal wind at 850 hPa averaged between 80°E and 100°E (*right*: a circle and shade, respectively). The vertical axis indicates time. On the left, the lines show the 8-day simulations using the initial times every 2 days from 2 April to 20 May 2008, and the large (small) circles indicate that the model simulated some low-pressure systems less than 990 hPa (1,000 hPa) over the Bay of Bengal

ignored in the discussion. Therefore, we can conclude that the model was able to capture the higher probability of the cyclogenesis in late April than during the other period. Here, a new question might be raised: What factor determined the simulated high probability of cyclogenesis? The shade on the right side in Fig. 2 shows the latitude-time diagram of zonal wind at 850 hPa averaged over 80°E and 100°E. Around the period of cyclogenesis, a large-scale westerly wind maximum shifted from the equator to ~10°N. This might suggest that the large-scale environment was related to the high probability of cyclogenesis. In the next section, we will discuss the characteristics of observed large-scale environments.

Discussion

Here, we analyze the observed large-scale field which seems to be related to the simulated probability of the cyclogenesis. The preferable condition for the cyclogenesis has been suggested in the previous studies (Camargo et al. 2007) to interpret the active cyclogenesis regions and periods. Figure 3 shows the genesis potential which considers the four factors favorable for the cyclogenesis: large absolute vorticity at 850 hPa, weak vertical shear, large potential intensity, and large relative humidity at 600 hPa. The potential intensity is a kind of latent instability which considers atmospheric temperature, moisture, and SST (Bister and Emanuel 2002). In order to remove the short-time influence of Nargis itself on the environments, we applied a running mean of 15 days to the dataset. In early April, the peaks of large genesis potential occurred around 5°–10° latitudes both in the northern and the southern hemispheres. In late April, the maximum in the northern hemisphere started to move northward, while the maximum in the southern hemisphere disappeared. Nargis was generated during this northward shift of large genesis potential. After mid-May, the genesis potential over the Bay of Bengal is reduced, associated with the seasonal change. Although Nargis itself could still influence part of the large-scale field, the northward shift of the maximum genesis potential apparently occurred with longer time scale than the lifetime of Nargis. Figures 3c–e show the individual factors related to the genesis potential. All of the four factors were preferable to the cyclogenesis in late April in 2008. This result is consistent with previous studies in that the genesis potential and cyclogenesis are larger in spring and autumn than in winter and summer over the North Indian Ocean. In other words, the cyclogenesis over the Bay of Bengal is large during the transient periods between summer and winter monsoons. Therefore, it is expected that the monsoon onset controls the timing of cyclogenesis.

Figure 4 is a preliminary result which shows the relation between the timing of westerly wind onset and the timing of the first cyclogenesis between April and June from 1975 and 2008. Here, the westerly wind onset was defined as the time when the zonal wind field averaged over the Bay of Bengal exceeded 2 m/s. In order to remove the transient influence of cyclones themselves, additional criterion that the zonal wind more than 4 m/s is sustained 15 days after the onset. The westerly onsets

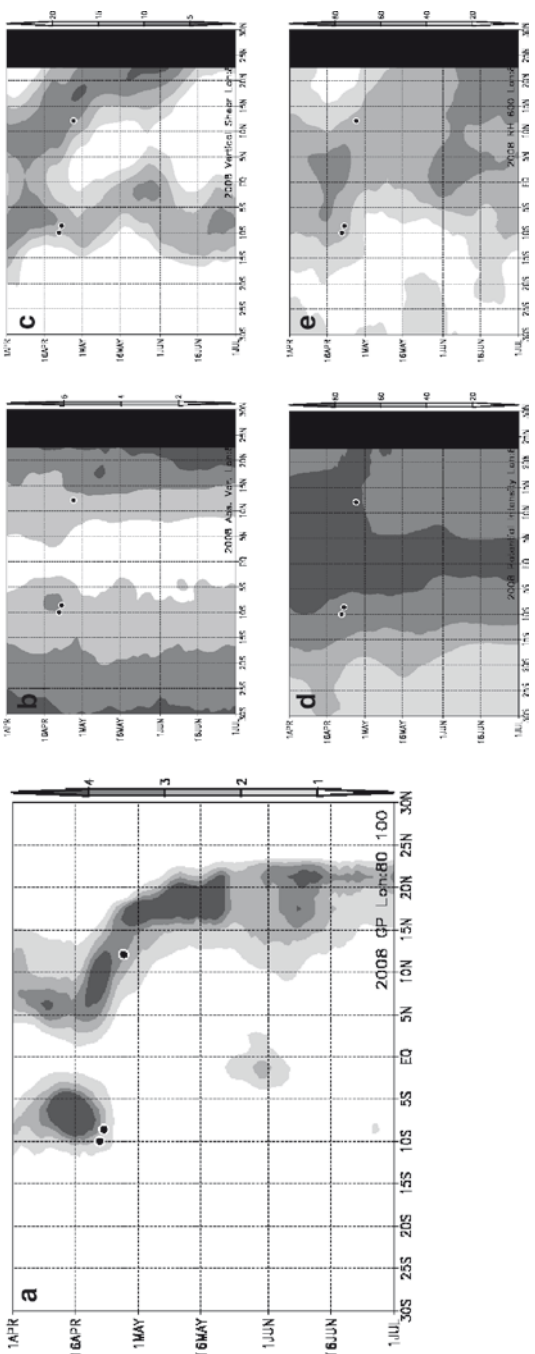

Fig. 3 Longitude-time diagram of the environmental factors related to cyclogenesis (dark shade indicates preferable condition for cyclogeneses) averaged between 80°E and 100°E. (**a**) genesis potential calculated using the following four factors; (**b**) absolute vorticity at 850 hPa; (**c**) vertical shear of the horizontal wind between 850 and 200 hPa; (**d**) potential intensity calculated using SST and vertical profile of temperature and moisture; and (**e**) relative humidity at 600 hPa. Circles indicate the location and time of observed cyclogenesis

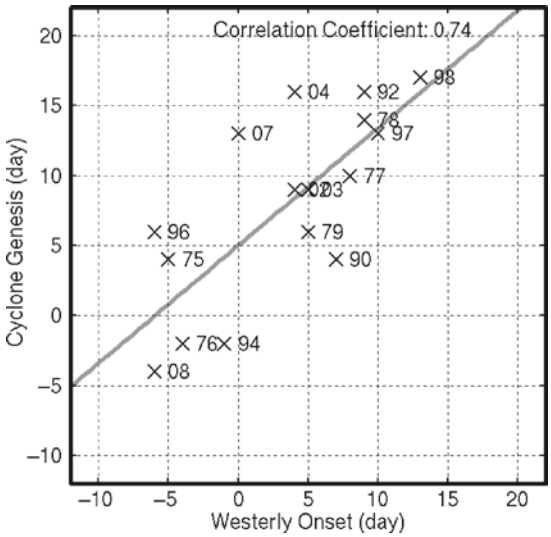

Fig. 4 Relation between the timings of westerly onset and the cyclogeneses over the Bay of Bengal. The time of westerly onset (abscissa) is defined as the time when the zonal wind field averaged over the Bay of Bengal (80°E–100°E, 5°N–15°N) first exceeded 2 m/s. In order to remove the transient influence of cyclones themselves, additional criterion that the zonal wind more than 4 m/s was sustained 15 days after the onset was used. The NCEP reanalysis data was used for the zonal wind field. The time of cyclogenesis (ordinate) is the time when the best-track data (University of Hawaii) first identified tropical cyclones between April and June in each year. Digits near the marks (X) indicate the year. During the analyzed period between 1975 and 2008, the following years (9/34) had no cyclones over the Bay of Bengal: 1981, 1983, 1984, 1986, 1988, 1993, 1995, 2001, and 2005. The regression line is $y = 0.84x + 5.02$ with the correlation coefficient of 0.74

and cyclogeneses show a good correlation. In 2008, for example, both the genesis of Nargis and westerly onset occurred earlier than the average. Since this is only a speculation, we should examine other indices for the monsoon onset that are typically used in the previous studies and are less affected by the cyclones themselves. We should also focus on the intraseasonal monsoon dynamics because it could be related to both the cyclogeneses (Murakami et al. 1984) and monsoon onsets (Webster et al. 1998).

Summary

We have examined the probability of the genesis of Cyclone Nargis using the global/regional cloud-system resolving model, NICAM, with the horizontal grid intervals of 14 and 7 km. Although the time and location of the cyclogenesis were not simulated precisely in most cases, the model simulated higher probability of

cyclogenesis around the period of actually observed cyclogenesis. The simulated high probability seems to be attributed to the high genesis potential around the monsoon onset period. This result shows that the probability of cyclogenesis around the monsoon onset might be predictable, if the model can forecast the timing of monsoon onset. The timing and location of cyclogenesis seems to be predictable only when the source of cyclogenesis is strong in the initial condition. Although a vortex moving northward over the Bay of Bengal seems to be related to the genesis of Nargis in the observation, it was not able to control the location and timing of cyclogenesis in our simulation.

Acknowledgment The present study was supported by Core Research for Evolutional Science and Technology, Japan Science and Technology Agency (CREST, JST) and by KAKENHI 20740266. The simulation discussed in this study was performed on the National Institute for Environmental Studies (NIES) supercomputer system (NEC SX-8R/128M16), and on the Earth Simulator at the Japan Agency for Marine-Earth Science and Technology. The potential intensity was calculated using the FORTRAN program on the website of Dr. Kerry Emanuel. The best-track data were obtained from the University of Hawaii. The analysis data used here are JMA GPV, JCDAS reanalysis, and NCEP final analysis.

References

Bister M, Emanuel KA (2002) Low frequency variability of tropical cyclone potential intensity. 1. Interannual to interdecadal variability. J Geophys Res 107, doi:10.1029/2001JD000776

Camargo SJ, Emanuel KA, Sobel AH (2007) Use of a genesis potential index to diagnose ENSO Effects on tropical cyclone genesis. J Clim 20:4819–4834

Murakami T, Nakazawa T, He J (1984) On the 40–50 day oscillations during the 1979 northern hemisphere summer. Part I: phase propagation. J Meteorol Soc Jpn 62:440–468

Satoh M, Matsuno T, Tomita H, Nasuno T, Iga S (2008) Nonhydrostatic icosahedral atmospheric model (NICAM) for global cloud resolving simulations. J Comp Phys 227:3486–3514. doi:10.1016/j.jcp. 2007.02.006

Webster PJ, Magana VO, Palmer TN, Shukla J, Tomas RA, Yanai M, Yasunari T (1998) Monsoons: processes, predictability, and the prospects for prediction. J Geophys Res 103: 14451–14510

Simulation of the North Indian Ocean Tropical Cyclones Using the Regional Environment Simulator: Application to Cyclone Nargis in 2008

Mohammed Haggag, Takao Yamashita, Kyeong Ok Kim, and Han Soo Lee

Keywords Storm surge simulation • Wind stress forcing

Introduction

Countries facing the North Indian Ocean (NIO) are threatened by the storm surges associated with tropical cyclonic storms. Several studies have been performed for the storm surge simulation in the NIO. Examples of studies confined to the Bay of Bengal are those performed by Das (1972), John and Ali (1980), and of studies confined to the Arabian Sea Dube et al. (2004) developed a location-specific vertically integrated shallow water model that covers the northern part of the Bay of Bengal with a horizontal grid resolution of 3 km to study the storm surge of cyclones in 1974, 1985, 1988, 1989, 1991, 1994, and 1999. Dube et al. (2004) used an idealized wind stress forcing that had been computed by the empirical formula given by Jelesnianski (1972). Developed a location-specific storm surge model for the coastal regions of Myanmar to carry out simulations for the 1975-Pathein, 1982-Gwa, 1992-Sandoway, and 1994-Sittewe cyclones. The model had horizontal grid resolution of 9 km and the idealized wind stress forcing computed by the wind model. Kim et al. (2008) developed a wind-wave-surge coupled process-based

M. Haggag (✉), T. Yamashita, and H. Soo Lee
Department of Development Technology, IDEC, Hiroshima University,
1-5-1Kagamiyama, Higashi Hiroshima, 739-8529, Japan

M. Haggag
Irrigation and Hydraulics Department, Faculty of Engineering, Cairo University,
P.O. Box 12211, Giza, 12613, Egypt
e-mail: haggag-moh@hiroshima-u.ac.jp

K.O. Kim
Department of Civil and Environmental Engineering, Sungkyunkwan University,
Chunchun-dong 300, Jangan-gu, Suwon, 440-746, Republic of Korea

Y. Charabi (ed.), *Indian Ocean Tropical Cyclones and Climate Change*,
DOI 10.1007/978-90-481-3109-9_11, © Springer Science+Business Media B.V. 2010

model for simulating the storm surge. The model consists of a meso-scale atmospheric model, a third-generation wave model and an ocean circulation model. Kim et al. (2008) introduced an additional sea-surface shear stress by wave dissipation into the current model considering energy transfer from winds to currents through whitecapping breaking.

This article describes the application of the coupled process-based cyclone surge simulation model (Kim et al., 2008) to the simulation of cyclone Nargis in the Bay of Bengal. The cyclone surge model is a part of the Regional Environment Simulator (RES) defined as a dynamically coupled atmosphere-ocean-land model (Haggag et al., 2008). Compared to earlier storm surges modeling activates in the NIO, RES provides a concurrent interaction between atmosphere-wave-current system, a realistic meteorological forcing that drives wave and current models rather than using empirical idealized forcing and potential of having high horizontal-grid resolution that enables accurate representation of the coastlines and enables representation of most of the islands, rivers, and the irregular coastal terrain.

Climatic Factors Affecting the Tropical Storms in the NIO

In the NIO, the frequency of tropical cyclones is much higher over the Bay of Bengal when compared with the Arabian Sea. Highest frequency is seen during pre-southwest monsoon season (March–May) and post-southwest monsoon (September-November) seasons. Murty and Neralla (1992) showed that severe cyclonic events over the Bay of Bengal do not occur during the monsoon regimes when the wind shear is very high thereby preventing cyclones from acquiring its highly organized vertical structure. Figure 1 shows the percentage probability of

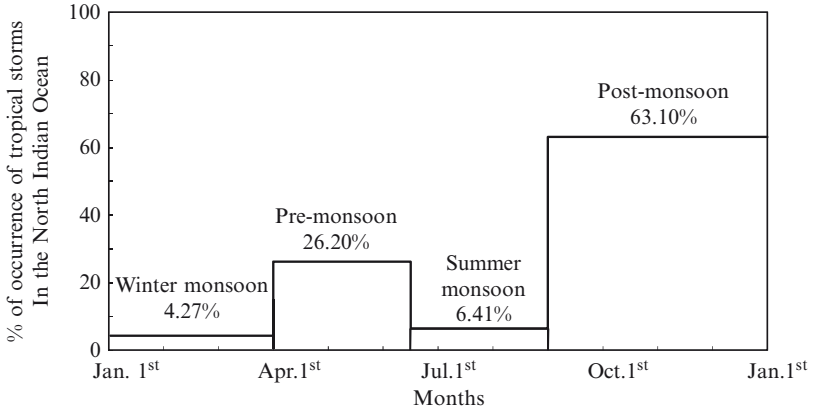

Fig. 1 Probability of occurrence of tropical storms in the North Indian Ocean

occurrence of tropical storms in the NIO. Ninety percent of the tropical storms occurred before and after the monsoon time while a limited number of storms coincide with the monsoon. The source of data in Fig. 1 is Joint Typhoon Warning Data Center (JTWC 2008) including a total of 187 tropical storms from 1975 to 2008. The destruction due to storm surge's flooding is a serious concern along the coastal regions of India, Bangladesh, and Myanmar. In particular, the low lying deltaic regions of Bangladesh and Myanmar are most vulnerable to storm surges. Historical records of tropical cyclones in the NIO show that millions of people died and property worth billions of dollars was destroyed in the NIO countries. Among the 20 deadliest cyclones in world history (not shown), 14 of these have occurred in the NIO and resulted in a death toll exceeding 2.3 million persons. The emerging consensus among climate scientists is that the trend toward stronger and more destructive storms appears to be linked to global warming, and specifically to the impact of global warming on higher ocean temperatures, which drives convection energy and moisture into these storms and makes them more powerful. In the Bay of Bengal, even with the present sea-level and weather conditions, the area is prone to some of the most disastrous coastal flooding in the world caused by storm surges associated with tropical cyclones.

The historical records of the tropical storms in the NIO in the period from 1945 to 2008 show a total number of 638 storms (JTWC 2008). It is easily distinguished that there are two patterns for the frequency of occurrence of the tropical storms in the NIO. The first pattern with frequent tropical storms lasted from 1945 to 1976 with a total number of 476 storms and the second pattern with less frequent storms lasted from 1977 to the present. The existence of those two different extremes suggested a link with a global climatic phenomenon. The Pacific Decadal Oscillation (PDO) is a pattern of climatic variability in the Pacific Ocean that shifts phases on at least inter-decadal time scale, usually about 20–30 years. The PDO is detected as warm or cool surface waters in the Pacific Ocean. During a warm phase (positive phase), the west Pacific becomes cool (warm) and part of the eastern ocean warms (cool) or negative phase, the opposite pattern occurs (Fig. 2). Figure 3 shows the number of annual

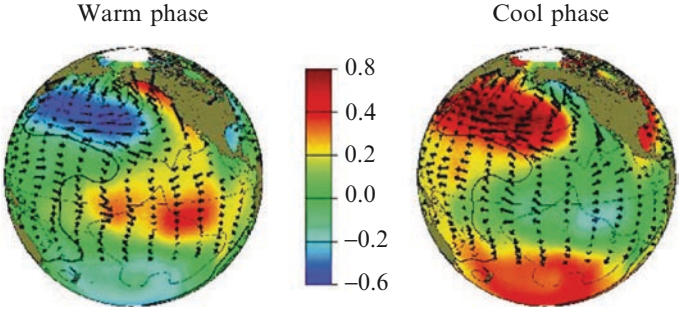

Fig. 2 Typical wintertime sea-surface temperature (*shaded*), sea-level pressure (*contours*), and surface wind stress (*arrows*) anomaly patterns during warm and cool phases of PDO (http://jisao.washington.edu/pdo/)

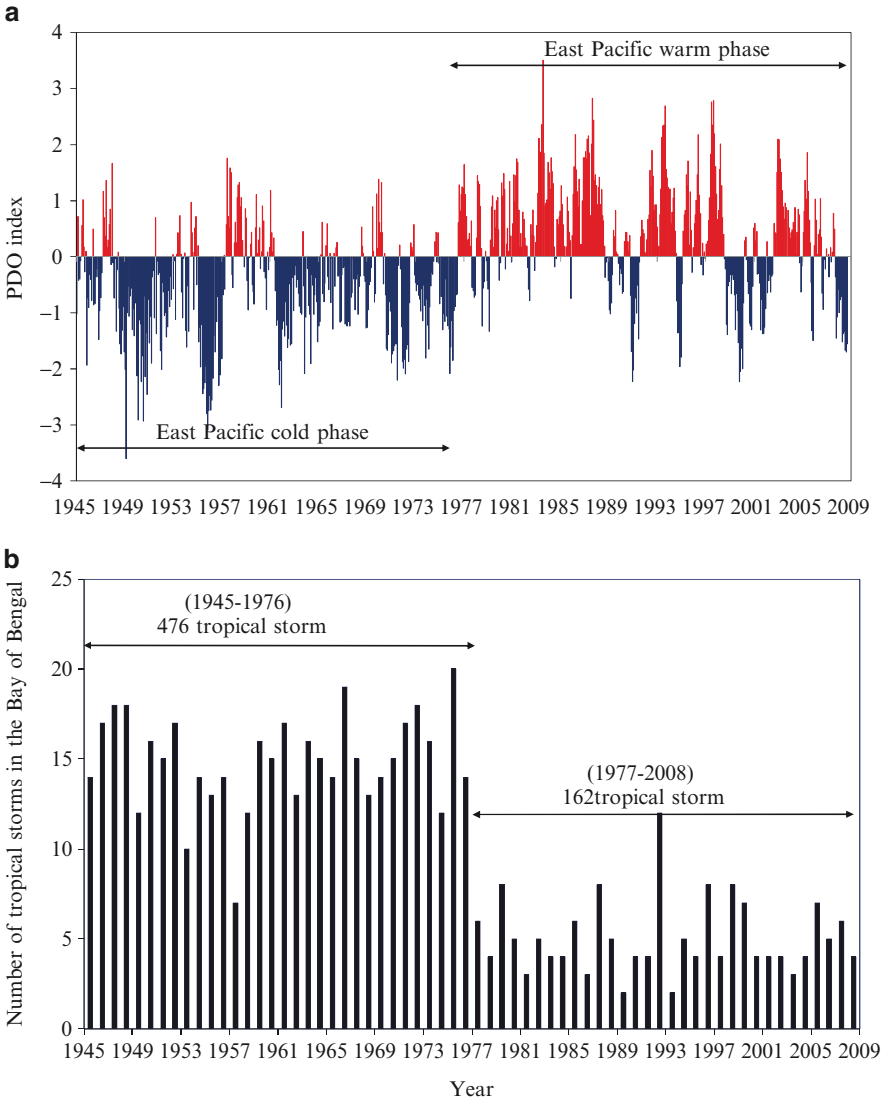

Fig. 3 (**a**) Monthly values for the Pacific Decadal Oscillation (PDO) index (1945 September 2008) and (**b**) the annual number of tropical storms in the NIO

tropical storms which occurred in the NIO (mostly in the Bay of Bengal) from 1945 to 2008 and the PDO in the corresponding time period. The abrupt shift from cold to warm PDO in 1976 coincided with a period of decreased number of tropical storms in the NIO. The Indian Ocean follows a pattern similar to the west Pacific which cools when the eastern Pacific warms in the warm phase and warms when the eastern Pacific cools in the cool phase. The total number of tropical storms in

the NIO during the cold phase (1945–1976) was 476 storms while the total number of storms during the warm phase (1977–2008) was 162 storms. A possible reason for the strong correlation between the western Pacific Ocean and the NIO could the Indonesian throughflow. The Indonesian throughflow that transports water between the Pacific Ocean and the Indian Ocean through the Indonesian archipelago transports large amounts of relatively warm water to the Indian Ocean. The PDO cyclic trend shown in Fig. 3 reveals that nowadays we are in the beginning of a new cool phase in the eastern Pacific which implies a warm phase in the other side of the Pacific and the Indian Ocean. In the next 30 years (2007–2037), all countries in East and south Asia will be threatened by severe climatological conditions along with frequent occurrence of tropical cyclones and its associated storm surge hazards.

RES's Cyclone Surge Simulation System

The models used in the cyclone surge simulation system are the meso-scale atmospheric model (MM5, Grell et al., 1996), the third-generation ocean wave model (WW3, Tolman, 2002), and the Princeton ocean model (POM). Figure 4 shows a schematic of the models used in the cyclone surge simulation with the different interactions among the models. The coupler is developed to exchange data among the different models within the parallel computing system. The flux coupler and models start at the same time; each model calculates its own variables and transfers data to the coupler at designated time intervals.

The coupler task is to continuously transfer data, such as atmospheric forcing and breaking stress, to the other models that need such data as forcing or boundary terms. The Multiple Program Multiple Data (MPMD) methodology using MPI libraries is applied to couple the models. The momentum flux transfer process between wind and ocean surface through waves takes three forms of energy transfer; (1) wind to waves, (2) wind to mean current, and (3) wave to mean current via wave breaking. For fully developed wind waves, wave breaking adjusts the energy balance between wind input and wave motion resulting in the generation of mean current. In the saturated state of wave fields, the rate of wind energy input may be equivalent to the whitecapping wave energy dissipation rate. It means that the energy from wind changes to mean current and turbulence through whitecapping wave breaking. The total shear stress to mean flow $\left(TS_{stress}\right)$ is the summation of the effective wave-breaking stress $\left(EWB_{stress}\right)$ by whitecapping and the direct shear stress $\left(DS_{stress}\right)$ by wind; the relation can be expressed as follows:

$$TS_{stress} = EWB_{stress} + DS_{stress} \tag{1}$$

Kim et al. (2008) stated that the total shear stress to mean flow is equivalent to the total wind stress $\left(TWD_{stress}\right)$ expressed as:

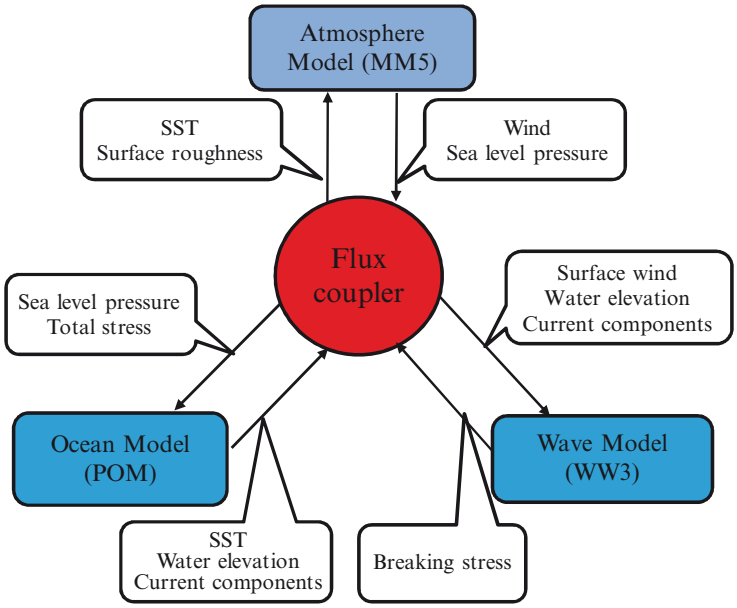

Fig. 4 Interactions in the cyclone surge simulation system

$$TWD_{stress} = \rho_a u_*^2 = \rho_a C_D \,|U_{10}|\, U_{10} \tag{2}$$

$$C_D = \left(0.63 + 0.066\,|U_{10}|\right) \times 10^{-3} \tag{3}$$

Where ρ_a is the air density, u_* is the friction velocity, C_D is the drag coefficient, and U_{10} is the 10 m horizontal wind component. The DS_{stress} can be assumed as a percentage of the TWD_{stress} as follows:

$$DS_{stress} = \upsilon\, TWD_{stress} \tag{4}$$

An additional shear stress component that works on mean current generation comes from wave-breaking dissipation by whitecapping. A part of wave dissipation stress changes into mean current. Kim et al. (2008) defined an effective wave dissipation stress factor (δ) that is being transferred to mean current as follows:

$$EWB_{stress} = \delta\, WB_{stress} \tag{5}$$

where WB_{stress} is the shear stress caused by the surface roller of a whitecapping breaker.

The effective wave dissipation stress factor represents the portion of the wave energy dissipation by whitecapping that is transferred to the mean current generation. In this coupled model, the total stress caused by wind is computed assuming

calm sea ($\upsilon = 1$), the additional effective wave dissipation contribution is computed using $\delta = 0.1$ (Kim and Yamashita, 2004, 2005). δ is determined based on a series of idealized numerical experiments performed with the coupled model assuming idealized winds and water depth.

The existence of variable mean current and water surface level affects the wave propagation through affecting the wave celerity and the total water depth. Wave celerity and water depth has a direct effect on several wave characteristic and processes (refraction, diffraction, and shoaling). Horizontal depth-averaged current components and surface water elevation are calculated in the ocean circulation model; they are sent to the wave model each time step through the flux coupler. Typically, the stand-alone wave models assume constant horizontal current components and constant surface elevation. In this coupling, the wave model uses the received current and elevation fields and recomputes the refraction terms each time step.

Storm Surge Computations

The storm surge computation is forced by the cyclone meteorological fields computed using the MM5 model. The MM5 modeling in this study includes totally three domains. Figure 5 shows the bathymetry of the finest domain used in the storm surge computations. The cyclone is simulated from 00 UTC 29 April to 00 UTC 4 May in 2008. Figure 6 shows the pressure and the wind vector fields of the cyclone over the Irrawaddy delta just after landfall in May 2, 2008. The minimum CSLP of the Nargis just after landfall is found to be 966 hPa, and the maximum

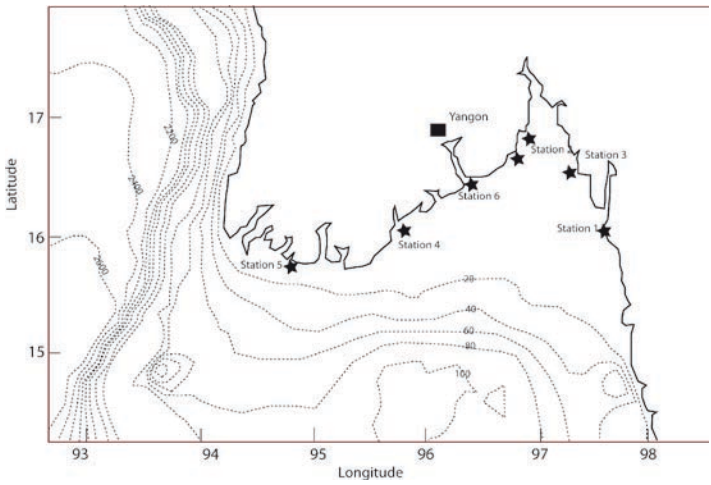

Fig. 5 Storm surge computational domain with locations at which computed water levels were extracted

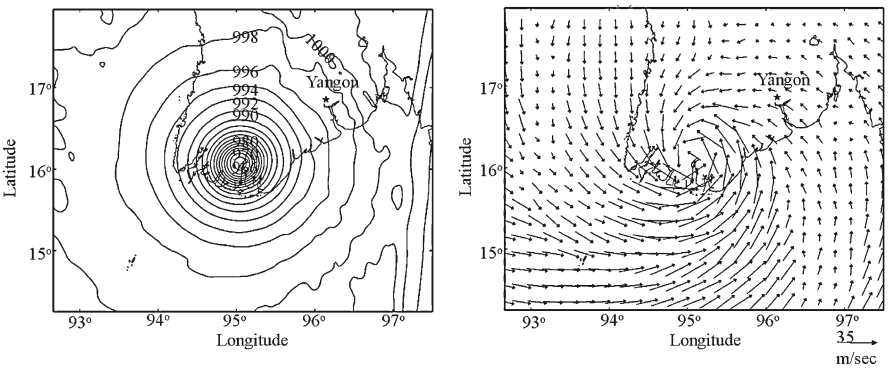

Fig. 6 The computed sea-level pressure and wind magnitude distribution at the landfall of cyclone Nargis

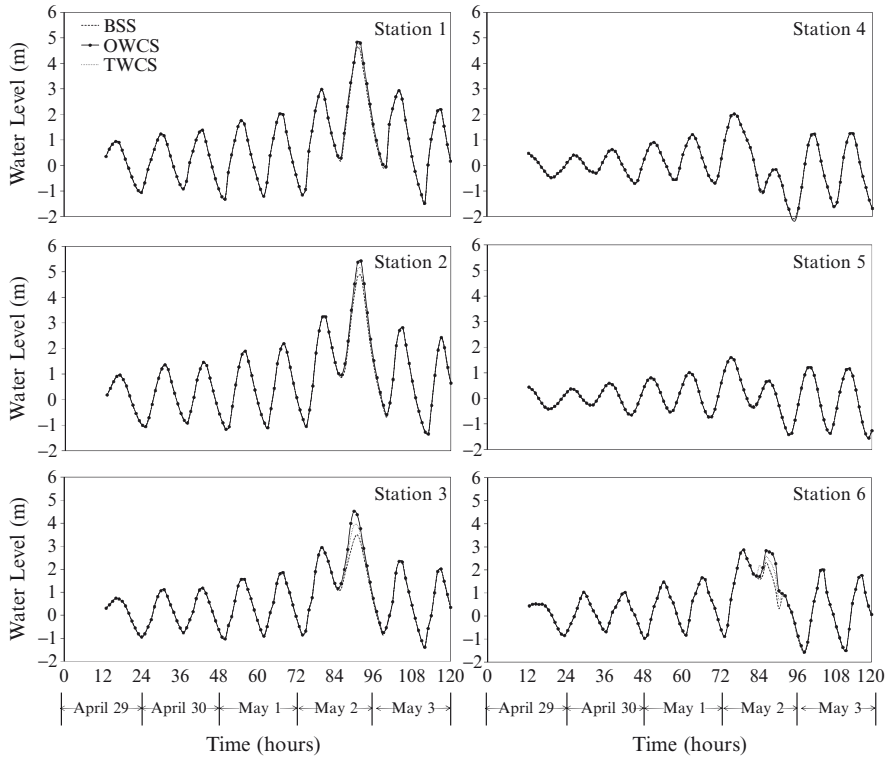

Fig. 7 Computed water levels at several stations along the Irrawaddy delta from April 29 to May 4 in 2008 using different sea-surface stress computations. Bulk Stress Scenario (BSS), One-Way Coupling Scenario (OWCS) and Two-Way Coupling Scenario (TWCS)

wind speed is found to be 35 m/s. Unfortunately observations are neither available for water levels nor for significant wave heights in the area, this limits our ability to enhance and verify the performance of the storm surge model. Three different scenarios for the sea-surface stresses are considered: the first scenario is called bulk stress scenario (BSS) with stress comes from the bulk method in the stand-alone POM model. The second stress scenario is called one-way coupled scenario (OWCS) that considers wave-breaking stress without current effects to wave. The third scenario is called two-way coupled scenario (TWCS) that fully considers wave–current interactions.

Figure 7 shows the computed water levels at several stations from April 29 to May 4 in 2008 using the previously described stress scenarios (BSS, OWCS and TWCS). The stations located in the shallow water of the Bay of Martaban (station 1, 2, 3) show higher water levels compared to points located in the outer delta (station 4 and 5). Maximum computed water level found at station 2 with a computed value of 5.5 m (18 ft) at the mid-day of May 2 in 2008, which is close to the reported figure by several media and newspapers after the cyclone disaster in Myanmar. Figure 7 shows the effect of the additional wave-breaking stress on storm surge. However, this effect is small but it cannot be neglected. This effect can be seen at locations with surge levels exceeding 3 m (station 1, 2, 3 and 6) and cannot be seen at locations with small surge levels (station 4 and 5). The water levels computed from the OWCS are higher than those computed from the TWCS or from the BSS. This emphasizes that the additional wave-breaking stress is acting on intensifying the surge by adjusting the energy balance between wind input and wave motion. The effect of wave–current interaction is not significant compared to the wave–surge interactions. Figure 8 shows the computed surge residual water levels, which is the difference between the total surge level, from OWCS, and the tidal elevations, at several stations along the Irrawaddy delta (stations 1, 2, 3, 4, 5, and 6).

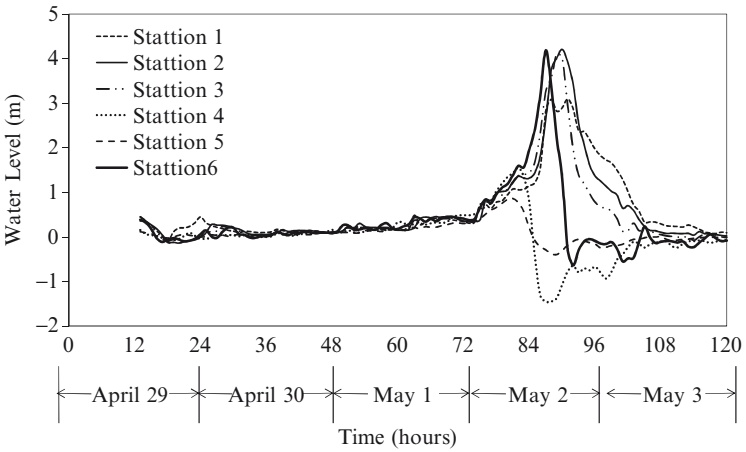

Fig. 8 Computed residual water levels (total water level-tide) at several stations along the Irrawaddy delta from April 29 to May 4 in 2008. The total water level is computed using the OWCS

References

Das PK (1972) A prediction model for storm surges in the Bay of Bengal. Nature 239:211–213
Dube SK, Chittibabu P, Sinha PC, Rao AD, Murty TS (2004) Numerical modelling of storm surge in the head Bay of Bengal using location specific model. Natural Hazards 31(2):437–453
Grell G, Dudhia J, Stauffer D (1996) A description of the fifth generation Penn State/NCAR Mesoscale Model (MM5). NCAR Technical Note (NCAR/TN-398 + STR), p 117
Haggag M, Yamashita T, Lee HS, Kim K (2008) A coupled atmosphere and multi-layer land surface model for improving heavy rainfall simulation. Hydrol Earth Syst Sci Discuss 5:1067–1100
Jelesnianski CP (1972) SPLASH I: landfall storms. NOAA Technical Memorandum, NWS-TDL-46, Washington DC, p 52
John B, Ali A (1980) The numerical modelling of storm surges in the Bay of Bengal. Quart J Roy Meteorol Soc 106:1–8
JTWC, Joint Typhoon Warning Center (2008) http://metocph.nmci.navy.mil/jtwc.php
Kim K, Yamashita T (2004) Hindcast of storm surge and wave fields of typhoon 9918 by wind–wave–current coupled model. Annu J Coastal Eng, JSCE 51:236–240 (In Japanese)
Kim K, Yamashita T (2005) Reanalysis of storm surge caused by cyclone in 1991 in Bay of Bengal: effects of whitecapping dissipation in wave-surge coupled model. Annu J Coastal Eng, JSCE 52:211–215 (In Japanese)
Kim KO, Yamashita T, Choi BH (2008) Coupled process-based cyclone surge simulation for the Bay of Bengal. Ocean Modelling 25:132–143
Murty TS, Neralla VR (1992) On the impossibility of the co-existence of monsoons and severe storm surges in the Bay of Bengal. Natural Hazards 6:281–285
Tolman HL (2002) User manual and system documentation of Wave Watch-III version 2.22. TN-No 222, NCEP MMAB, pp 133

Simulation of Track and Intensity of Gonu and Sidr with WRF-NMM Modeling System

Sujata Pattanayak and U.C. Mohanty

Keywords Meso-scale models • the Non-hydrostatic Meso-scale Model

Introduction

Tropical cyclones are organized convective activities, developed over warm tropical oceans. The Indian region is unique in nature than any other region of the world, as far as the genesis and death toll due to tropical cyclone is concerned. The tropical cyclones affect this region in two seasons: Pre-monsoon (April–May) and Post-monsoon (October–December). The peak frequency is found to be in the months of May and November. Though considered to be much weaker in intensity and smaller in size as compared to the cyclones of other regions, the Bay of Bengal storms are exceptionally devastating, especially when they cross the land. This is mainly due to shallow bathymetry, nearly funnel shape of the coastline, and the long stretch of the low-lying delta region entrenched with large number of river systems leading to high storm surges and coastal inundations. The Bay of Bengal contributes about 5% of the global annual tropical storms. At the same time, Arabian Sea contributes 1–2% of the global annual tropical storms. Therefore, reasonably accurate prediction of these storms has great importance to reduce the loss of valuable lives.

In recent years meso-scale models are extensively used for the prediction of different weather events worldwide. In the present study, WRF-NMM is used to simulate the pre-monsoon cyclone Gonu and the post-monsoon cyclone Sidr generated over Arabian Sea and Bay of Bengal respectively. The performance of the model has been evaluated and compared with observations and verifying analysis. Again, the advancement of data assimilation techniques indeed improves the forecast skill of the meso-scale models in wide ranges. A brief description of the meso-scale

S. Pattanayak (✉) and U.C. Mohanty
Centre for Atmospheric Sciences, IIT Delhi, Hauz Khas, New Delhi, 110016, India

Y. Charabi (ed.), *Indian Ocean Tropical Cyclones and Climate Change*,
DOI 10.1007/978-90-481-3109-9_12, © Springer Science+Business Media B.V. 2010

model used for the present study is given in Section 2. The numerical experiments and the data used are presented in Section 3. The synoptic situation for the above-mentioned cyclones is described in Section 4. The results are presented in Section 5, and the conclusions are in Section 6.

Model Description

The Non-hydrostatic Meso-scale Model (NMM) core of the Weather Research and Forecasting (WRF) system was developed by the National Center for Environmental Prediction (NCEP)/National Oceanic and Atmospheric Administration (NOAA). The WRF-NMM is designed to be a flexible, state-of-the-art atmospheric simulation system that is efficient on available parallel computing platforms. The WRF-NMM model is a fully compressible, non-hydrostatic model with a hydrostatic option (Janjic et al., 2001; Janjic, 2003a, b). The horizontal Arakawa E-grid staggering is used for computational efficiency. The model uses a terrain following hybrid sigma-pressure vertical coordinate. The dynamics conserve a number of first- and second-order quantities including energy and enstrophy (Janjic 1984). Forward–backward schemes are used for the horizontally propagating fast-waves and implicit scheme is used for the vertically propagating sound waves. Adams-Bashforth scheme and Crank-Nicholson scheme are used for horizontally and vertically propagating waves. The Geophysical Fluid Dynamic Laboratory (GFDL) long-wave and short-wave radiation schemes are incorporated in the model.

Numerical Experiments and Data Used

Two sets of numerical experiments are carried out with the above-mentioned meso-scale model. In the first experiment, i.e., in the control simulation (CNTL), the model has been integrated up to 72 h in a single domain with the horizontal resolution of 27 km along with 51 levels up to a height of 30 km in the vertical for both the cases. For case-1, i.e., for the Arabian Sea cyclone Gonu, the model is integrated with five different initial conditions, i.e., 00 UTC 02 June 2007, 12 UTC 2 June 2007, 00 UTC 3 June 2007, 12 UTC 3 June 2007, and 00 UTC 4 June 2007. Again, for case-2, i.e., for the Bay of the Bengal cyclone Sidr, the model is integrated with five different initial conditions, i.e., 00 UTC 12 November 2007, 12 UTC 12 November 2007, 00 UTC 13 November 207, 12 UTC 13 November 2007, and 00 UTC 14 November 2007. The initial and lateral boundary conditions to a limited area model are usually provided from the large-scale analysis and forecasts available at different NWP centers in the world. The NCEP Global Forecast System (GFS) analyses and forecasts ($1^\circ \times 1^\circ$ horizontal resolution) are used to provide the initial and lateral boundary conditions respectively. Again, in order to improve the initial analysis

fields for the model integration, an attempt has been made to initialize WRF-NMM model with WRF-VAR system. Hence, in the second experiment, i.e., in the data assimilation (DA), the impact of the observational datasets has been investigated by incorporating the available conventional and nonconventional datasets over the Indian region. Hence, for both the cases (Gonu & Sidr), the model is integrated with five different initial conditions each, as mentioned above with the improved initial conditions through WRFVAR system (Table 1).

Systems Descriptions

The tropical storm Gonu developed as a depression over the east central Arabian Sea with center near lat 15.0°N, long 68.0°E at 18 UTC 1 June 2007. It moved westwards and intensified into a cyclonic storm at 09 UTC 2 June 2007 near lat 15.0°N, long 67.0°E. It remained in that stage for 15 h, i.e., up to 00 UTC 3 June 2007. By 00 UTC 3 June 2007, it intensified into a severe cyclonic storm with the central pressure of 988 hPa and centered at lat 15.5°N, long 66.5°E and the storm remained in that stage for the next 18 h, i.e., up to 18 UTC 3 June 2007. Continuing its northwestward movement, it further intensified into a very severe cyclonic storm by 18 UTC 3 June 2007 and lay centered at lat 18.0°N, long 66.0°E with the central pressure of 980 hPa. It sustained in that stage for the next 21 h, i.e., up to 15 UTC 4 June 2007. By 15 UTC 4 June 2007, the system moved west–northwestwards and further intensified as a super cyclonic storm and lay centered at lat 20.0°N, long 64.0°E with the minimum central pressure of 920 hPa. It remained in the super cyclonic storm stage for the next 6 h, i.e., up to 21 UTC 4 June 2007. Then the storm further moved in northwestward direction and weakened into a very severe cyclonic storm by 21UTC 4 June 2007 and lay centered over northwest Arabian Sea at lat 20.5°N, long 63.5°E with the minimum central pressure of 935 hPa. The storm remained in that stage for the next 48 h, i.e., up to 21 UTC 6 June 2007. Then the storm gradually weakened, moved northwestward, and crossed the Makran coast near lat 25.0°N, long 58.0°E between 3 and 4 UTC 7 June 2007 as a cyclonic storm. The cyclone Sidr developed over southeast Bay near lat 10.5°N, long 91.5°E as a depression at 00 UTC 12 November 2007. As the storm picked up speed, the sea became turbulent with the gale force winds blowing even harder. On 13 November, Cyclone Sidr moved over southeast Bay and adjoining areas and moved northwestwards, concentrating into a severe cyclonic storm with the minimum central pressure of 968 hPa with a core of hurricane wind. It further intensified and reached the minimum central pressure of 944 hPa on 15 November with a core of winds in east central Bay. This is an estimated 655 km south–southwest of Chittagong port, 580 km south–southwest of Cox's Bazar port and 595 km south of Mongla port (near lat 17.0°N and long 89.2°E). Then it further moved in a northerly direction and cross Khulna-Barisal coast of Bangladesh in the evening of 15 November 2007.

Table 1 Vector displacement errors (in km) for both the cases (Gonu & Sidr)

Initial time of model integration	00 h		12 h		24 h		36 h		48 h	
	CNTL	DA	CNTL	DA	CNTL	DA	CNTL	DA	CNTL	DA
Gonu-1(0200)	100.0	65.0	95.0	55.0	88.5	64.3	128.1	72.2	142.0	77.5
Gonu-2(0212)	60.8	55.0	70.0	50.5	88.3	66.0	124.2	127.5	272.3	144.0
Gonu-3(0300)	32.0	25.0	65.4	54.0	140.7	95.0	188.0	135.2	225.0	175.4
Gonu-4(0312)	59.1	55.0	102.3	72.0	168.0	95.8	202.4	124.8	325.4	196.8
Gonu-5(0400)	50.1	24.4	84.1	61.1	125.1	79.5	223.6	102.5	371.0	155.0
Sidr-1(1200)	118.0	89.4	98.3	105.0	78.5	144.3	148.1	222.2	202.1	277.5
Sidr-2(1212)	80.8	55.5	71.1	59.7	172.3	166.5	248.2	277.5	372.3	44.0
Sidr-3(1300)	22.2	55.5	74.5	44.4	180.7	165.0	228.9	175.5	295.6	305.8
Sidr-4(1312)	35.1	70.1	115.9	78.4	248.2	175.5	323.6	246.2	546.6	496.5
Sidr-5(1400)	55.5	44.4	124.1	101.1	200.1	119.5	323.6	262.9	571.4	355.3
Mean error	61.36	53.93	90.07	68.12	149.04	117.14	213.87	174.65	332.37	222.78
Percentage of improvement	**13.8**		**32.2**		**27.2**		**22.5**		**49.2**	

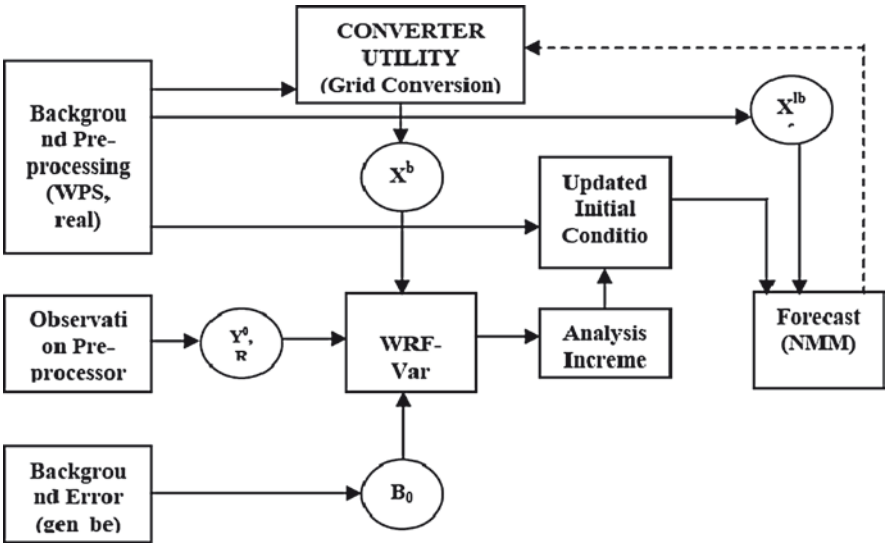

Fig. 1 Flowchart for the development strategy of initialization of WRF-NMM with 3-DVAR

Results and Discussion

The results for the above-mentioned two cases are presented in this section. The upgraded code of WRF-VAR for WRF-NMM system is also described. The results with the updated initial condition through the WRF-VAR system are presented.

Figure 1 shows the strategy followed to develop the utility to initialize WRF-NMM with 3DVAR system.

Conclusion

From the present study, the following broad conclusions have been derived. The WRF-VAR system is successfully upgraded for WRF-NMM which is clearly demonstrated through the flowchart mentioned above (Fig. 2). The WRF-NMM model could simulate most of the features of the cyclones Gonu and Sidr with reasonable accuracy. The significant improvement of 27.2% and 49.2% are there from the day-1 and day-2 forecasts respectively with the DA experiments from that of the CNTL simulations.

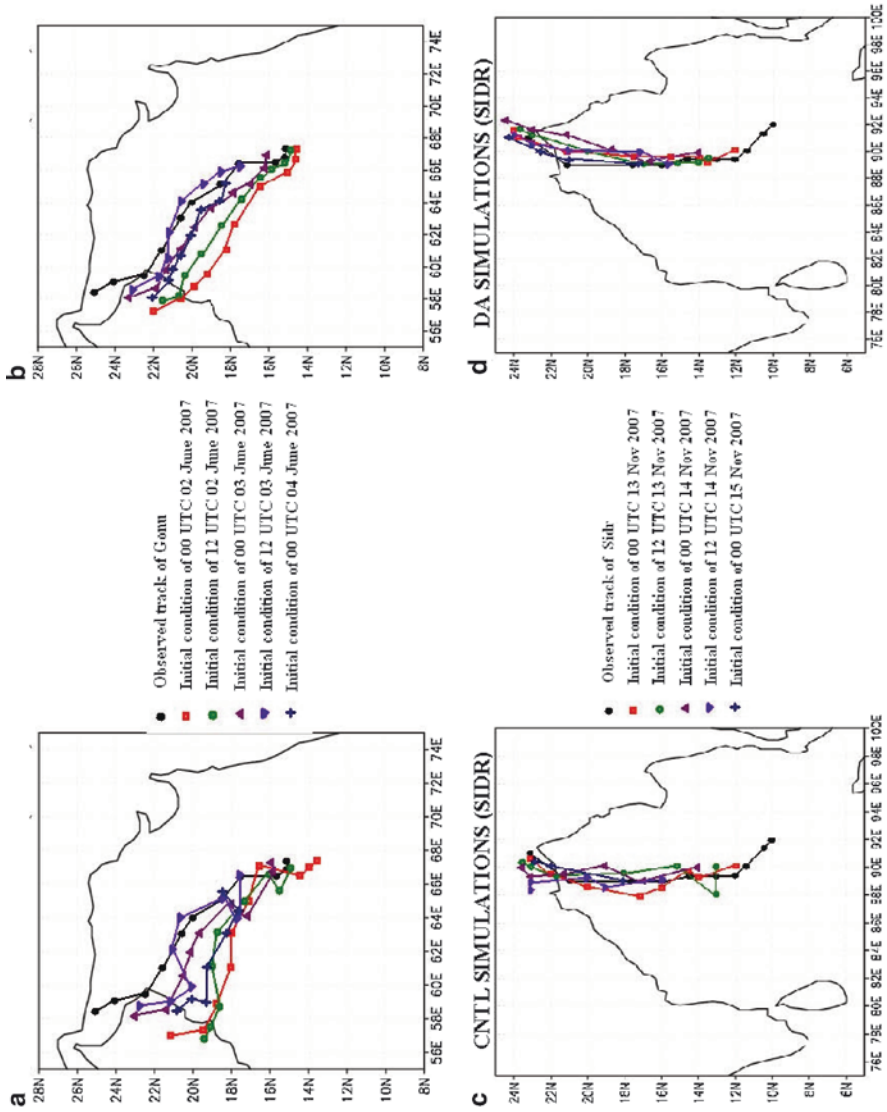

Fig. 2 Tracks of the cyclones from different initial conditions: (**a**) tracks of the cyclone Gonu from CNTL experiments; (**b**) tracks of the cyclone Gonu from DA experiments; (**c**) tracks of the cyclone Sidr from CNTL experiments; and (**d**) tracks of the cyclone Sidr from DA experiments

Acknowledgments We sincerely thank Mesoscale Microscale Meteorology (MMM) Division of NCAR for providing WRF-ARW modeling system and their valuable scientific help on the development aspect. We thank NCEP for providing the WRF-NMM system and the real-time large-scale analyses as well as forecasts of Global Forecast System (GFS). The authors also gratefully acknowledge the IMD for providing observational datasets and best-fit track of the cyclones Gonu and Sidr.

References

Barker DM, Huang W, Guo YR, Bourgeois AJ, Xiao QN (2004) A three-dimensional variational data assimilation system for MM5: implementation and initial results. Mon Wea Rev 132:897–914

Janjic ZI (1984) Non-linear advection schemes and energy cascade on semi-staggered grids. Mon Wea Rev 112:1234–1245

Janjic ZI (2003a) A nonhydrostatic model based on a new approach. Meteorol Atmos Phys 82:271–285

Janjic ZI (2003b) The NCEP WRF Core and further development of its physical package. Fifth International SRNWP Workshop on Non-Hydrostatic Modeling, Bad Orb, Germany, 27–29 October

Janjic ZI, Gerrity JP Jr, Nickovic S (2001) An alternative approach to nonhydrostatic modeling. Mon Wea Rev 129:1164–1178

Mandal M, Mohanty UC, Das AK (2006) Impact of satellite derived wind in mesoscale simulation of Orissa super cyclone. Indian J Mar Sci 35(2):161–173

Mandal M, Mohanty UC, Raman S (2004) A study of the impact of parameterization of physical processes in prediction of tropical cyclones over the Bay of Bengal with NCAR/PSU mesoscale model. J Int Soc Prevent Mitig Nat Hazards 31(2):391–414

Mohanty UC, Mandal M, Raman S (2004) Simulation of Orissa Super Cyclone (1999) using PSU/NCAR mesoscale model. J Int Soc Prevent Mitig Nat Hazards 31(2):373–390

Pattanayak S, Mohanty UC (2008) A comparative study on performance of MM5 and WRF models in simulation of tropical cyclones over Indian seas. Curr Sci 95(7):923–936

Part III
Operational Tropical Cyclone Forecasting & Warning Systems

Monitoring and Prediction of Cyclonic Disturbances Over North Indian Ocean by Regional Specialised Meteorological Centre, New Delhi (India): Problems and Prospective

Ajit Tyagi, B.K. Bandyopadhyay, and M. Mohapatra

Keywords Intraseasonal and interannual variation • numerical weather prediction

Introduction

Tropical cyclones are the most devastating phenomena among all natural disasters, having taken more than half a million lives all over the world in the last 5 decades. India Meteorological Department (IMD) monitors and predicts cyclonic disturbances over North Indian Ocean and provides early warning services for management of cyclones. IMD, New Delhi acts as a Regional Specialised Meteorological Centre (RSMC) – Tropical Cyclone for the World Meteorological Organisation (WMO)/ Economic and Social Cooperation for Asia and the Pacific (ESCAP) Panel Member countries, viz. Pakistan, Oman, Bangladesh, Sri Lanka, Thailand, Maldives, and Myanmar. The area of responsibility of RSMC, New Delhi is shown in Fig. 1. The broad functions of RSMC, New Delhi are as follows:

1. Round-the-clock watch on weather situations over the North Indian Ocean.
2. Analysis and processing of global meteorological data for diagnostic and prediction purposes.
3. Detection, tracking, and prediction of cyclonic disturbances in the Bay of Bengal and the Arabian Sea
4. Running of numerical weather prediction (NWP) models for tropical cyclone track and storm surge predictions.
5. Implementation of the Regional Cyclone Operational Plan of WMO/ESCAP Panel.
6. Issue of Tropical Weather Outlook and Tropical Cyclone Advisories to the Panel countries.

A. Tyagi (✉), B.K. Bandyopadhyay, and M. Mohapatra
India Meteorological Department, Mausam Bhavan, Lodi Road, New Delhi, 1100 03
e-mail: ajit.tyagi@gmail.com

Y. Charabi (ed.), *Indian Ocean Tropical Cyclones and Climate Change*,
DOI 10.1007/978-90-481-3109-9_13, © Springer Science+Business Media B.V. 2010

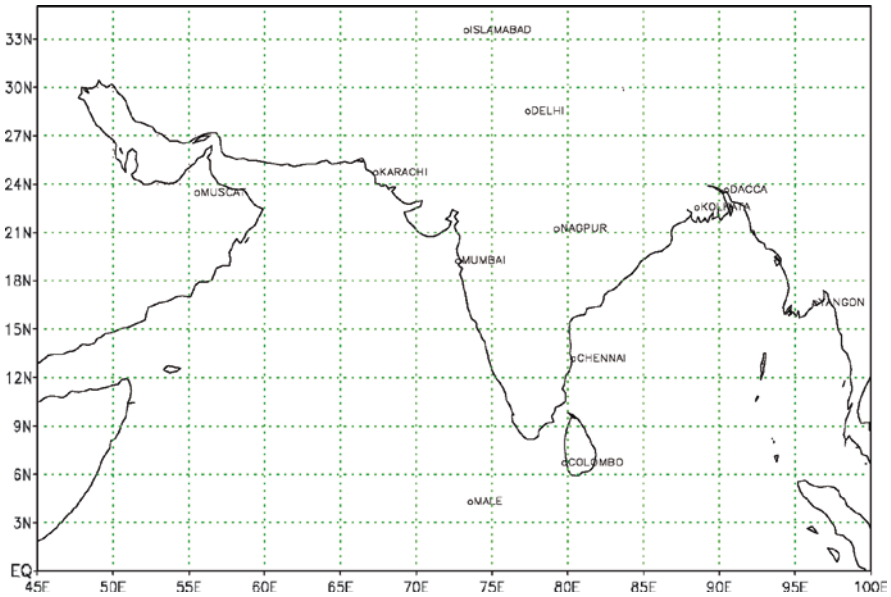

Fig. 1 Area of responsibility of RSMC- Tropical Cyclone, New Delhi

7. Collection, processing, and archival of all data pertaining to cyclonic disturbances viz. wind, storm surge, pressure, rainfall, damage report, satellite- and Radar-derived information, etc. and their exchange with panel member countries.
8. Preparation of comprehensive annual reports on cyclonic disturbances formed over the North Indian Ocean every year.
9. Preparation of annual review report on various activities including meteorological, hydrological, and disaster preparedness and prevention activities of panel member countries.
10. Research on storm surge, track, and intensity prediction techniques.
11. Interaction with National Disaster Management Authority and National Disaster Management, Ministry of Home Affairs, Govt. of India to provide timely information and warnings for emergency support services. RSMC, New Delhi also coordinates with National Institute of Disaster Management (NIDM) for sharing the information related to cyclone warning.

The intraseasonal and interannual variations of cyclonic disturbances over the North Indian Ocean and adjoining land regions are presented and analyzed in Section “Intraseasonal and Interannual Variation.” The cyclone warning procedure followed by RSMC, New Delhi is presented and discussed in Section “Cyclone Warning Procedure of RSMC, New Delhi.” The problems and perspective of existing early warning system in RSMC, New Delhi are analyzed in Section “Problems

and Perspective of Existing Early Warning System." The broad conclusions and future scope are presented in Section "Conclusions."

Intraseasonal and Interannual Variation

The low-pressure systems over the North Indian Ocean are classified based on the associated sustained maximum wind at the surface level. According to IMD criteria (IMD 2003), a low-pressure system is considered as Low Pressure Area, if the sustained maximum surface wind is less than 17 knots, a depression, if it is 17–27 knots, a deep depression, if it is 28–33 knots, a cyclonic storm (C), if it is 34–47 knots, a severe cyclonic storm, if it is 48–63 knots, a very severe cyclonic storm, if it is 64–119 knots and a super cyclonic storm if it is more than or equal to 120 knots. The systems with the intensity of depressions and above are considered as cyclonic disturbances. In the present study, severe cyclonic storm, very severe cyclonic storm, and super cyclonic storm have been together considered as severe cyclones (S). Similarly, depressions and deep depressions (D) have been considered as one category. The frequency of cyclonic disturbances over the North Indian Ocean shows large-scale intraseasonal and interannual variation. The mean frequencies of total cyclonic disturbances (D + C + S), only cyclones (C + S), and only severe cyclones (S) along with their standard deviation (SD) and coefficient of variation (CV) based on data of 1891–2007 as given in Cyclone e-Atlas of IMD (IMD 2008a) are shown in Table 1. The frequencies of cyclones and severe cyclones show bimodal behavior, being maximum in May and November. The frequency of total cyclonic disturbances is maximum in October, followed by November, August, and September.

Cyclone Warning Procedure of RSMC, New Delhi

The details of the cyclone warning activity including observational system, analysis, prediction, and warning dissemination are given in Cyclone Manual published by IMD (2003). This manual is under revision at present due to various developments in observation system, analysis tools, prediction techniques, and warning dissemination system. Brief descriptions on various aspects of cyclone warning are given below.

Observational System

A brief description of different types of observational network of IMD and observations collected from networks are given below:

Table 1 Mean SD and CV of frequency of cyclonic disturbances over the North Indian Ocean

	D + C + S			C + S			S		
Period	Mean	SD	CV (%)	Mean	SD	CV(%)	Mean	SD	CV(%)
Jan	0.15	0.36	235.53	0.07	0.25	370.71	0.02	0.13	761.55
Feb	0.04	0.20	475.32	0.02	0.13	761.55	0.01	0.09	1081.67
Mar	0.06	0.24	398.12	0.04	0.20	475.32	0.02	0.13	761.55
Apr	0.33	0.53	157.57	0.26	0.46	178.53	0.15	0.38	259.80
May	0.99	0.92	93.17	0.69	0.75	108.06	0.49	0.69	141.64
June	1.31	1.09	83.08	0.52	0.68	129.89	0.17	0.40	234.13
July	1.31	1.13	86.06	0.38	0.67	177.10	0.07	0.29	417.50
Aug	1.54	1.09	71.17	0.25	0.45	182.79	0.03	0.16	619.09
Sept	1.47	1.04	70.65	0.41	0.63	154.01	0.16	0.39	241.99
Oct	1.91	1.04	54.67	0.94	0.83	88.65	0.41	0.62	150.65
Nov	1.63	1.10	67.58	1.13	0.94	83.55	0.69	0.84	120.64
Dec	0.74	0.77	104.76	0.44	0.56	126.88	0.21	0.43	202.22
JF	0.20	0.42	213.74	0.09	0.28	328.52	0.03	0.16	619.09
MAM	1.38	0.89	64.21	0.99	0.77	77.79	0.65	0.73	113.12
JJAS	5.62	2.31	41.16	1.56	1.28	82.47	0.43	0.66	154.60
OND	4.27	1.75	40.95	2.51	1.21	48.35	1.32	1.16	88.47
Annual	11.48	3.40	29.60	5.15	1.86	36.20	2.42	1.58	65.20

Surface Observatories

IMD has a good network of surface observatories satisfying the requirement of World Meteorological Organization (WMO). There are 559 surface observatories in IMD. The data from these stations are used on real-time basis for operational forecasting. Recently, a number of moored ocean buoys including Meteorological Buoy (MB), Shallow Water (SW), Deep Sea (DS), and Ocean Thermal (OT) buoys have been deployed over the Indian Sea, under the National Data Buoy Programme (NDBP) of the Department of Ocean Development (DOD), Government of India. The existing buoy network is shown in Fig. 2a. IMD has also recently set up a network of 125 automated weather stations (AWS) in the country (Fig. 2b) which help in monitoring cyclonic disturbances (Bhatia et al. 2008).

Upper Air Observatories

There are at present 62 Pilot Balloon Observatories, 39 Radiosonde/Radiowind observatories, and 01 Radiosonde Observatory. The upper air meteorological data collected all over the country are used on real-time basis for operational forecasting. The short-period averages of Radiosonde data and normal of Radiowind data have been published. A Wind Profiler/Radio Acoustics Sounding System has been installed. The instrument is capable of recording upper air temperature up to 3 km and upper wind up to 9 km above sea level.

Cyclone Detection Radar

There are 11 S-band Cyclone Detection Radar (CDR) stations, viz. Kolkata, Paradip, Visakhapatnam, Machilipatnam, Chennai, Sri Harikota, Karaikal, Kochi, Goa, Mumbai, and Bhuj (Fig. 2c). Out of these 11 stations, 6 stations (except Chennai, Kolkata, Sri Harikota, Visakhapatnam, and Machilipatnam) are using

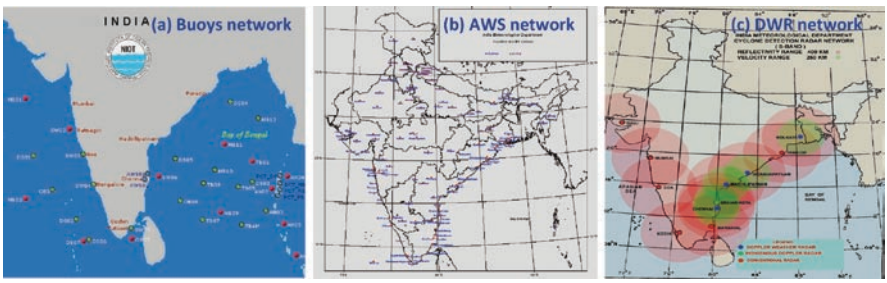

Fig. 2 (**a**) Existing buoys network over North Indian Ocean and (**b**) Automatic Weather Stations network (**c**) S-band conventional cyclone detection radar and DWR network

conventional S-band radars. Doppler Weather Radars (DWR) provides vital information on radial velocity within a tropical cyclone which is not available in conventional radar. Conventional radar provides information on reflectivity and range only, whereas a DWR provides velocity and spectral width data along with various meteorological, hydrological, and aviation products which are very useful for forecasters in estimating the storm's center, its intensity, and predicting its future movement. The monitoring of a small-scale, short-lived cyclone 'Ogni' IMD (2008b) and high impact cyclone, 'SIDR' (RSMC, New Delhi 2008) by DWR has been demonstrated by the existing DWRs.

Satellite Observation

India has launched Geo-stationary Satellite METSAT, now named KALPANA-I, on September 2002 purely for meteorological applications. It is positioned over the equator at 74°E. Another Geostationary satellite under INSAT series (INSAT-3A) was launched in April 2003 with the meteorological payloads identical to those of INSAT-2E which became operational since May 2003. It is positioned over the equator at 93.5°E. Both these satellites provide imageries in visible (VIS), Infrared (IR), and Water Vapor (WV) channels. In addition INSAT-3A is also equipped with Charged Coupled Device (CCD) cameras capable of providing imageries in VIS, Near IR (NIR), and Short-Wave IR (SWIR) channels with greater resolution. During a cyclone situation, data from KALPANA-1 are processed at hourly/half hourly intervals to assess the location and intensity of cyclonic disturbances out at sea. In addition to above, products like outgoing long-wave radiation, quantitative precipitation estimates, sea-surface temperatures, cloud-motion vectors, water-vapor-derived wind vector, and isotherm analysis on enhanced infrared images are also generated on operational mode and posted on the website of IMD.

IMD transmits processed imagery, meteorological and facsimile weather charts to field forecasting offices distributed over the country using the Meteorological Data Dissemination (MDD) facility, through INSAT in broadcast mode. The bulletins providing description of the cloud organization and coverage are also sent as advisory to forecasting offices every synoptic hour. When cyclones are detected in satellite imagery, these bulletins are sent every hour. Such advisories are also transmitted to the neighboring countries. Two MDD receiving stations are also operating in neighboring countries at Sri Lanka and Male. Processed satellite imagery, analyzed weather charts, and conventional synoptic data are uplinked to the satellite in C-band. Satellite broadcasts these data to MDD receiving stations in S-band. MDD receiving stations analyze weather imagery and other data to generate required forecast. The processing system is also being used for generating analogue type of cloud imagery data which are transmitted through INSAT-3C to field stations using S-band broadcast capability of the satellite along with other conventional meteorological data and fax charts. Dvorak technique (Dvorak 1984) is used to estimate the intensity of the system.

Analysis

The synoptic charts are prepared and analyzed every 3 h to monitor tropical cyclones over the North Indian Ocean. Cloud imageries from Geostationary Meteorological Satellites INSAT-3A and METSAT (KALPANA-1) are the main sources of information for the analysis of tropical cyclones over the data-sparse region of North Indian Ocean. Data from ocean buoys also provide vital information. Ship observations are also used critically during the cyclonic disturbance period. The direction and speed of the movement of a tropical cyclone are determined primarily from the 3 hourly displacement vectors of the center of the system and by analyzing satellite imageries. When the system comes closer to the coastline, the system location and intensity are determined based on hourly observations from Cyclone Detection Radar and Doppler Weather Radar stations as well as coastal observatories. The AWS stations along coast are also very useful as they provide hourly observations on real-time basis (Bhatia et al. 2008). The water-vapor-derived wind vector and cloud motion vectors in addition to the conventional wind vectors observed by Radio Wind (RW) instruments are very useful for monitoring and prediction of cyclonic disturbances especially over the sea region (Bhatia et al. 2008). The various kinds of analytical procedure are described in Cyclone Manual (IMD 2003). At present the mean error of center estimated by RSMC, New Delhi is about 0.5° latitude/longitude (IMD 2003).

Prediction Systems in Operational Use

(a) *Quasi-Lagrangian Model (QLM):* The QLM, a multilevel fine-mesh primitive equation model with a horizontal resolution of 40 km and 16 sigma levels in the vertical, is being used for tropical cyclone track prediction in IMD. The integration domain consists of 111x111 grid points centered over the initial position of the cyclone. The model includes parameterization of basic physical and dynamical processes associated with the development and movement of a tropical cyclone. The two special attributes of the QLM are: (i) merging of an idealized vortex into the initial analysis to represent a storm in the QLM initial state and (ii) imposition of a steering current over the vortex area with the use of a dipole. The initial fields and lateral boundary conditions are derived based on global model (T-80 and T254) forecasts obtained online from the National Centre for Medium Range Weather Forecasting (NCMRWF), India. The model is run twice a day based on 00 UTC and 12 UTC initial conditions to provide 6 hourly track forecasts valid up to 72 h. The track forecast products are disseminated as a World Weather Watch (WWW) activity of RSMC, New Delhi. The mean forecast error of QLM for the year 2007 is 92, 136, 252, and 320 for 12, 24, 48, and 72 h forecast (RSMC 2008)

(b) *Limited Area Model (LAM):* The operational forecasting system known as Limited Area Forecast System (LAFS) is a complete system consisting of data decoding and quality-control procedures, 3-D multivariate optimum interpolation scheme for objective analysis, and a semi-implicit semi-Lagrangian multilayer primitive equation model. The model is run twice a day based on 00 UTC and 12 UTC observations. The horizontal resolution of the model is 0.75° × 0.75° latitude/longitude. With 16 sigma levels in the vertical. First-guess and boundary conditions for running the LAFS are obtained on-line from global forecast model being operated by the NCMRWF. During cyclone situations, the model is run by including Holland vortex scheme. The forecast products are disseminated as a WWW activity of RSMC, New Delhi.

(c) *Non-hydrostatic Meso-scale Model MM-5 (Version 3.6):* The non-hydrostatic model MM-5 is being run on operational basis daily once based on 00 UTC initial conditions for the forecast up to 72 h. The horizontal resolution of the model is 45 km with 23 sigma levels in the vertical. The domain of integration covers the area between latitude 25°S–45°N and longitude 30°E–120°E. National Centre for Environmental Prediction (NCEP) analysis and 6 hourly forecasts are used as initial and boundary conditions to run the model. During cyclone situations, the model is run by including Holland vortex scheme. The forecast products are disseminated as a WWW activity of RSMC, New Delhi.

(d) *WRF Model:* The WRF model is run experimentally at IMD during a cyclone period. It is also run in Indian Institute of Technology (IIT), Delhi with different resolution using NCEP data and the prediction is made available to IMD.

(e) *Other Models:* Apart from the models run in IMD, the model product from other centers like ECMWF, UKMO, JMD, NCMRWF (T254), and Indian Air Force (MM5) are considered. Various stations models like CLIPPER, Chaos/ Senaric algorithim model developed by Space Application Centres, Indian Space Research Organisation, Ahmedabad run operationally in IMD for track prediction.

(f) *Storm Surge Model:* For the operational storm surge prediction, IMD uses both nomograms developed by IMD and Dynamical Storm Surge Model developed by IIT, Delhi. The nomograms are based on the numerical solution to the hydrodynamical equations governing motion of the Sea. The nomograms are prepared relating peak surge with various parameters such as pressure drop, radius of maximum wind, vector motion of the cyclone, and offshore bathymetry. The dynamical model of IIT Delhi is fully nonlinear and is forced by wind stress and quadratic bottom friction following the method of numerical solution to the vertically integrated mass continuity and momentum equations. The updated version of the model currently in operational use covers an analysis area lying between latitude 2.0°N and 22.25°N and longitude 65.0°E and 100.0°E. The method uses a conditionally stable, semi-implicit, finite difference stair-step scheme with staggered grid for numerical solution of the model equation. The bottom stress is computed from the depth-integrated current using conventional quadratic equation. The bathymetry of the model is derived from Naval Hydrographic charts applying cubic spline technique.

Products Generated by RSMC, New Delhi

RSMC, New Delhi prepares and disseminates the following RSMC bulletins.

(i) *Tropical Weather Outlook:* Tropical Weather Outlook is issued daily at 0600 UTC in normal weather for use of the member countries of WMO/ESCAP Panel. This contains description of synoptic systems over North Indian Ocean along with information on significant cloud systems as seen in satellite imageries. In addition, a special weather outlook is issued at 1700 UTC when a tropical depression lies over the North Indian Ocean.

(ii) *Tropical Cyclone Advisories:* Tropical cyclone advisories are issued at 3 h intervals based on 00, 03, 06, 09, 12, 15, 18, and 21 UTC observations. The time of issue is HH + 03 hours. These bulletins contain the current position and intensity; central pressure of the cyclone; description of satellite cloud imagery; expected direction and speed of movement; and forecast of winds, squally weather, and state of the sea in and around the system. Tropical cyclone advisories are transmitted to panel member countries through global telecommunication system (GTS) and are also made available on real-time basis through Internet at IMD's website: http://www.imd.ernet.in and http://www.imd.gov.in.

(iii) *Tropical Cyclone Advisories for Aviation:* Tropical Cyclone Advisories for aviation are issued for international aviation as soon as any disturbance over the North Indian Ocean attains or is likely to attain the intensity of cyclonic storm within the next 6 h. These bulletins are issued at 6 h intervals based on 00, 06, 12, 18 UTC synoptic charts and the time of issue is HH + 03 hours. These bulletins contain present location of cyclone in lat./long., max sustained surface wind (in knots), direction of past movement and estimated central pressure, forecast position in Lat./Long, and forecast winds in knots valid at HH + 6,HH + 12, HH + 18 and HH + 24 hours in coded form. The tropical cyclone advisories are transmitted on real-time basis through GTS and AFTN channels to designated International Airports of the region prescribed by ICAO.

(iv) *Bulletin for Indian coasts:* These bulletins are issued on every 3 h interval based on the standard eight synoptic observations at 00, 03, 06, 09, 12, 15, 18, and 21 UTC when the system intensifies into a cyclonic storm over the North Indian Ocean. This bulletin contains present status of the cyclone, i.e. location; intensity, past movement and forecast intensity and movement; likely landfall point and time; and likely adverse weather including heavy rain, gale wind and storm surge. Expected damage and action suggested are also included in the bulletins. This bulletin is completely meant for national users and these are disseminated through various modes of communication including All India Radio, Telephone/Fax, Print and electronic media. It is also posted on cyclone page of IMD website.

Cyclone Warning Dissemination System

IMD's Area Cyclone Warning Centres (ACWCs) at Chennai, Mumbai, and Kolkata and Cyclone Warning Centre (CWCs) at Bhubaneswar, Visakhapatnam, and Ahmedabad are responsible for originating and disseminating cyclone warnings at the regional level. In addition to the conventional network like telephone, fax, e-mail, Internet, and SMS, IMD has installed specially designed receivers within the vulnerable coastal areas for transmission of warnings to the concerned officials and people using broadcast capacity of INSAT satellite. This is a direct broadcast service of cyclone warning in the regional languages meant for the areas affected or likely to be affected by the cyclone. There are 352 cyclone warning dissemination system (CWDS) stations along the Indian coast; of these 100 digital CWDS are located along the Andhra coast. The bulletins through CWDS are transmitted every hour. The warning is selective and will be received only by the affected or likely to be affected stations. The service helps the public in general and the administration, in particular, during the cyclone season.

Problems and Perspective of Existing Early Warning System

As a result of increase in requirements of meteorological support, it has become necessary to provide adequate and realistic observations for frequent initialization of numerical weather prediction models for short-to-medium range forecasting of tropical cyclones. The thrust areas of RSMC, New Delhi include: (i) improvement in scientific understanding, (ii) improvement in forecast techniques, (iii) improvement in telecommunication measures, and (iv) collaboration with research institutions. IMD has taken up various technological upgradation measures with respect to tropical cyclones in its modernization program, which will eventually help in addressing the above-mentioned thrust areas and requirements. Main features of ongoing modernization program include: to replace most of the remaining existing old conventional CDRs by the state of Art S-Band Doppler Weather Radar augmentation of AWS network, installation of dense network of automatic rain gauge stations, high-power computing system, more objective forecasting system, and better telecommunication facility for warning dissemination. At present, the operational cyclone landfall forecast error for 24 h is about 150 km. With the modernization program, the error is likely to reduce by about 10–15% in the next 2 years.

Conclusions

RSMC, New Delhi is well-equipped for monitoring and prediction of cyclonic disturbances over the North Indian Ocean. However, the average landfall error of cyclone for 24 h forecast issued by IMD is about 150 km. With the completion of

the ongoing modernization program, the error is likely to reduce by about 10–15% in the next 2 years.

References

Bhatia RC, Das S, Mohapatra M, Roy Bhowmik SK (2008) Use of satellite and AWS data for weather Prediction. IMD Met Monogr Synop Met No 6/2008. India Meteorological Department, New Delhi, India, pp 109–121

Dvorak VF (1984) Satellite observed upper level moisture pattern associated with tropical cyclone movement. In: Proc 15th American Met Sec Conf on Hurricane and Tropical Meteorology, pp 163–168

IMD (2003) Cyclone Manual. India Meteorological Department, New Delhi, India

IMD (2008a) Track of storm and depressions over the Indian Seas during 1891–2007, 'Cyclone e-Atlas of IMD'. IMD, New Delhi, India

IMD (2008b) A report on the cyclonic storm, 'OGNI' 2006' Published by Cyclone Warning Division. IMD, New Delhi, India

RSMC, New Delhi (2008) A report on cyclonic disturbances over the North Indian Ocean during 2007. IMD, New Delhi

Evaluation of the WRF and Quasi-Lagrangian Model (QLM) for Cyclone Track Prediction Over Bay of Bengal and Arabian Sea

Y.V. Rama Rao, A. Madhu Latha, and P. Suneetha

Keywords Quasi-Lagrangian model • the Weather Research and Forecasting (WRF) model

Introduction

Quasi-Lagrangian model (QLM) for cyclone track prediction is the operational limited area model used in India Meteorological Department (IMD) for providing numerical guidance in cyclone forecasting operations (Mathur 1991, Prasad and Rama Rao 2003). QLM is specially tailored for providing cyclone track forecasts using the methodology of a synthetic vortex superimposed on gridded fields to correct the location and intensity of the vortex in the initial fields. QLM has a horizontal resolution of 40 km and 16 sigma levels in the vertical. It is integrated in a domain of about 4,400 × 4,400 km^2 area that is centered on the initial position of the cyclone. The special feature of the QLM is an idealized vortex, which is generated from the current storm parameters; and a Dipole, which is generated based on the estimated storm speed and direction.

Recently, IMD implemented the Weather Research and Forecasting (WRF) model in the research mode. The model has a horizontal resolution of 20 km and 31 sigma levels in vertical, with domain of 0°–30°N; 65°E–105°E. Using this model, some case studies were conducted to examine the usefulness of this high-resolution advanced mesoscale models for the Indian region. The track forecast experiment results up to 3 days were compared with the operational QLM forecast. In the present study, we have selected two severe cyclonic storms namely (i) Super Cyclone "GONU" over Arabian Sea during 01–07 June, 2007, and (ii) very severe

Y.V.R. Rao (✉)
NHAC, India Meteorological Department New Delhi, 110003, India
e-mail: ramarao@imdmail.gov.in

A.M. Latha and P. Suneetha
Andhra University, Visakhapatnam (AP), India

Y. Charabi (ed.), *Indian Ocean Tropical Cyclones and Climate Change*,
DOI 10.1007/978-90-481-3109-9_14,

cyclonic storm "SIDR" over Bay of Bengal during 11–16 November 2007. Also sensitivity experiments were conducted with the WRF model to test the impact of various microphysical and cumulus parameterization schemes in capturing the track and intensity of the systems.

Data and Methodology

In the present study, the initial analysis and the lateral boundary conditions for running the QLM and WRF model are obtained from GFS, NCEP, USA Global real-time analyses and 6 hourly forecasts at 1° × 1° lat./long. In the present experiment, using the initial conditions from 2 to 5 June 2007 and from 13 to15 November 2007, the 72h forecasts are generated with the WRF and QLM models. WRF model sensitivity experiments with four combination of microphysical (WSM 3 simple ice scheme, Ferrier et al. and Lin et al.) and cumulus (Kain-Fritsch, Betts-Miller-Janjic, and Grells Devenyi Ensemble) schemes (Skamarock et al. 2005) were conducted. Here, we give detailed results of QLM and WRF experiment results for the above case.

Forecast Experiment

Case 1: Super Cyclone "GONU" Over Arabian Sea During 01–07 June, 2007

Synoptic Situation

A low-pressure area developed in the head of prevailing monsoon surge on 31 May 2007. It concentrated into a depression in the night of 1 June over east central Arabian Sea and lay centered at 1800 UTC near lat. 15.0°N and long. 68.5°E. Initially, the system moved in westerly direction and concentrated into a deep depression at 0300 UTC of 2 June and into a cyclonic storm "GONU" at 1200 UTC and lay centered near lat. 15.0°N and long. 67.0°E. It further intensified into a severe cyclonic storm at 0000 UTC of 3 June and lay centered at 15.5°N and long. 66.5° Satellite picture showing open eye at 0600 UTC of 4 June 2007. Moving in a northwesterly direction it intensified into a very severe cyclonic storm during the night of 4 June and into a super cyclonic storm at 1500 UTC and lay centered near lat 20.0°N and long. 64. 0°E. Moving in a west-northwesterly direction, it lost its intensity and crossed the Oman coast as a very severe cyclonic storm and in the morning of 6 June. Throughout its life span, the upper air ridge line remained to the north of the system. After crossing the Oman coast, it emerged in the Gulf of Iran and started to move in a north-northwesterly direction. It made second landfall over

Iran coast near long. 58.5° E in the morning of 7 June 2007 as a cyclonic storm. Moving in the same direction, it weakened gradually and it was seen a well-marked low-pressure area over Iran and its neighborhood on 8 June 2007.

Model Forecast

QLM Forecast

In Fig. 1, QLM west-to-east crosssection of tangential wind (kts) and temperature analysis through the center (20.5°N/63.5°E) for 00 UTC of 5 June 2007 initial analysis (a) without idealized vortex (b) with idealized vortex is given. It shows that without vortex initialization the analysis is not able to capture the cyclonic structure. After vortex initialization, the analysis shows minimum strength of winds at the center with increased wind speed to the left and right quadrant with maxima of more than 80 kts to the right about 50 km away from the center. The temperature field also shows warm core extending up to 300 hPa. In Fig. 1c the mean sea-level

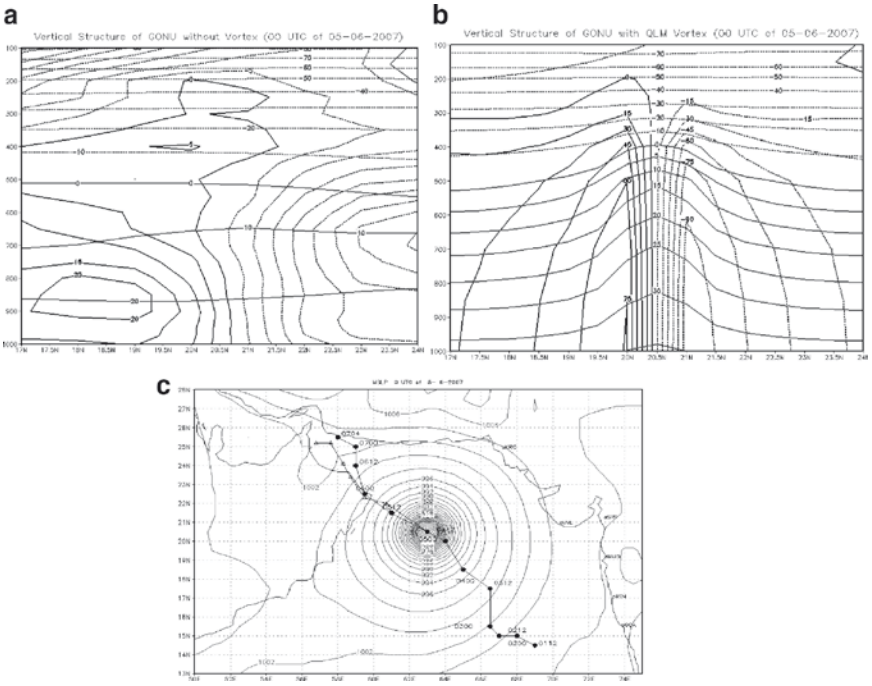

Fig. 1 QLM west to east cross section of tangential wind (kts) analysis through the center (20.5ºN/63.5ºE) for 00 UTC of 5 June 2007 initial analysis (**a**) without idealized vortex (**b**) with idealized vortex (**c**) QLM mean sea level pressure (hPa) analysis for 00 UTC of 5 June 2007 and 72 hours track forecast based on 5 June/00 UTC initial conditions with idealized vortex (circle: observed; triangle: predicted)

pressure (hPa) analysis based on 5 June/00 UTC initial conditions and 72 h track forecast with idealized vortex (circle: observed; triangle: predicted) is given. It shows the model was able to capture the track to the northwest movement of the storm; however, the track shows slightly west of the observed on 3 June and remaining days it is able to follow closely with the observed track. It is also observed that the forecast track was slower than the observed on 2, 3, and 4 June 2007.

WRF Forecast

The WRF model forecasts are produced using four combinations of microphysical and physical parameterization schemes. In Exp.1 WSM 3 Simple Ice scheme and KF scheme, Exp. 2 Ferrier et al. and BMJ scheme, Exp. 3 WSM 3 Simple Ice scheme and Grells Devenyi ensemble scheme, and Exp. 4 WSM 3 Simple Ice scheme and Grells Devenyi ensemble scheme respectively. The wind analysis at 850 hPa (m/s) based on 00 UTC of 3 June 2007; observed and 72 h forecast track based on the above four experiments are given in Fig. 2. It shows that, in Exp.1 the model forecast track is close to the observed. In other experiments, the model was able to capture the northwest movement of the system; however, the forecast track is left to the observed. Also, it was observed that the forecast track shows slow

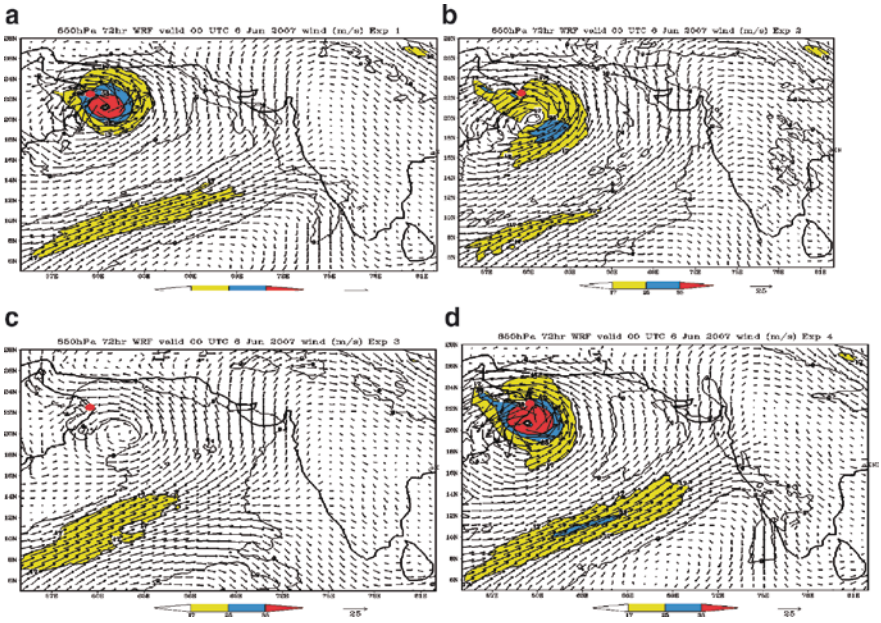

Fig. 2 WRF 72 hours forecast wind at 850hPa (ms^{-1}) based on 00 UTC of 3 June 2007 and valid for 6 June 2007 (**a**) based on Exp. 1 (**b**) based on Exp. 2 (**c**) based on Exp. 3 (**d**) based on Exp. 4 (closed circle: observed position on 6 June 2007)

movement in Exp. 2 and in other cases it is slightly slower than observed. In 72 h forecast, only Exp. 2 and 4 were able to capture the more than 33 m/s where the observed system was very severe cyclonic storm with wind speed of 38 m/s. In the other two experiments it was not able to capture the intensity of the system. The 72 h forecast 850 hPa (m/s) wind fields valid for 00 UTC of 7 June 2007, only Exp. 2 was able to capture the intensity more than 25 m/s where the observed system was cyclonic storm with wind speed of 27 m/s. In the other three experiments, it was not able to capture the intensity, since the forecast system was over the land. It is also interesting to note that the observed system crossed the Oman coast as very severe cyclonic storm on the 6 June morning and moved in a north-northwesterly direction emerging in the Gulf of Iran and made second landfall over Iran coast near long. 58.5°E on 7 June 2007 morning, however, the model experiments are not able to capture the recurvature of the storm after the first landfall near the Oman coast and model weakened the system after the landfall.

Case 2: Very Severe Cyclonic Storm "SIDR," Bay of Bengal During 11–16 November 2007

Synoptic Situation

An upper air cyclonic circulation lay over southeast Bay of Bengal and adjoining area of south Andaman Sea during 8–10 November, 2007. Initially, moderate upper-level wind shear inhibited organization, while strong diffluence aloft aided in developing convection. During this period easterly wave was also active. The vertical wind shear over the region decreased gradually and the circulation became more defined. Under the influence of these scenarios a low-pressure area formed at 0300 UTC of 11 November over southeast Bay of Bengal and its neighborhood. It concentrated into a depression on same day and lay centered at 1430 hrs IST over southeast Bay of Bengal near lat. 10.0°N and long. 92°E, about 200 km south-southwest of Port Blair. Moving slightly northwestwards it intensified into a deep depression and lay centered at 1800 UTC of 11 November near lat. 10.5°N and 91.5°E. It intensified into cyclonic storm SIDR and lay centered at 0300 UTC of 12 November near lat. 10.5°N and 91.0°E, about 220 km southwest of Port Blair. It moved in the northwesterly direction, further intensified into severe cyclonic storm and lay centered at 1200 UTC of same day near lat. 11.5°N and long. 90.0°E. Remaining practically stationary it intensified into a very severe cyclonic storm and lay centered at 1800 UTC of 12 November. The system moved northwestward direction till 0000 UTC of 13th. Afterwards the system moved in a near northerly direction up to 1200 UTC of 15 November and then the system recurved and moved in a north-northeasterly direction. It crossed west-Bangladesh coast around 1700 UTC near longitude 89.8°E as a very severe cyclonic storm and lay centered at 1800 UTC near lat. 22.5°N and long 90.5°E,

about 100 km south of Dhaka (Bangladesh). The system then weakened rapidly into a cyclonic storm while moving northeastwards and lay centered at 2100 UTC on 15 November near lat 23.5°N and long. 91.0° E, about 70 km southwest of Agartala (India). It further weakened into a depression and lay centered at 0300 UTC of 16 November near lat. 24.5°N and long. 91.5°E, about 50 km north of Agartala. It lay as a well-marked low-pressure area over northeastern states at 1200 UTC of 16 November.

Model Forecast

QLM Forecast

In Fig. 3, the mean sea-level pressure (hPa) analysis based on 14 and 15 November/00 UTC initial conditions and 72 h track forecast of each individual day with idealized vortex is given. It shows, based on 14 November, the 48 h forecast showing the landfall point along the West Bengal coast west to the observed; however, it shows the landfall time at 21 UTC of 15 November which was close to the observed. The 24 h forecast based on 15 November shows the landfall point along the Bangladesh coast, close to the observed; however, the predicted track shows northwards movement, where as the observed track made a recurvature after 12 UTC of 15 November just 5 h before the landfall.

WRF Forecast

The 72 h forecast wind at 850 hPa (m/s) based on 00 UTC of 13 November 2007 valid for 00 UTC of 16 November 2007 is given in Fig. 4. The 72 h forecast except in Exp. 3, all other experiments show intensity more than 33 m/s as observed; however, in Exp. 2, the maximum strength is shown over the Orissa coast since the

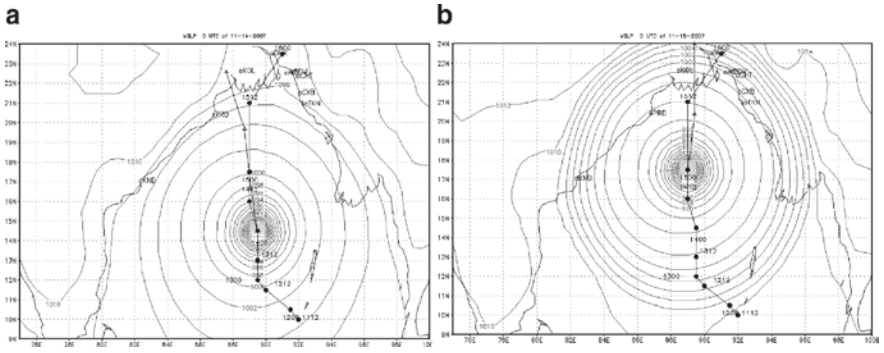

Fig. 3 (**a**) QLM mean sea level pressure (hPa) analysis for 00 UTC of 14 Nov. 2007 and 72 hours track forecast based on 14 Nov./00 UTC initial conditions with idealized vortex (**b**) based on 15 Nov. 2007 (circle: observed; triangle: predicted)

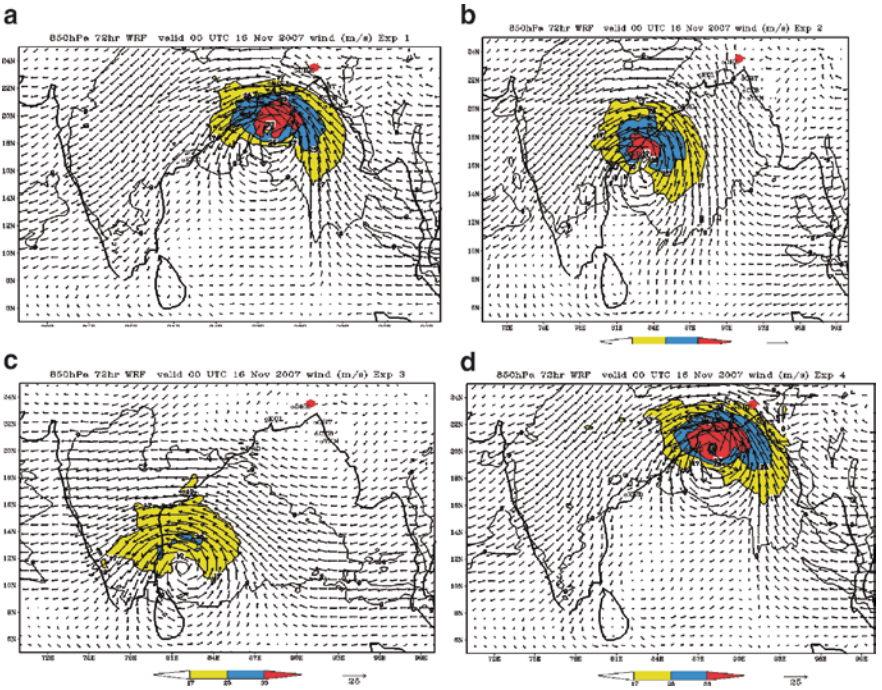

Fig. 4 WRF 72 hours forecast wind at 850hPa (ms^{-1}) based on 00 UTC of 13 Nov. 2007 and valid for 16 Nov. 2007 **(a)** based on Exp. 1 **(b)** based on Exp. 2 **(c)** based on Exp. 3 **(d)** based on Exp. 4 (closed circle: observed position on 16 Nov. 2007/00 UTC)

system moved west-northwest and in Exp. 1 and 4, it was over the head bay of West Bengal. The 48 h forecast based on 00 UTC of 14 November 2007 in Exp. 4 shows slow northwards movement, in Exp. 1 and 2 the model forecast track shows slightly north-northwest, in Exp. 3 it is northwest to the observed. In 48 h forecast, except in Exp.3, all other experiments show maximum wind along the West Bengal-Bangladesh coast. In Exp. 1 and 2 the intensity of more than 25 m/s was maintained as observed. It is also observed that in all the experiments the movement of the track forecast was slower than observed.

Track Forecast Errors

Forecast verification has been carried out by computing the direct position error (DPE) – the geographical distance between the predicted location of the storm and the verifying position at valid hour. The results are presented in Table 1 for the period ranges from 12 to 72 h for each individual day of experiment for the two cases considered and the QLM operational forecast errors from 1998 to 2007. The mean of all cases considered in this study at each forecast hour is also shown in

Table 1 Forecast Errors 2-7 June 2007 and 11-17 November 2007 Direct Position Error (DPE) (in km) and QLM Forecast errors during 1998-2007. (*Legend*: DPE is the geographical distance between the predicted location of the storm and the verifying position at valid hour)

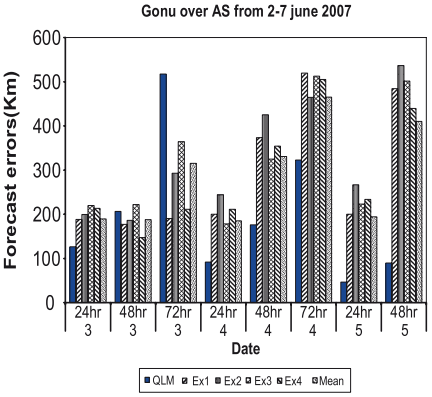

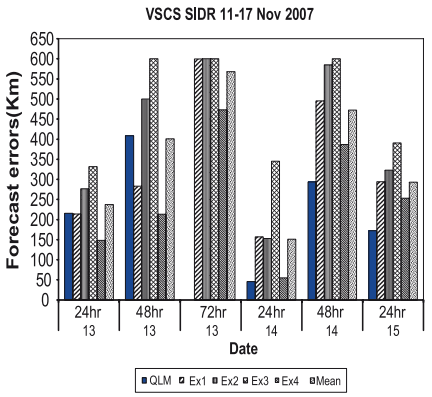

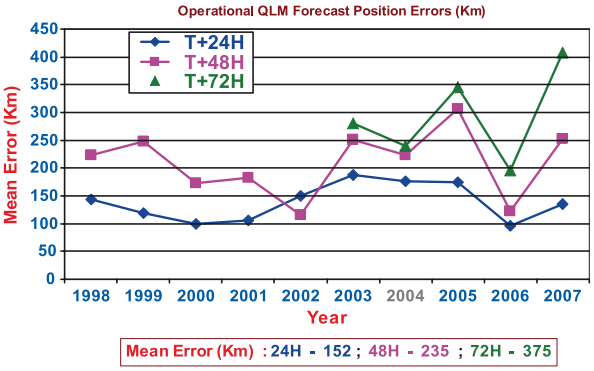

June 2007	3	3	3	4	4	4	5	5
	24hr	**48hr**	**72hr**	**24hr**	**48hr**	**72hr**	**24hr**	**48hr**
QLM	126	206	517	92	176	322	47	89
Ex1	188	177	190	200	373	519	200	484
Ex2	199	186	293	244	425	464	266	536
Ex3	219	222	364	178	324	512	223	501
Ex4	213	147	211	211	354	505	233	439
Mean	189.	188	315	185	330	465	194	410
Nov. 2007	13	13	13	14	14	15	-----	-----
	24hr	**48hr**	**72hr**	**24hr**	**48hr**	**24hr**	-----	-----
QLM	215	408		45	293	172	-----	-----
Ex1	213	282	599	157	495	294	-----	-----
Ex2	276	499	1126	152	585	323	-----	-----
Ex3	331	799	1664	345	1058	424	-----	-----
Ex4	148	213	473	54	386	253	-----	-----
Mean	237	440	966	151	563	293	-----	-----

the Table. During the last 10 years, the QLM errors are 152 km for 24 h; 235 km for 48 h and 375 km for 72 h, respectively. It is seen that the mean error for "GONU" 2–7 June 2007 of 24 h forecast is about 190 km, which increases to

about 250 km for 48 h forecast and 400 km for 72 h forecast. In this case QLM has shown 100 and 200 km in 24 and 48 h forecast. In the case of "SIDR" 11–16 November 2007, the QLM track errors have increased in the initial stage where the models are not able to capture the northerly movement of the system and the error reduced before landfall of 24–48 h. It has shown errors in the range 45–215 km in 24 h; around 300 km in 48 h. The average WRF errors are noticed to be 250 km for 24 h; 500 km for 48 h; 600 km for 72 h. The large average errors are due to westwards bias in Exp. 2. The WRF model forecast errors are less in Exp. 4 varying 55–250 km in 24 h and around 250 km in 48 h. The forecast errors have also been computed in terms of the "Vector Difference" and the "Angular Deviation." It was noticed that the Vector Difference showed negative value for all the WRF experiments with more than 200 km, showing the slow bias of the model, and Angular Deviation also shows negative values showing the predicted track to the left of the actual track.

Concluding Remarks

The present study evaluated the performance of the quasi-Lagrangian model with high-resolution state-of-art WRF model for cyclone track prediction over the Indian seas. Experiments were carried out for the most recent major severe cyclonic storms in the Bay of Bengal and Arabian Sea which occurred during 2007 and performance of the model was evaluated. QLM, because of the advantage of vortex initialization scheme and dipole winds which control the track forecast, the track forecast errors are minimum up to 48 h compared with the WRF model. The skill of the QLM is still limited in handling those cases which have an erratic behavior or sudden change in the speed and direction of movement. Attempts are underway to improve the model performance by increasing the horizontal resolution and boundary domain, etc. The WRF model forecast shows large variation in forecasted tracks for different physics combinations. Thus, cyclone track prediction is shown sensitive to convection and microphysical process. In the case of north-westward moving storm "SIDR," all the four experiments have shown similar results of northwest movement, whereas, for "SIDR" recurving system, the model shows large variation in track forecast by different schemes. In this case, the microphysics Lin et al. and Cumulus scheme KF is found to be better than other combinations for track prediction; however, more experiments with different combinations of convection schemes and cloud microphysics are required to further quantify the results. In both the cases the model showed slow bias and track was more westwards compared to the observed. The WRF model was able to capture the intensity after 48 h forecast. It may be due to poorly defined initial structure of the system in initial analysis. It is also observed that the initial position errors are more than 50 km from the observed position, which will also have large impact on the track forecast by the model. Further improvement can be expected with the vortex initialization/relocation, and 3D data assimilation in the WRF model can improve the track forecast.

References

Skamarock WC, Klemp JB, Dudhia J, Gill DO, Barker DM, Wang W, Powers JG (2005) 'A Description of the Advanced Research WRF Version 2' NCAR Technical Note-468

Prasad K, Rama Rao YV (2003) Cyclone track prediction by quasi-Lagrangian limited area model. Meteol Atmos Phys 83:173–185

Mathur MB (1991) The National Meteorological Center's quasi-Lagrangian Model for hurricane prediction. Mon Wea Rev 119(6):1419–1447

Simulation of Tropical Cyclones Over Indian Seas: Data Impact Study Using WRF-Var Assimilation System

Krishna K. Osuri, A. Routray, U.C. Mohanty, and Makarand A. Kulkarni

Keywords High-density wind coverage • vortex

Introduction

The track and intensity prediction of TCs require accurate representation of the vortex in the model initial conditions. The sparsity of observations, both near the vortex and in the surrounding environment, causes either undetectability in standard analyses or poor analysis with ill-defined centers and locations. So, much emphasis over the years has been laid on improving the initial conditions of NWP models, particularly high-resolution mesoscale models in a number of ways. The initial errors obviously have a major impact on the forecast of cyclone tracks using numerical models. One way of overcoming the above difficulty is by improving the initial analysis with the assimilation of conventional and nonconventional observations, which include the development and testing of a range of assimilation methods in the numerical weather prediction (NWP) model. Unfortunately, conventional measurements used to initialize forecast models are unavailable over vast areas of the tropical oceans. So, the high-resolution data required for numerical prediction of TC can be derived by tracking cloud features in the satellite imageries, which provide a large amount of data over data-void regions of the oceans. These derived winds can be used to improve the initialization of the model for the TC forecast. The ability to provide high-density wind coverage over large regions of the tropics makes satellite winds particularly useful for studying TCs (Velden et al. 1998).

Several studies have demonstrated that the inclusion of near-storm observations can substantially improve cyclone predictions. Pu et al. (2008) demonstrated the

K.K. Osuri (✉), A. Routray, U.C. Mohanty, and M.A. Kulkarni
Centre for Atmospheric Sciences, Indian Institute of Technology, New Delhi, 110016
e-mail: India mohanty@cas.iitd.ernet.in

Y. Charabi (ed.), *Indian Ocean Tropical Cyclones and Climate Change*,
DOI 10.1007/978-90-481-3109-9_15, © Springer Science+Business Media B.V. 2010

impact of aircraft dropsonde and satellite wind data on landfalling cyclones. Zhang et al. (2007) showed the impact of multisatellite data on initialization and simulation of Hurricane Lili's (2002) rapid weakening phase. Singh et al. (2008) showed the impact of SSM/I and Qscat satellite observations on Orissa super cyclone with MM5 model. The Mandal and Mohanty (2006) study showed the positive impact of assimilation of satellite-derived wind in simulation of TC over Bay of Bengal using MM5 modeling system, although their study was limited to only one case. Soden et al. (2001) demonstrated the impact of satellite winds on GFDL model forecast.

The main objective of the study is to improve the model's initial condition using satellite-derived winds through sophisticated WRF-3DVAR assimilation system and its subsequent impact on the simulation of track and intensity of the Indian Seas cyclones. Section 2 describes the numerical experiments and data used. The results obtained along with related discussions are presented in Section 3. Finally the conclusions are provided in Section 4.

Numerical Experiments and Data Used

The two numerical experiments used were: the CNTL experiment without assimilation, which utilizes the FNL analysis as the initial and lateral boundary condition, and the second, 3DVAR with the assimilation of satellite-derived wind to improve initial condition through WRF-3DVAR. All the model-simulated parameters are compared with India Meteorological Department (IMD) observations. The Tropical Rainfall Measuring Mission (TRMM) rainfall is used to validate the model-simulated rainfall. In this context, four TCs, namely Nargis (28 April–3May 2008), Sidr (14–16 November 2007), Gonu (2–8 June 2007), and Akash (13–16 May 2007) are simulated using the WRF model with 27 km resolution. These cyclones will be referred to as case-1, case-2, case-3, and case-4, respectively. The WRF assimilation system used the derived wind from INSAT WV channels and CMVs; surface wind from QSCAT and wind speed from SSM/I over the sea surface. For BOB TCs, the experimental domain was fixed to 3°N–28°N, 77°E–102°E centered at 15.5°N and 89.5°E. For Arabian Sea TC, the domain was fixed to 5°N–30°N, 48°E–78°E as 17.5°N and 63°E domain center. The model is integrated with 51 sigma levels vertically (up to 10 hPa). Except for the assimilation of these additional data, the model configuration for the both CNTL and 3DVAR are identical in all other aspects.

Results

Figure 1 shows the initial 10-m surface wind of case-1 and case-3 valid at 00UTC of 28 April 2008 and 00UTC of 2 June 2007 respectively and initial position errors for all cyclone cases (Fig. 1g) from 3DVAR and CNTL experiments. In case-1, a

strong wind (6–8 m/s) is found to the right of the cyclone in 3DVAR (Fig. 1b) whereas in CNTL (Fig. 1a), wind is very weak. The south-westerlies of the vortex are also increased and are well-organized in 3DVAR rather than CNTL. Similarly, for case-3, the enhancement is essentially in the position of the vortex and is well-represented in the 3DVAR analysis (Fig. 1d). Strong wind flow (14–16 m/s) over southern part of the vortex is also noticeable whereas it is less marked in CNTL (Fig. 1c). Same features are also found in case-2 and case-4 (figures are not provided). The initial position error Fig. 1(e) clearly indicates the initial position improvement in 3DVAR analyses than CNTL (NCEP) analyses in case-2, case-3, and case-4. There is no improvement in the position of the vortex in case-1. There is a mean position error improvement of 25% from 3DVAR than CNTL. It is well-known that the reduction in initial position error of the cyclonic vortex causes better track prediction (Holland 1984).

Impact of Model Simulation

Storm Track, and Its VDEs

The storm tracks from MSLP as obtained from CNTL and 3DVAR experiments along with the best-fit track provided by IMD is illustrated in Fig. 2a–d for case-1 to case-4, respectively. The Vector Displacement Errors (VDEs) for all experiments are calculated with respect to the IMD best position. There is noticeable improvement in the track of the cyclones in all the cases simulated by 3DVAR experiment compared to that of the CNTL experiment. Figure 3e demonstrated the error statistics of mean VDEs of all the cyclone cases. It is interesting to note that the mean VDEs show statistically significant improvement of 19%, 41%, and 64% in 24, 48, and 72-h forecasts. Table 1 represents the landfall errors for all individual cases. The landfall position error is improved 12%, 31%, 69%, and 33% in case-1, case-2, case-3, and case-4, respectively. The landfall time errors are also reasonably improved.

Statistical Verification

Figure 3a and b provide the root mean square error (RMSE) of predicted storm intensity in terms of MSLP (hPa) and maximum sustained 10-m wind (m/s). It can be easily noticed that the values of RMSE are smaller for all the four cyclone cases simulated from 3DVAR experiment as compared with CNTL except for case-1. In case-1 the 3DVAR resulted in a deeply intensified cyclone than the actual observations, which may be the probable reason for the slightly higher error. Equitable Threat Score (ETS) and bias at different thresholds of rainfall (mm) for the three cases viz. case-1, case-3, and case-4 have been computed and given in Fig. 4.

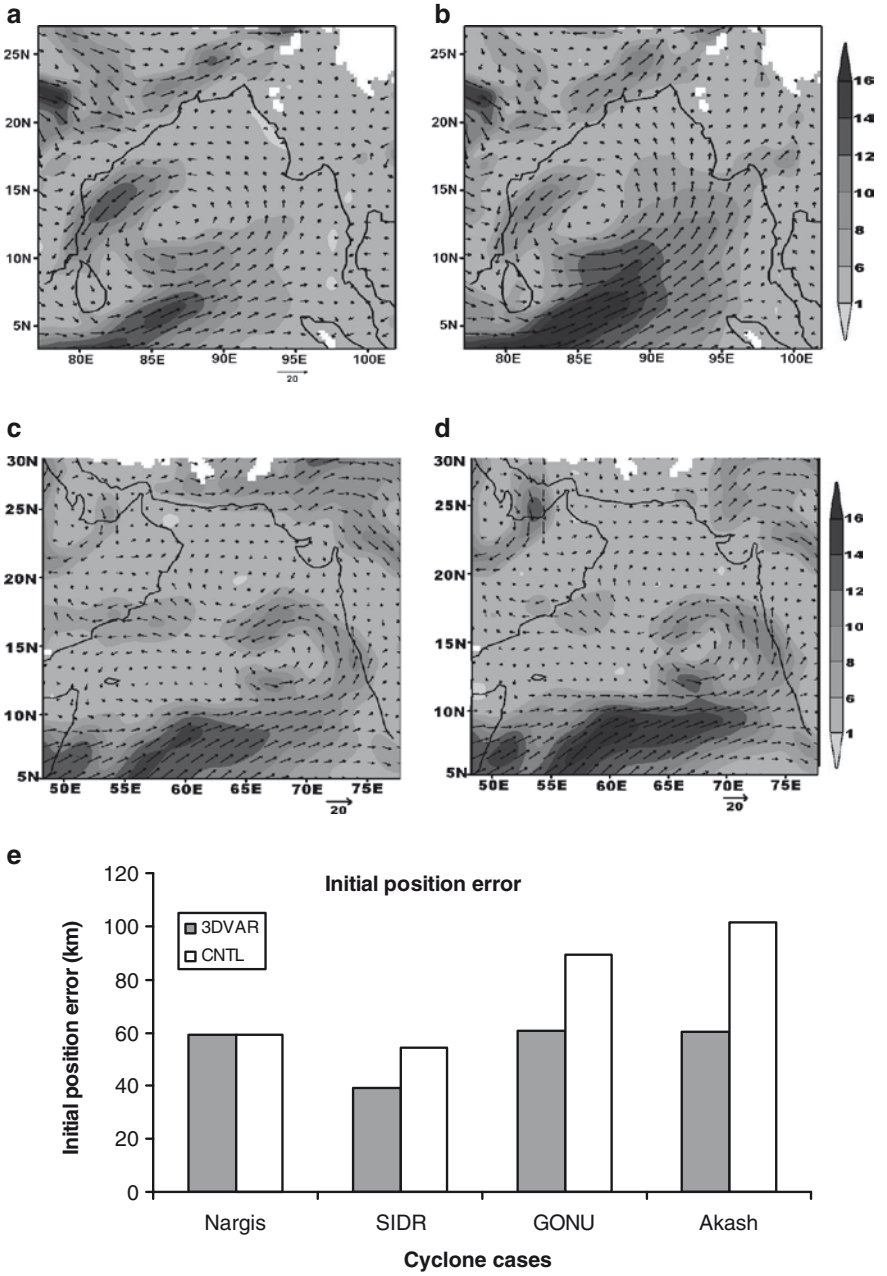

Fig. 1 10-m surface wind at initial time (**a**) CNTL (**b**) 3DVAR for case-1. Similarly (**c**), (**d**) are same as (**a**), (**b**) for case-3 respectively. (**e**) Initial position error (km) for all cases

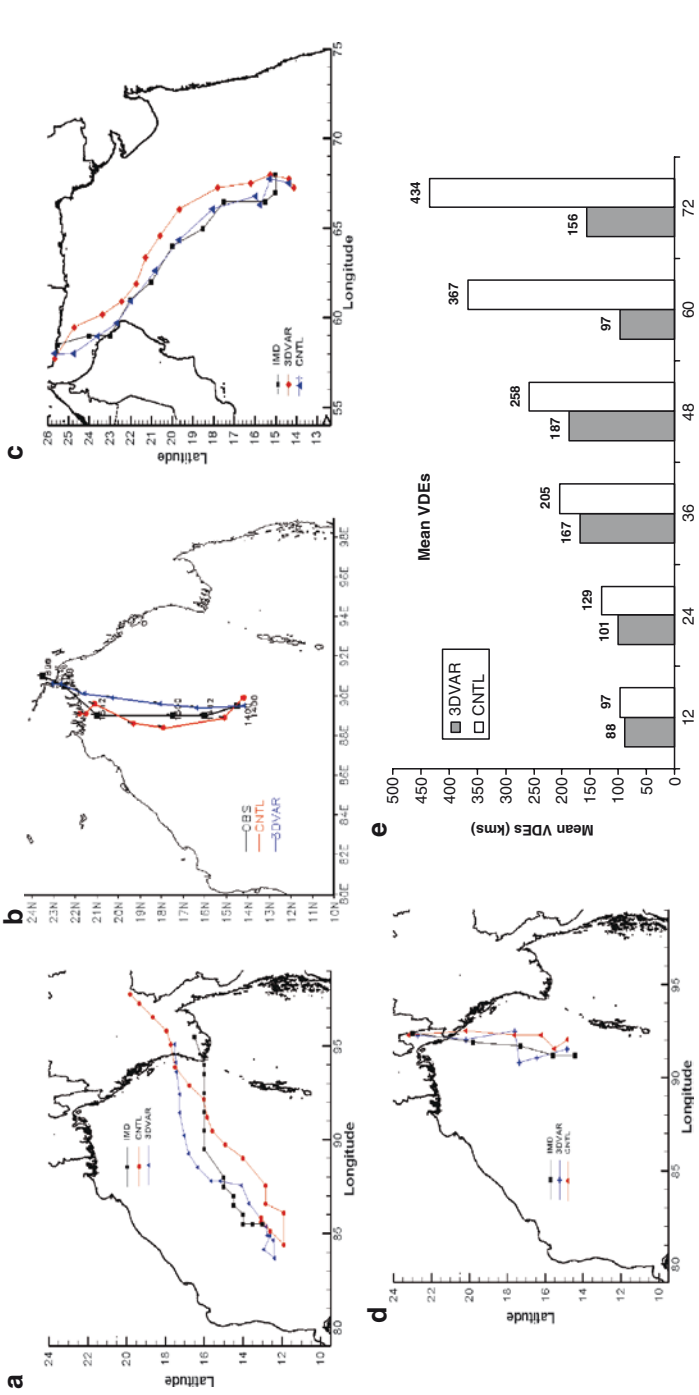

Fig. 2 Model-simulated tracks from CNTL and 3DVAR along with IMD best-fit track for (**a**) case-1 (**b**) case-2 (**c**) case-3, (**d**) case-4. (**e**) Mean vector displacement errors (km)

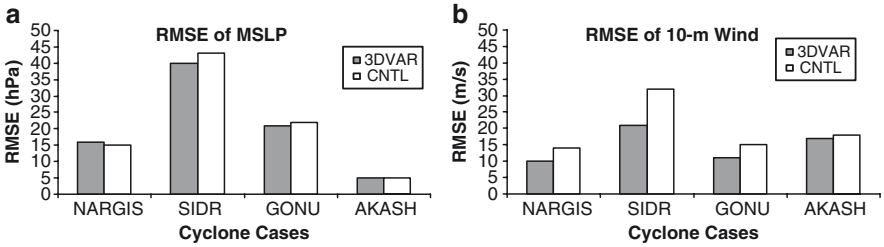

Fig. 3 Error statistics, RMSE of (**a**) MSLP and (**b**) 10-m wind from 3DVAR (dark) and CNTL (white) for all cyclone cases

Table 1 Landfall errors for all individual cyclone cases

	Landfall error (km)		Time errors (h)	
CycloneCases	3DVAR	CNTL	3DVAR	CNTL
NARGIS	196	223	3	25
SIDR	52	77	–3	–6
GONU	24	79	–9	–21
AKASH	51	77	–6	–3

It can be observed that for lower thresholds of rainfall there is a large improvement in 3DVAR simulations (ETS is higher and Bias is lower) than CNTL. Though the differences of ETS and bias for high-threshold values of rainfall between 3DVAR and CNTL simulations have reduced, 3DVAR have performed better.

Diagnosis of Simulation

Some diagnostics studies have been carried out to understand what aspects of the circulation fields are improved following the assimilation of satellite derived winds. Here we are providing only one case study (for case-3). This diagnostic study is carried out at maximum intensity time 1200 UTC of 5 June 2007 for case-3 (GONU) from both CNTL and 3DVAR experiments.

Figure 5a–d shows the simulated oceanic latent heat flux (LHF) and corresponding 850 hPa level wind. From these figures, it is clear that the LHF is significantly increased in the 3DVAR experiment, which can be attributed to the strong wind at 850 hPa level, than in the CNTL. The corresponding 850 hPa wind indicates a strengthening of surface wind over the area of maximum LHF, suggesting the role of increased winds in extracting heat energy from the ocean surface. Figure 6 shows the simulated east–west cross section of vorticity (a–b) and vertical velocity (c–d) through storm center from the CNTL and 3DVAR experiments for case-3. The 3DVAR experiment (Fig. 6b) shows strong vorticity (6–18 $\times 10^{-5}$/s) near the surface

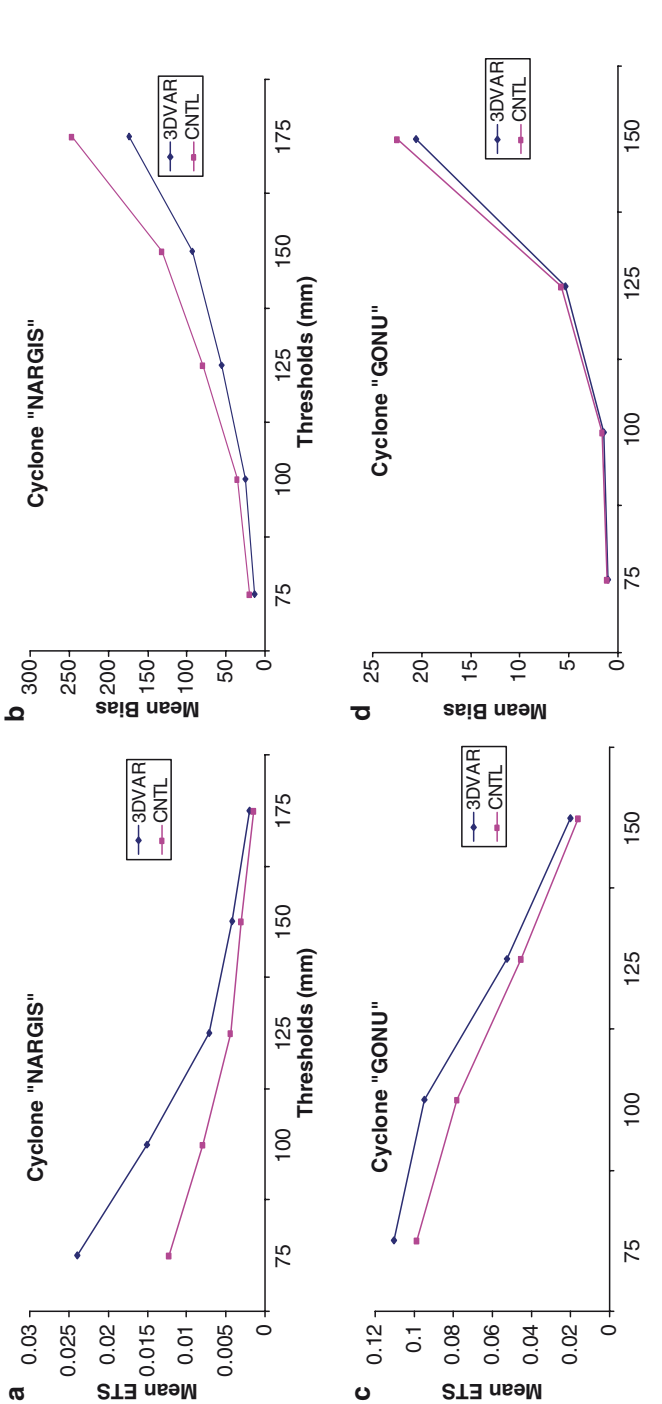

Fig. 4 Statistical precipitation skill score averaged over entire simulation time for different thresholds (**a**) ETS and (**b**) Bias for case-1 (NARGIS). (**c**), (**d**) are same as (**a**), (**b**) but for case-3 (GONU)

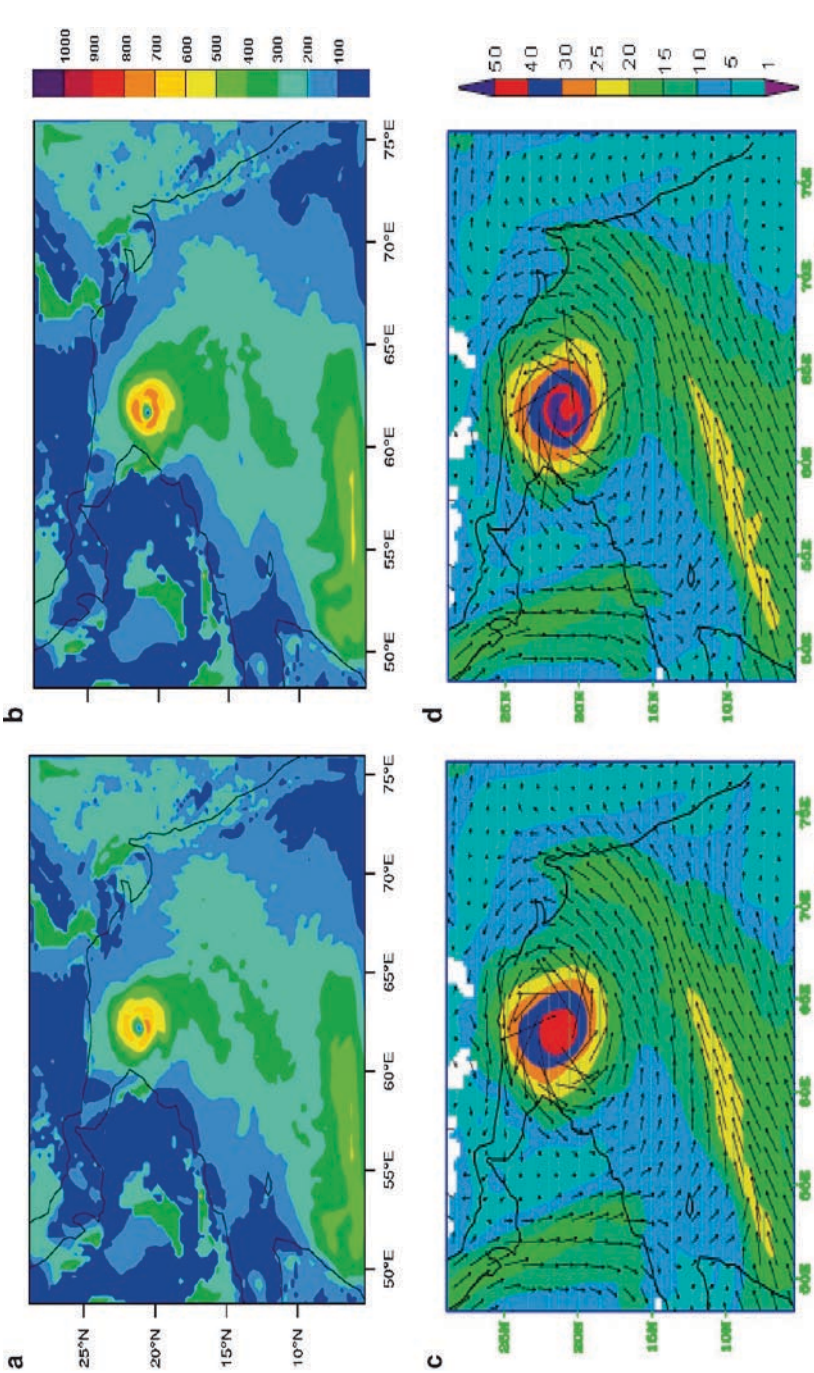

Fig. 5 Spatial distribution of LHF (w/m^2) (**a**) CNTL; (**b**) 3DVAR; (**c**) and (**d**) are corresponding wind (m/s) at 850 hPa level for case-3 valid at 1200 UTC of 5 June 2006

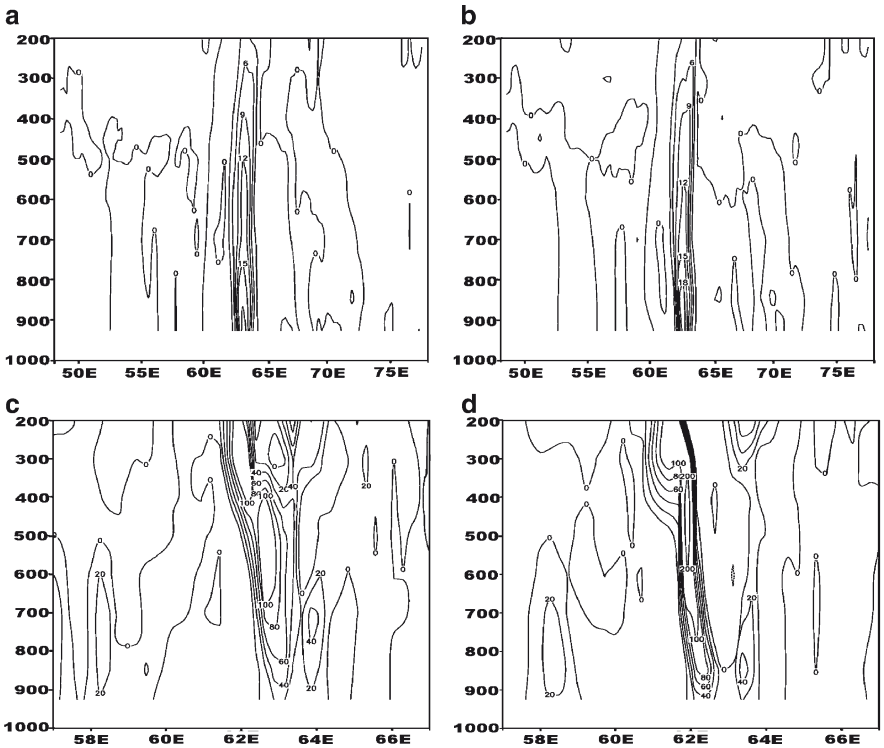

Fig. 6 Vertical cross section of vorticity in 10^{-5}/s through cyclone center for (**a**) CNTL (**b**) 3DVAR; (**c**) and (**d**) are same as (**a**) and (**b**), respectively, but for vertical velocity (cm/s) valid at 1200 UTC of 5 June 2007

and it is weak (6–15 × 10^{-5}/s) in the CNTL experiment (Fig. 6a). Two narrow strips of strong upward motions are found in the 3DVAR experiment of the order of 40–200 cm/s in the eastern part of the eye wall. But in the CNTL experiment, spread upward motions of the order of 20–100 cm/s are simulated. Very narrow upward motions in the 3DVAR experiment represent the simulation of strong cyclone with close center, which was not the case in the CNTL experiment (in which the area of upward motion is spread).

Summary

The prediction of TC tracks remains a challenging problem. Since improved track prediction depends heavily upon improved specification of the initial conditions, it is important to assess the impact of satellite observations (SSMI, QSCAT, INSAT)

which covers most of the data-sparse tropical oceans. As shown here, the assimilation of these winds is able to make a significant contribution to the reduction in track error (in 3DVAR experiment). Although the impact of the winds varied from storm to storm, statistically significant reductions in the forecasted track error were obtained for all TCs. The initial position error reduction improvement is about 20–25%. The 24-h and 48-h VDEs improvements are 20% and 40%, respectively. This improved percentage of average VDEs may increase or decrease if number of cases is increased. The spatial distribution of simulated 24-h accumulated rainfall also matches well with the TRMM observation from the 3DVAR experiment than that from the CNTL experiment as the position of the vortex is improved. The average RMSE of MSLP and 10-m maximum wind also supported the better performance of 3DVAR than the CNTL simulations with the improvement of 2–5% for MSLP and 20–25% for wind. The ETS and bias at different threshold also support the better simulation of precipitation in 3DVAR than CNTL. Diagnostic study indicates the intensification of the storm can be attributed to increased low-level convergence of warm air, latent heat release in the eye wall, and surface pressure drop in the inner core of the storm following the assimilation of satellite-derived winds. With this experiment, it is clear that the assimilation of satellite winds substantially improved the accuracy of the initial values and hence the model forecast.

References

Aberson SD, Franklin JL (1999) Impact on hurricane track and intensity forecasts of GPS Dropwindsonde Observations from the first-season flights of the NOAA Gulfstream-IV Jet Aircraft. Bull Am Meteor Soc 80:421–427

Holland GJ (1984) Tropical cyclone motion: a comparison of theory and observations. J Atmos Sci 41:68–75

Mandal M, Mohanty UC (2006) Impact of satellite derived wind in mesoscale simulation of Orissa super cyclone. Indian J Mar Sci 35(2):161–173

Pu Z, Xuanli Li, Velden CS, Aberson SD, Liu WT (2008) The Impact of aircraft Dropsonde and satellite wind data on numerical simulations of two landfalling tropical storms during the tropical cloud systems and processes experiment. Weather Forecast 23:62–79

Singh R, Pal PK, Kishtawal CM, Joshi PC (2008) The impact of variational assimilation of SSM/I and QuikSCAT Satellite observations on the Numerical Simulation of Indian Ocean Tropical Cyclones (2008). Weather Forecast 23:460–476

Soden BJ, Velden CS, Tuleya RE (2001) The impact of satellite winds on experimental GFDL hurricane model forecasts. Mon Wea Rev 129:835–852

Velden CS, Olander TL, Wazong S (1998) The impact of multispectral GOES-8 wind information on Atlantic tropical cyclone track forecasts in 1995, Part I: Dataset methodology, description and case analysis. Mon Wea Rev 126:1202–1218

Zhang X, Xiao Q, Fitzpatrick PJ (2007) The impact of multisatellite data on the initialization and simulation of hurricane Lili's (2002) rapid weakening phase. Mon Wea Rev 135(2):526–548

Impact of Rain-Affected SSM/I Data Assimilation on the Analyses and Forecasts of Tropical Cyclones, and Study of Flow-Dependent Ensemble Background Errors, Over the Southwest Indian Ocean

R. Montroty, F. Rabier, S. Westrelin, G. Faure, Loïk Berre, and Laure Raynaud

Keywords 3D-Var data assimilation • ALADIN

Introduction

Tropical cyclones are tremendous natural hazards that threaten coastal populations worldwide, including in the Indian Ocean, the third most active basin. The purpose of this study is to perform data impact studies with the ALADIN Réunion Limited Area Model, which is the largest and the only tropical implementation of all of the versions of the ALADIN consortium. It allows special focus on the Indian Ocean area and a "tropicalized" 3D-Var data assimilation.

Studies are performed for several storms of the 2006/2007 cyclonic season of the Southwest Indian Ocean (SWIO) basin. That season proved to be very active with ten named storms, four of which attained the "major hurricane" wind threshold of 50 m/s. Satellite data have proven most invaluable when trying to initialize NWP models, since the oceanic zones over which the cyclones develop are, by nature, data-sparse. Yet, the occurrence of clouds or rain proves to be a challenge when trying to assimilate satellite data: nonlinear processes predominate and the use of refined, costly numerical methods might be required. These computational costs are usually found to be prohibitive and cloudy/rainy data assimilation usually is a missing component in most operational centers. This proves to be of critical importance when dealing with tropical cyclones the data-sparse core, where observations are systematically rejected.

R. Montroty (✉), F. Rabier, L. Berre, and L. Raynaud
CNRM/GMAP/OBS, CNRS/GAME, Météo France, Toulouse, FRANCE

S. Westrelin and G. Faure
LACy/Météo France, La Réunion, FRANCE

Y. Charabi (ed.), *Indian Ocean Tropical Cyclones and Climate Change*,
DOI 10.1007/978-90-481-3109-9_16,

Data and Methodology

Of the few centers that do not suffer from this crucial observational lack, the NCEP and the JMA have been assimilating rain rates while the European Center for Medium Range Weather Forecasting (ECMWF) has implemented a 1D-Var inversion for cloudy/rainy areas, which uses complex moist physical schemes to retrieve a Total Column Water Vapor (TCWV)-equivalent from the rainy radiances, which is then used as pseudo-observation in the 4D-Var assimilation. In collaboration with the ECMWF and to bypass the costly 1D-Var inversion, we investigated a statistical multilinear regression that fits TCWV with the brightness temperatures of the SSM/I instrument, relying on the ECMWF analyses. The algorithm is then applied to assimilate cloudy/rainy TCWV in the 3D-Var of ALADIN Réunion. Impacts of the 3D wind bogus are also investigated. We further used our reference simulation to downscale to 4 km using the latest non-hydrostatic French model, AROME, over a SWIO-centered domain, using dynamical adaptation. Figure 1 presents the joint coverage of both SSM/I clear-sky pixels (treated as radiances) and cloudy/rainy pixels (treated as TCWV) in a 3D-Var assimilation network of TC Favio, on 18 February 2007 at 18Z. One can clearly see the doubled amount of information thanks to SSM/I TCWV as well as much better coverage of rainy areas with this technique.

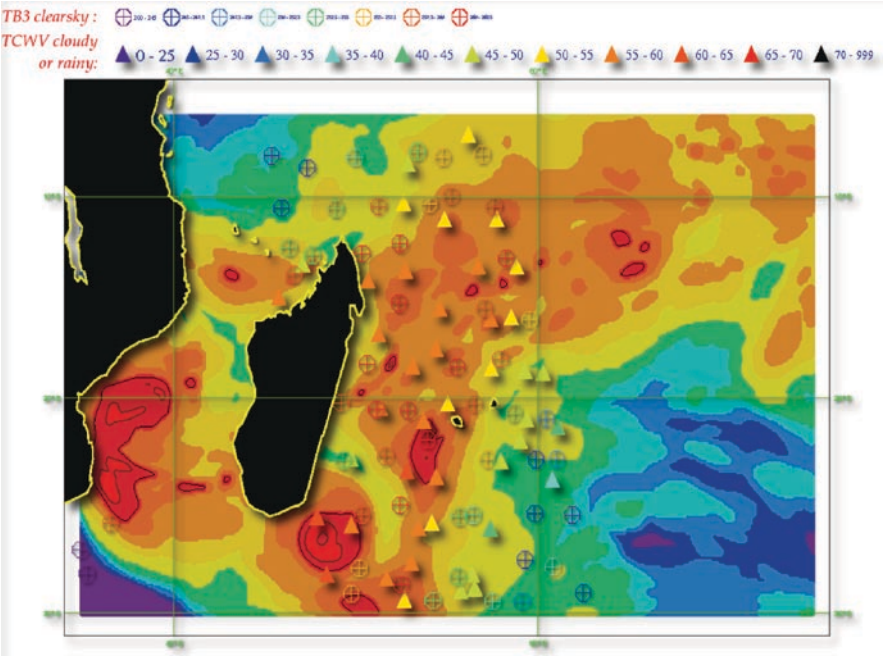

Fig. 1 Map of added SSMI rainy/cloudy radiances (triangles) to the already assimilated clear-sky radiances (crossed-out circles) in the analysis of TC Favio, 18 February 2007 at 18Z

Discussion and Results

In order to complement our study on observational impacts, we have studied the flow-dependence of background error standard deviations of the day in the Aladin-Reunion area, and in particular their space and time variations as a function of cyclonic location and intensity. For this purpose, results from a six-member global assimilation ensemble have been used. The results reflect the larger uncertainty in the vicinity of cyclones, implying that observations should be given larger weightage in these regions. Impact studies on the 2007/2008 season were performed. We find that over a period of 2 months, the use of background error variances "of the day" have a neutral impact on track forecasting but that an improvement of intensity forecasts is seen at longer lead times, indicating that the environmental conditions are better described when data assimilation is constrained by those ensemble-derived errors. Figure 2 presents three meteorological cases: intense TC Ivan (20080215 at 12Z) in the upper panel, intense TC Jokwe (2008031012 at 09Z) in the middle panel, and a standard "calm weather" day (20080402) on the SWIO basin. It is clear that both the position and intensity of the cyclone are easily noticed in those background error maps. This denotes a great potential for use in standard data assimilation systems as a way to measure model uncertainties and refine the use of observations in the vicinity of larger errors.

Finally, we performed a few case studies of tropical cyclones Sidr & Nargis using Météo-France's global model ARPEGE, using the rain-affected data assimilation in order to diagnose potential improvements to track and intensity forecasts in the North Indian Ocean. Figure 3 presents the vorticity background error variances at 850 hPa in the case of TY Nargis on 5 May 2008 at 00Z. Again, the ensemble captures the background errors well and they are maximal where the typhoon is located.

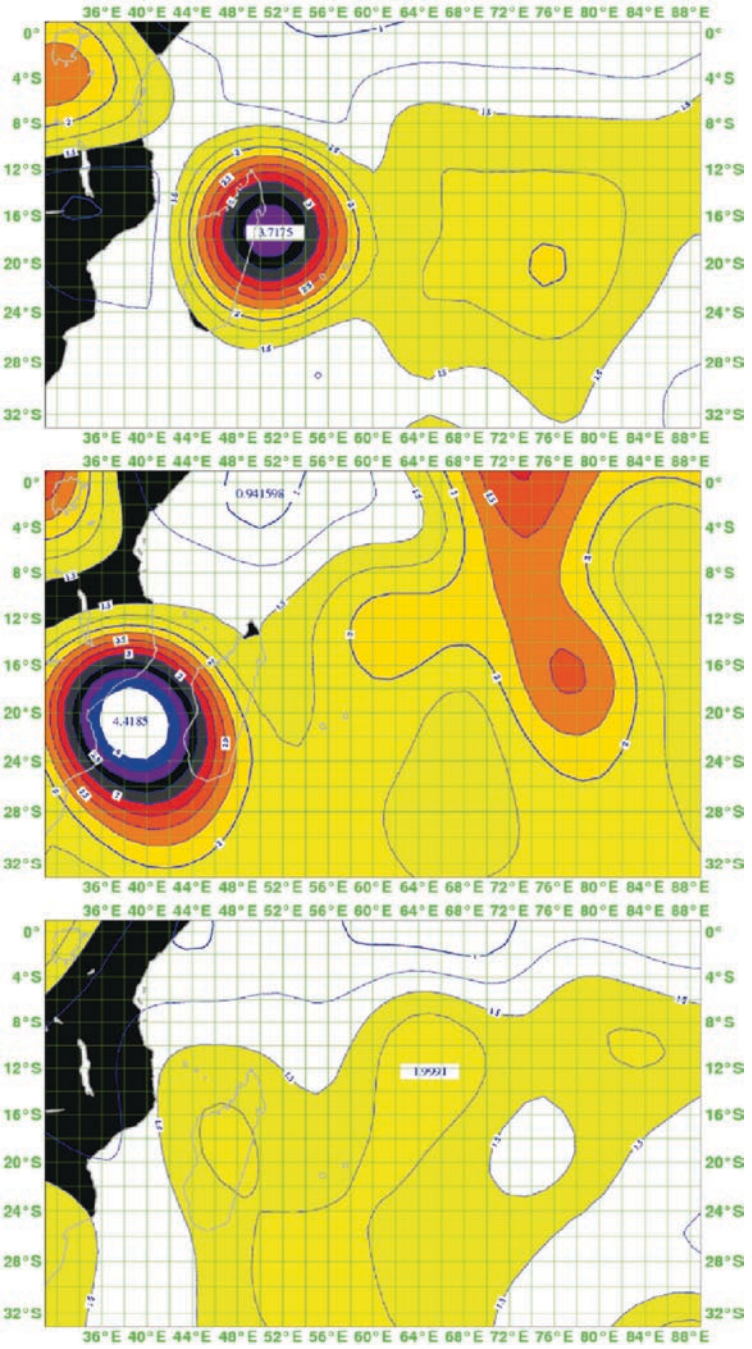

Fig. 2 Maps of background error standard deviations for vorticity (s^{-1}) at 850 hPa in three meteorological cases: TC Ivan (*upper panel*), TC Jokwe (*middle panel*), and standard calm weather on the domain (*bottom panel*)

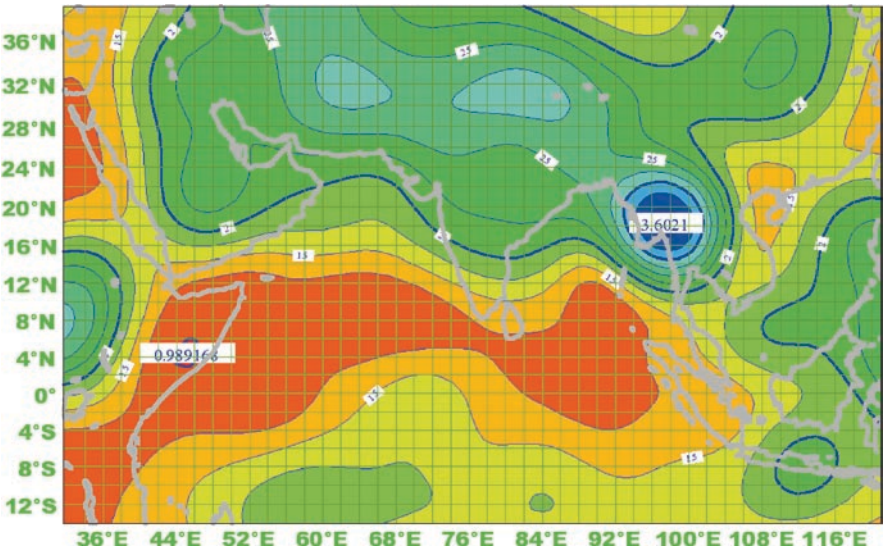

Fig. 3 Map of background error standard deviations for vorticity (s^{-1})at 850 hPa for TY Nargis on 5 May 2008 at 00Z

Statistical Forecasting of Tropical Cyclones for Bangladesh

Saleh A. Wasimi

Introduction

Bangladesh being a densely populated country and mostly deltaic region with many people living in thatched cottages along the coast is afflicted severely when lashed by a tropical cyclone (TC). TCs in the region have claimed by far more lives than anywhere else in the world – 49% of the world's total fatalities by cyclone is in Bangladesh alone and 22% in India (Ali 1996). The tropical cyclones that hit Bangladesh are mostly formed in the Bay of Bengal and their destructive force is primarily due to the accompanying storm surge, whose development is influenced by unique features such as shallow bathymetry and near funnel shape of the Bay (Mandal et al. 2007). As cyclones at different oceans are formed at different times, it is now well established that regional climate and weather patterns play an important role in cyclogenesis (JTWC Annual tropical cyclone reports 2007; Vecchi and Soden 2007). The climate of the region around Bangladesh besides its latitudinal and longitudinal location is influenced by the presence of the highest mountains to its north and northeast. In summer (May–October), a low-pressure system is created in northwest India by heating of landmass that marks the position of the monsoon trough, which causes wind to blow northeast from the Bay of Bengal over the shallow ocean waters to Bangladesh and then get deflected by the mountains to northwest. In winter (November–March), the monsoon trough is over the Bay of Bengal and cold airmass over land in north India moves outward through Bangladesh into the Bay of Bengal in southwest direction. The transition period (May or November) is when the wind is slowest offering ideal conditions for tropical cyclones to form over warm waters.

The factors that affect the formation of tropical cyclones are a topic of research and we still have a long way to go to fully understand the causes (Lee et al. 2008). Why some irregular atmospheric disturbances transform into cyclones and others do not is a perplexing question for the scientists. Once formed, cyclones derive their

S.A. Wasimi (✉)
CQ University, Rockhampton, Queensland 4702, Australia
e-mail: s.wasimi@cqu.edu.au

Y. Charabi (ed.), *Indian Ocean Tropical Cyclones and Climate Change*,
DOI 10.1007/978-90-481-3109-9_17, © Springer Science+Business Media B.V. 2010

energy from the latent heat of condensation of water vapor, and rapid intensification of cyclones generally occur when their translation speed is between 3 and 8 m/s (Zeng et al. 2007) – at lower speeds negative feedback from cold waters from upwelling deprives them of the energy, and at higher speeds, the shape gets asymmetric resulting in nonuniform angular acceleration. Many studies point to the fact that warm sea-surface temperature (SST) above 26°C, conditional instability and high relative humidity in the middle troposphere, and low vertical wind shear are prerequisites for the genesis of cyclones (Webster et al. 2005). Kotal et al. (2009) developed a genesis parameter for the Bay of Bengal as the product of four variables, namely vorticity at 850 hPa, middle tropospheric relative humidity, middle tropospheric instability, and the inverse of vertical wind shear. DeMaria et al. (2001) defined a genesis parameter for the North Atlantic basin based on SST, midlevel moisture, vertical shear, and vertical instability. ENSO has a significant role to play in the frequency and intensity of cyclones, which has been established (Camargo et al. 2007; Emanuel 2008). Ralph and Gough (2009) have shown that even in the same ocean, such as Eastern North Pacific, TCs can have different characteristics based on the main development region (MDR) of its formation.

Historical data on cyclones of the Bay of Bengal is available since 1877 (Singh et al. 2001; Islam and Peterson 2009), but its accuracy in early years is doubtful because dates, positions, and intensities are deduced through estimates and compromise among various reports using synoptic and climatological judgment (FNMOC 1998). However, reliable data (though primarily from satellite imagery) on the formation of major tropical cyclones in the Bay of Bengal, their tracks and their wind speeds at 6 h intervals are available since 1971 from the Joint Typhoon Warning Centre (JTWC) in Hawaii – detailed information on each TC is available in graphical and tabular forms. Frank and Young (2007) question the reliability of JTWC data but corrections of their data were made later to improve the quality of data. JTWC uses a number of numerical models and an expert system TAPT to predict the tracks and characteristics of the TCs, but frequently those turn up to be very different from the reality. Nicholls (2001) notes in this context that statistical and numerical analyses are complementary, and together are more reliable than numerical analysis alone. Aberson (2009) identifies some pitfalls of statistical analysis and emphasizes the need to be cautious with statistical inferences. Nevertheless, Kotal et al. (2008) demonstrates that statistical analysis of the TCs in the Bay of Bengal yields useful results.

This study attempts to perform some statistical analysis with a view to developing a model that is capable of predicting the cyclonic activity over Bangladesh. There is considerable literature available on forecasting of cyclones. A brief summary of the forecasting techniques in use is presented in Tropical Cyclone Forecasting. These forecasting techniques have been very useful to save lives. However, the forecasting techniques are considered reliable for up to 72 h. In Bangladesh context, where majority of the population in the coastal areas is rural poor living on subsistence farming in deltaic flats, a forecast lead time of several weeks or months can be of enormous benefit. Where physics-based models do not seem to offer any plausible solution to the problem of long-term forecasting, a black box model such

as a regression model or Box-and-Jenkins type of models have been applied in many areas of science to derive useful knowledge in long-term outlooks. This is the primary strategy and motive that underpins this analysis. There can be many steps in statistical analysis beginning from prewhitening or detrending of data to residual analysis. To accomplish all the tasks comfortably an open-source free software product WEKA has been used. The software package has not been described in this chapter, but detailed information about the product is available in Ali and Wasimi (2007). In Section Is There a Trend in Cyclonic Activity over Bangladesh? the trend characteristic of cyclonic activity in Bangladesh is analyzed. The fourth section is on data selection process and source. The fifth section is on statistical modeling. The chapter ends with some concluding remarks.

Tropical Cyclone Forecasting

The destructive power of a TC lies in its maximum sustained wind speed and the atmospheric pressure drop that it creates, which is responsible for violent seas. Forecasting in this context may mean several things or their combinations. Forecasting can be of the maximum sustained surface wind speed, height of the storm surge, or track of the TC. Forecasting of the maximum sustained surface wind speed has not received much attention in published literature because normally a cyclone would attain its maximum potential intensity unless an adverse factor such as strong steering current or high vertical wind shear prevails. Commonly, Dvorak's (1984) method of analyzing satellite data is used to estimate a cyclone's intensity. Most of the focus of published literature, however, is on the track of a TC. The forecasting techniques for cyclone tracking can be loosely grouped into the categories of persistence-based, climatology-based, synoptic technique-based, satellite-based, dynamics-based, and statistics-dynamics-based.

Persistence-based techniques use some sort of polynomial fit to extend the path already traced out into the future. In advanced methods a form of regressive filter such as Kalman filter is used. In climatology-based technique, searching is done in the historical record to find similar cyclones within a preset spatial, seasonal, and translational velocity range of the cyclone to be forecasted. The forecast track is derived as the mean of all these cyclones. A significant number of meteorologists believe that cyclones are carried by the steering current along its way. According to them, therefore, a cyclone's track can be determined by the direction of the environmental flow. Synoptic technique-based methods use historical observations of a cyclone's translation in the context of its relative location with features such as subtropical ridge, upper-level troughs, and quasi-stationary features such as Tibetan High. Satellite-based techniques involve interpreting satellite imagery of cloud patterns. The pioneering work in this regard was done by Dvorak. Cloud bands in outer circulation can indicate the direction of translation. Dynamics-based techniques are essentially numerical models solving analytical equations, which can range from simple conceptual models to complex distributed models integrated over many days

on a global domain. Statistics-dynamics-based techniques use output from a numerical model to be filtered by statistical parameters, which are obtained from statistical screening of past storms.

Intuitively, statistics-dynamics-based techniques are the most reliable because it uses both physics and statistics. This is supported by evidences at many cyclone forecasting centers. For example, CSUM used by JTWC, NHC90 used by NHC (National Hurricane Center), and SD75 used by China showed consistent improved performance over other techniques. The usefulness of the dynamical component begins to fade as we extend the forecasting lead time beyond 72 h. Therefore, when we are seeking a forecasting lead time of several weeks or months, the only tool available to us is apparently statistical techniques.

Is There a Trend in Cyclonic Activity over Bangladesh?

Development of a statistical model often requires that the data satisfy the condition of wide sense stationarity. If the data is not stationary, usually data transformation is implemented to render stationarity in the data. One such basic transformation is detrending. Whether detrending is required would depend on if there is any trend in the data. To seek an answer to this question, historical cyclone activity in Bangladesh is analyzed.

EM-DAT (The OFCA/CRED International Disaster Database, Brussels, Belgium) has time series data of the number of destructive tropical storms that lashed Bangladesh over the years. This information is captured in Fig. 1. Khan et al. (2000) after analyzing data of the Bay of Bengal for the period 1877–1998 obtained from

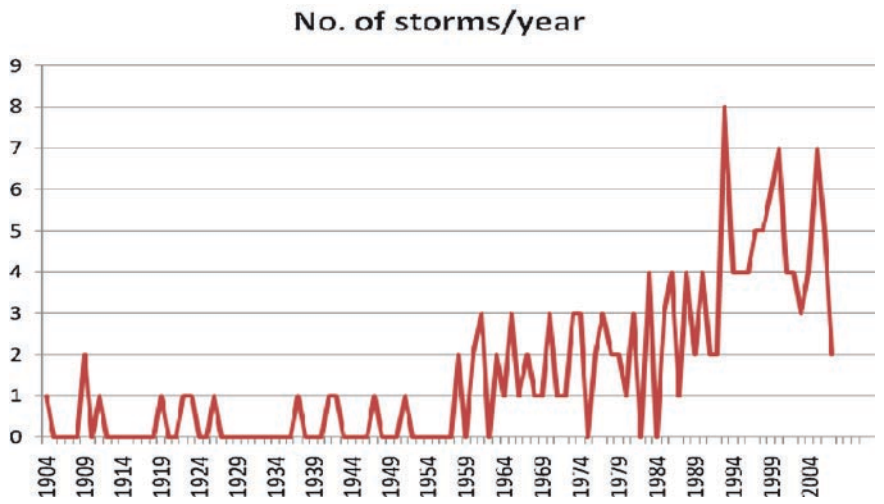

Fig. 1 Number of destructive tropical storms in Bangladesh occurring annually

the India Meteorological Department (IMD) claim that there is a positive trend in cyclonic activity with a gradient of 0.0027 per year in May and 0.0067 in November, which is correlated with rising SST with a significance level of above 90%. In this study, an independent investigation is done using the concept of NTA proposed by Kwon et al. (2007). The focus is only on TC, but not on tropical depressions. A TC is assumed to be formed when the maximum sustained surface winds (MSSW) is 34 knots or above. A tropical depression has a wind speed of 33 knots or less. This is in accordance with the Global Tropical Cyclone Climatic Atlas (GTCCA) and also with WMO classification Islam and Peterson (2009). According to Kwon et al. Normalized Typhoon Activity (NTA) is given by the relation

$$\mathrm{NTA} = \sum \frac{1}{4}\left(\frac{V_{\max}}{V_{\mathrm{TY}}}\right)^2$$

where the summation is over the total cyclone duration, $V_{\max}$ is maximum wind speed at 6 h intervals, V_{TY} is typhoon wind speed, which is 64 knots, and division by 4 is because cyclone information is issued four times a day by JTWC. JTWC data is used in this analysis.

To look into the significance in trend of annual NTA of the Bay of Bengal, rather than seeking a significant numeric value for the slope, which can be doubtful unless confidence intervals are properly captured, a nonparametric approach was adopted that can yield a simple "yes" or "no" answer to the question if the cyclone activity is really increasing. In this approach, first, a jack-knife analysis was done where the data were divided roughly into two equal parts: one part consisting of data for the period 1971–1989 and the other part consisting for the period 1990–2008. Next, Wilcoxon signed-rank test (Miller and Miller 1999) was performed with the alternative hypothesis that the mean for the period 1990–2008 is greater than the mean for the entire period, which is 1971–2008. The annual mean NTA for the entire period is 8.10. T^+ for the hypothesis test is found to be 102, T^- is found to be 69, and $T = 69$. The critical T value at 1% level of significance is 33 and at 5% level of significance is 47. The critical values are lower than the T value, and therefore, we cannot reject the null hypothesis. To seek further corroboration of this statistical inference more tests were performed. In published literature, there are three methods, which have been recommended by WMO and other agencies to test for the existence of significant trends in time series data – Mann-Kendall (M–K) test, Spearman rank correlation (SRC) test, and the least squares linear regression (LR) test. LR test outcome has been presented earlier as performed by Khan et al. M–K test is a nonparametric test (for details see Xu et al. 2005) which requires the data to be prewhitened if there is autocorrelation in the data. A plot of autocorrelation function (ACF) showed no significant autocorrelation and therefore no prewhitening was necessary. After doing the computations, it has been found that $S = 100$, Var $(S) = 5{,}846$ and $Z = 1.31$. Since Z is less than the critical value of 1.96 for 95% confidence level, the null hypothesis could not be rejected. For the SRC test (for details see Khaliq et al. 2009) Σd_i^2 is found to be 7,374, $r_{\mathrm{SRC}} = 0.1259$, and $t_{\mathrm{SRC}} = 0.75$. The critical t value for 5% level of significance is 2.02 and therefore the null

hypothesis could not be rejected for this situation as well. Thus, both parametric and nonparametric analyses lead consistently to one conclusion that there is no sufficient evidence to infer that cyclonic activities are increasing in the Bay of Bengal though it contradicts with the inferences made earlier by Khan et al. (2000) and Webster et al. (2005). One criticism that can be made of the analysis just presented is the shortness in the length of the data. This criticism would not affect the modeling efforts made in this chapter because the intended projection into the future is of much shorter length compared to the past period analyzed.

In fact further analysis by the author of other variables, which could be related to the cyclonic activity over Bangladesh revealed that it cannot be conclusively established if there is any trend in any of the variables. Nor could it be established if there is any temporal change in the standard deviation of the data. These analyses were routinely done mostly visually using the software package WEKA. It is therefore, perhaps, logical to state that simple statistical relationship can be developed from the data without the need to perform any kind of transformation of the data.

Data Selection and Source

Two aspects of tropical cyclones, which are important in Bangladesh context are rapid intensification and recurvature. Rapid intensification causes the cyclone to attain devastating levels of maximum sustained surface winds (MSSW). There exists a relationship between MSSW and MSLP (minimum sea-level pressure), which in turn determines the height of the storm surge. For a tropical cyclone situation the relationship between MSSW and MSLP can be dynamically captured by a cyclostrophic wind equation of the form $V_m = a(b - p)^c$, where V_m is MSSW in knots, p is MSLP in millibars, and a, b, and c are constants determined by least squares. There are other methods as well which are used to capture the wind–pressure relationships such as by Atkinson and Holliday (1977) and Dvorak (1975). In this study the analysis of the cyclone data of the Bay of Bengal for the period 1971–2008 yields the following cyclostrophic equation.

$$V_m = 6.0(1011 - p)^{0.67} \tag{1}$$

Equation 1 has a coefficient of determination (R-square) value of 0.9558 and is different from the relationships given by Brown et al. (2009) for other oceans. This R-square value is also higher than that reported by Brown et al. for other oceans. This means that if we know MSSW, we can reliably estimate MSLP, which in turn can be used to estimate the height of the storm surge that would hit Bangladesh coast using a two-dimensional hydrodynamic model. Hydrodynamic modeling is not within the scope of this study, and therefore, the focus has been confined within the hydro-meteorological variables that contribute to MSSW.

However, the other aspect of a cyclone, we cannot ignore is the track. Cyclones do not form within a band of 5° latitude around the equator because of the low

Coriolis effect. In the Bay of Bengal it forms mainly in the region 5°N–15°N and 85°E–95°E. Once formed a cyclone tends to move poleward and westward. If this is the case, Bangladesh would not be in the path of a cyclone. When a cyclone changes its course and turns eastward, the process is called recurvature. With recurvature Bangladesh coast is likely to fall into the path of a cyclone formed in the Bay of Bengal. Thus, for TC predictive purposes recurvature as a response variable should be considered along with MSSW.

The hydro-climatic factors, which have been identified to influence rapid intensification and recurvature in TCs of the Bay of Bengal from literature survey and correlation analysis within MDR are sea-surface temperature (SST), ocean temperature up to a depth of 60 m, sea-level pressure (SLP), vertical wind shear, latent heat flux (proxy for atmospheric moisture), wind speed, and curl of wind; and outside MDR are atmospheric temperature over land in Delhi and ENSO. Data on MSSW of cyclones, their tracks, and wind speed were obtained from JTWC in Hawaii (1971–2008). SST and other ocean–atmosphere interface data were obtained from NOAA-NCDC-ERSST. Vertical water temperature profile data was obtained from Carton-Giese SODA data. Climatic indices and other data were obtained from KNMI. The temperature data of Delhi was obtained from IMD.

Since the focus of this study is long-term forecasting, only monthly values were used in the statistical analysis. The dependent variables were the NTA, which follows from the concept of kinetic energy of a cyclone, and recurvature, which has been considered as a binary variable with 0 indicating no recurvature and 1 indicating at least one recurvature. Each independent variable had at most 12 values, six values at lags 1–6 and six values of standard deviation within MDR also for lags 1–6. The truncation at lag 6 is based on the assumption that the system memory for the genesis of a cyclone does not extend beyond 6 months. Also, lag 0 data were not considered since we are interested in prediction of one or more months in advance. Obviously, such a selection of independent variables would have significant cross-correlations. To avoid problems associated with high cross-correlations such as multicollinearity problem it is necessary to restrict use of multiple highly correlated variables as inputs in the formulation of a forecasting model.

Statistical Modeling

Statistical modeling in this study has been done using the software package WEKA. It is an open-source data-mining tool developed at The University of Waikato, New Zealand. The software is downloadable for free from the web site http://www.cs.waikato.ac.nz/ml/weka/. WEKA is written in java and therefore can be used with any platform. Once successfully installed the opening window will look similar to Fig. 2. WEKA has graphical user interface (GUI) and therefore there is no need to write the code to run any program. Once we click on the explorer button, it will come up with the menu where we can enter the data as external files and select the statistical method that we wish to apply. WEKA has provisions for preprocessing

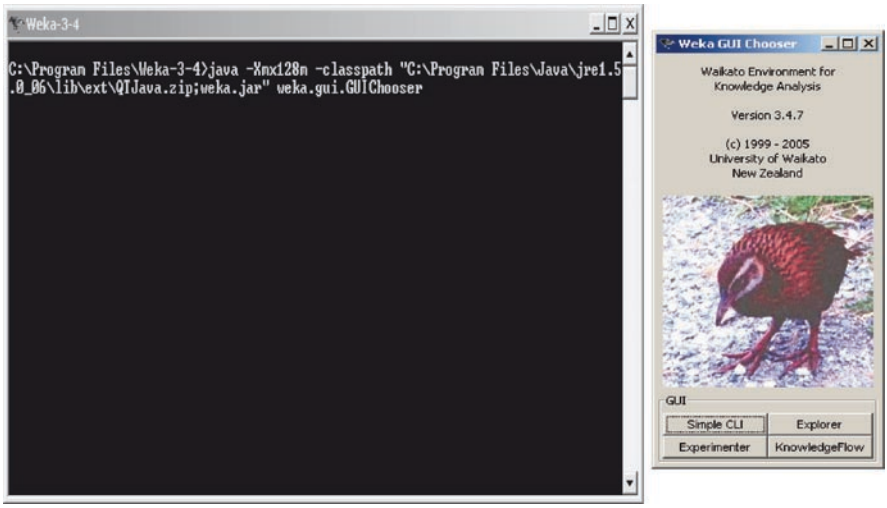

Fig. 2 WEKA opening window

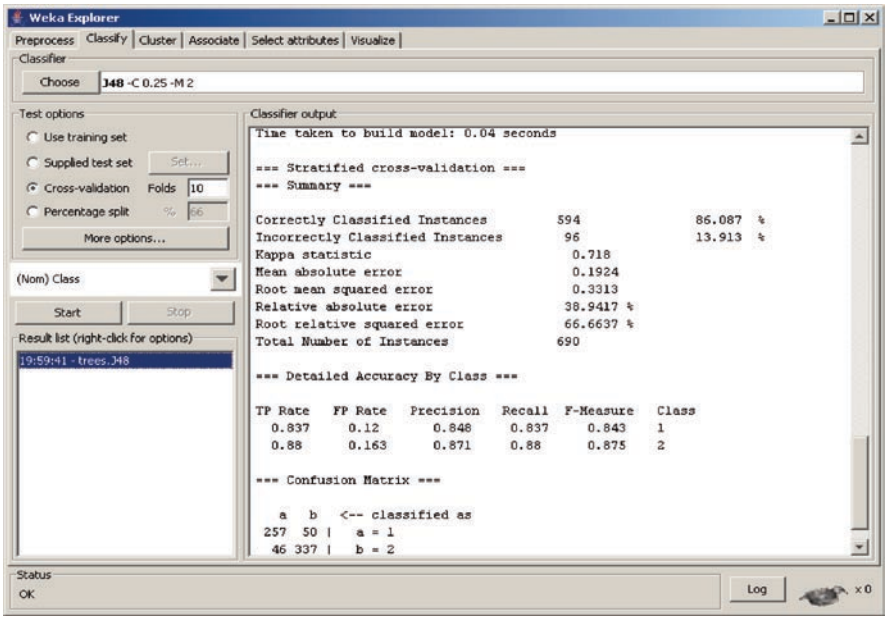

Fig. 3 The output screen of WEKA

or prewhitening of data if required. Once the program is executed by clicking on the *Start* button the output screen will look similar to Fig. 3. The output can be viewed on the screen, saved as a text file, or printed. For further information the reader is referred to Ali and Wasimi (2007).

The first step that was undertaken in the development of the statistical model was to perform a principal component analysis of the input variables. This yielded nine significant principal components. It was therefore decided for simplicity that each model – one on NTA and the other on recurvature – will be allowed to have a maximum of nine independent variables and no two of them can have a cross-correlation, which has been identified as significant in the correlation analysis procedure. For the NTA model a stepwise linear regression model was adopted. In the first iteration the two independent variables, which were selected by the procedure are SLP_{t-2}, and $D57T_{t-2}$, where $D57T_{t-2}$ is the subsurface water temperature at a depth of 57 m 2 months earlier. The first procedure yielded an *R*-square value of 0.62. Next these two variables were removed from the database and stepwise regression was done again. In the second iteration SST_{t-2} was selected. For the third iteration SST_{t-2} was removed from the database before rerunning the stepwise regression procedure, which resulted in $Wind_{t-2}$ to be selected as the next variable. The procedure kept on being repeated till nine independent variables were selected, which ultimately yielded an *R*-square value of 0.84. For the recurvature model a similar procedure was followed. In the first iteration SST_SD_{t-2} was selected, in the second iteration $CWind\_SD_{t-2}$ was selected, and so on, where SST_SD_{t-2} is the standard deviation of SST within MDR and $CWind\_SD_{t-2}$ is the standard deviation of the curl of the wind within MDR.

Linear regression models as the name implies linearize the real-world relationships, which are hardly ever linear. To check the nonlinearity of the problem two techniques on artificial intelligence were applied to the data; one is artificial neural networks (ANN) and the other is the support vector machines (SMO). For the NTA model ANN yielded an *R*-square value of 0.94 and SMO yielded an *R*-square value of 0.81 compared to 0.84 by linear regression for nine independent variables. These have been essentially curve-fitting exercises and their suitability as a predictive tool can only be judged if part of the data is used for model development and the rest of the data are used for model testing. The industry practice is to use 70% of the data for training and 30% of the data for testing. With testing for predictability, the ANN approach turned out to be the best in selecting the number of the independent variables that is most suitable for prediction. The ANN approach for the best NTA model suggested that six independent variables can be used, which are SLP_{t-2}, $D57T_{t-2}$, SST_{t-2}, $Wind_{t-2}$, LHF_SD_{t-2}, and VW_Sheart_{t-1}, where LHF stands for latent heat flux and VW_Shear stands for vertical wind shear. The ANN approach further suggested that the best recurvature model comprises of the four variables: SST_SD_{t-2}, $CWind\_SD_{t-2}$, SLP_{t-2}, and $D57T_{t-2}$. The probability of correct prediction for NTA with these variables is around 0.70 and that for recurvature is around 0.61.

Conclusion

The main cyclone seasons in the Bay of Bengal are October–November and May, when devastating cyclones make landfall. Advance warning of the category of a cyclone is now available a few days ahead. Due to poor infrastructure in the region

and agriculture being the primary economic activity, a forecast of at least a month in advance would be of immense benefit to the population. With that in view a forecasting model comprised of hydro-climatic variables with a forecast lead time of several months was attempted. It has been found that development of such a model is possible, which would be able to predict if a powerful cyclone is likely or unlikely in the coming season with about a months lead time. Few of the interesting discoveries made during this modeling exercise are that ENSO has no influence on the predictability or on the land temperature. The factors that control the formation of future cyclones entirely lie within the main development region. While the absolute values of the hydro-meteorological parameters tend to influence the NTA, it is the variation of these parameters that tend to influence the recurvature. It should however be pointed out here that the analysis has been done with limited data. The conclusions could be different if longer periods of data are analyzed or a different ocean is considered.

The statistical analysis in this study was mostly confined within the framework of regression analysis, and the final result was the selection of the hydro-meteorological variables that can serve as explanatory variables. No final regression model has been presented in order to leave the option to an analyst of selecting any linear or nonlinear models. The cyclones that hit the coast of Bangladesh are fairly predictable in terms of time of the year when they can be expected, but unpredictable as to their ferocity and track. The modeling approach suggested in this chapter is capable of predicting the likelihood of these two characteristics about a month in advance. For a more useful picture on prediction a hydrodynamic model depicting the storm surge is relevant because the fatalities and destruction are not caused so much by the wind as by the storm surge.

References

Aberson SD (2009) Regimes or cycles in tropical cyclone activity in the North Atlantic. Bull Am Meteor Soc 90:39–43. doi:10.1175/2008BAMS2549.1

Ali A (1996) Vulnerability of Bangladesh to climate change and sea level rise through tropical cyclones and storm surges. Water Air Soil Pollut 92:171–179

Ali S, Wasimi SA (2007) Data mining: methods and techniques. Thomson, Australia, p 299

Atkinson GD, Holliday CR (1977) Tropical cyclone minimum sea level pressure/maximum sustained wind relationship for the western North Pacific. Mon Wea Rev 105:421–427

Brown DP, Franklin JL, Landsea C (2009) A fresh look at tropical cyclone pressure-wind relationships using recent reconnaissance-based "best track" data (1998–2005). NOAA/NWS/NCEP/Tropical Prediction Center, Miami, FL. http://ams.confex.com/ams/pdfpapers/107190.pdf. Accessed on 17 April 2009

Camargo SJ, Emanuel KA, Sobel AH (2007) Use of a genesis potential index to diagnose ENSO effects on tropical cyclone genesis. J Climate 20:4819–4834

DeMaria M, Knaff JA, Connell BA (2001) A tropical cyclone genesis parameter for the North Atlantic. Wea Forecast 16:219–233

Dvorak VF (1975) Tropical cyclone intensity analysis and forecasting from satellite imagery. Mon Wea Rev 103:420–462

Dvorak VF (1984) Tropical cyclone intensity analysis using satellite data. National Oceanic and Atmospheric Administration, Washington, DC, NOAA-TR-NESDIS-11

Emanuel K (2008) The hurricane-climate connection. Bull Am Meteor Soc 89:ES10–ES20. doi:10.1175/BAMS-89-5-Emanuel

FNMOC (1998) Data base description for global tropical cyclone tracks (GTCT). Public release for distribution by Fleet Numerical Meteorology and Oceanography Center, Asheville

Frank WM, Young GS (2007) The interannual variability of tropical cyclones. Mon Wea Rev 135(10):3587–3598

Islam T, Peterson RE (2009) Climatology of landfalling tropical cyclones in Bangladesh 1877–2003. Nat Hazards 48:115–135

Khaliq MN, Ouarda TBMJ, Gachon P, Sushama L, St-Hilaire A (2009) Identification of hydrological trends in the presence of serial and cross correlations: a review of selected methods and their application to annual flow regimes of Canadian rivers. J Hydrol 368:117–130

Khan TMA, Singh OP, Rahman MS (2000) Recent sea level and sea surface temperature trends along the Bangladesh coast in relation to the frequency of intense cyclones. Mar Geodesy 23:103–116

Kotal SD, Bhowmik SKR, Kundu PK, Das AK (2008) A statistical cyclone intensity prediction (SCIP) model for the Bay of Bengal. J Earth Syst Sci 117(2):157–168

Kotal SD, Kundu PK, Bhowmik SKR (2009) Analysis of cyclogenesis parameter for developing and nondeveloping low-pressure systems over the India Sea. Nat Hazard. doi: 10.1007/s11069-009-9348-5

Kwon HJ, Lee W-J, Won S-H, Cha E-J (2007) Statistical ensemble prediction of the tropical cyclone activity over the western North Pacific. Geophys Res Lett 34:L24805. doi:10.1029/2007GL032308

Lee C-S, Cheung KKW, Hui JSN, Elseberry RL (2008) Mesoscale features associated with tropical cyclone formations in the western North Pacific. Mon Wea Rev 136(6):2006–2023

Mandal M, Mohanty UC, Sinha P, Ali MM (2007) Impact of sea surface temperature in modulating movement and intensity of tropical cyclones. Nat Hazards 41:413–427

Miller I, Miller M (1999) John E. Freund's mathematical statistics, 6th edn. Prentice Hall, Englewood Cliffs, NJ

Nicholls N (2001) Atmospheric and climatic hazards: Improved monitoring and prediction for disaster mitigation. Nat Hazards 23:137–155

Ralph TU, Gough WA (2009) The influence of sea-surface temperatures on Eastern North Pacific tropical cyclone activity. Theor Appl Climatol 95(3–4):257–264

Singh OP, Khan TMA, Rahman MS (2001) Has the frequency of intense tropical cyclones increased in the north Indian Ocean? Curr Sci 80(4):575–580

Vecchi GA, Soden BJ (2007) Effect of remote sea surface temperature change on tropical cyclone potential intensity. Nature 450. doi: 10.1038/nature06423

Webster PJ, Holland GJ, Curry JA, Chang H-R (2005) Changes in tropical cyclone number, duration, and intensity in a warming environment. Science 309:1844–1846

Xu ZX, Takeuchi K, Ishidaira H, Li JY (2005) Long-term trend analysis for precipitation in Asian Pacific FRIEND river basins. Hydrol Process 19:3517–3532

Zeng Z, Wang Y, Wu C-C (2007) Environmental dynamical control of tropical cyclone intensity – an observational study. Mon Wea Rev 135(1):38–60

JTWC (2007) Annual tropical cyclone reports. Joint Typhoon Warning Center, Pearl Harbor, Hawaii

THORPEX and Its Application for Nargis by Ensemble Prediction

Tetsuo Nakazawa, David Parsons, and Takuya Komori

Keywords Nargis TC • numerical probabilistic weather forecast systems • THORPEX

THORPEX

THORPEX is a 10-year international global atmospheric research program under the World Meteorological Organization (WMO)/World Weather Research Program (WWRP) to accelerate improvements in the accuracy of 1-day to 2-week high-impact weather forecasts and in society's utilization of weather products. The program was established in May 2003 by the 14th WMO Congress. THORPEX is a key research meteorological component of the WMO Natural Disaster Reduction and Mitigation Programme. It will contribute to WMO's goal to halve the number of deaths due to natural disasters of meteorological, hydrological, and climatic origin over the next 15 years, by conducting a series of regional and global projects, including experiments on improvements in forecast skill, targeted satellite and in situ observation, data assimilation, numerical probabilistic weather forecast systems, and demonstrations on societal and economic benefits of improved forecasts. Asian THORPEX Regional Committee (ARC) is the focal point in the Asian region to implement the THORPEX-related activities for tropical cyclones, severe rainfalls, MJO, and sand/dust storms.

T. Nakazawa (✉)
Meteorological Research Institute, Japan Meteorological Agency

D. Parsons
THORPEX International Program Office, WMO

T. Komori
Numerical Prediction Division, Japan Meteorological Agency

Y. Charabi (ed.), *Indian Ocean Tropical Cyclones and Climate Change*,
DOI 10.1007/978-90-481-3109-9_18,

JMA Weekly Ensemble Prediction of Nargis

As an example of THORPEX application, using the JMA weekly ensemble prediction system (Table 1), the evolution of Nargis has been examined, especially focusing on landfalls on Myanmar, by changing initial times.

Figure 1 shows the ensemble track forecasts of Nargis with different initial times, from April 23–29 every 2 days. It is notable that several members from April 23 could simulate the landfall of Nargis on Myanmar.

Figure 2 shows the number of members which forecasted landfall on Myanmar and genesis in different initial times. The number of landfall/genesis members increases in time, with some decrease on April 27 and 28. At the initial time of April 23, out of 50, there are 18 members which forecasted landfall on Myanmar. An evolution of the sea-level pressure for Nargis in an ensemble member, which simulated the landfall on Myanmar, starting from April 23, is shown in Fig. 3.

We can see the presence of Nargis more easily in the ensemble spread, as is shown in Fig. 4. This shows the ensemble spread of the sea-surface pressure in the ensemble forecasts with the initial time of April 23. As expected, the region with large spread, shown by warm colors, implies the occurrence of Nargis within the variability (position and intensity).

Summary

As an example of THORPEX application, using the JMA weekly ensemble prediction system, the evolution of Nargis has been examined, especially focusing on landfalls on Myanmar, by changing initial times. Out of 51 members (including the control run), there are more than 30% of members, which predicted the landfall on Myanmar before the genesis period. Nargis was formed on April 27 and landed on May 2 and thus the duration is 5 days; however, the JMA ensemble data show that there are several members showing landfall on Myanmar even 7 days earlier than the landfall date (May 2, 2008). Some members tend to move northward toward the northern

Table 1 Specification of the JMA Weekly ensemble forecast system

Initial time	12UTC
Forecast hours	216 h
Horizontal resolution	TL319 (0.5625°, 60 km)
Vertical resolution	60 Levels (surface ~ 0.1 hPa)
Number of members	51 (50 members + control run)
Perturbation generation	Singular vector method
SV calculation area	North hem.: 30°N–90°N Tropics: 20°S–30°N
Resolution for SV calc.	T63L40
Norm for perturbation	Total energy

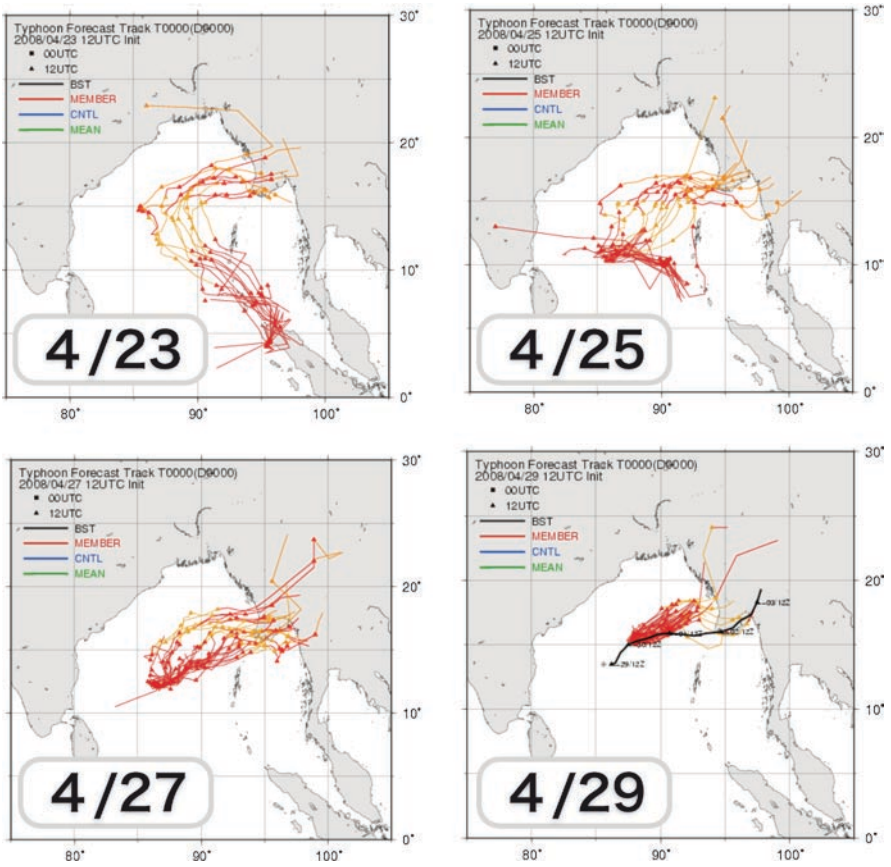

Fig. 1 Ensemble track forecasts of Nargis with different initial times

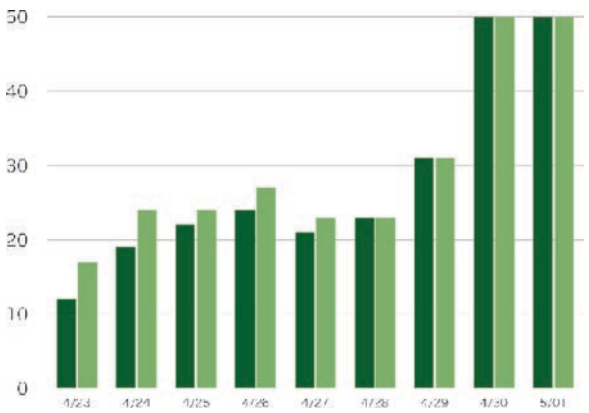

Fig. 2 Number of members, which forecasted Nargis landfall (dark green) and genesis (light green) with different initial times

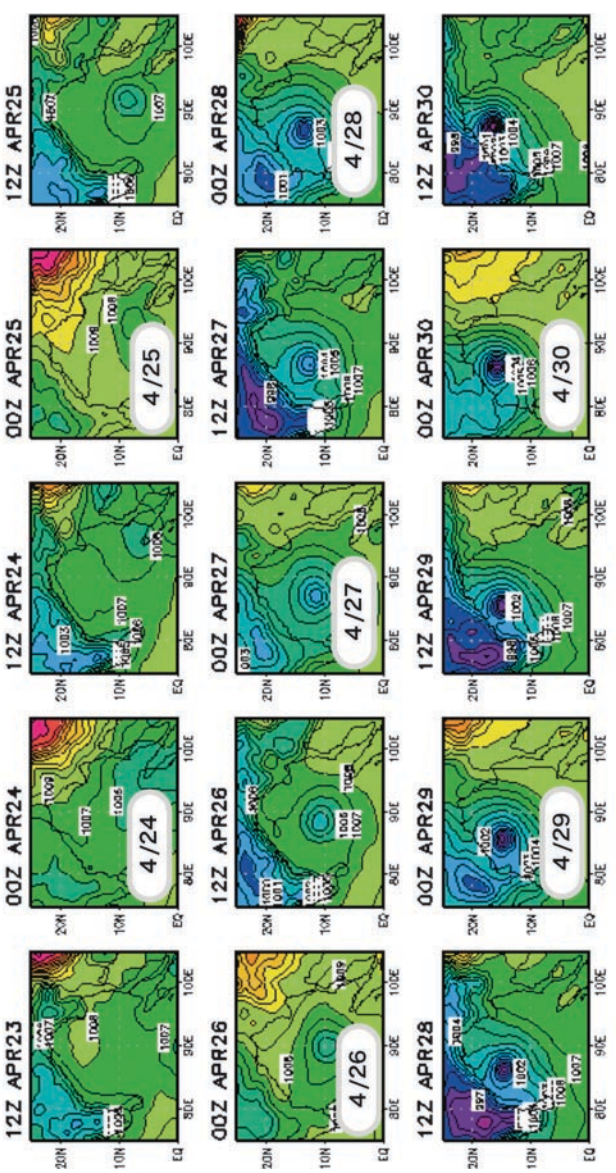

Fig. 3 An evolution of the sea-level pressure for Nargis in an ensemble member, which simulated the landfall in Myanmar, starting from April 23

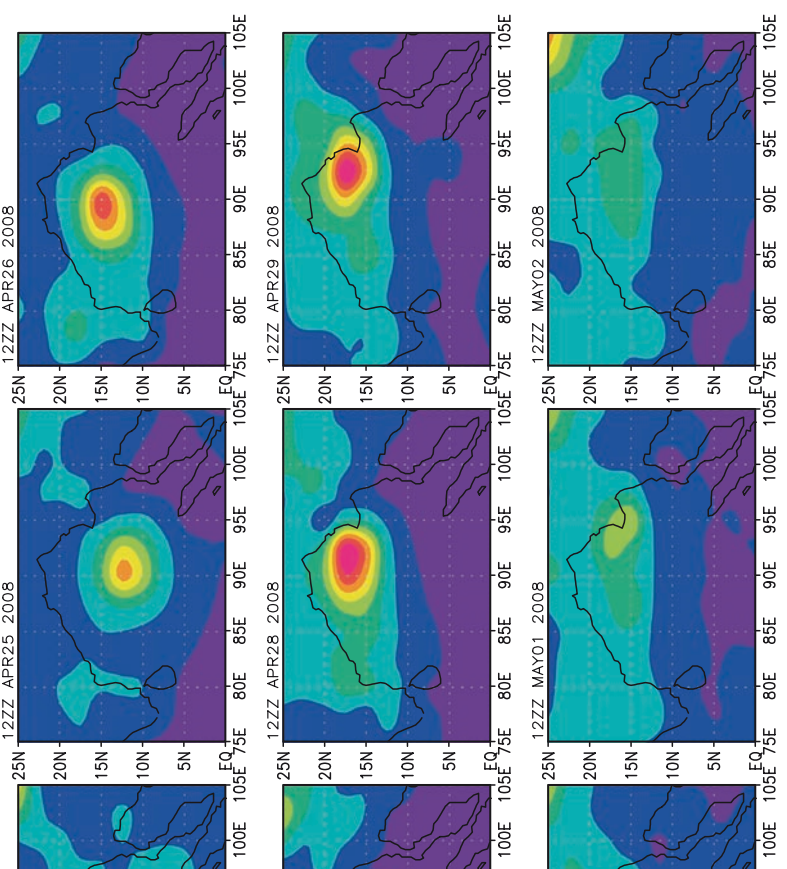

Fig. 4 Ensemble spread of the sea-surface pressure for Nargis from April 24 to May 2. Red (blue) color denotes the region with large (small) spread

Bay of Bengal. When we checked the reason for the track difference, we found that the steering flow, integrated between 1,000 and 300 hPa, tends to be south-westerlies for Myanmar landfall cases, but southerlies for non-landfall cases. The number of landfall predicting members gradually increases in time, suggesting that the JMA ensemble forecast data is capable of being utilized for early warning purposes.

Cyclone Gonu: The Most Intense Tropical Cyclone on Record in the Arabian Sea

Mohammad Dibajnia, Mohsen Soltanpour, Rob Nairn, and Mohammadreza Allahyar

Keywords 2DH and 3D numerical modeling • sediment transport

Introduction

The Oman Sea and its neighboring countries' (Iran and Oman) coastlines are subject to tropical cyclone influence on an infrequent basis; however, these cyclones can generate extremely large sea states. In general, cyclones generated in the Arabian Sea tend to travel either due west toward Oman or recurve north to strike Pakistan or India. They rarely enter the Oman Sea. Recently, in early June 2007, cyclone Gonu entered the Oman Sea and large waves were experienced along the Iranian and Omani coastlines. This cyclone had an unusual path, traveling much further west and north than the typical cyclone. Significant wave heights in excess of 4 m were measured at Chabahar located on the south coast of Iran bordering the Oman Sea.

A detailed investigation of the wave climate on the Oman Sea coastline of Iran has been recently carried out in support of a comprehensive study of coastal zone

M. Dibajnia (✉)
Associate, Baird & Associates, Canada
e-mail: mdibajnia@baird.com

M. Soltanpour
Assistant Prof., Civil Engineering Department,
K.N. Toosi University of Technology, Iran
e-mail: soltanpour@kntu.ac.ir

R. Nairn
Principal, Baird & Associates, Canada
e-mail: rnairn@baird.com

M. Allahyar
Head of Coastal Engineering Office,
General Directorate of Coast and Port Engineering,
Ports and Maritime Organization, Iran
e-mail: allahyar@ir-pso.com

Y. Charabi (ed.), *Indian Ocean Tropical Cyclones and Climate Change*,
DOI 10.1007/978-90-481-3109-9_19, © Springer + Business Media B.V. 2010

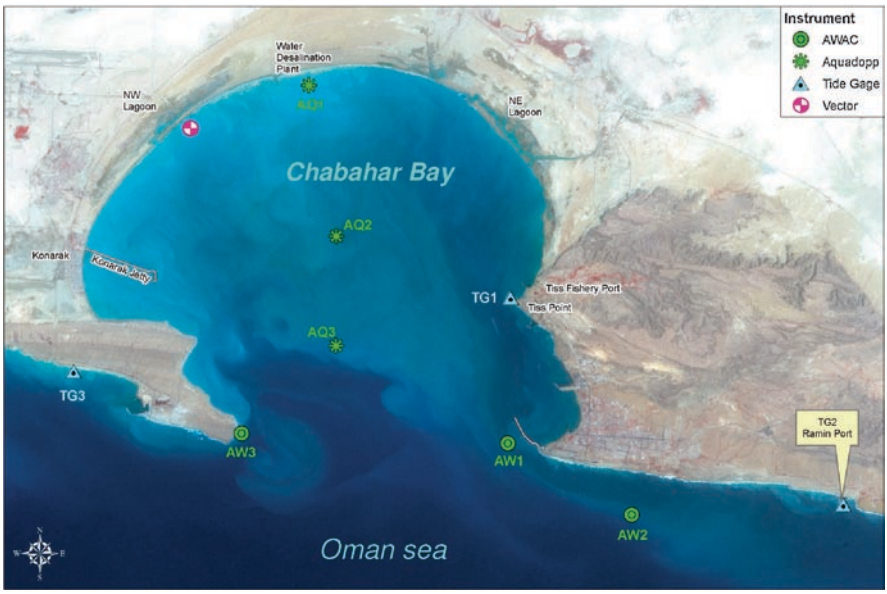

Fig. 1 Instrument locations during cyclone Gonu event (June 2007)

processes (project MONITOR SB&B by Ports and Maritime Organization of Iran) in Chabahar Bay area. The project involved an extensive 1-year field measurement campaign, a 25-year wave hindcast for the Oman Sea and various 2DH and 3D numerical modeling of hydrodynamics and sediment transport in Chabahar Bay. The field measurement campaign involved measurements of waves and currents at six locations, water levels at three locations, and winds at one location. Figure 1 shows locations of the instruments at the time of cyclone Gonu. The present paper provides a summary of cyclone wave climate investigation conducted in the above study for the Oman Sea.

Historical Tropical Cyclones

An assessment of historical tropical cyclones was undertaken using the following tropical cyclone datasets:

- The US Navy Joint Typhoon Warning Center (JTWC) "Best Track" digital dataset. The current version of this dataset covers the period from 1945 to 2003.
- Historical Tropical Storm and Depression tracks available from the India Meteorological Department in printed format. These data were used to evaluate cyclones occurring prior to 1945.

Assessment of Digital "Best Track" Data (1945–2003)

The JTWC "Best Track" data are based on a reanalysis of historical cyclone data to provide "best" estimates of each cyclone track and intensity on a 6-hourly basis. As the reanalysis of the data is undertaken on an irregular basis, the data provided are not fully up-to-date (i.e., to 2008). The "Best Track" tropical cyclone database was searched for storms within radial distances ranging from 250 to 1,000 km from Chabahar Bay near the eastern end of the Iranian coastline on the Oman Sea, as shown in Fig. 2. In the figure, cyclones that have peak wind speed data available are shown in color that varies with the wind speed. There were only 23 tropical cyclone tracks, starting in 1977, that contained wind speed data. It is also important to note that the wind speed estimates for the cyclones were likely derived by means of Dvorak analysis (using satellite imagery of cloud patterns), and are not the result of aircraft reconnaissance or Dropsonde data.

Figure 2 shows that the majority of the cyclones have occurred south and east, and at a significant distance from the Iranian coastline. This is important in that the height associated with cyclone-generated wave conditions reduces significantly with distance. The closest cyclone event to Iran in the "Best Track" dataset occurred in 1948 and was, at closest approach, approximately 250 km from Chabahar.

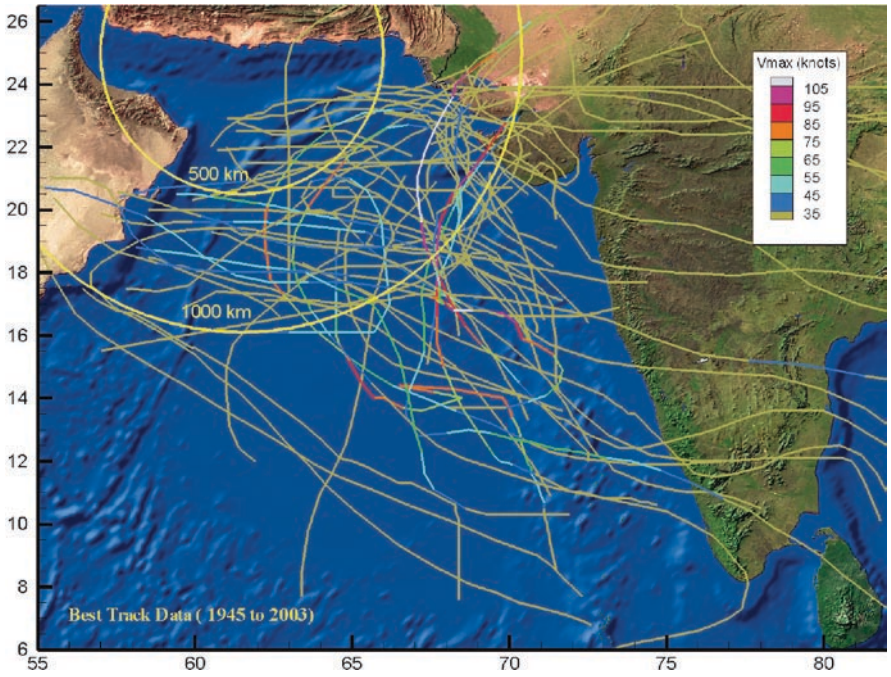

Fig. 2 Tropical storm tracks within 1,000 km of Chabahar on the Oman Sea Coastline

We note that cyclone Gonu, which is not in the Best Track dataset, approached in closer proximity to the Iranian coastline.

In general, the cyclones tend to travel either due west toward Oman or recurve north to strike Pakistan or India. Cyclones in close proximity to Iran (<300 km) are relatively infrequent. The dataset indicates that there are two distinct tropical cyclone periods: May to July; and September to November. As the southwest monsoon becomes more prominent during the summer months, the potential for tropical cyclones to develop is reduced.

Assessment of India Meteorological Department Cyclone Data

The India Meteorological Department compiled an extensive summary of cyclonic storm tracks for the period from 1877 to 1970. Review of the historical cyclone tracks showed that a number of Severe Tropical Storms entered the Oman Sea that would potentially generate large waves that would impact the Iranian shoreline. These events included storms from the following time periods: June 1889, June 1890, May 1898 and April 1901. The associated cyclone tracks are shown in Fig. 3.

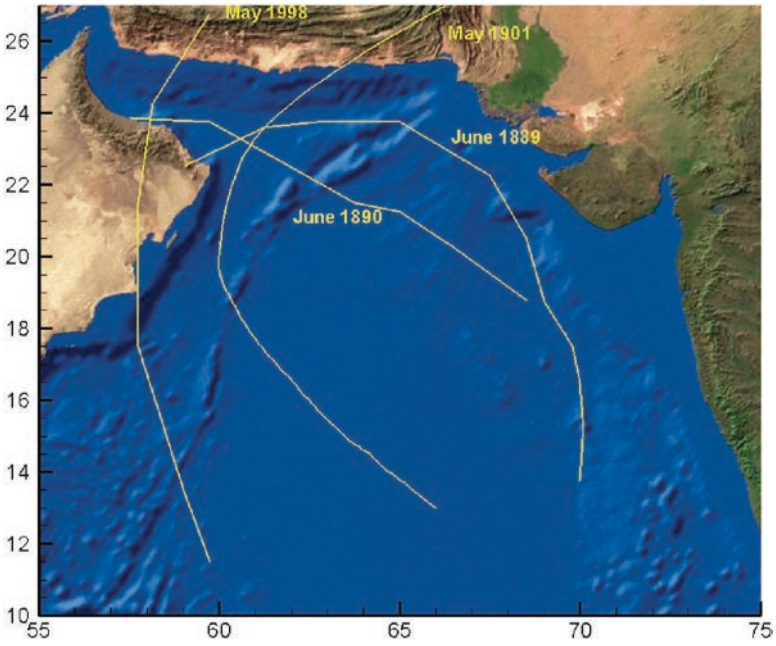

Fig. 3 Historical Cyclones from India Meteorological Dataset

It is worth noting that the "Best Track" data do not show the presence of storms with Severe Tropical Storm strength in as close proximity to the Iranian shoreline as the data from late 1800s and early 1900s. This may potentially indicate that there has been a temporal shift in the tropical cyclone climatology of this region. However, it is difficult to determine if there has been any significant change in cyclone frequency and patterns due to climate change. It is also possible that the wind speed estimates for the tropical cyclone events in the late 1800s and early 1900s may not be reliable. To verify the accuracy of these historical storms would require investigation into archival records.

Cyclone Gonu 2007

Cyclone Gonu, which existed from June 1 to 7, 2007, was the most intense tropical cyclone on record in the Arabian Sea. It developed from an area of persistent convection in the eastern Arabian Sea, and intensified to a Category 5 cyclone with maximum wind speeds of 250 kPh (140 knots) by June 4. The cyclone moved in a northwest direction, making landfall at the eastern-most tip of the Arabian Peninsula in Oman and then proceeded into the Oman Sea. The storm decreased in intensity as it moved northward from Oman.

AW2 sensor (Fig. 1) located in 30 m depth at Chabahar measured wave for this time period. Figure 4 provides a time-series plot showing significant wave height and peak wave period measured during Gonu. The waves achieved a maximum significant wave height of approximately 4.2 m with an associated period of 10 s. A maximum wind speed of 16 m/s from SE direction was measured in the evening on June 6.

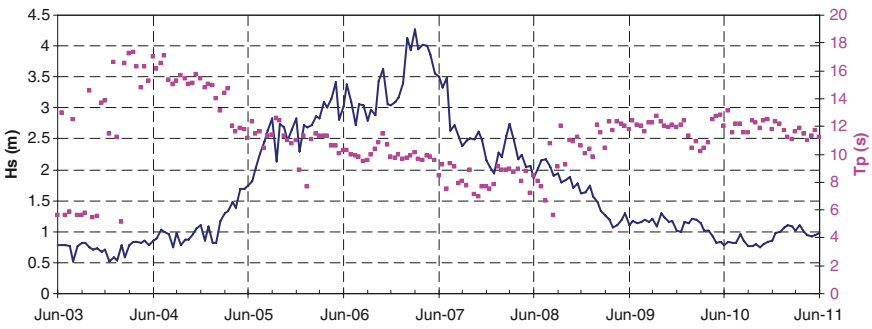

Fig. 4 Time series of waves at Chabahar (30 m depth) during Gonu

Simulation of Cyclones

Numerical modeling of tropical cyclone wave generation was used in this study to both simulate historical storm events and to investigate potential design wave conditions. The WAVAD model, as summarized in Resio (1981) and Resio and Perrie (1989), was used for the tropical cyclone wave simulations. This model was utilized for both purposes of computational efficiency and its accuracy in rapidly changing wind fields, such as occur in a tropical cyclone. Over 200 model simulations were carried out.

WAVAD is a second-generation (2G) spectral wave model that maintains equilibrium between the wind source and non-linear wave energy flux with an assumed f-4 shape for the wave spectrum. Inputs to the WAVAD model consist of a regular grid defining the shoreline and bathymetry in the region of interest as well as a spatially and temporally varying wind field defined at the grid points. Output from the model includes the spectral wave energy densities at all grid locations, from which standard parameters such as significant wave height (*Hs*), peak wave period (*Tp*), peak wave direction, and wave directional spreading are derived. The model grid had 191 longitudinal grid points and 171 latitude grid points at an equal resolution of 0.1°. A time step of 15 min was used in all of the simulations. A total of 23 frequencies were employed, ranging from 0.039 to 0.317 Hz, in conjunction with a directional resolution of 15° (24 directional bins). There are no calibration parameters within the WAVAD model.

The cyclone wind field model that was used to drive the WAVAD wave model was based on the parametric representation of Holland (1980). Input data to the wind field generation model included the cyclone path, and the peak wind speed, cyclone central pressure, distance to the maximum wind speeds (Rmax), and an empirical shape factor ("B"), all defined on a 6-hourly basis. Estimates of Rmax and B were derived from recent work by Willoughby et al. (2004) for Atlantic Ocean hurricanes. The output wind fields are defined on an hourly basis.

The results of numerical simulation of cyclones Gonu and the 1889 cyclone are presented here. Input parameters for cyclone Gonu were based on currently available track data from JTWC for this cyclone. It is important to note that these data are not complete and should be considered preliminary in nature; these data may vary in the future when more detailed reanalyses are carried out. For the 1889 cyclone, the India Meteorological Department reference (1979) does not identify the specific maximum wind speeds associated with reported cyclone events. It is only noted if the wind speed is greater than 50 knots. Therefore, cyclone simulations were carried out assuming a constant peak wind speed of 90 knots.

Figure 5 shows the maximum significant wave height estimated at each grid point throughout the passage of Gonu. Peak wave heights adjacent to the cyclone were in the order of 10 m when the cyclone entered the Oman Sea but reduced as the intensity of the cyclone decreased with time. Figure 6 shows a time series comparison to the waves measured at Chabahar. Excellent agreement was achieved between the measured and hindcast waves. Note that background wave conditions in the Indian Ocean were not included in the simulation, which would have little effect on the peak of the storm event but could affect the magnitude of lesser wave conditions before and after the cyclone passage.

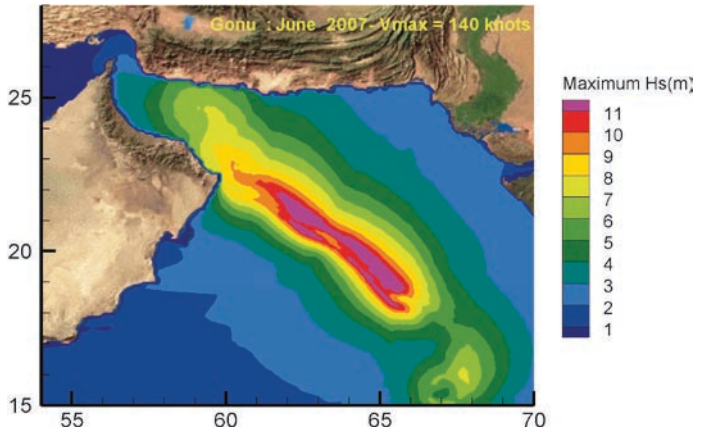

Fig. 5 Predicted maximum significant wave height in Arabian and Oman seas during Gonu

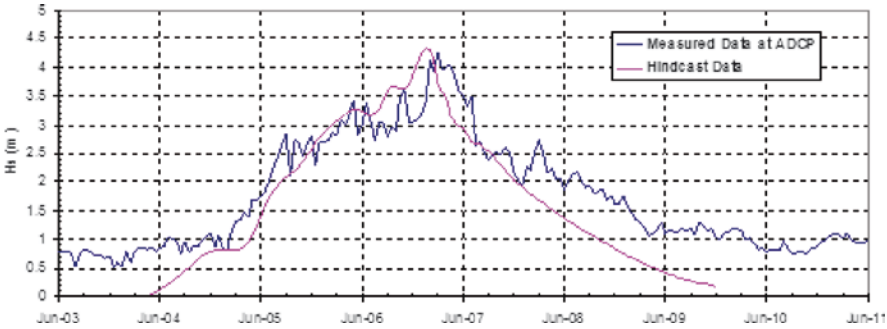

Fig. 6 Time series comparison of wave height at Chabahar (30 m depth)

Contour plot of the maximum significant wave height calculated at each grid point during the 1889 cyclone simulation is presented in Fig. 7. It may be noted that this cyclone event may have potentially created very large wave conditions along both Iranian and Omani coastlines in the Oman Sea. As noted previously, there is a fundamental concern as to the accuracy of this early data. There have been no similar events or cyclone tracks since 1945. However, the recent occurrence of cyclone Gonu does indicate the possibility that such events might readily occur.

Conclusion

Cyclone Gonu, which occurred from June 1 to 7, 2007, was the most intense tropical cyclone on record in the Arabian Sea. This cyclone entered the Oman Sea with high wind conditions, generating waves in excess of 9 m. Older historical tropical cyclone data (prior to 1945) indicate the occurrence of several cyclones within the Oman Sea and striking Iran, particularly in the late 1800s and early 1900s. Tropical cyclone

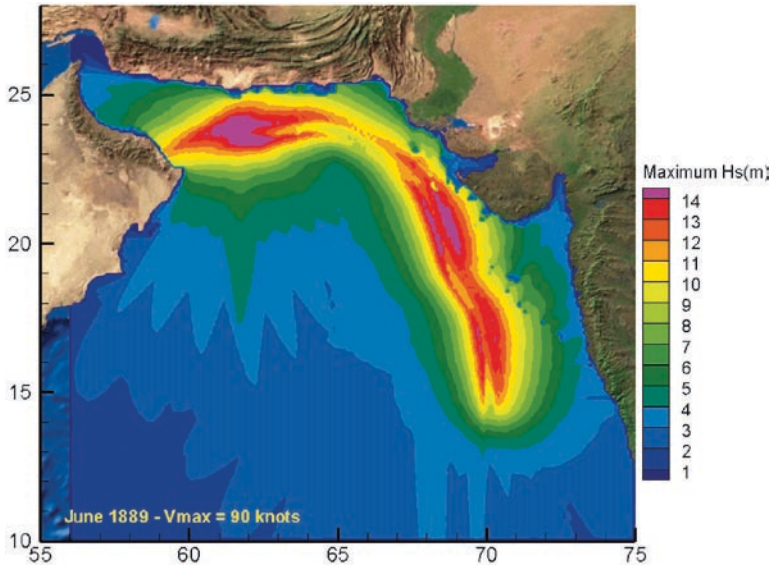

Fig. 7 Predicted maximum significant wave height in Arabian and Oman seas during the 1889 cyclone

data from the last 30 years, including Gonu, indicate maximum offshore design significant wave heights of up to 8.8 m along Iranian coastline. If the cyclone track data from the late 1800s and early 1900s are considered reliable, the potential for even larger cyclone design wave heights is feasible. As this potential variability in design wave height has a significant impact on the costs associated with coastal infrastructure, we recommend that a more detailed investigation of these historical events be carried out. Such an investigation would require research into historical records with a view to establishing the track and intensity of these events.

The data employed in this study have shown that there may be considerable temporal variability in the frequency of occurrence of tropical cyclones in the Arabian and Oman Seas, raising the possibility of climate change effects. We note that the technical community remains divided as to the potential effects of climate change on the frequency and intensity of tropical cyclones. A recent Statement on Climate Change effects by the World Meteorological Organization (2006), and one of the most thorough studies conducted by a number of cyclone experts, Henderson-Sellers et al. (1998) have indicated that there is insufficient historical information to determine if tropical cyclones are being affected by global warming.

References

Henderson-Sellers (1998) Tropical cyclones and global climate change: a Post-IPCC assessment. Bull Am Meteorol Soc 79:19–38

Holland G. (1980). An analytic model of the wind and pressure profiles in hurricanes. Mon Wea Rev 108:1212–1218

India Meteorological Department (1979) Tracks of storms and depressions in the Bay of Bengal and the Arabian Sea 1877–1970.

Resio D, Perrie W (1989) Implications of an f^{-4} equilibrium range for wind-generated waves. J Phys Oceanogr 19:193–204

Resio D (1981) The Estimation of wind-wave generation in a discrete spectral model. J Phys Oceanogr 11(4):510–525

Statement on Tropical Cyclones and Climate Change (2006). The World Meteorological Organization

Willoughby HE, Rahn ME (2004) Parametric representation of the primary hurricane vortex. Part I: observations and evaluation of the Holland (1980) model. Mon Wea Rev 132:3033–3048

The US Navy Joint Typhoon Warning Center (JTWC) "Best Track" digital dataset
http://metocph.nmci.navy.mil/jtwc.php

Real-Time Prediction of SIDR Cyclone Over Bay of Bengal Using High-Resolution Mesoscale Models

D.V. Bhaskar Rao and D. Srinivas

Keywords Quantitative weather prediction • mesoscale atmospheric models

Introduction

Tropical cyclones are known to be the most devastating of all natural disasters. These are intense vortices associated with lower surface pressure, strong winds exceeding 16 m/s, torrential rains, and storm surge. Numerical models based on well-defined dynamical and physical processes provide quantitative weather prediction. Numerical modeling studies of tropical cyclones are being continuously attempted since the 1960s to understand the physical and dynamical mechanisms of tropical cyclone development and movement. With the developments in atmospheric modeling and computer technology, mesoscale atmospheric models with non-hydrostatic dynamics are currently being used for tropical cyclone studies. In the present study, real-time numerical prediction experiments were performed of an intense tropical cyclone "SIDR" over the North Indian Ocean with NCAR WRF and MM5 models. The model-predicted intensification and movement of the tropical cyclone with these two different models have been compared to discuss the relative merits of MM5 and WRF mesoscale models.

Description of the Models

MM5 and WRF models, developed and sourced from National Center for Atmospheric Research (NCAR), are the two high-resolution mesoscale models used in the present study for the prediction of "SIDR" cyclone of Bay of Bengal

D.V.B. Rao (✉)
Department of Meteorology and Oceanography, Andhra University, Visakhapatnam, India
e-mail: dvb_1949@yahoo.com

D. Srinivas
D. Hari Prasad, Jackson State University, USA

Y. Charabi (ed.), *Indian Ocean Tropical Cyclones and Climate Change*,
DOI 10.1007/978-90-481-3109-9_20,

Table 1 Differences between the MM5 and WRF models

MM5	WRF
Terrain following height (sigma-*z*) vertical coordinate	Terrain following hydrostatic pressure vertical coordinate
Arakawa B-grid	Arakawa C-grid
First-order (time-filtering) leapfrog time integration scheme	Second-order Runge–Kutta split-explicit time integration
Advection formulation (no conservation properties)	Conserves mass, momentum, entropy, and scalar using flux from prognostic equations
Second-order center differencing for advection	Fifth-order upwind or sixth-order centered differencing for advection

Table 2 The details of parameterization schemes

Physical process	MM5	WRF
Cumulus convection	Kain-Fritsch2	Grell-Devenyi ensemble
Planetary boundary layer	Medium range forecast	Mellor-Yamada
Cloud microphysics	Simple ice	Lin
Radiation	Dudhia's shortwave/longwave simple cloud	RRTM for longwave and Dudhia scheme for shortwave
Soil model	Multilayer soil model	Noah land-surface model

(BOB). The MM5 model was made available through public domain in the 1990s, which has been widely used for scientific studies of atmospheric processes of different time and spatial scales (Dudhia 1993; Grell et al. 1994). The WRF model is designed to be the next generation model after MM5, incorporating the advances in atmospheric simulation system suitable for a broad range of applications (Skamarock et al. 2005). Both are primitive equation models with non-hydrostatic dynamics and suitable for idealized simulations, real-time numerical weather prediction and data assimilation. Both these models have versatility to choose the domain region of interest; horizontal resolution; interactive nested domains and with various options to choose parameterization schemes for convection, planetary boundary layer (PBL), explicit moisture; radiation; and soil processes. However, there are differences between MM5 and WRF as given in Tables 1 and 2.

The MM5 model used equations in terrain following σ coordinates, solved in Arakawa B grid with Leapfrog time integration scheme with time-splitting technique. The WRF model equations use mass-based terrain following coordinate system and solved in Arakawa-C grid, Runge–Kutta second- and third-order time integration techniques. The parameterization schemes that are available with the WRF model are advanced versions as improved after the release of the MM5 modeling system. In the present study a comparison of near real-time predictions of a BOB tropical cyclone "SIDR" with the MM5 and WRF models is attempted to assess the relative merits of these two models and their applicability for tropical cyclone prediction.

Description of the "SIDR" Cyclone

SIDR, whose life cycle spanned 11-16 November 2007, was graded as a severe cyclonic storm with an attained intensity in terms of the minimum central sea-level pressure (CSP) as 944 hPa and the maximum wind speed (MW) of 115 knots. It was identified as a low-pressure system at 03 UTC of 11 November 2007 over southeast BOB and its neighborhood. It developed into a depression and lay centered at 09 UTC of the same day, moved slightly northwestwards and intensified into a deep depression and lay centered at 19 UTC of 11 November. It intensified into a cyclonic storm, "SIDR" and lay centered at 03 UTC of 12 November about 220 km near 10.5N, 91E. It moved in the northwesterly direction, further intensified into a severe cyclonic storm, remained stationary and then intensified into a very severe cyclonic storm at 18 UTC of 12 November. The system moved slightly northwestwards thereafter till 00 UTC of 13 November. Afterward the system moved in a nearly northward direction up to 12 UTC of 15 November and then the system recurved and moved in a north-northeasterly direction. Finally, it crossed the west-Bangladesh coast around 17 UTC of 15 November. The system weakened rapidly into a depression at 03 UTC of 16 November.

Description of the Data and Model Experiments

For the present study, the model is designed to have an interactive two-way nested to three with horizontal resolutions of 90, 30, and 10 km covering the BOB and the neighboring region as shown in Fig. 1. The model integrations were performed for 72 h starting from 00 UTC of each day of 11, 12, 13, and 14 November 2007. For both these two model integrations the initial conditions were taken from NCEP FNL data and the time-varying boundary conditions were taken from NCEP Global Forecast System fields at every 6 h interval and both these analyses are available at 1° resolution. The intensity and the track positions of the SIDR cyclone are taken from the reports of the IMD (India Meteorological Department, 2008) for comparison with the model results.

Results

In the present study, the results from "Real-time prediction experiments of the SIDR cyclone" are presented. The authors used "real time" as these predictions were made during the life cycle of SIDR over BOB and the results were shared with IMD and NCMRWF on a real-time basis. The real-time predictions were made with the MM5 model and experiments with the WRF model were performed later.

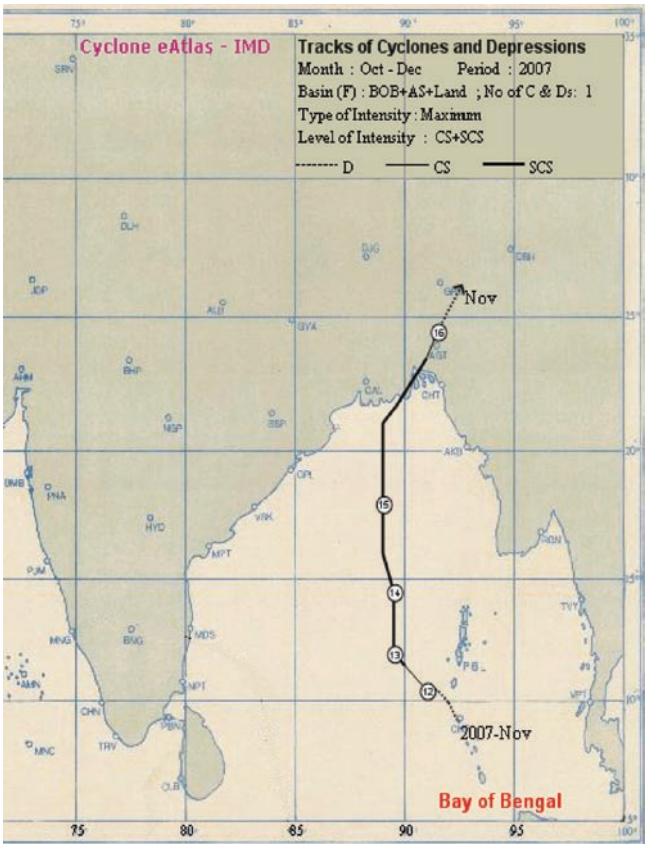

Fig. 1 Model domains with 90 (d01), 30 (d02), and 10 km (d03) resolution

As mentioned in the earlier section, four different predictions were made starting from 00 UTC of 11, 12, 13, and 14 November 2007. Model integrations were performed for 72 h with both the MM5 and WRF models to assess the performance and to examine their use in real-time prediction. The model-predicted CSP and MW associated with the cyclonic system were analyzed and compared with the reports from IMD. Similarly, the model-predicted track positions were compared with IMD estimates at 6 h interval. The time variations of the CSP and MW for the four predictions are presented in Fig. 2 and corresponding track positions are presented in Fig. 3. The results are described with reference to time as yymmddhh.

(1) The predictions with the integration starting from 07111100 show that the CSP variations have pre-deepening period of about 18 h followed by intensification up to 72 h The pre-deepening period was predicted 6 h earlier than the observations and the rate of intensification was higher than the observations. Observations show the attainment of steady state after 48 h where as the model shows continued intensification

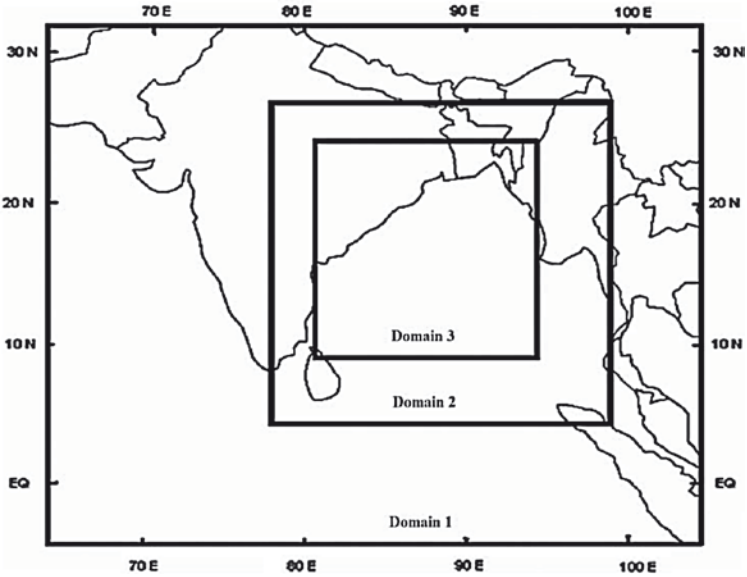

Fig. 2 Time variations of model-predicted CSP (hPa) (*left panel*) and MW (m/s) (*right panel*) at different times (**a**, **e**) at 07111100; (**b**, **f**) at 07111200; (**c**, **g**) at 07111300 and (**d**, **h**) at 07111400

up to 72 h. The magnitude of CSP predicted by the MM5 and the WRF models is at 48 h and nearly the same in magnitude as and in agreement with the IMD estimates. Corresponding time variation of MW shows steady increase up to 18 h followed by rapid rise up to 54 h with both the models. Both models show higher rate of intensification as compared to the observations and the WRF model shows higher intensification than the MM5 model. The WRF model shows attainment of near steady state after 54 h, whereas the MM5 model shows steady increase of MW up to 72 h. In this prediction, the WRF model shows better performance than the MM5 in terms of the period of rapid intensification and attainment of steady state closer to the observations, although the predicted magnitude is higher with the WRF model. The predicted rate of intensification and the attained intensity are higher with the WRF model than with the MM5 model.

An examination of the track positions show that both the models show a trend of movement similar to the IMD track positions. It is to be noted that the initial position of the center of the cyclone system is to the south of the observation by about 40 km. IMD track positions show cyclone movement toward northwest and then northward. The MM5 model shows north-northwest motion followed by north-northeast direction, where as the WRF model predicts, northwest and then northward movement. With these predicted tracks, both models show errors after 24 h. The track positions with the WRF model seem to be slightly better as the northwest followed by northward movement is similar to the IMD reports. The vector track errors are noted to be 187 (109), 119 (104), and 119 (293) km with WRF (MM5) model at 24, 48, and

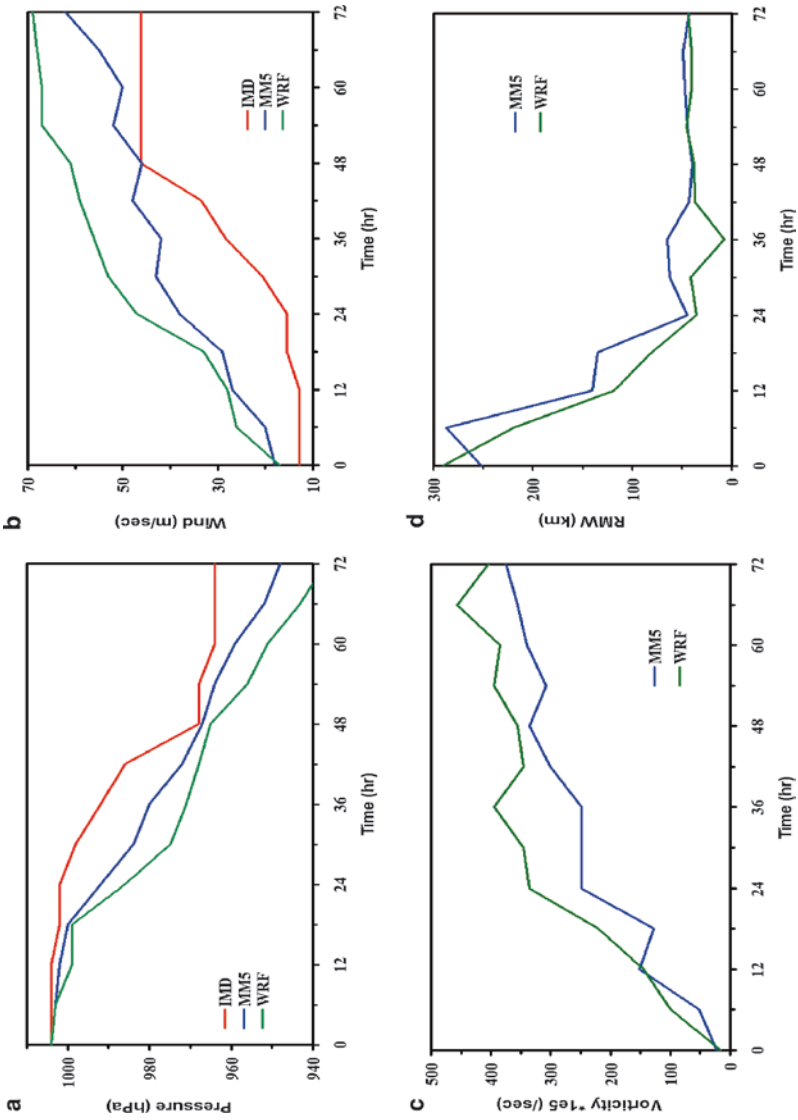

Fig. 3 Model-predicted 72-h track positions as predicted from (**a**) 07111100; (**b**) 07111200; (**c**) 07111300; and (**d**) 07111400 (up to 48 h) along with corresponding IMD reported positions

72-h prediction times, respectively. It is to be noted that except at 24 h, the vector track errors are less than 120 km with the WRF model as compared to consistent higher errors in the range of 143–293 km with the MM5 model.

(2) With the model integration starting from 07111200, both the MM5 and WRF models show rapid intensification after 18 h (Fig. 2b). The time variation of CSP shows start of rapid intensification after 18 h as compared to the intensification from 07111200 itself (start of model integration) up to 24 h and steady state thereafter. The WRF model produces higher intensity than the MM5 model and is closer to the observations up to 36 h. It is to be noted that the time variations of the MW show intensification during the first 30 h followed by slight decreased rate of intensification although the time variation of CSP shows deepening period to start after 18 h. The predicted track positions starting from 0711200 up to 07111500 along with IMD positions are shown in Fig. 2b. In this prediction, the MM5 model shows a very good track prediction similar to the IMD estimates whereas the WRF model predicts northwest movement. The vector track errors range up to 380 km with the WRF model whereas the errors are below 150 km with the MM5 model.

(3) For the prediction with initial time of 07111300, the WRF model shows better performance than the MM5 model. IMD reports show the minimum CSP to be around 968 hPa at 07111300, which remained constant for 36 h and then decreased up to 54 h attaining a minimum value of 942 hPa. The MM5 model prediction shows the CSP as 1002 hPa at the starting time (07111300) decreases gradually up to 54 h and then increases, indicating weakening of the storm. In contrast, the WRF model had 1008 hPa as CSP at the initial time, remained nearly constant up to 42 h, and then decreased rapidly up to 60th hour and then started increasing till 72 h. As per the IMD reports, the time variation of the MW shows nearly constant wind speed of 46 m/s up to 36 h and then increasing to 60 m/s at 60 h. The MM5 model shows a gradual increase from about 18 m/s at the initial time reaching a value of 45 m/s at 36 h and then decreasing to 35 m/s at 48 h and increases to attain 50 m/s at 54 h and then rapidly decreased *t* reach a value of 30 m/s at 60 h. The WRF model had an initial wind speed of 10 m/s gradually increased to about 16 m/s at 36 h and then rapidly increased to attain a value of 60 m/s at 54 h and then slowly decreased up to 72 h. It is to be noted that, in the prediction starting from 07111300, the initial strength of vortex is much weaker than the observed storm as the CSP (MW) difference was 40 hPa (36 m/s) and 34 hPa (28 m/s) in the WRF and MM5 models. However, the WRF model shows the intensification between 36 and 54 h forecast period agreeing with the observations, but the rate of intensification is much higher in WRF prediction and the attained maximum wind with WRF prediction is same as that of the observations. At this time the MM5 model could not predict the intensification as of the observations. However, both the WRF and MM5 models predict the weakening of the storm after 60 and 54 h respectively as of the observations.

The predicted track positions along with the IMD estimates are presented in Fig. 3a. From this time (07111300) the IMD track shows consistent northward movement followed by northeast direction up to 60 h followed by northeastward movement. Both the MM5 and WRF models predict northward track but fail to

predict the movement toward northeast. The WRF model shows motion toward the west side of the IMD track whereas the MM5 model predicts toward east. The vector track errors range up to a maximum of 350 and 370 km with the MM5 and WRF models, respectively. However, the errors with WRF model have a maximum of 156 km up to 54 h prediction and then the errors rapidly increase to reach a value of 371 km at 72 h. In contrast, the errors with MM5 are 162 km at 36 h and reach a maximum of 350 km at 60 h. The decrease of errors after 60 h in MM5 prediction is for a wrong reason as the model-predicted storm shows northwest direction where the observed storm recurved in the northeast direction (Table 3).

(4) The prediction experiment starting from 07111400 has limited prediction value as the observed storm shows intensification for 36 h and then weakens as per the IMD reports. The predicted time variation of CSP (Fig. 2c) shows better performance with the WRF model than with the MM5 prediction. The MM5 model does not predict any intensification throughout the 72-h period as the CSP remains constant around 1,000 hPa. In contrast, the WRF model with initial CSP of 1,000 hPa shows rapid decrease after 6 h attaining a minimum of 980 hPa at 30 h and then gradually rises. This prediction with the WRF is significant as it predicts the period of intensification (6–30 h) and the pressure drop 20 of hPa, which are similar to the IMD reports of the intensification period (12–30 h) and the pressure drop of 20 hPa. Although, the minimum attained CSP value with the WRF model is higher than the observations, the time variation of MW shows corresponding variations in the wind strength. The IMD reports wind speed of 46 m/s at initial time, remain constant for 12 h, and then increase to a value of 60 m/s at 30 h. The MM5 model has an initial value of 15 m/s which slowly intensifies to attain a value of 30 m/s at 18 h and then slowly decreases to reach 20 m/s at 72 h. In contrast, the WRF model also starts with initial strength of 15 m/s, rapidly increases to attain about 46 m/s at 24 h, remains same up to 36 h, and rapidly decreases to attain 20 m/s at 54 h. These results indicate the prediction with the WRF model to be superior to the MM5 model prediction as the WRF model could predict the period of intensification and pressure drop as of the observations. However, the rapid intensification in terms of wind speed is higher than the observations. The model predicted track starting from 07111400, along with IMD track positions are shown in Fig. 3. Starting from this time, the IMD track positions show near northward movement up to 36 h and then northeast direction. Both the MM5 and WRF models show near northward movement

Table 3 Model-predicted vector track errors with different initial times

Initial time of integration →	07111100		07111300		07111300		07111400	
Prediction time (h) ↓	MM5	WRF	MM5	WRF	MM5	WRF	MM5	WRF
00	71	78	93	99	41	29	48	56
24	109	187	59	103	25	128	273	143
48	104	119	100	299	292	124	238	156
72	293	119	143	378	65	372		

thereafter up to 72 h indicating the models' inability to predict change of direction toward northeast after 42 h.

The WRF model shows better prediction than the MM5 model as the WRF-predicted track is closer to the observations up to 36 h. The vector track errors also indicate better performance with the WRF model with the errors to be below 156 km. The MM5 model shows relatively slower motion and the model-predicted storm did not show land fall up to 07111600. MM5 model shows errors to be 164 km at 12 h increasing to 273 km at 24 h and 238 km at 48 h. The above description of the model-predicted time variations of CSP and MW show superior performance of the WRF model. The WRF model shows higher rate of intensification in all the four predictions with different initial times of integration. The WRF model could predict the period of intensification agreeing with the observations, whereas the intensification is more gradual in the MM5 prediction. It is also to be noted that the initial strength of the cyclone system is much weaker in the third and fourth predictions and the models are not expected to fare better with such differences at the initial time. However, the WRF model shows intensification indicating better dynamics and physics in the WRF model. Both models could predict the movement of the SIDR cyclone similar to the observations in all the four predictions. However, the WRF model shows better prediction with less track errors in three of the four predictions and could not fare better only with the integration starting from 07111200.

References

Dudhia J (1993) A non-hydrostatic version of Penn State–NCAR mesoscale model (1993): validation tests and simulation of an Atlantic cyclone and cold front. Mon Wea Rev 121:1493–1513

Grell G, Dudhia J, Stauffer DR (1994) A description of the fifth generation Penn State/NCAR mesoscale model (MM5). NCAR Tech. Note, NCAR/TN-398 + STR, p 122

Skamarock WC, Klemp JB, Dudhia J, Gill DO, Barker DM, Wang W, Powers JG (2005) A description of the advanced research WRF version 2. NCAR/TN-468 + STR, 88 pp

Performance Evaluation of DGMANs NWP Models During Gonu

Sultan Salim Al-yahyai and Fawzi Bader Hilal Al-Busaidi

Keywords Consortium for small-scale modeling (COSMO) • High-resolution Model (HRM)

Introduction

HRM: **H**igh-**R**esolution **M**odel **HRM** is a hydrostatic mesoscale NWP model. It has been developed at The Deutscher Wetterdienst (DWD) and currently used in more than 30 universities and national weather services. It solves for surface pressure, temperature, water vapor, cloud water, cloud ice, and horizontal wind components (u, v) explicitly, in addition with several surface/soil parameters. It uses regular or rotates latitude/longitude grid using Arakawa C-grid and Hybrid vertical coordinate based on Simmons and Burridge (Simmons and Burridge, 1981). Different sub-grid scale processes are parameterized including radiation, convection, and soil processes. **COSMO**: **Co**nsortium for **S**mall-scale **Mo**deling **COSMO** was formed in October 1998. It is a non-hydrostatic limited-area atmospheric model, to be used both for operational and for research applications by the members of the consortium. The consortium members include Germany, Switzerland, Italy, Greece, Poland, and Romania.

Case Study Configuration

During this study, both models have been rerun during the period 3–6 June 2007 based on the German Global Model GME 00/12UTC analysis.

S.S. Al-yahyai (✉) and F.B.H. Al-Busaidi
Directorate General of Meteorology and Air NavigationOman
e-mail: s.alyahyai@met.gov.om; f.albusaidi@met.gov.om

Y. Charabi (ed.), *Indian Ocean Tropical Cyclones and Climate Change*,
DOI 10.1007/978-90-481-3109-9_21,

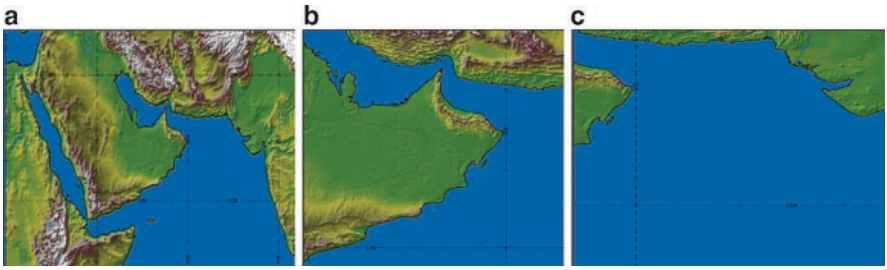

Fig. 1 Operational and case study model domain (**a**) HRM_28, (**b**) operational HRM_07/Cosmo_07; and (**c**) case study HRM_07/Cosmo_07

Figure 1a and b shows the operational domain for 28- and 7-km resolutions, respectively. It is clear that the 7-km domain does not cover the area of Gonu during the period of the study; therefore, the 7-km domain was shifted southeasterly to cover the area 14°–29°N and 48.5°–63.5°E as shown in Fig. 1c.

For the purpose of the study, comparison data were collected from different sources. Best Track and wind intensity information were collected from the Joint Typhoon Warning Center JTWC website archive. On the other hand, pressure intensity reports were collected from the DGMAN archive. The pressure intensity reports were originated at the Cyclone Warning Center of India CWCI. Moreover, the rainfall information was collected from the department of hydrology, Oman. The rest of the paper will be organized as follows: initial data analysis, track evaluation, rainfall evaluation, conclusion, and future work.

Initial Data Analysis

German Global Model GME is the deriving global model for the operational runs at DGMAN. GME is currently running on 40-km resolution and 40 vertical layers. Therefore, GME is the deriving model for the study; in this section we will evaluate the GME analysis during the Gonu case. Figure 2 shows comparison between Gonu Best Track and the track generated from the GME 00/12 UTC analysis. From the figure we can notice the deviation on the cyclone center according to GME analysis. This deviation reached more than one degree on 5 June 00 UTC analysis and on 6 June 00UTC analysis as shown in Fig. 3.

With respect to the pressure intensity we can see from Fig. 4 that the pressure drop on the GME analysis is much weaker than the estimated pressure drop of Gonu during the whole period of the study. The minimum pressure on the GME analysis was 990 hpa on 5 June 12 UTC, while the minimum estimated pressure was 934 hpa on 4 June 09 UTC.

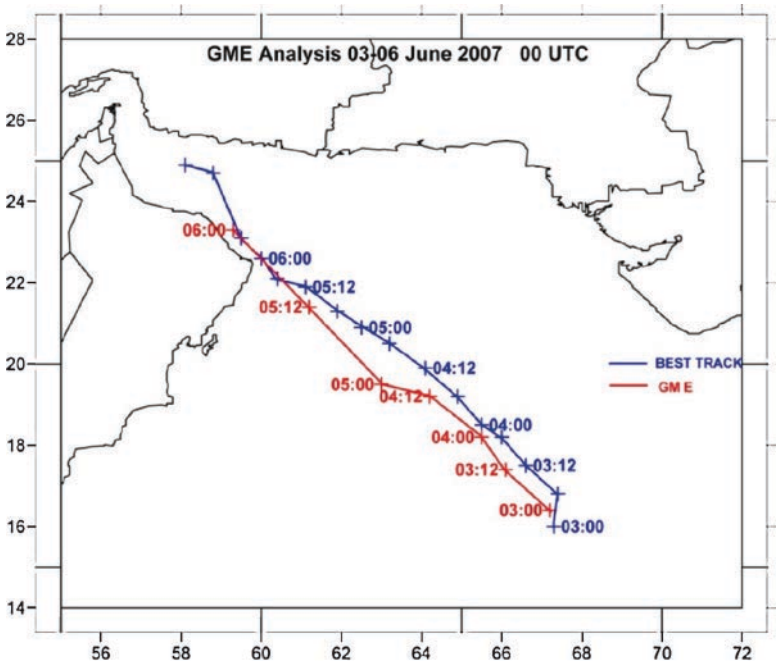

Fig. 2 Gonu Best Track and Track frobm GME 00/12 UTC analysis

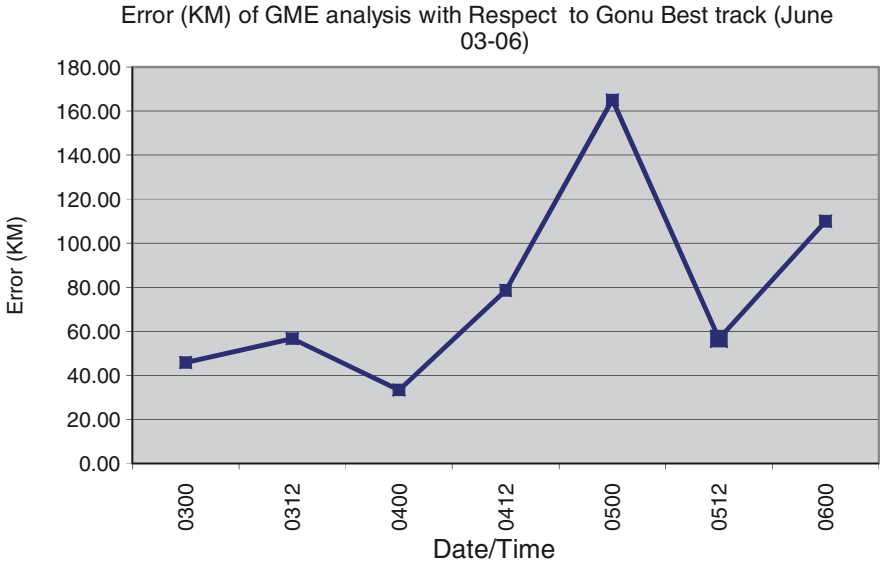

Fig. 3 Error (KM) of GME analysis with respect to Gonu Best track

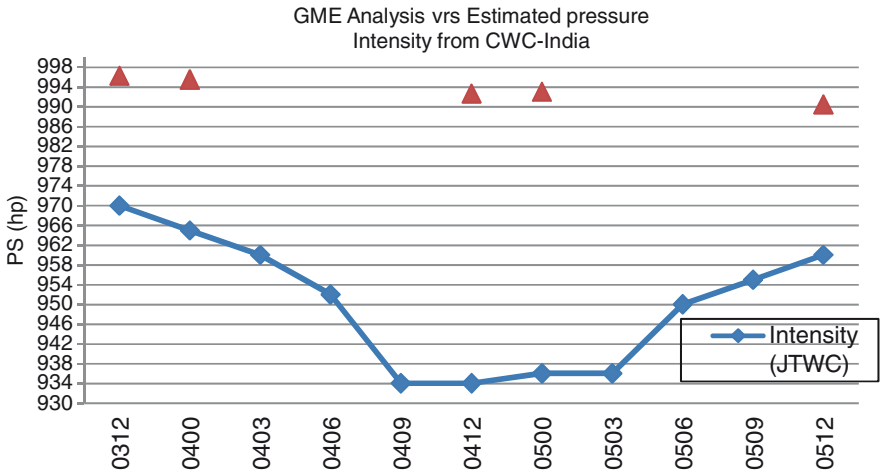

Fig. 4 Pressure intensity comparison between GME analysis and estimated pressure intensity from the JTWC

Track Evaluation

In this section we compare forecasted tracks from both HRM/COSMO using different model runs against Gonu Bets Track. We have also included the forecasted tracks from JTWC models to include at least one tropical cyclone specialized model (JTWC) against our models which are not tropical cyclone specialized models. The details of the forecasted tracks are shown on Fig. 5. The figure shows model run starting from 3 June, 00 UTC to 5 June, 12 UTC. Figure 5 shows that the DGMAN NWP model track forecasts are in agreement with the specialized JTWC model track forecast, and they all suggested that Gonu will make landfall in the area between Masera Island and Ras- Alhad during 3 June for both 00/12 UTC. Starting from 4 June, JTWC made a significant change in the track forecast as the 12 UTC run forecasted Gonu to make landfall in Muscat. While both HRM and COSMO did not predict such a scenario, they only started predicting the landfall in Muscat during the 12 UTC run of 5 June with some variation from the JTWC model forecast.

Wind Intensity Evaluation

Figure 6 shows estimated wind intensity from JTWC and the wind forecasted from different model runs of COSMO and HRM models of both 28 and 7 km resolution. HRM_28 km and HRM_07 were not able to forecast wind speed of more than 45

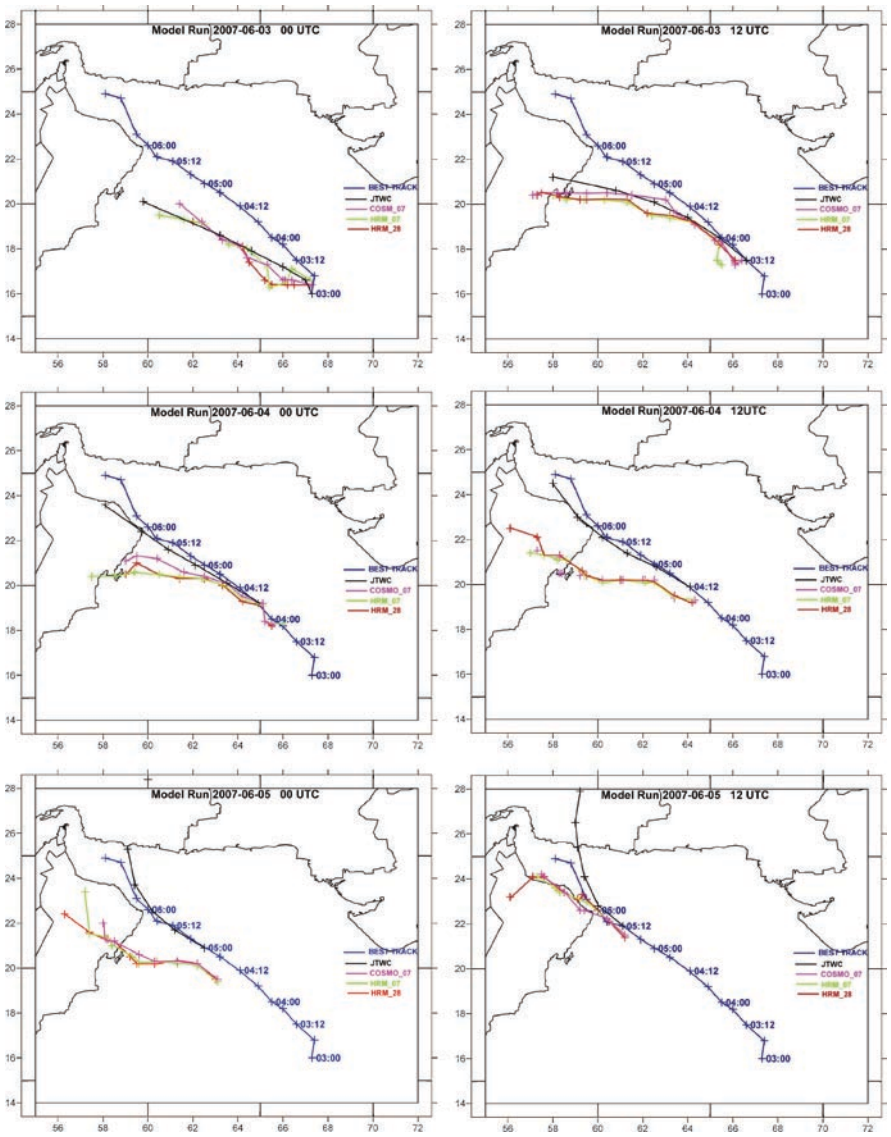

Fig. 5 Gonu Best Track and track forecast from different models and model runs. Best Track (blue), HRM_28 (red), HRM_07 (green), COSMO (pink) JTWC (black)

knots during the whole period, while the estimated wind from JTWC reached up to 140 knots. On the other hand, COSMO model was able to forecast wind speed up to 60 knots which according to the Area Cyclone Warning Services (ACWC's) from India classification was a "Severe Cyclonic Storm" while Gonu was classified as "Super Cyclonic Storm" (wind >120 knots).

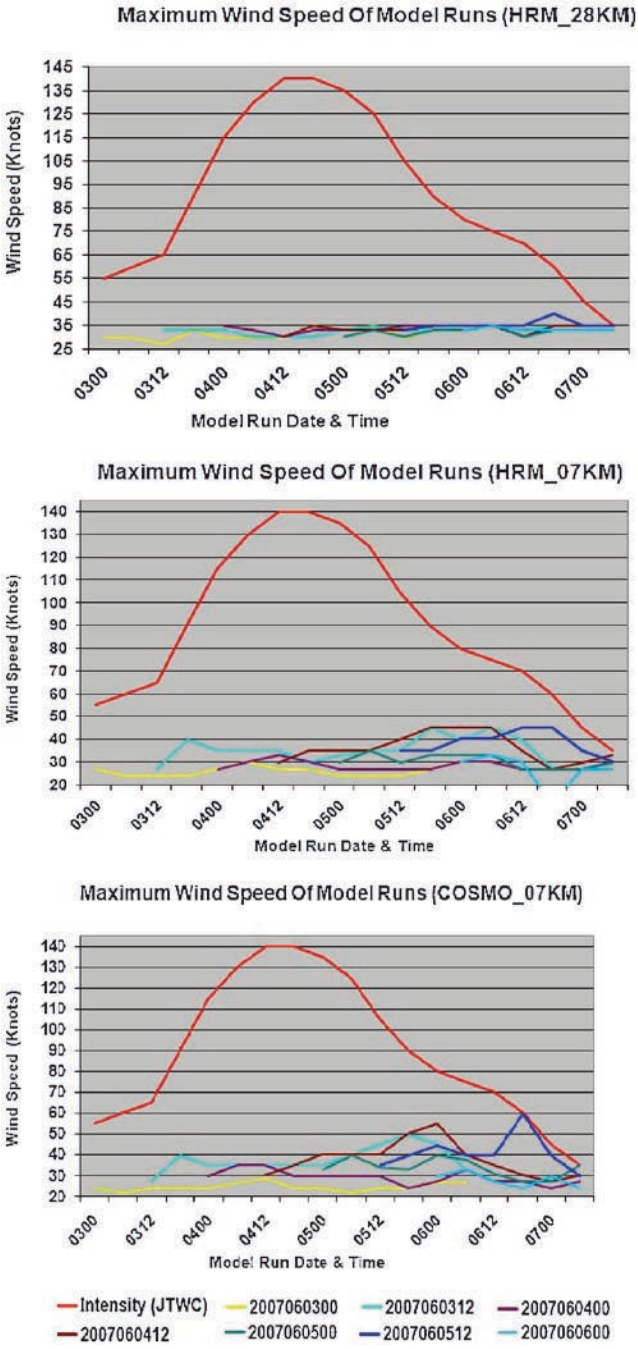

Fig. 6 Estimated wind speed intensity and wind forecast from HRM/COSMO

Rainfall Evaluation

Figure 7 shows the 48-h recorded rainfall (top left chart) between the period of 5–7 June and forecasted rainfall amount from different model based on 5 June 00UTC run. HRM_28 was not able to forecast the maximum recorded rainfall of (900 mm). It forecasted up to 400 mm. On the other hand, HRM_07 and COSMO models predicted rainfall of more than 1,000 mm. Location Weiss; all the models predicted two different maxima, the first maxima is far to the south from the recorded maximum. The Second maxima of both HRM_07 and COSMO model (787 mm, 745 mm, respectively) is located closer with the recorded maximum.

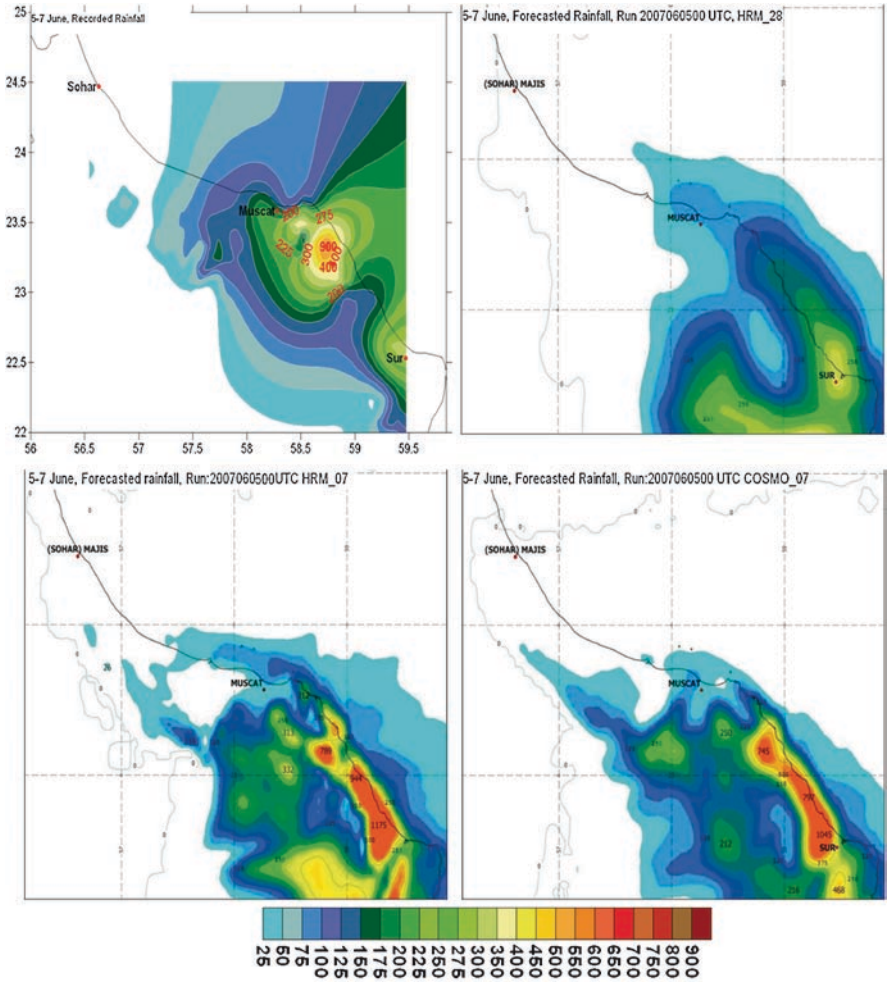

Fig. 7 48h recorded (*top left*) rainfall amount and forecasted amount from different models based on June 5th 00UTC run. HRM_28 (*top right*), HRM_07 (*bottom left*), COSMO (*bottom right*)

Conclusion

This paper presented an evaluation of DGMAN's NWP models during Gonu during the period 3–6 June 2007. The study included rerun of HRM and COSMO models for the same period. Track forecast, cyclone intensity, and associated rainfall were investigated. Moreover, we also evaluated the analysis of German Global model for the same period because it was the deriving global model for both regional models. From the evaluation study we can summarize the following:

- GME (driving model) mislocated Gonu's center and underestimated the associated wind and pressure drop.
- Clear dependency between GME forecast quality and HRM/COSMO forecast quality.
- Even though HRM/COSMO are not TC specialized models, both have given the signal for Gonu.
- COSMO_07 were able to forecast Gonu as Severe Cyclonic Storm starting from 12UTC run of 4th June 2007.
- On average COSMO shows 5% improvement of track forecast and 3% on the wind intensity over HRM.
- Both HRM_07 and COSMO_07 have signaled 48-h rainfall of more than 900 mm starting on June 5th with reasonable spatial and good amount of agreement with the recorded rainfall.
- DGMAN plans to introduce a 3Dvar data assimilation system in the second half of 2009, and then the effect of the 3Dvar on the performance of both models will be investigated. Moreover, a new version of HRM model is being developed to include tropical cyclone bogus scheme. The new scheme will be tested for tropical cyclone track predictability using Gonu case in our domain. Finally, the effect of the initial state and lateral boundary condition of the deriving model GME was clear in the performance of both HRM and COSMO models. To avoid depending on one source for the deriving model, we plan to introduce a short-range ensemble forecast SREF. The SREF system will also be tested for Gonu Case.

References

Al-katheri Ahmed, Radi AJJAJI, DHANHNI Abdullah, Assimilation and simulation of Cyclone Gonu (2007) using the UAE WRFVAR system [online]. Available at: http://www.mmm.ucar.edu/wrf/users/workshops/WS2008/abstracts/P5-08.pdf [accessed 28 March 2009]

India Meteorological Department, Cyclone Warning Services (ACWC's) [online]. Available at: http://www.imd.gov.in/main_new.htm [accessed 28 March 2009]

Regional and Mesoscale Meteorology Branch (RAMMB). Tropical Cyclone GONU [online]. Available at:http://rammb.cira.colostate.edu/products/tc_realtime/storm.asp?storm_identifier=IO022007 [accessed 28 March 2009]

Simmons, A. J., and D. M. Burridge, 1981: An energy and angularmomentum conserving vertical finite-difference scheme and hybrid vertical coordinates. Mon. Wea. Rev., 109, 758–766

Capabilities of Using Remote Sensing and GIS for Tropical Cyclones Forecasting, Monitoring, and Damage Assessment

Lotfy Kamal A. Azaz

Keywords GIS • Remote Sensing • Tropical cyclones • Monitoring • Damage assessment

Introduction

Natural Disasters occur frequently around the world, and their incidence and intensity seem to be increasing in recent years. The disasters such as floods and cyclones often cause significant loss of life, large-scale economic and social impacts, and environmental damage. For example, Cyclone Gonu was the strongest tropical cyclone on record in the Arabian Sea, and tied for the strongest tropical cyclone on record in the northern Indian Ocean and was the strongest named cyclone in this basin. On June 5 it made landfall on the eastern-most tip of Oman with winds of 150 km/h (90 mph). Gonu dropped heavy rainfall near the eastern coastline, reaching up to 610 mm (24 in.), which caused flooding and heavy damage. The cyclone caused about $4 billion in damage and nearly 50 deaths in Oman, where the cyclone was considered the nation's worst natural disaster. Planning to mitigate the impact of such incidents has become even more critical, given the prediction of increased climatic extremes associated with an "enhanced greenhouse effect." UN stressed the need for special attention to be given to planning ahead for natural disasters and to reducing long-term vulnerability in those countries at highest risk. It is quite obvious that space technology inputs are crucial for disaster management as it is the only means to obtain needed real-time data in remote and inaccessible areas. Satellite systems are the only tools that remain unaffected by the disasters for assessing the vulnerability of the region (Fig. 1). Therefore, using remote sensing with the help of geographic information system (GIS) for tropical cyclones forecasting,

L.K.A. Azaz (✉)
Geography Department, College of Arts and Social Sciences, Sultan Qaboos University, P.O. Box 42, 123, Alkhoud, Oman
e-mail: Lotfy_Azaz@Yahoo.co.uk

Y. Charabi (ed.), *Indian Ocean Tropical Cyclones and Climate Change*,
DOI 10.1007/978-90-481-3109-9_22,

Fig. 1 and 2 The impacts of Gonu Cyclone in Oman; the cyclone caused about $4 billion in damage and nearly 50 deaths

monitoring, and damage assessment can play a significant role for planning to alleviate such consequences caused by tropical cyclones (Fig. 2).

The Need for Warning Systems for Tropical Cyclones

It is possible to minimize the potential risk by developing disaster early warning strategies, prepare and implement developmental plans to provide resilience to such disasters, and to help in rehabilitation and post-disaster reduction. Exact and timely forecasting and warning systems are of significant importance in the struggle against tropical cyclones to mitigate their impacts on the population and economy. Using GIS and satellite systems data offer a magnificent technological potential for addressing critical information needs during all phases of disaster management, which include mitigation and preparedness, response, recovery, and relief.

Capabilities of GIS and Remote Sensing for Tropical Cyclones Forecasting

Weather Satellite systems forecast and advance warnings of severe weather conditions, which can minimize loss of life and damage. The main contribution of satellite systems in this field is monitoring and tracking cyclone paths and forecasting.

Only unexpected changes in direction and intensity of the cyclones limit the accuracy of early warnings to some extent, but in general the system functions quite satisfactorily.

The short-term forecasts are the most accurate as they contain the most detailed data about predictions of cloud cover, temperature, precipitation type, wind speed, and direction associated with the cyclone. Special forecasts predicting the position/location, intensity, expected movement, developments, and dissipation are also available to enable civic agencies and relief organizations to take urgent action regarding evacuation, cleaning up, recovery, etc.

Remote sensing is the primary method of observing tropical cyclones, which spend most of their lifetime over the ocean. Satellite systems provide comprehensive and multitemporal coverage of large areas in real time, and therefore, they are valuable resources for continuous detailed monitoring of atmospheric as well as surface parameters related to cyclones such as surface currents, ocean color, sea level, sea-surface temperature, cyclone-induced upwelling, primary production, and ocean eddies. All these parameters that are essential for tropical cyclones forecasting can be extracted from remote-sensing data. Several satellites are available that can be used prior, during, and after the event.

Several agencies monitor weather systems using remote-sensing imagery to monitor, track, and forecast cyclone activity, and these cyclone-tracking products need to be overlaid with ground information to forecast the impact of the cyclone, which can be done with the help of GIS. Prior to a cyclone, remote-sensed high-resolution sensors such as GeoEye-1, QuickBird, IKONOS, and SPOT-5 data helps to locate where previous hazard events have occurred, where they are likely to occur in the future, and the costs associated with historical events (Figs. 3, 4, 5).

Capabilities of GIS and Remote Sensing for Tropical Cyclones Monitoring

During the event, mapping of inundated area can be utilized using remotely sensed data such as MODIS images. Another type of satellite available for identifying flooded areas is the radar satellites, such as Radarsat. Radar has the advantage of capability to penetrate clouds, and can be used to differentiate between water and land. Therefore, it can provide accurate maps of flood extent. After the disaster, remote sensing can be used to determine the extent of landscape change and monitor the progress of recovery. Remote sensing allows a larger land mass to be studied in a shorter amount of time than is possible with traditional ground cover study methods (Fig. 6).

The spatial resolution of an image determines the ability to view individual features such as buildings and bridges. It also affects the ability to monitor and assess damage conditions, and depends on the nature of the hazard itself, for example, flooding, winds pressure, and storm surge. High-resolution imagery is very useful for bringing the flooding into context. It can show in detail things like buildings,

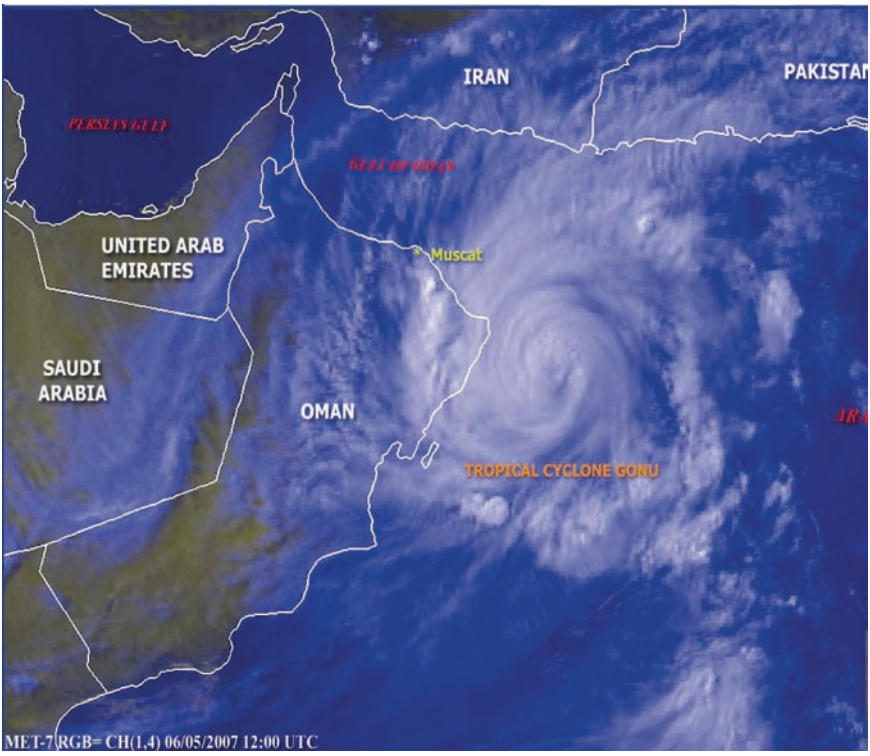

Fig. 3 The development of cyclone Gonu from METEOSAT satellite images taken 5th, of June 2007. These images are used to forecast the cyclone track and take the proper procedures by local authorities

roads, etc. overlaid on the flooded areas. Resolution of approximately 10 m or smaller are necessary to detect the presence and location of individual buildings, while high-resolution imagery of 1 m or less can distinguish damage conditions of individual buildings. Widespread flooding can be detected and monitored using less-detailed moderate-resolution imagery.

Satellite Imagery with multispectral resolution from Satellite Sensors such as LandSat and ASTER can distinguish physical materials with different reflectance values in different portions of the electromagnetic spectrum, and so features of interest, such as construction materials, water, and vegetation, can be identified by unique characteristics. The use of multispectral remote sensing systems is therefore critical for the separation of constituent materials within an image and for the interpretation of images of damage for pre- or post-disaster assessment (Fig. 7).

Land cover categories can be extracted from remotely sensed data. Then, it can be used to estimate the particular land cover classes that may be inundated by cyclones. This can enable planners to better assess their region's risk and vulnerability. With this type of information, planners are better able to prioritize and target mitigation and preparedness activities for their area. Remote sensing gives state and government agencies the ability to view the damage from multiple vantage points.

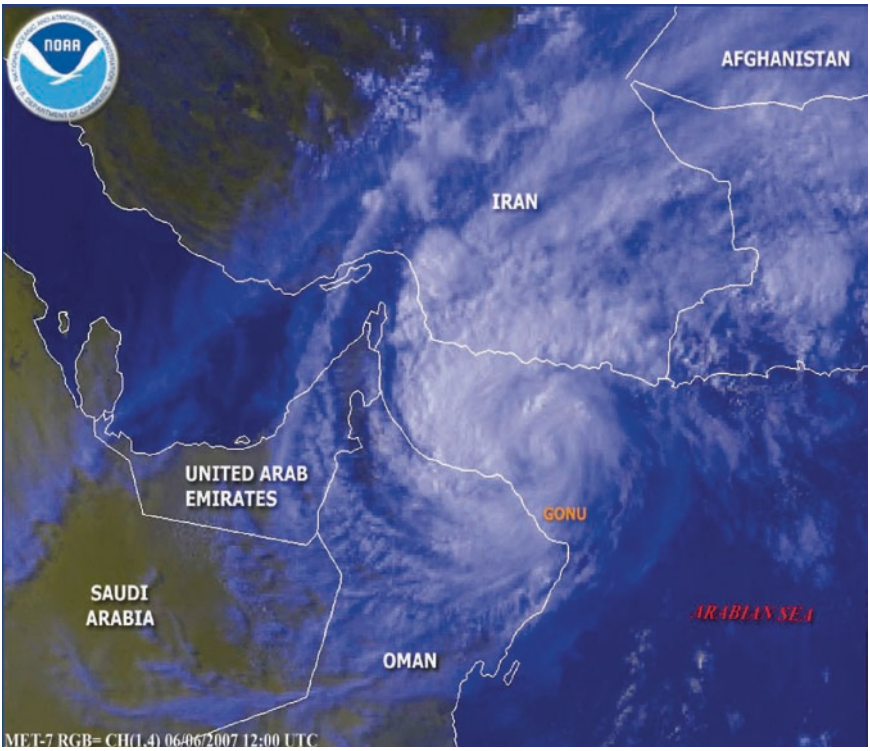

Fig. 4 The development of cyclone Gonu from METEOSAT satellite images taken on 5 June 2007. These images are used to forecast the cyclone track and take the proper procedures by local authorities

Due to the great number of earth observation programs that are available now with different types of data sets, GIS comes as a very powerful tool to collect, store, manipulate, analyze, and display of these different types of data. In addition, GIS allows for the combination of the different kinds of spatial data, with nonspatial data, attribute data, and use them as useful information in the various stages of disaster management. GIS plays an important role in case of cyclone mapping and mitigation.

Capabilities of GIS and Remote Sensing for Tropical Cyclones Damage Assessment

Nowadays, we have access to information and techniques provided by remote sensing and GIS that have proven their usefulness in disaster management. Many types of disasters, such as floods and cyclones, have certain features that satellite can detect. In addition to the capability of remote sensing to monitor such events

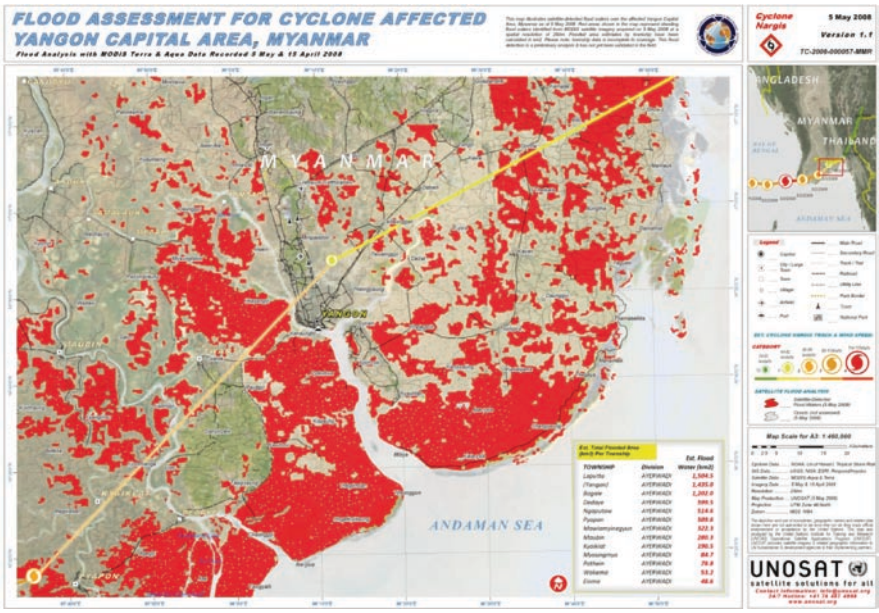

Fig. 5 The Illustrates satellite-detected flood waters over the affected Yangon capital area, Myanmar as of 5 May 2008. Red areas shown in the map represent standing flood waters identified from MODIS satellite imagery acquired on 5 May 2008

during the time of occurrence, it can assist in damage assessment as well, providing a quantitative base for relief operation. After that, it can be used to map the new situation and update the geographical database used for the reconstruction of an area.

Satellite imagery and aerial photography incorporated with geographic information systems (GIS) can give emergency officials a wealth of information for assessment, analysis, and monitoring of natural disasters such as cyclones damage from small to large regions around the globe. Urban planners, coastal managers, and local communities can better prepare for the next natural disaster by learning from past experiences. Satellite imagery and GIS can enable emergency management and community planners to better prepare for natural disaster impacts on their region.

The mitigation measures are very effective when GIS is applied to the whole process. For the flood preparedness phase, mapping topological flood risk is the first task that can be implemented using GIS, where a preliminary flood risk zoning map can be produced. Using contour lines will help to extract Digital Elevation Model (DEM) to obtain the areas of lower elevation. These areas can be detected and immediate help would be provided for these areas in order to help those in danger.

Disaster management plan consists of two phases that take place before disaster occurs, i.e., disaster prevention and disaster preparedness, three phases that happen

Fig. 6 IKONOS satellite images – Pre and Post Hurricane atrina – 2005

after the occurrence of a disaster, i.e., disaster relief, rehabilitation, and reconstruction. In disaster prevention phase, GIS is used to manage the large volume of data needed for the hazard and risk assessment. For the flood preparedness phase, mapping topological flood risk is the first task that can be implemented using GIS, where a preliminary flood risk zoning map can be produced. Using contour lines will help to extract Digital Elevation Model (DEM) to obtain the areas of lower elevation (Figs. 8).

In disaster preparedness phase, it is a tool for the planning of evacuation routes, for the design of centers for emergency operations, and for integration of satellite data with other relevant data in the design of disaster warning systems.

In the disaster relief phase, GIS is extremely useful in combination with Global Positioning System in search and rescue operations in areas that have been devastated and where it is difficult to orientate. In the disaster rehabilitation phase, GIS is used to organize the damage and the post-disaster census information, and in the

Fig. 7 Flood hazard map in ISE city produced through the integration of remote sensing and GIS

evaluation of sites for reconstruction. A proper structure of information system for disaster management should be present to tackle the disaster and to manage it. The remote sensing and GIS database can be used to create elaborate and effective Disaster Management Information System.

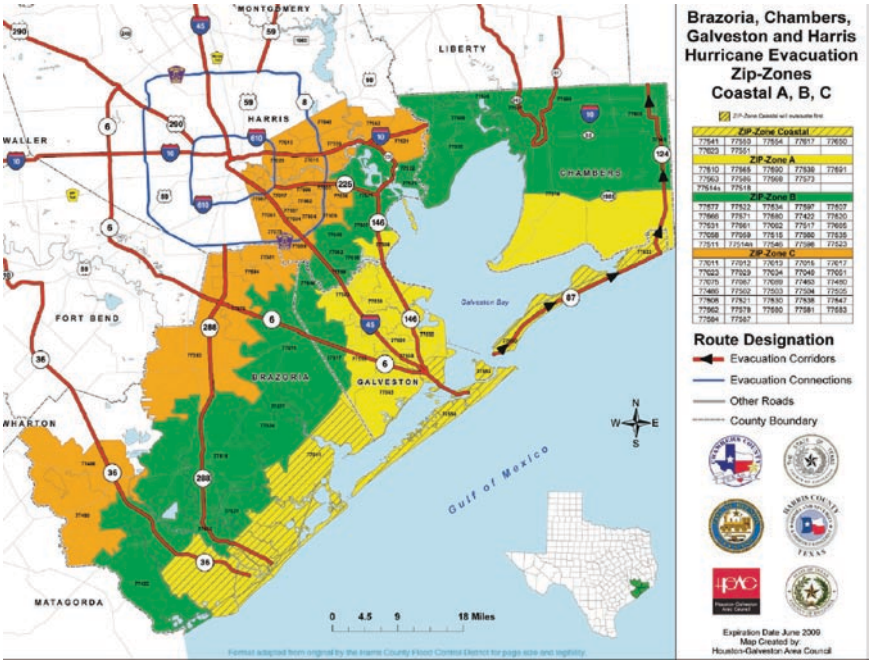

Fig. 8 Evacuation plan map produced by GIS

Conclusions

An integrated approach using scientific and technological advances should be adopted to mitigate and manage natural hazards. Remote sensing and GIS database can be used to create elaborate and effective Disaster Management Information System as a part of the national policy for natural disaster management.

Coppock (1995), Emani (1996), and Eastman, Emani, Hulina, Johnson, Jiang, and Ramachandran (1997) reviewed the integration of GIS and natural hazards risk modeling studies with an emphasis on real-time disaster decision support. These reviews prove that GIS evolves into real-time risk management decision support systems. In general, a GIS is a spatially referenced information system that can support decision making in emergency planning, response, recovery, and mitigation activities.

References

Chen SH, Jakeman AJ, Norton JP (2008) Artificial intelligence techniques: an introduction to their use for modelling environmental systems. Math Comput Simul 78(2–3):379–400. Special issue: Selected papers of the MSSANZ/IMACS 16th biennial conference on modelling and simulation, Melbourne, Australia, 12–15 December 2005

Coppock JT (1995). GIS and natural hazards: an overview from a GIS perspective. In: Carrara A, Guzzetti F (eds) Geographical information systems in assessing natural hazards, vol 6, Kluwer, Netherlands, pp 21–34

Cova TJ, Church RL (1997) Modelling community vulnerability using GIS. Int J Geogr Inf Syst 11:763–784

Cutter SL (2005) Hazards measurement. In: Kempf-Leonard K (Editor(s)-in-chief) Encyclopedia of social measurement. Elsevier, New York, pp 197–202

De Silva F, Pidd M, Eglese R (1993) Spatial decision support systems for emergency planning: an operational research/geographic information systems approach to evacuation planning. In: Sullivan J (ed) International emergency management and engineering conference, Society for computer simulation, pp 130–133

Dymon UJ (1993) Map use during and after hurricane Andrew. Natural Hazards Research Center, University of Colorado, USA

Dymon UJ, Winter NL (1993) Evacuation mapping: the utility of guidelines. Disasters 17:12–24

Eastman JR, Emani S, Hulina S, Johnson A, Jiang H, Ramachandran M (1997) Applications of geographic information systems (GIS) technology in environmental risk assessment and management. In: UNEP (ed) The Idrisi project. Clark labs for cartographic technology, Worcester, MA, pp 1–10

Emani S (ed) (1996) GIS applications in hazard assessment and management. UNITAR, Geneva

Feidas H, Kontos T, Soulakellis N, Lagouvardos K (2007) A GIS tool for the evaluation of the precipitation forecasts of a numerical weather prediction model using satellite data. Comput Geosci 33(8):989–1007

Jayaraman V, Chandrasekhar MG, Rao UR (1997) Managing the natural disasters from space technology inputs. Enlarging the scope of space applications. Acta Astronaut 40(2–8):291–235

Lanza L, Siccardi F (1995) The role of GIS as a tool for the assessment of flood hazard at the regional scale. In: Carrara A, Guzzetti F (eds) Geographical information systems in assessing natural hazards. Kluwer, The Netherlands, pp 199–217

Lipschultz MS (1988) Application of floodplain management by local government using GIS technology. In: Proceedings of the twelfth annual conference of the association of state floodplain managers, special publication 19. Natural Hazards Research and Applications Information Center, Nashville, TN, pp 321–348

Mather M (1993) Maps in action for protecting Trinidad and Tobago from disasters. In: Merriman PA, Browitt CWA (eds) Natural disasters: protecting vulnerable communities. Thomas Telford, London, pp 365–373

Simpson JJ, (Ben) Tsou YL, Schmidt A, Harris A (2005) Analysis of along track scanning radiometer-2 (ATSR-2) data for clouds, glint and sea surface temperature using neural networks. Remote Sens Environ 98(2–3):152–181

Verstappen HT(1995) Aerospace technology and natural disaster reduction, Natural hazards: monitoring and assessment using remote sensing technique. Adv Space Res 15(11):3–15

Zerger A, Smith DI (2003) Impediments to using GIS for real-time disaster decision support. Comput Environ Urb Syst 27:123–141

Part IV
Assessment of Risk and Vulnerability from Tropical Cyclones, Including Construction, Archival and Retrieval of Best-Track and Historic Data Sets

On Developing a Tropical Cyclone Archive and Climatology for the South Indian and South Pacific Oceans

Y. Kuleshov, L. Qi, D. Jones, R. Fawcett, F. Chane-Ming, J. McBride, and H. Ramsay

Keywords El Niño-Southern Oscillation (ENSO) phenomenon

Introduction

Tropical cyclones (TCs) are the most dangerous and damaging weather phenomena to regularly affect countries in the South Indian (SIO) and the South Pacific (SPO) Oceans. The year-to-year impact varies, and historical records demonstrate significant interannual variability in TC frequency and spatial distribution of TC tracks. Additionally, the climate is changing on a global scale (IPCC 2007) and it is important to understand how a warmer climate may affect TC activity. Numerous studies on TC activity in various regions of the northern and southern hemispheres have been completed with the aim of developing TC climatologies and establishing driving forces behind TC temporal and spatial variability.

Many studies have focused on related TC activity to the El Niño-Southern Oscillation (ENSO) phenomenon. In the northern hemisphere, a significant reduction (*increase*) of TC activity is observed over the Atlantic basin during El Niño (*La Niña*) events (e.g., Gray 1984). Significant spatial and temporal variations of TC activity over the western North Pacific associated with the ENSO phases have been reported (e.g., Chan 2000). ENSO also affects TC frequency in the North Indian Ocean, with a reduction in TC activity over the Bay of Bengal during El Niño events (Singh et al. 2000). In the southern hemisphere (SH), attempts to

Y. Kuleshov (✉), L. Qi, D. Jones, and R. Fawcett
National Climate Centre, Australian Bureau of Meteorology, Australia

F. Chane-Ming
Laboratoire de Physique de l'Atmosphère et des Cyclones, Université de la Réunion, France

J. McBride and H. Ramsay
Centre for Australian Weather and Climate Research, Bureau of Meteorology, Australia

Y. Charabi (ed.), *Indian Ocean Tropical Cyclones and Climate Change*,
DOI 10.1007/978-90-481-3109-9_23,

develop a TC climatology for the Australian region have been made by Holland (1984), who analyzed data for the period 1958–1979, and Nicholls (1985) who examined records of Australian TC numbers from 1909/10 to 1982/83. A nonlinear rising trend, with fewer TCs observed at the beginning of the century, was attributed to improvements in observing systems and networks. However, variations in TC activity occur around this trend and Nicholls (1985) found a strong and stable relationship between TC numbers and TC days in the Australian region and Darwin pressure.

El Niño events cause TC activity in the SPO to occur further eastward than normal and also to bring about a general suppression of TC activity in the Coral Sea and north Australian region (Gray 1988; Ramsay et al. 2008). Basher and Zheng (1995), analyzing spatial patterns and relationships of TCs in the western SPO to the Southern Oscillation Index (SOI) and sea-surface temperature (SST), found that the geographical distribution of TC incidence shifts eastward and northward during negative SOI phases and vice versa. The western SIO is also a region of high TC activity in the SH – it accounts for 14% of global TC occurrences. Climatological associations and characteristics of TCs in the western SIO (5°–25°S, 50°–75°E) during 1972–1991 were studied by Jury (1993), however, no statistically significant correlation between the SOI and TC numbers was found. The earlier studies mainly focused on studying variations in occurrences of TCs in different regions of the SH. However, a comprehensive TC climatology for the SH that includes other TC characteristics (e.g., intensity, density, and flux) had not yet been developed. The present work applies a uniform statistical approach to analysis of TC activity in the SIO and the SPO with respect to changes in oceanic and atmospheric conditions related to the ENSO phenomenon.

Data

To accurately assess whether a significant change in TC activity has occurred in the historical record, a reliable and homogeneous TC database is essential. The first attempt to develop a TC archive for the SH (south of the equator, 30°E–120°W) was by Kuleshov and de Hoedt (2003). Recently, the TC archive for the SH (the SHTC) has been further developed at the National Climate Centre (NCC), Australian Bureau of Meteorology (Kuleshov et al. 2008) and now it consists of the TC best track data for the 1969/70–2006/07 TC seasons. Based on the data from the SHTC archive, the present study is aimed at summarizing the extensive existing knowledge by applying a uniform approach to analysis of TC activity in the SIO (defined here as the area west of 135°E) and the SPO (defined here as the area east of 135°E). The division of the SH into the SIO and SPO in the current study is derived from the local minimum in the average annual number of TCs at around 130°E–135°E. Our analysis only considers TCs from the 1981/82 SHTC season onwards, due to the questionable quality of TC intensity records prior to about 1980.

Climatology

To analyze characteristics of the TC climatology, we have employed the NCC's vortex tracking computer package. The package is a set of FORTRAN programs that generate a wide range of statistics based on the data from the SHTC archive. The package was originally developed at the University of Melbourne, and subsequently further developed and updated at the Australian Bureau of Meteorology (Murray and Simmonds 1991; Jones 1994). The package statistics are derived from the individual TC positions using a dual process of interpolation. The first step involves interpolation in the time domain, using bicubic splines to compute the intermediate data along the tracks based on the raw system positions. This is to ensure consistency in statistics along system tracks. The second interpolation involves the distribution of data from the raw and interpolated systems using a Cressman weighting scheme applied to the specified output grid. In this study, TC characteristics such as cyclone hours, system density, system flux, system intensity, and intensity tendency have been computed using the methodology described in detail in Jones (1994). In the SPO, a noticeable eastward displacement of TC genesis position during El Niño seasons compared to La Niña seasons (see Kuleshov et al. (2008) for a list of these ENSO seasons) is observed, in agreement with the earlier studies.

Analysis of TC hours stratified by ENSO warm and cold phases reveals an area with increased TC hours over the eastern part of the SIO during La Niña seasons. The opposite relationship occurs over the northern regions of the SPO – that is, increased TC hours are noted during El Niño seasons with two major maxima located in the Coral Sea and around Vanuatu (Fig. 1).

ENSO has a significant impact on the annual average TC transport, as shown by the differences between El Niño and La Niña seasons in Fig. 2. In La Niña seasons the peak fluxes over the SIO are higher than those in El Niño seasons, while in the SPO, the fluxes in La Niña seasons are somewhat weaker than those in El Niño seasons (figures not shown). The major flux center in the SH is located at about

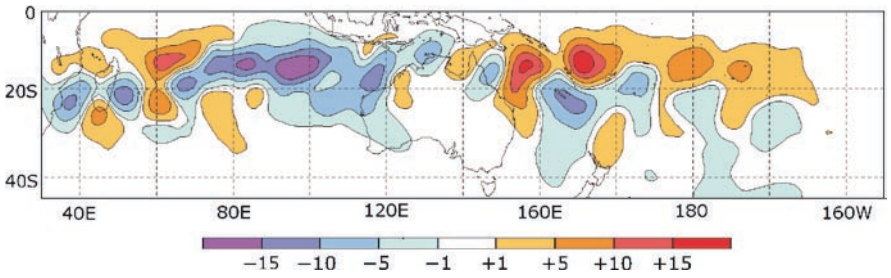

Fig. 1 The TC hour difference between El Niño seasons and La Niña seasons

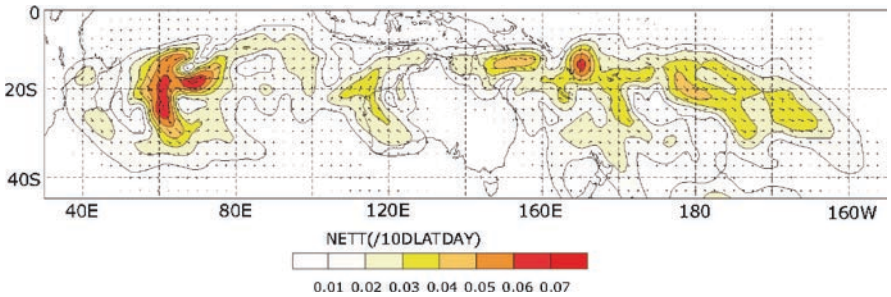

Fig. 2 Difference in average annual TC transport between El Niño seasons and La Niña seasons

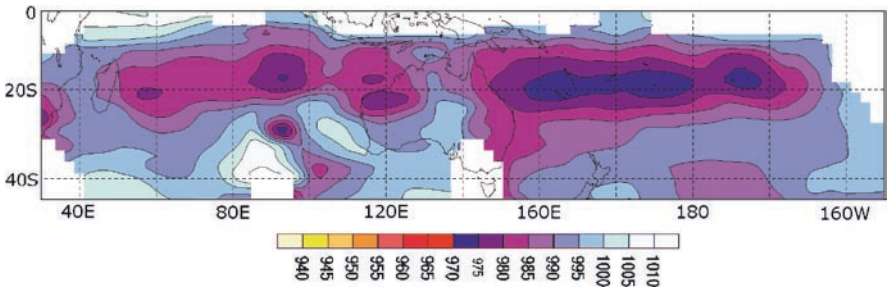

Fig. 3 Average annual TC intensities for El Niño seasons

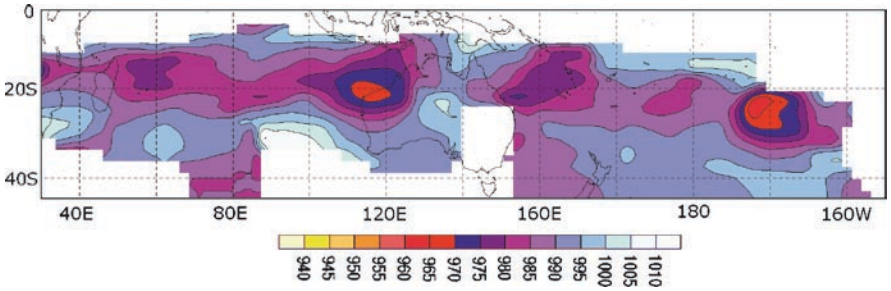

Fig. 4 Average annual TC intensities for La Niña seasons

65°E in the SIO (Fig. 2). The climatological location of average annual TC intensity reveals that generally TCs intensify while moving in the areas between the equator and around 20°S, and then weaken in the higher latitudes, presumably as they encounter colder SSTs and stronger vertical wind shear associated with mid-latitude systems. In El Niño seasons, there are four major maxima of TC intensity located along about 20°S and positioned around 90°E, 115°E, 165°E, and 155°W, respectively (Fig. 3).

Over the SPO during La Niña seasons (Fig. 4), the area with TC mean central pressure of 980 to 970 hPa is significantly weaker than in El Niño seasons. The region of maximum

intensity (970–980 hPa) around 90°E in the SIO during El Niño seasons (Fig. 3) is not evident during La Niña seasons (Fig. 4), while another TC intensity center in the area around 20°S, 115°E intensifies in La Niña seasons – representing the area of the most intense TC activity in the Australian region (Fig. 4). The results from the TC intensity tendency analysis demonstrate that, over the SIO and the SPO, cyclone systems mostly develop in the areas north of about 20°S, and start to weaken south to it.

SST, vertical wind shear, lower tropospheric vorticity, and mid-tropospheric relative humidity are investigated in this study as primary large-scale environmental parameters to examine their contribution to variations in TC characteristics related to the ENSO phenomenon. From the results of the composite analysis, it is found that each individual field studied here can explain some of the TC variations. Composites have been carried out for El Niño and La Niña seasons of the large-scale parameters known to have an influence on tropical cyclogenesis on a climatological basis, following Gray (1968), McBride (1995), and others. Care should be taken in interpreting these results as all interannual variations of all six of the components of the Gray genesis parameter are themselves highly correlated to indices of ENSO; so the parameters are not independent. In the northern hemisphere, particularly the North Atlantic, it is well established that ENSO affects interannual variability of TC activity primarily through vertical wind-shear variations (e.g., Gray 1984). In the southern hemisphere it is less obvious that this should be the case. This is because the SH cyclogenesis regions are characterized by quite large values of vertical wind shear, with a north–south gradient of strong westerly shear pole-ward of 20°S and a tendency toward weak or even easterly shear near the equator. This is supported by our findings in which the El Niño versus La Niña shear differences are not easily interpreted (not shown). Similarly, the SST difference composites (also not shown) simply reproduce the large-scale structure of the SST patterns of ENSO and show little or no in situ relationship to TC activity. Physically, one would expect modification of SH cyclone behavior by ENSO to be through the vertical motion fields, associated with the well-documented variations in the upward and downward branches of the Walker Cell with ENSO, and through low-level vorticity. The reason for the latter is that ENSO affects the strength of the easterly and westerly winds close to the equator. Given a much smaller influence on the trade winds pole-ward of 20°S, this variation in low-latitude zonal flow will bring about large differences in the vorticity of the monsoon trough. For example, in an El Niño event the low-latitude westerlies extend far into the central Pacific, bringing about a monsoon trough and low-level cyclonic vorticity far into the central Pacific. The Gray genesis parameter does not contain large-scale vertical motion. This field is represented through the proxy of mid-level relative humidity, which has a positive anomaly when the vertical motion is upward and a negative anomaly when there is subsidence. The composites of low-level vorticity and relative humidity are shown in the upper and lower panels of Fig. 5.

As can be seen from casual inspection of Fig. 5, the major mechanism through which ENSO affects TC activity across the SPO is through large-scale vertical motion, which provides convection and so feeder or precursor convective systems, and through the relative vorticity in the monsoon trough, mainly through the changes in the low-latitude westerlies equator-ward of the trough. Some of these conclusions were previously obtained by Ramsay et al. (2008).

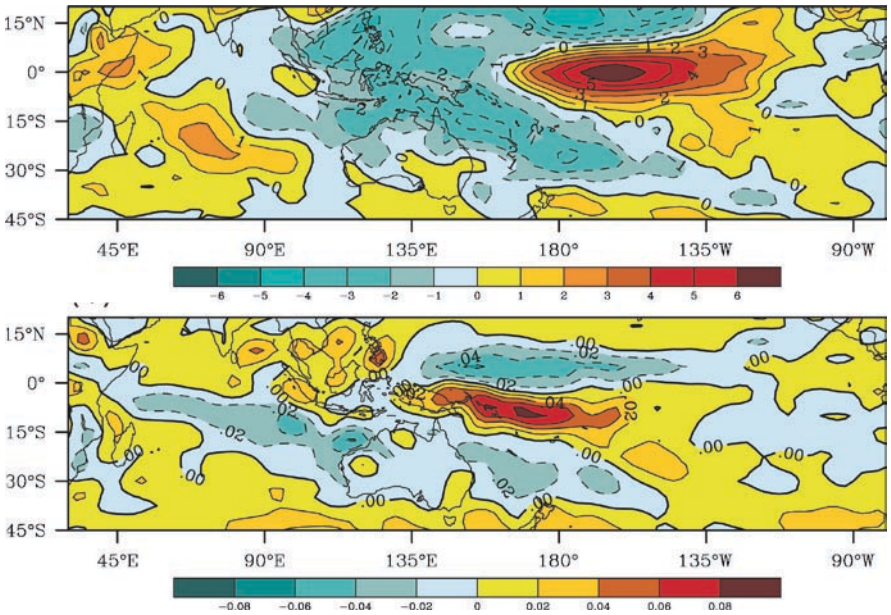

Fig. 5 Differences between El Niño and La Niña seasons. *Upper panel*: Relative humidity difference: the actual field is a composite of relative humidity anomaly in El Niño seasons. *Lower panel*: Low-level relative vorticity difference: the plot is a relative vorticity anomaly composite in La Niña seasons

Trends

Trends in TC occurrences and intensity, and possible physical mechanisms for change, have much been discussed widely in recent years. A major uncertainty with all analyses of TC intensity, in particular, is that of data homogeneity and quality. For example, McBride (2008) suggests that the increased occurrences of the strongest TCs around Australia might be due to inhomogeneities in the data. Similar conclusions have been made for the northern hemisphere (Landsea et al. 2006). In this study, the statistical significance of the linear trends in the various TC time series was assessed in three ways. The first is the standard linear regression approach, based on the assumption of identically independently normally distributed residuals. Because the TC data, being (non-negative) integer-valued, depart considerably from this assumption, we have also calculated the statistical significances by Monte Carlo simulation (5,000 iterations) involving resampling the time series with and without replacement. We have also subjected the TC time series to two single break-point testing procedures, a parametric one based on the null hypothesis that the data are normally distributed, and an analogous nonparametric one based on the Mann-Whitney statistic, the nonparametric one being of greater

relevance given the characteristics of the data. A minimum of four seasons on either side of the break was imposed in the assessment. One motivation for the use of break-point analysis is that it can identify artificial changes in the data, which might not be evident in trends or raw time series. The two most critical issues impacting on the homogeneity of TC records, and the associated confidence in climate change analyses, are changes in analysis practice and in the quality of satellite data. If step changes in the TC data coincide with known changes in data quality and/or observation techniques then a case might be made for the changes to be artificial.

Lastly, because both these approaches (linear regression and breakpoint analysis) merely lead to the rejection of the null hypothesis of no change, without establishing the departure from no change as being specifically linear or step-change (e.g.), we have compared three competing models (constant, linear, step-change) under leave-one-season-out cross-validation, to determine which of the three models generates the least root-mean-square-error (RMSE). Analyzing TC occurrences, the following intensity thresholds (in terms of mean central pressure) were used; 995 hPa or lower (*970 hPa or lower*) for a system to be counted as a TC (*a severe TC*). Examining changes in severe TCs, six thresholds were explored – 945, 950, 955, 960, 965, and 970 hPa, to explore the consistency of the results for severe TCs. Changes in TC occurrences in the SH, the SIO, and the SPO were analyzed over the 26-year period 1981/82 to 2006/07, as complete SH intensity records start in 1981/82. Over this period, there are no significant trends in the annual numbers of TCs (SPO, SIO, SH) attaining a life-time mean central pressure of 995 hPa or lower, or in the numbers of severe TCs (mean central pressure of 970 hPa or lower) in these three regions. Positive trends in 945 and 950 hPa TCs in the SIO (and consequently the SH) are statistically significant, but appear to be influenced to some extent by changes in data quality. As TC observation and analysis techniques in the regions of the SH evolved, the trends in TC numbers appear to be affected, at least to some extent, by step changes, which may reflect data homogeneity issues rather than climate trends.

Concluding Remarks

A comprehensive TC climatology for the SIO and SPO has been developed. Data from the TC archive for the SH have been stratified between El Niño and La Niña seasons, and significant changes in TC occurrences and cyclogenesis in terms of geographical distribution and intensity of maxima have been found. It has been demonstrated through composite analysis and physical reasoning that these changes are primarily associated with changes in vertical motion following Walker Cell movements and in low-level relative vorticity associated with changes in low-latitude/equatorial zonal flow. There are no simple changes in vertical shear or in situ SST that follow the modifications of cyclone behavior by ENSO. Trends in occurrences of TCs in the SH, the SIO and the SPO have been examined in detail. For the 1981/82 to 2006/07 period, there are no apparent trends in the total numbers of TCs reaching 995 hPa, or in the numbers

of severe TCs (mean central pressure of 970 hPa or lower) in these three regions. Positive trends in 945 and 950 hPa TCs in the SIO (and consequently the SH) are statistically significant, but appear to be influenced by changes in data quality to some extent and therefore should not be taken at face value. Attempts have been made to prepare consolidated TC global datasets (e.g., Kossin et al. 2007; Kuleshov et al. 2008) and there are further plans to continue these efforts. However, consolidation of historical data from various regions is currently limited by the inhomogeneity of TC observation and analysis practice. We believe that an international project on re-analysis of the historical TC data under should be initiated under the WMO umbrella in order to obtain globally homogeneous records, something required to address the important question of how TC activity is changing and its possible relationship with global climate change more generally.

References

Basher RE, Zheng X (1995) Tropical cyclones in the Southwest Pacific: spatial patterns and relationships to Southern Oscillation and sea surface temperature. J Clim 8:1249–1260

Chan JCL (2000) Tropical cyclone activity over the western North Pacific associated with El Niño and La Niña events. J Clim 13:2960–2972

Gray WM (1968) Global view of the origin of tropical disturbances and storms. Mon Wea Rev 96:669–700

Gray WM (1984) Atlantic seasonal hurricane frequency. Part I: El Niño and 30 mb quasi-biennial oscillation influences. Mon Wea Rev 112:1649–1668

Gray WM (1988) Environmental influences on tropical cyclones. Aust Meteor Mag 36:127–139

Holland GJ (1984) On the climatology and structure of tropical cyclones in the Australian/south-west Pacific region: I. data and tropical storms. Aust Meteor Mag 32:1–15

IPCC (2007) IPCC WG1 AR4 Report: ipcc-wg1.ucar.edu/wg1/wg1-report.html

Jones DA (1994) A numerical vortex finding, tracking, and statistics package. BMRC Research Report, No. 41, 35pp

Jury MR (1993) A preliminary study of climatological associations and characteristics of tropical cyclones in the SW Indian Ocean. Meteorol Atmos Phys 51:101–115

Kossin JP, Knapp KR, Vimont DJ, Murnane RJ, Harper BA (2007) A globally consistent reanalysis of hurricane variability and trends. Geophys Res Lett 34:L04815. doi:10.1029/2006GL028836

Kuleshov Y, de Hoedt G (2003) Tropical cyclone activity in the southern hemisphere. Bull Austral Met Ocean Soc 16:135–137

Kuleshov Y, Qi L, Fawcett R, Jones D (2008) On the El Niño-Southern Oscillation and tropical cyclone activity and trends in the Southern Hemisphere. Geophys Res Lett 35:L14S08, doi:10.1029/2007GL032983

Landsea CW, Harper BA, Hoarau K, Knaff JA (2006) Can we detect trends in extreme tropical cyclones? Science 313:452–454

McBride JL (1995) Tropical cyclone formation. Chapter 3 of global perspectives on tropical cyclones Russell Elsberry (ed) World Meteorological Organization

McBride JL (2008) Interannual variability of tropical cyclones near Australia: Implications for the response to global warming. Eos Trans. AGU 89, West Pac Geophys Meet Suppl Abstracts U34A-08

Murray RJ, Simmonds I (1991) A numerical scheme for tracking cyclone centres from digital data Part I: development and operation of the scheme. Aust Meteor Mag 39:155–166

Nicholls N (1985) Predictability of interannual variations of Australian seasonal tropical cyclone activity. Mon Wea Rev 113:1144–1149

Ramsay HA, Leslie LM, Lamb PJ, Richman MB, Leplastrier M (2008) Interannual variability of tropical cyclones in the australian region: role of large-scale environment. J Clim 21:1083–1103
Singh OP, Khan TMA, Rahman MS (2000) Changes in the frequency of tropical cyclones over the North Indian Ocean. Meteorol Atmos Phys 75:11–20

Improving the Australian Tropical Cyclone Database: Extension of the GMS Satellite Digital Image Archive

M. Broomhall, I. Grant, L. Majewski, M. Willmott, D. Jones, and Y. Kuleshov

Keywords Digital image archive • the GMS satellite

Introduction

Japan's GMS series of satellites were, and MTSAT-1R currently is, located at a nominal sub-satellite of 0°S, 140°E in geostationary orbit to retrieve imagery for meteorological purposes. This suite of satellites has been active since 14 July 1977 when the first of five GMS satellites was launched. The Bureau did not start receiving imagery from GMS until late 1977 and it was not until early in 1978 that imagery was received regularly. The Bureau now has an archive of meteorological satellite data extending over 30 years. The best use of this data can be achieved by converting it all to a single format, which can be utilised within computer-based analysis systems. As the Bureau uses McIDAS as its primary visualisation and image-processing tool it was decided that all historical data should be converted to a format that would allow it to be utilised within McIDAS. The image data format within McIDAS is called AREA format, so all of the historical imagery needed to be converted to AREA file format. A search of relevant literature was undertaken to ascertain if others had attempted to resurrect scanned imagery in this manner. While no evidence of this was apparent it did reveal that the Japanese Meteorological Agency's (JMA) Meteorological Satellite Centre (MSC) had a significant part of their archive in a digital format (JMA,1980). This format is known as archived Visible Infrared Spin Scan Radiometer (VISSR) and will be referred to herein as VISSR format. These archive data comprise much of the IR imagery that the Bureau only has as scanned tiff files. Converting the VISSR data to AREA format is far more desirable as the quality of

M. Broomhall (✉), I. Grant, L. Majewski, and M. Willmott
Observation and Engineering Branch, Bureau of Meteorology, Melbourne, Australia

D. Jones and Y. Kuleshov
National Climate Centre, Bureau of Meteorology, Melbourne, Australia,

Y. Charabi (ed.), *Indian Ocean Tropical Cyclones and Climate Change*,
DOI 10.1007/978-90-481-3109-9_24,

digital data does not degrade over time. This chapter concentrates on the processes involved in converting scanned imagery to AREA format as it will be needed to fill in the data gap and the conversion of VISSR to AREA in comparison is a trivial matter.

The GMS Satellite

The GMS series of satellites were spin stabilised and deployed into geostationary orbit with a nominal sub-satellite point (SSP) on the equator at 140° East longitude. The imaging system comprised both an IR and visible scanning array which imaged the Earth as its optical system spun past on each revolution, with a scanning mirror stepping the field of view each revolution. The visible imaging system of GMS1 had four detectors imaging each scan line therefore having four times the resolution of IR imagery. The visible imagery had a resolution of 1.25 km with a spectral bandpass of 0.55–0.75 micrometres and the IR imagery had 5 km resolution with a spectral bandpass of 10.5–12.5 micrometres. The appearance of GMS1 and an illustration of the scanning method are shown in Fig. 1 (BOM 1979).

The Reception, Distribution, and Display Method

GMS used the Data Utilisation system, which consisted of the following segments:

- A master control station in Japan that received the data from the satellite, reprocessed it to VISSR format, which was in turn archived to tape, reprocessed it to

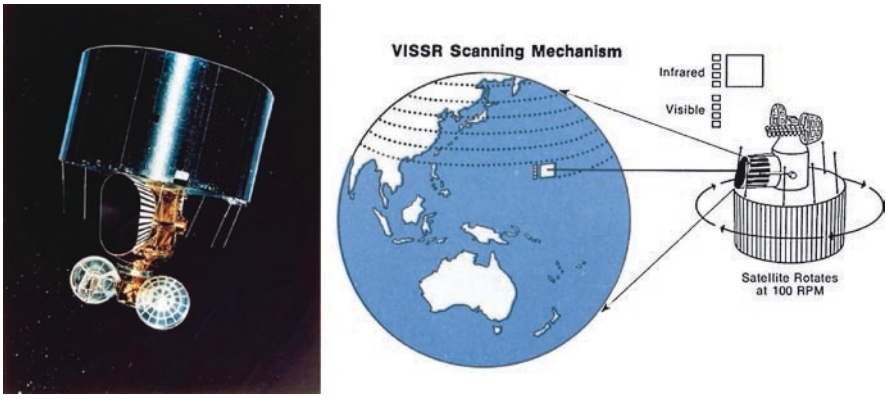

Fig. 1 Artists impression of GMS1 and an illustration of the spin scan method used to image the Earth

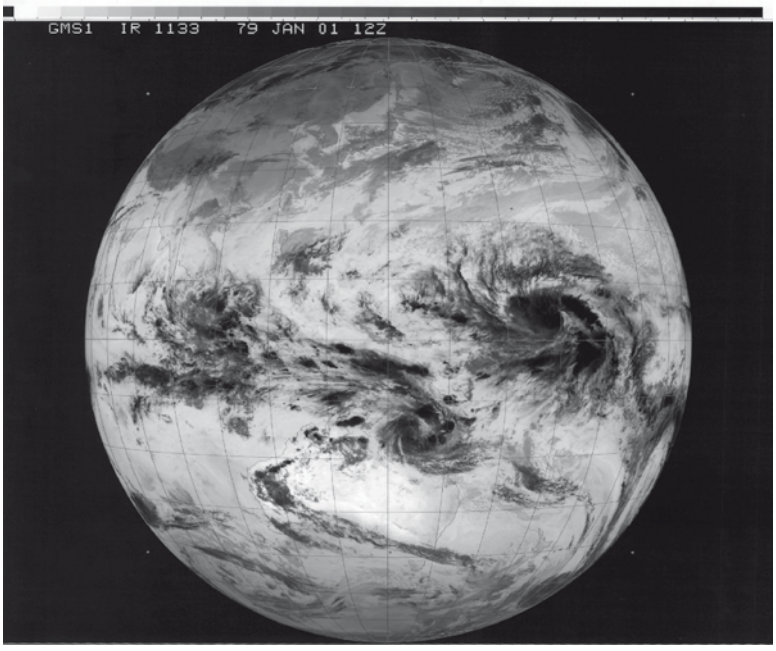

Fig. 2 HR-FAX image displayed here at low quality. This is the GMS 1 IR image for 1133 UTC on January 1, 1979

High Resolution facsimile format (HR-FAX) and transmitted it back to the satellite.

- The Satellite itself transmitted the analogue HR-FAX signal to the Western Pacific region.
- A receiving station complete with laser facsimile printing equipment.

The HR-FAX image produced by this process was printed to a 2' × 2' photo-negative from which contact prints were made and disseminated to forecasters. An example of an HR-FAX image can be seen in Fig. 2.

This image had coastlines and navigation lines spaced 10° apart imbedded in the image when it was reprocessed. The image also contains, a calibration bar at the very top, image type and date stamped into picture. These images were the Bureaus GMS archive.

From Photo-Negative to AREA Format

Converting the photo-negatives to AREA format involved removing the actual image of the globe from the photo-negative scan, retrieving calibration information by utilising the scale bar and navigating the image. The following will explain the calibration and navigation procedures.

Retrieving Calibration Information

The scale bar consists of 32 rectangular boxes, each of which represents a single 6-bit greyscale level and a specific temperature range.

Figure 3 shows sections of the scale bar with the left-hand end representing warmer temperatures, starting at approximately 300 K with each successive box representing a temperature, which is 1.75 K cooler. It is obvious here that the right-hand side of the bar contains boxes which are indistinguishable from one another.

As the final McIDAS AREA format requires a temperature scale with 8-bit values some interpolation is required. The photo-negatives were scanned as 8-bit tiff files so that the entire image, including the scale bar had already been converted to 8-bit values. Each of the 32 boxes now had an 8-bit greyscale representing the same temperature scale. The new greyscale to temperature curve was constructed by interpolating between 32 known values to give 256 temperatures for corresponding greyscale values. This gave a scale that had four times the resolution of the original scale. This temperature scale was then written into the new AREA file header.

Navigating the Images

In order to successfully track any feature within a series of satellite images, the images must be consistently navigated or georeferenced. The navigation on the scanned images would have originally been done by visual interpolation of the position of a feature between the navigation lines imprinted into the image. McIDAS uses a navigation header, which contains parameters for orbital and attitudinal parameters

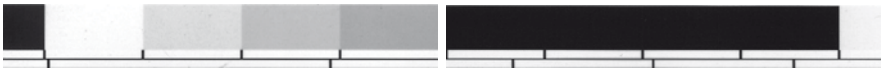

(a) Left hand end of the scale bar (b) Right hand end of the scale bar

Fig. 3 Two sections of the scale bar from Fig. 1. The LHS represents the warm end of the scale, the RHS the cold end of the scale. (**a**) Left hand end of the scale bar. (**b**) Right hand end of the scale bar

to navigate each GMS image through computation. Each pixel should correspond to a unique position on the Earth and have a unique latitude and longitude position. If the scanned images are to be converted to McIDAS AREA format then there must be a navigation header created for each image. The first issue is then to establish known points within the scanned imagery that have a defined latitude and longitude. The most obvious approach is to use the intersections of the navigation lines. These are drawn at 10° intervals for both latitude and longitude with the primary lines at the equator (0°S) and 140°E. Identifying the intersections is simple with the naked eye but can be problematic with an automated process.

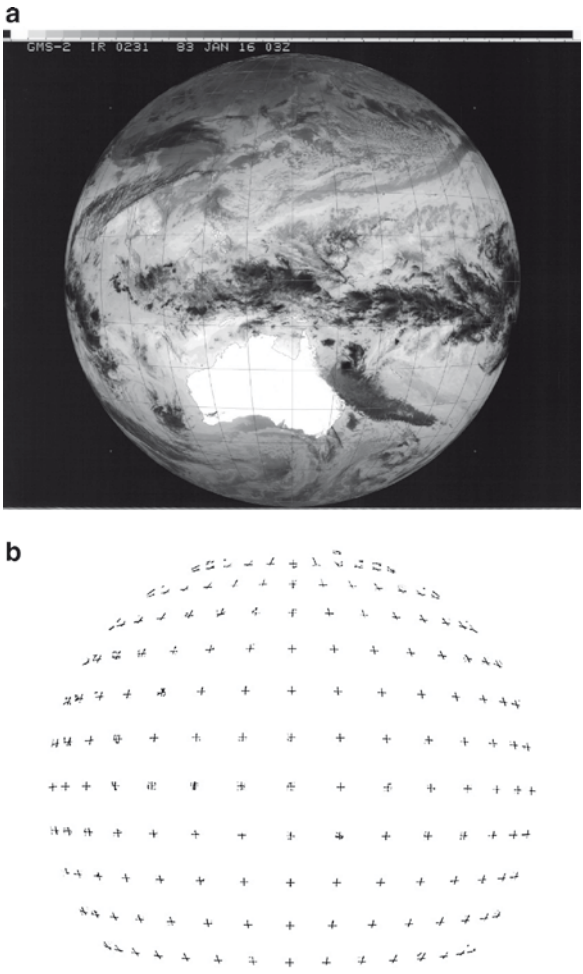

Fig. 4 The contrast enhancement technique is applied only where an intersection is likely. The exact centre pixel of each intersection is then easy to identify with an automated process. This method almost completely removes the background image

The first step is to extract the required part of image from the scanned photo-negative (a process which will not be discussed herein). Step 2 requires highlighting the navigation lines so that the intersection can be more readily found with automated processes. A contrast enhancement technique from Pham and Maeder (1989) is utilised. This highlights pixels that have a high level of contrast from the surrounding pixels. The process, however, is very slow and hence a method to target the areas where the intersection should be and adjust for orientation of the navigation lines was developed. The contrast enhancement process was only run in these locations. The result of this process is shown in Fig. 4.

When complete, the contrast enhancement allows a known latitude and longitude to be assigned to pixel positions within the image as the intersections are now easy to identify. These registered positions can then be used to apply navigation to each pixel in the image. As the ultimate goal is to convert the scanned image data into McIDAS AREA files, a method was found that used McIDAS in the navigation process, which effectively removed a final conversion step. The process also made use of an implementation of the Levenberg-Marquardt algorithm (LMA) for curve fitting called MPFIT (Markwardt 2008) as part of an optimisation process. This process started with a donor McIDAS AREA file with its own calibration and navigation header sections. The navigation header was altered so that it was reasonably close to fitting the scanned image. The alteration was done based on knowledge gained while converting archived VISSR files to McIDAS AREA format and experimentation. Using the donor AREA file, a set of pixel positions for known latitude and longitudes was produced utilising commands within McIDAS. This

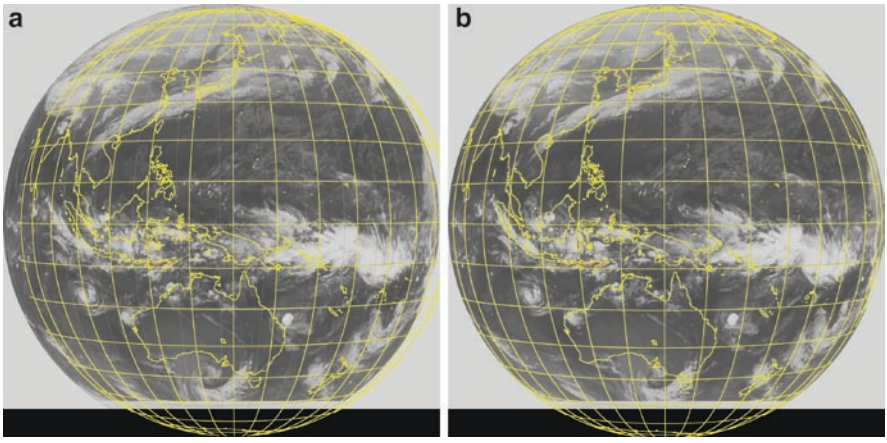

Fig. 5 Screen output from McIDAS of a poor guess (**a**) and the result of this after the optimisation process (**b**)

gave two sets of registered pixel positions that were compared. The comparison was done by calculating the absolute distance between the two sets of pixel values at the same latitude/longitude positions. The optimisation process utilised a Levenberg-Markwardt algorithm (LMA) to alter parameters within the navigation header until the absolute distance comparison was minimised.

An example of this output is shown in Fig. 5. Image (a) shows an exaggerated bad guess where the initial parameters are chosen to be far from the best estimate. Image (b) shows the final result after the optimisation process was run through and altered the navigation parameters to achieve the best fit.

Known Issues and Problems

This project is not complete but a method has been developed to calibrate, navigate, and convert the Bureau scanned GMS archive to McIDAS AREA format. There are still issues to resolve and improvements to be made. The major calibration issue is the lack of contrast at the cold end of the scale bar. In some cases the last 4–6 scale bar boxes cannot be separated by their greyscale value. This makes it very difficult to produce a sensible calibration curve. This lack of resolution at the cold end of the temperature scale may hinder some TC reanalysis techniques such as the Dvorak technique. The biggest issue with the navigation of the images is the manner in which they were scanned. If an image was not placed correctly within the scanning apparatus then it is possible that the image has an artificial tilt introduced. Presently, no method has been considered to identify and then to correct for any induced tilt.

Conclusion

While this remains a work in progress it appears that a viable technique to convert scanned HR-FAX imagery for quantitative computer-based analysis to digital McIDAS AREA has been developed. Utilising data derived from the imagery, knowledge provided by various user manuals and McIDAS algorithms, conversion of the Bureau of Meteorology GMS-scanned imagery to AREA files is now possible. A significant part of the GMS IR archive in VISSR format has been obtained from JMA extending over the period from December 1978 to January 1989 with a sizable gap of missing data. The 14 months of missing data (from November 1979 to March 1981) will have to be filled using the conversion processes outlined above. When this project is complete, the Bureau will have 30 years of continuous satellite data covering the Western Pacific including the Australian region. When available, this 30-year satellite meteorological record will allow analysis of longer-term trends and provide the ability to utilise modern techniques to re-analyse, in particular, hazardous weather phenomena such as tropical cyclones.

References

JMA (1980) The GMS users guide: issue 1. Meteorological Satellite Centre, Japan Meteorological Agency, Haneda, Tokyo

Pham B, Maeder A (1989) Removal of navigational lines from GMS images. Australian Meteorological Magazine 37:93–97

BOM (1979) GMS: geological meteorological satellite. Bureau of Meteorology, Commonwealth of Australia

Markwardt C (2008) Markwardt IDL Library. URL: http://cow.physics.wisc.edu/~craigm/idl/idl.html, Last accessed (01/12/2008)

URL: http://cow.physics.wisc.edu/~craigm/idl/idl.html, Last accessed (01/12/2008)

Coastal Vulnerability Assessment Based on Historic Tropical Cyclones in the Arabian Sea

Chris Blount, Hermann M. Fritz, and Ahmed Hamoud Mohammed Al-Harthy

Keywords Coastal vulnerability assessment • storm surge model description

Introduction

In the last 1200 years, three catastrophic tropical cyclones have been documented to strike the Sultanate of Oman. Cyclone Gonu, the most recent in 2007, caused over $4 billion damage and left high water marks of over 5 m. Here the model applied in Fritz et al. (2009) is described in detail and is used to estimate the storm surge and storm track from the two major historic events recorded previously in 1890 and 865. According to the facsimile original British documents found in Bailey (2008), "the 1890 cyclone remains the most devastating coastal disaster in Oman's recorded history: A severe cyclone accompanied with heavy and continuous rain, occurred here [Muscat] and all along the coast from Soor to Suwaik on the 4th and 5th [of June]. … The quantity of rain which was registered at the Civil Hospital from the commencement of the storm to the end, a period of about 24 hours, was 11 inches and 24 cents. Mattrah being open to the north-east wind the furry of the storm was principally expended there and several [ships] were washed ashore. … The disastrous were unfortunately not confined only to these two towns,

C. Blount (✉)
Graduate Research Assistant, Civil and Environmental Engineering, Georgia Institute of Technology, Savannah, GA, 31407, USA
e-mail: chris.blount@gatech.edu

H.M. Fritz
Associate Professor, Civil and Environmental Engineering, Georgia Institute of Technology, Savannah, GA, 31407, USA
e-mail: fritz@gatech.edu

A.H. M. Al-Harthy
Director of Meteorology, Department of Meteorology, Directorate General of Civil Aviation and Meteorology, Muscat, Sultanate of Oman
e-mail: a.alharthy@met.gov.om

Y. Charabi (ed.), *Indian Ocean Tropical Cyclones and Climate Change*,
DOI 10.1007/978-90-481-3109-9_25,

but extended right into the interior as far as the Semaeel valley on one side and the Wadi Beni Gafir on the other".

The records continue by stating that the entire Batineh region was affected and that the Sultan estimated at least 727deaths directly attributable to the storm. Over 100,000 date trees, which constituted the principal wealth of the country, were destroyed, and it was estimated that it would take 15 years to recover from the agricultural loss. The 865 cyclone occurred on May 2 and "the whole of the country between Gobrah and Sohar was laid waste and several people were carried away by the overflooded condition of the valleys into the sea." The May and June landfall dates of these major historic cyclones impacting Oman coincide with cyclone Gonu. Based on the historic information, multiple tracks were simulated applying the ADCIRC storm surge model developed by Luettich et al. 1992. Since no water-level data are available only qualitative comparisons are possible between the model results and the descriptions of the flooded areas.

Methodology

Storm Surge Model Description

The fully nonlinear, barotropic, depth-integrated hydrodynamic model ADCIRC-2DDI was used to perform the storm surge computations (Luettich et al. 1992). The primitive governing continuity is given as:

$$\frac{\partial \xi}{\partial t} + \frac{1}{R\cos\varphi}\left[\frac{\partial UH}{\partial \gamma} + \frac{\partial \left(VH\cos\varphi\right)}{\partial \varphi}\right] = 0 \tag{1}$$

where ξ is the free-surface elevation, U and V are the depth-averaged horizontal velocities, $H = h + \xi$ is the total water depth, h is the bathymetric depth, and φ and λ are the degrees of latitude and longitude, respectively. The primitive momentum equations in the λ and φ directions, respectively, are given as:

$$\frac{\partial U}{\partial t} + \frac{1}{R\cos\varphi}U\frac{\partial U}{\partial \lambda} + \frac{V}{R}\frac{\partial U}{\partial \varphi} - \left(\frac{\tan\varphi}{R}U + f\right)V = -\frac{1}{R\cos\varphi}\frac{\partial}{\partial \lambda}\left[\frac{p_s}{\rho_0} + g\left(\xi - \alpha\eta\right)\right] + \frac{\tau_{s\lambda}}{\rho_0 H} - \tau_* U \tag{2}$$

$$\frac{\partial V}{\partial t} + \frac{1}{R\cos\varphi}U\frac{\partial V}{\partial \lambda} + \frac{V}{R}\frac{\partial V}{\partial \varphi} - \left(\frac{\tan\varphi}{R}U + f\right)U = -\frac{1}{R\cos\varphi}\frac{\partial}{\partial \varphi}\left[\frac{p_s}{\rho_0} + g\left(\xi - \alpha\eta\right)\right] + \frac{\tau_{s\varphi}}{\rho_0 H} - \tau_* V \tag{3}$$

where $f = 2\Omega\sin\Phi$ is the Coriolis force, Ω is the angular speed of the Earth, p_s is the atmospheric pressure, g is gravitational acceleration, η is the Newtonian equilibrium tide potential, α is the effective Earth elasticity factor, ρ_0 is the reference density of water, $\tau_{s\lambda}$ and $\tau_{s\phi}$ are the applied free-surface stresses; $\tau_* = C_f(U^2 + V^2)^{1/2}/H$ is the bottom friction, and C_f is the bottom friction coefficient. Here the friction coefficient has been chosen as the hybrid form, as implemented by Luettich and Westerink (1999)

$$C_f = C_{f_{\min}}\left[1+\left(\frac{h_{break}}{H}\right)^{\theta}\right]^{\frac{\gamma}{\theta}} \tag{4}$$

where the values $C_{f\min} = 0.003$, $h_{\text{break}} = 2$ m, $\theta = 10$, and $\gamma = 1.3333$ are taken in accordance to Westerink et al. (2008). This formulation, which causes a more realistic wetting/drying front, creates a Manning-type friction law below the break depth h_{break} and a Chezy friction law deeper than the break depth (Mukai et al. 2002; Westerink et al. 2008). ADCIRC uses the generalized wave continuity equation (GWCE), which is a manipulation and combination of the primitive continuity and momentum equations, to prevent spurious oscillations in the solution. The GWCE depends on a numerical constant τ_0 that sets the balance between the pure wave form and the primitive form of the continuity equations. The correct selection of τ_0 is related to the bottom friction (Kolar et al. 1994) and as such the recent versions of ADCIRC allow for spatially and temporally variable τ_0 to be calculated on the fly. The model uses a Galerkin finite element approach based on linear triangles. Details on the current implementation of the GWCE and the finite element model can be found in the implementation manual (Luettich and Westerink 2004).

Hurricane Wind Model Description

Recently, two hurricane wind models were implemented into ADCIRC by Mattocks, Forbes, and Ran (2006). The first represents an axisymmetric version of the Holland (1980) gradient wind model. The second is an asymmetric version of the Holland model which uses the forecast information available from the National Hurricane Center or the Automated Tropical Cyclone Forecasting (ATCF) best-track data. For the Indian Ocean, ATCF best-track data can be obtained from the Joint Typhoon Warning Center (JTWC) or the advisories from the JTWC and RSMC, New Delhi, storm advisories can be reconstructed into this format. The pressure distribution is determined by the following relation:

$$P(r,\theta) = P_c + (P_n - P_c)\exp\left[-\left(R_{\max}(\theta)/r\right)^B\right] \tag{5}$$

where P is the pressure at radius r and angle θ, P_c is the central pressure, P_n is the synoptic (or far field) pressure, and R_{max} is the radius to maximum winds as a function of θ. The shape parameter B specifies the shape of the wind profile and is defined as:

$$B = \frac{\left[\left(V_{max} - V_T\right)/WR\right]^2 \rho_a e}{\left(P_n - P_c\right)} \tag{6}$$

where V_{max} is the maximum sustained 1 min wind speed in the cyclone, V_T is the translational speed of the storm, ρ_a is the density of air, and WR is a wind reduction factor used to adjust the speeds from outside the planetary boundary layer to the surface level. Assuming the winds are in gradient wind balance, the tangential velocity can be found as follows:

$$V_{asym} = \sqrt{\frac{B}{a}\left(\frac{R_{max}(\rho)}{r}\right)\left(P_n - P_c\right)\exp\left[-\left(R_{max}(\rho)/r\right)^B\right] + \left(\frac{rf}{2}\right)^2} - \left(\frac{rf}{2}\right) \tag{7}$$

The direction of the wind is then adjusted by a cross-isobar frictional inflow angle. The synthetic vortex has been shown to give very good approximations to the H*Wind surface wind analysis developed by the National Oceanic and Atmospheric Administration (NOAA) Atlantic Oceanographic and Meteorological Laboratory (AOML) Hurricane Research Division, which is considered the best hurricane wind estimates available in the USA. The lack of inland wind decay remains as a deficit of the synthetic vortex. The reader should note that the ADCIRC code was modified by the ADCIRC development group from the release version used (47.27) to account for the change to the eastern hemisphere from its native western hemisphere.

Grid Development

The finite element grid domain was chosen to incorporate all of the Arabian Sea north of 9°N latitude as nearly all cyclones developed in the basin initiate north of this. The domain includes all major connected water bodies (the Persian Gulf, the Gulf of Oman, and the Gulf of Aden) except for the Red Sea which is replaced by a wave radiation boundary specified at the shallow and narrow Bab al-Mandab between Djibouti and Yemen. The coastline was obtained from the global, self-consistent, hierarchical, high-resolution shoreline database (Wessel and Smith 1996). The bathymetry was obtained from National Geophysical Data Center's ETOPO1 1 arc-minute global relief model (Amante and Eakins 2008). The grid was developed using the surface-water modeling system (SMS) mesh generator based on the scalar paving density function. The size of each element was determined by combining the M_2 wavelength to grid size ratio and the topographic length-scale

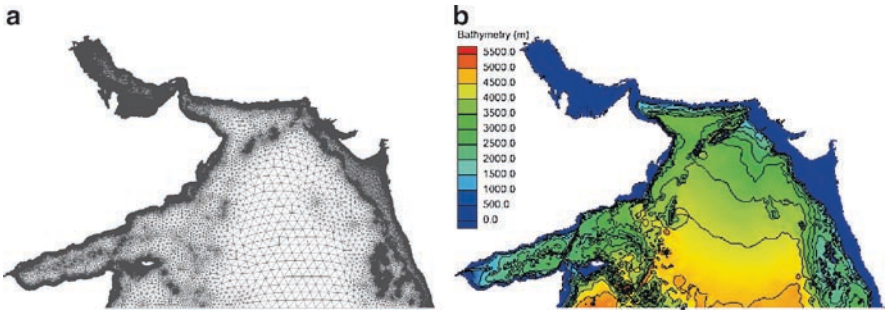

Fig. 1 Arabian Sea: (**a**) finite element mesh containing 125,511 nodes and 231,770 elements; (**b**) corresponding bathymetry obtained from ETOPO1

criteria according to Mukai et al. (2002) with target values of $\lambda/x = 100$ and $\alpha = 1.0$. The target minimum and maximum element sizes were 1 km and 80 km, respectively. The resulting mesh (Fig. 1) contained 125,511 nodes and 231,770 elements.

Hypothetical Storm Tracks and Parameter Selection

Since no wind measurements are available for the historic cyclones under consideration, a representative wind field is selected. For all simulations, the cyclone wind parameters where held constant and approximated by the JTWC data corresponding to the highest wind speed for cyclone Gonu (145 kt and 914 mb at 12:00 June 4, 2007). The selected track points were chosen to maintain relatively constant translational speed over 6 h periods corresponding to the temporal resolution of JTWC data.

The hypothetical tracks approximating the two cyclones in the simulations are shown in Fig. 2. The initial estimate of the 1890 storm track (Track 1) was obtained by digitizing a storm track figure received from the Department of Meteorology in Muscat, Sultanate of Oman. Track 2 represents a hypothetical case of a storm propagating roughly parallel to the south shore of the Gulf of Oman. Tracks 3–6 are modifications of the approach angle of the cyclone. The area of landfall was kept in accordance with Track 1 as the landfall area may be historically accurate based on the digitized figure.

Results and Discussion

The simulations indicate that the 1890 track based on historical records (Track 1) appears to compare more favorably to the 865 description of the most intense flooding between Sohar and Gobrah (Fig. 3a). The maximum storm surge is approximately

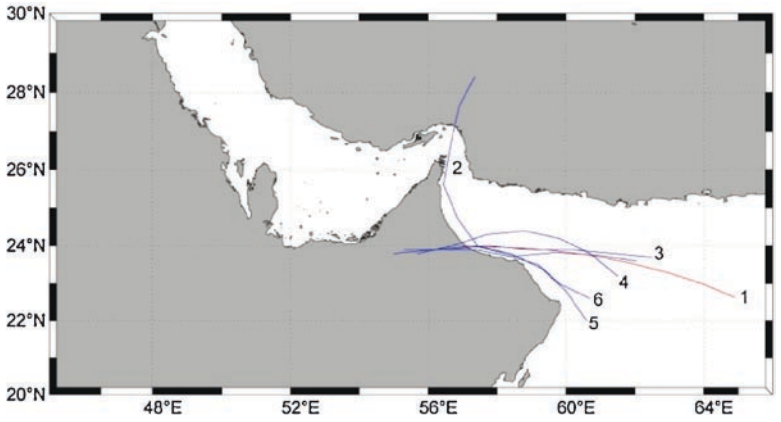

Fig. 2 Tracks used for the simulations: Track 1 is the 1890 obtained from government records and subsequent tracks are permutations of Track 1

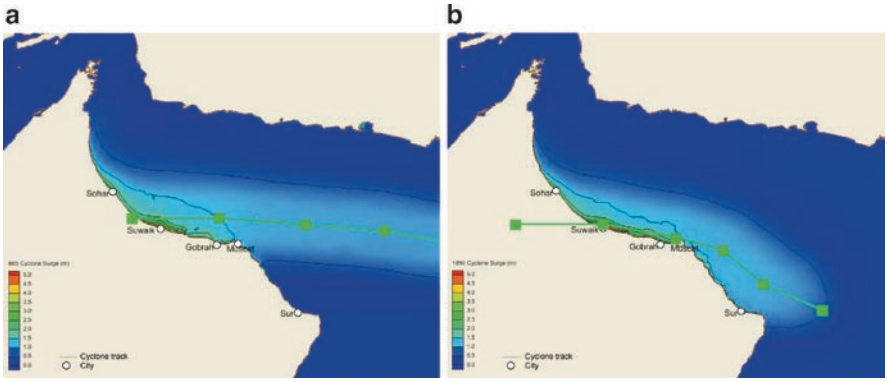

Fig. 3 Tropical cyclone tracks estimated from storm surge simulations: (**a**) the 865 cyclone, and (**b**) the 1890 cyclone

4.75 m at Suwaik with surge levels exceeding 2.5 m near Sohar and mostly between 2 and 2.5 m near Gobrah. The surge level is still above 1 m southeast of Muscat. In order to flood from Sur to Suwaik, it appears that the 1890 storm may have paralleled the shoreline more than previously assumed (Fig. 3b). Tracks 5 and 6 yield similar results except that Track 5 yields a storm surge south of Ras al Hadd that is not described in the historical text. Track 6 is most likely closer to the actual track because the edge of the surge distribution is near Sur which is in accordance with records. The peak storm surge from Muscat to Sur remains mostly between 1 and 1.5 m with intermittent peaks exceeding 2.5 m. The peak storm surge near Muscat and Mattrah is 2.3 m inside the harbor. The peak storm surge rapidly increases from around 2 m at Qurm to 3.3 m at Gobrah. The peak surge for the 1890 storm is

determined to be 5.4 m again at Sohar. On the northern side of the track at landfall, the storm surge maintains a level exceeding 2 m past Sohar. These results suggest that the initial path of the 1890 cyclone could have been similar to cyclone Gonu without turning northwards towards Iran, but making landfall near Suwaik.

Conclusions

A high resolution storm surge model (ADCIRC) was used to estimate the storm surge induced by the 865 and 1890 tropical cyclones which are known to have devastated Omani coastlines. British records give some description of the impact and the inundated areas for both storms. Simulations were carried out with ADCIRC to estimate the storm surge distribution and the appropriate track for each storm based on the historical descriptions. Storm parameters were selected in accordance with the peak wind field of cyclone Gonu (the strongest storm recorded in the Arabian Sea). These results suggest that for the 1890 cyclone to match the significant impact, as described in historical British records, the storm could possibly have followed a path closer to shore than originally thought (based on government records). However, the track obtained from the government records appears to match the 865 cyclone storm surge. As the economical development of Oman continues along the northern coast, an understanding of the coastal vulnerability will increase in importance. This became evident with cyclone Gonu which caused over $4 billion in damage. For a detailed assessment of the coastal flood hazards several advanced features will have to be incorporated in the model. This includes adding higher-resolution bathymetry near the coast and high-resolution topography (including important hydraulic features) governing inundation such as dunes. This will allow the inclusion of the wadi flow, which will highlight the interplay between wadi runoff and the inland effects of cyclones. Coupling a short-wave model with the storm surge model will also increase the estimated storm surge through wave-induced set-up and this will reveal the relative contributions of surge and waves to high water marks. The coast of Oman represents a unique setting in this respect. The bathymetry from Ras al Hadd to Muscat is steep which will decrease the storm surge but will likely increase the affect of waves. The storm surge flooding hazard is expected to increase in the rare event of a cyclone landfall along the shallow shelf between Muscat, Oman, and Al Fujayrah, United Arab Emirates. A hypothetical worst case would likely involve a cyclone landfall perpendicular to the shoreline, which along a similarly shallow and converging coastline has caused storm surge up to 10 m during Hurricane Katrina (Fritz et al., 2008).

Acknowledgments The authors would like to thank the ADCIRC development team for use of their code. Special thanks go to Dr. Christina Forbes and Dr. Jason Fleming at the Institute of Marine Sciences at the University of North Carolina for ADCIRC-related support. The Meteorology Department of the Sultanate of Oman provided the historic records.

References

Amante C, Eakins BW (2008) ETOPO1 1 Arc-Minute Global Relief Model: procedures, data sources and analysis, National Geophysical Data Center, NESDIS, NOAA, US Department of Commerce, Boulder, CO, August 2008

Bailey RW (ed) (2008) Records of Oman: 1867–1947. 8 vols. Archive Editions, Buckinghamshire, England

Fritz HM, Blount C, Sokoloski R, Singleton J, Fuggle A, McAdoo BG, Moore A, Grass C, Tate B (2008) Hurricane Katrina Storm Surge Reconnaissance. J Geotech Geoenv Eng ASCE 134(5):644–656, doi:10.1061/(ASCE)1090-0241

Fritz HM, Blount C, Albusaidi FB, Al-Harthy AHM (2009) Cyclone Gonu Storm Surge in the Gulf of Oman. Proceedings of the First International Conference on Indian Ocean Tropical Cyclones and Climatic Change (in this volume)

Holland GJ (1980) An analytical model of the wind and pressure profiles in hurricanes. Mon Wea Rev 108:1212–1218

Kolar RL, Westerink JJ, Cantekin ME, Blain CA (1994) Aspects of nonlinear simulations using shallow water models based on the wave continuity equation. Comput Fluids 23(3):523–538

Luettich RA, Jr, Westerink JJ (1999) Elemental wetting and drying in the ADCIRC hydrodynamic model: upgrades and documentation for ADCIRC version 34.XX, Contractors Report, Department of the Army, US Army Corps of Engineers, Waterways Experiment Station, Vicksburg, MS, March 1999, 8p

Luettich RA, Westerink JJ (2004) Formulation and Numerical Implementation of the 2D/3D ADCIRC Finite Element Model Version 44.XX. (Available online at http://www.adcirc.org/adcirc_theory_2004_12_08.pdf)

Luettich RA, Jr, Westerink JJ, Scheffner NW (1992) ADCIRC: an advanced three-dimensional circulation model for shelves, coasts and estuaries, Report 1: theory and methodology of ADCIRC-2DDI and ADCIRC-3DL, Dredging Research Program Technical Report DRP-92-6, US Army Engineers Waterways Experiment Station, Vicksburg, MS, 137p

Mattocks C, Forbes C, Ran L (2006) Design and implementation of a real-time storm surge and flood forecasting capability for the State of North Carolina, UNC-CEP Technical Report, 103 pp

Mukai AY, Westerink JJ, Luettich RA Jr, Mark D (2002) Eastcoast 2001: a tidal constituent database for the western North Atlantic, Gulf of Mexico and Caribbean Sea, US Army Engineer Research and Development Center, Coastal and Hydraulics Laboratory, Technical Report, ERDC/CHL TR-02-24, September 2002, 201p.

Wessel P, Smith WHF (1996) A global self-consistent, hierarchical, high-resolution shoreline database. J Geophys Res 101(B4): 8741–8743

Westerink JJ, Luettich RA, Feyen JC, Atkinson JH, Dawson C, Roberts HJ, Powell MD, Dunion JP, Kubatko EJ, Pourtaheri H (2008) A basin- to channel-scale unstructured Grid Hurricane Storm Surge Model applied to Southern Louisiana. Mon Wea Rev 136:833–864. doi:10.1175/2007MWR1946.1

The International Best Track Archive for Climate Stewardship (IBTrACS) Project: Overview of Methods and Indian Ocean Statistics

David H. Levinson, Kenneth R. Knapp, Michael C. Kruk, Howard J. Diamond, and James P. Kossin

Keywords Climate Stewardship (IBTrACS) Project

Introduction

Despite the widespread interest in data that describes the distribution, frequency, and intensity of tropical cyclones worldwide, until recently no central repository for official data existed. Currently, there are six Regional Specialized Meteorological Center's (RSMC) and five Tropical Cyclone Warning Centers (TCWC) that forecast and monitor each of the tropical-cyclone-prone basins worldwide. On an annual basis each center analyzes and archives best track (BT) data: information on tropical cyclone positions, intensities, as well as other related parameters. To rectify this situation, the International Best Track Archive for Climate Stewardship (IBTrACS) Project was developed by NOAA's National Climatic Data Center under the auspices of the World Data Center for Meteorology, Asheville to collect and disseminate the historical tropical cyclone BT data from all available sources, merging the disparate data into one comprehensive dataset for the user community (Kruk et al. 2009). Unlike any other global tropical cyclone best track dataset, IBTrACS utilizes complex merging techniques, which necessarily account for the inherent differences between BT datasets while applying objective quality control procedures to flag potentially erroneous data points. Therefore, one of the primary goals of the IBTrACS project is for the data processing methods to remain open, such that desired user feedback on data quality can be collected more readily and assessed. In addition, data provenance is completely recorded in IBTrACS so that all observations and corrections, either through rigorous quality control or through user feedback, may be tracked and provided to users. This article will summarize

D.H. Levinson (✉), K.R. Knapp, H. J. Diamond, and J.P. Kossin
NOAA National Climatic Data Center, Asheville, NC, USA

M.C. Kruk
STG Incorporated, Asheville, NC, USA

Y. Charabi (ed.), *Indian Ocean Tropical Cyclones and Climate Change*,
DOI 10.1007/978-90-481-3109-9_26,

the purpose and vision of the project, the methods used to merge the data, and discuss results of computed basin-wide tropical cyclone statistics for both the North and South Indian Ocean basins.

Data

Tropical cyclone BT data are required by the World Meteorological Organization (WMO) to be reported by each of the RSMCs and TCWCs. These centers are designed to cover each major ocean basin: North Atlantic (NA), Eastern Pacific (EP), Western North Pacific (WP), Northern Indian Ocean (NI), Southern Indian Ocean (SI), and South Pacific (SP). In addition, other agencies track TCs in ocean basins where their country has an interest. The following agencies provided BT data for inclusion in the IBTrACS merged dataset for the North and South Indian Ocean basins:

- BoM: Australian Bureau of Meteorology
- IMD: India Meteorological Department (as RSMC New Delhi)
- JTWC: US Department of Defense Joint Typhoon Warning Center
- MFLR: MeteoFrance (as RSMC La Reunion)

Hereafter, these are collectively referred to as forecast centers. Best track data are generally produced by these centers for each tropical cyclone with an intensity of at least 25 kt (i.e., a minimal tropical depression). However, tropical cyclogenesis and cyclolosis dates, as well as reporting times, and intensities often vary by forecast center. Ideally, a global BT dataset should incorporate information from all available resources to ensure completeness, which was a fundamental objective of the IBTrACS project. Note that additional data for the southern hemisphere was obtained from Neumann (1999) and was included and added to the South Indian Ocean basin since it incorporated data sources not listed above.

Upon receipt of the electronic files, data were converted into a common format. The BT input files were obtained in numerous formats: NOAA data tape format (i.e., HURDAT; Jarvinen et al. 1984, Landsea et al. 2004), spreadsheet tables, various ASCII formats, and even photocopied storm reports that were then digitized by NOAA's Climate Database Modernization Program (Dupigny-Giroux 2007). All BT data were converted to Network Common Data Form (netCDF) format (Rew and Davis 1990), since it allows for the storage of many variables along with their descriptions, is supported by Unidata, and has software interfaces for use with numerous programming languages.

Methods

The first step toward a merged, global BT dataset was identifying large errors in track positions. These often tended to be keying errors when digitizing the track data (e.g., transposing numbers or repeating a position). The term "large" refers to gross errors that are approximately 111 km or more. Potential errors in a storm track were assessed based on how well a track followed a "smooth" path.

First, track positions were converted from latitude, longitude, and distance from the Earth's center to three-dimensional Cartesian coordinates (x, y, z), to avoid discontinuities at either the Dateline or Prime Meridian. The smoothness of any point along a TC track in Cartesian coordinates was estimated using a cubic-spline interpolation. Next, storm tracks were queried to determine which storms were identified by one or more forecast centers. An automated algorithm was then developed that identified storms reported by multiple forecast centers by sorting tracks temporally and spatially. Any tracks (from the same or different forecast centers) with at least two concurrent positions within 111 km were identified as one storm. Also, four track positions (equivalent to 1 day) were extrapolated beyond the end of the track to identify storms that were dropped by one center and picked up by another. Storms which crossed a geographic basin were identified as a single storm regardless of the intermediate storm intensity as it crossed basin boundaries (although a cross-basin storm flag is provided in the final data).

The time of each reported position was also assessed. In some cases, reports from different forecast centers had similar positions for a storm with some offset in time. An algorithm compared the distances between reported positions from different centers. When the algorithm found shorter mean distances between reported positions by shifting (either forward or backward) the time for a center in an increment of 6 h, then the correction was kept in IBTrACS. The time-check algorithm, however, cannot objectively determine which center was reporting the correct time. Out of all 16,539 tracks in IBTrACS, only 255 tracks required time adjustments.

In merging the time coordinate, the longest possible storm track was pieced together by using the first to the last position from all track data for a storm. Since some BT data contained once-daily or 12-h reports, the time coordinates were normalized to 6 h prior to merging by interpolating the position with cubic-splines and holding intensity based on maximum sustained winds (MSW) or minimum central pressure (MCP) constant during the time period (such that calculated indices would not vary between the daily and 6-h tracks). Storms unique to only one forecast center had no further adjustments. For the remaining 4,214 storms reported by multiple forecast centers globally, the IBTrACS position was the average position for each time step. Finally, once individual storms were identified, BT data were processed by merging time coordinates, addressing storm positions and storm intensities via MSW and MCP. The resultant central pressure provided in IBTrACS is simply the average from each of the reporting centers (although the ranges in pressures are also provided). However, the merging process was more complex for MSW due to differences in operating procedures at the forecast centers, which were addressed by converting all MSW values to the 10-min standard used by the World Meteorological Organization (WMO).

Indian Ocean Statistics

A fundamental advantage of the IBTrACS dataset is the ability to determine the statistical variability of BT data since the source data includes input from multiple forecast centers. This is also true for both the North and South Indian Ocean basins, which are covered by the forecast centers listed in Section "Data".

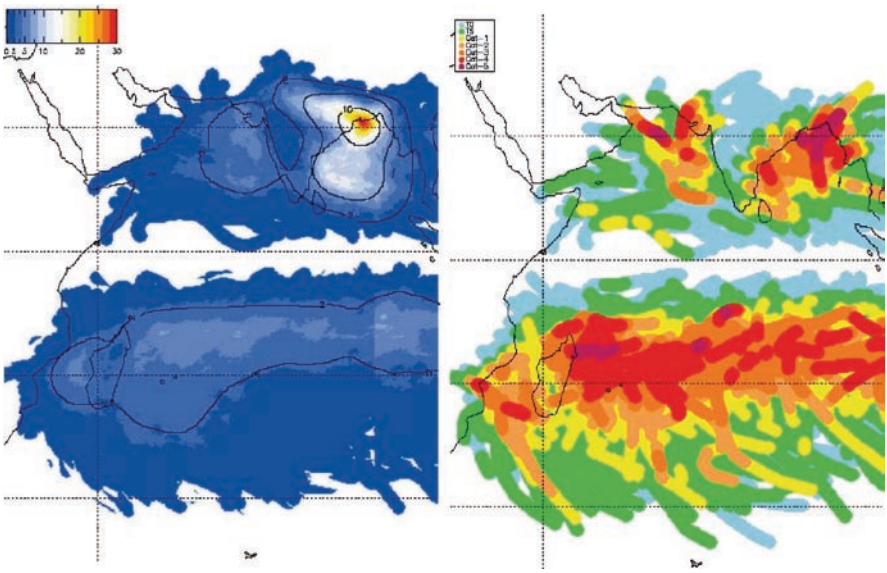

Fig. 1 (*Top*) frequency (counts decade-1 within 1o latitude/longitude for each tropical cyclone along its track), and (*bottom*) maximum intensity of each tropical cyclone in IBTrACS based on Saffir-Simpson categories. Note that the period of record used for the North Indian basin was 1945 to 2007, and for the South Indian basin was 1848 to 2007

Figure 1 shows the spatial variability of tropical cyclone frequency and maximum intensity for both the North and South Indian Ocean basins. In terms of frequency (top panel), which is displayed as counts decade-1, the highest frequency occurs in the Bay of Bengal in the North Indian basin, where as many as 30 tropical cyclones per decade are observed along and offshore of the southern coast of Bangladesh. The highest frequencies in the South Indian basin are distributed fairly evenly along the monsoon trough between 10° and 20°S.

In terms of the maximum intensity (bottom panel of Fig. 1), the spatial variability in the Indian Ocean has several regions where the strongest storms typically occur. In the North Indian basin, the Bay of Bengal is the focus for the most severe tropical cyclone activity, with several storms that have reached Category 5 intensity based on the Saffir-Simpson scale (Simpson 1974). Severe tropical cyclones are more evenly distributed in the South Indian basin, with a broad region in the western half of the basin east of Madagascar where numerous Category 4 and 5 tropical cyclones have been observed historically.

These regions of tropical cyclone activity in the Indian Ocean can also be seen in terms of the mean intensity and standard deviation of the intensity (Fig. 2). In the North Indian basin the highest mean intensity is observed in the northern portions of both the Bay of Bengal and the Arabian Sea. Note that the region of highest mean intensity is located near the coast and extending inland over coastal portions of Bangladesh and Myanmar. Obviously this has significant implications for

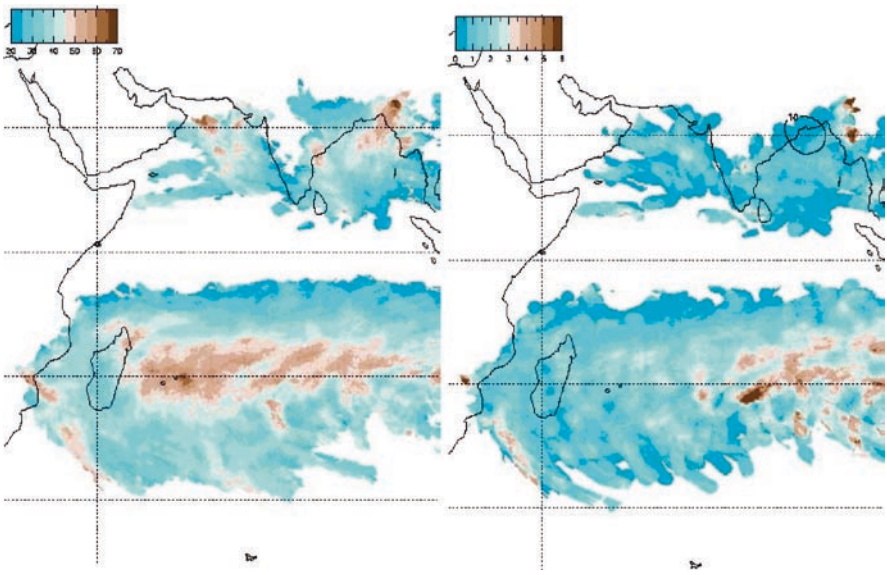

Fig. 2 (*Top*) mean intensity of every Indian Ocean tropical cyclone in IBTrACS, and (*bottom*) standard deviation of the maximum sustained winds for all Indian Ocean tropical cyclones in IBTrACS (units are in kt). The period of record used is the same as in Fig. 1

cyclone impacts due to the dense population centers in these areas. Over the South Indian basin the highest mean intensities once again cover a broad region of the basin east of Madagascar. Standard deviations of the observed cyclone intensities show that the forecast centers BT intensity estimates varied widely over the eastern half of the South Indian basin (bottom panel of Fig. 2). This region has the highest number of forecast centers tracking storms in the basin, as the Australian BoM tracks cyclones east of 90°E. For the North Indian basin, the situation is much different, with the largest variance observed over land after landfall.

Figure 3 shows the time series of the Power Dissipation Index (PDI), which is a measure of tropical cyclone activity that incorporates intensity over time (Emanuel 2005). In its simplest form the PDI is defined as the cube of the 6-h BT wind intensities, which are summed for all periods that a tropical cyclone was at tropical storm intensity (10-min wind ≥30 kt) or greater. In general, the South Indian basin is much more active than the North Indian basin, but both basins show significant interannual variability. Tropical cyclone activity in the North Indian basin is relatively low in most years, below 15 × 106 kt3, except for rare hyperactive seasons such as 2007 and 1998 when the PDI is a factor of three larger (>30 × 106 kt3). In contrast, for the South Indian basin most years are generally active, with occasional years with below normal activity. There is far more variability in the South Indian basin on account of the greater number of forecast centers tracking storms in this region.

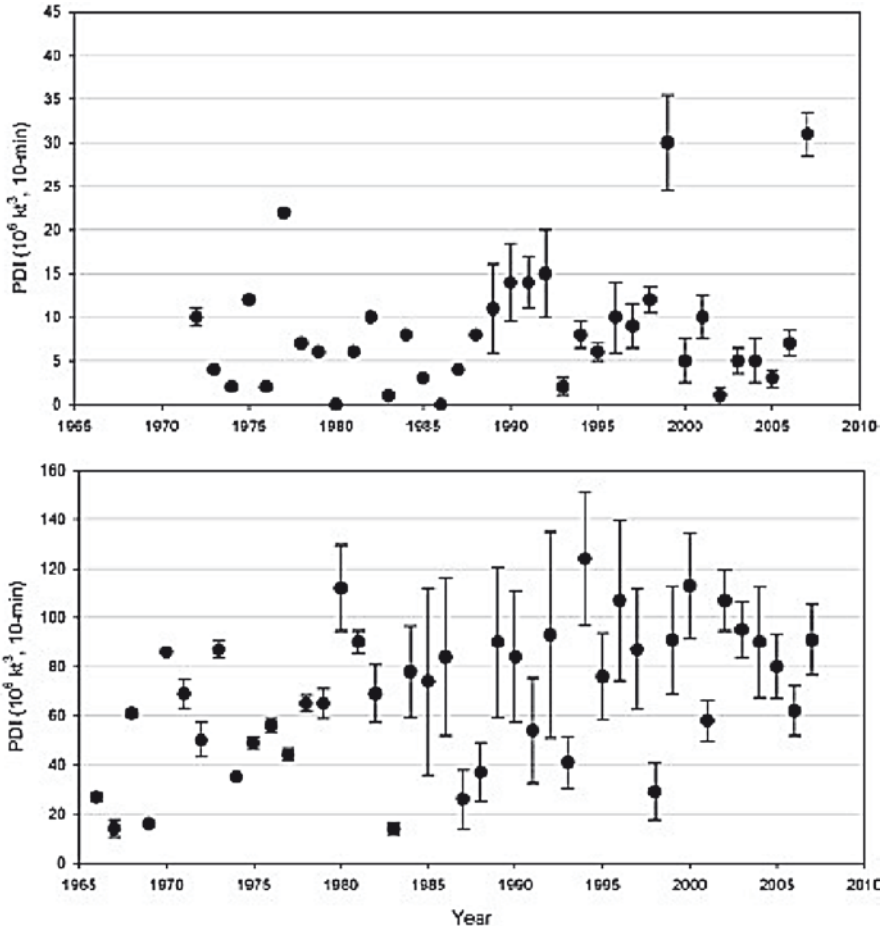

Fig. 3 Power Dissipation Index (PDI; in units of 106 kt3) for the North Indian Ocean basin (*top*) and the South Indian Ocean basin (*bottom*) determined using intensity data from the IBTrACS merged dataset. The whisker plots denote the range in PDI values based on those BT points reported by multiple forecast centers

Summary

This paper provided an overview of the best track dataset merging process used to develop a new global tropical cyclone dataset – the International Best Track Archive for Climate Stewardship (IBTrACS). The best track data provided in this archive are the positions and intensities (via minimum central pressure and/or maximum sustained wind) of each storm available from all resources and was derived using detailed quality assessments. In the process of merging the data from each of the forecast centers, statistics were calculated to provide information on the

variations in position and intensities. Also, prior to merging the best track data, quality assessments of the position and intensity were made. While some gross position errors were found and corrected, all intensity values were retained in the final data along with the quality assessment results. The IBTrACS positions and intensities are, therefore, the average position and intensity tracked by official forecast centers. It has been demonstrated that in creating a new global tropical cyclone best track dataset, it is imperative that best track data be included from all forecast centers. This is especially critical when analyzing global tropical cyclones since using data from any one center will likely result in missed TCs. One major advantage the IBTrACS dataset has over other available best track data is that it provides the full range of reported values for pressure, intensity, and position, for each 6-h time step. This information was previously unavailable for assessing data quality and variance.

References

Dupigny-Giroux L-A, Ross TF, Elms JD, Truesdell R, Doty SR (2007) NOAA's Climate Database Modernization Program rescuing, archiving, and digitizing history. Bull Am Meteor Soc 88:1015–1017

Emanuel K (2005) Increasing destructiveness of tropical cyclones over the past 30 years. Nature 436:686–688

Jarvinen BR, Neumann CJ, Davis MAS (1984) A tropical cyclone data tape for the North Atlantic Basin, 1886–1983: contents, limitations and uses. NOAA Technical Memo NWS NHC 22, NOAA/National Hurricane Center, Miami FL, 21 pp (available from NOAA/Tropical Prediction Center, 11691 S.W. 17th St., Miami, FL 33165-2149)

Knapp KR, Kossin JP (2007) New global tropical cyclone data from ISCCP B1 geostationary satellite observations. J Appl Remote Sens 1:013505

Kruk MC, Knapp KR, Levinson DH, Diamond HJ, Kossin JP (2009) An Overview of the International Best Track Archive for Climate Stewardship. Preprints, 89th Annual Meeting, Phoenix, AZ, Am Meteor Soc

Landsea CW et al. (2004) The Atlantic hurricane database re-analysis project: Documentation for the 1851–1910 alterations and additions to the HURDAT database. In: Murnane RJ, Liu KB (eds) Hurricanes and typhoons: past, present and future. Columbia University Press, New York, pp 177–221

Neumann CJ (1999) The HURISK model: an adaptation for the southern hemisphere (a user's manual). Prepared by Science Applications International Corporation (SAIC), US Naval Research Laboratory, Monterey, CA

Rew R, Davis G (1990) NetCDF – an interface for scientific data access. IEEE Comput Graph Appl 10:76–82

Simpson RH (1974) The hurricane disaster-potential scale. Weatherwise 27:169, 186

Remote Sensing Imagery Assessment of Areas Severely Affected by Cyclone Gonu in Muscat, Sultanate of Oman

Andy Y. Kwarteng

Keywords Remote sensing imagery assessment

Introduction

Cyclone Gonu, which was the strongest tropical cyclone to hit the Arabian Peninsula, affected the eastern parts of the Sultanate of Oman on June 4, 2007. The cyclone brought along strong and torrential rains, high waves, and strong winds. Gonu was first observed as an incipient tropical depression in the Indian Ocean on May 27 by weather satellites. Gonu peaked to category 5 on June 6 but was downgraded to category 1 by June 8, 2007. As the storm weakened, it moved through the Arabian Sea and made a landfall in Iran at 0.00 GMT on June 7, 2007. The most seriously affected areas in Oman included Sur, Quriyat, and parts of Muscat Governorate. In the city of Muscat, the torrential rains from Gonu turned wadis and roads to rivers, and low areas to lakes at the scale never recorded in the history of the Sultanate of Oman (Fig. 1). Some of the other major destructions caused by the cyclone in Muscat area included:

- Damage to desalination plants resulting in water shortages
- Damage to buildings and other infrastructure
- Damage to roads and bridges
- Uprooting of trees
- Severing of electricity supply and telephone network

Meteorological and environmental satellites provide unparalleled techniques to monitor the environment on a continuous basis. Cyclone Gonu is an excellent example of the usefulness of meteorological satellites to monitor, forecast, and to

A.Y. Kwarteng (✉)
Sultan Qaboos University; Remote Sensing and GIS Center, P.O. Box 33, Al Khod PC 123, Sultanate of Muscat
e-mail: kwarteng@squ.edu.om

Y. Charabi (ed.), *Indian Ocean Tropical Cyclones and Climate Change*,
DOI 10.1007/978-90-481-3109-9_27,

study this damaging phenomenon. From the analysis of imagery provided by the European Organization for the Exploitation of Meteorological Satellites (EUMETSAT) satellites and the forecast models used by the Oman Meteorological Service Department, more than 70,000 inhabitants were evacuated before Gonu affected the country. Nevertheless, Oman State News Agency reported the death toll of 49 and 27 missing. The total damage caused by cyclone Gonu was estimated at US$3.9 billion and it is considered the nation's worst natural disaster. The destruction from the cyclone would undoubtedly have been much higher without any information from remote sensing satellites. Weather and climate studies are increasingly becoming important and the contributions from satellites have exceeded expectation and are unequalled by any other technique. In addition, environmental studies have become quite prominent due to effects of global warming, desertification, ozone depletion, and El Niño.

Information extracted from satellite images and other sources can help managers and city planners to make critical decisions regarding the extent of wadi flooding and the type of buildings and infrastructures suitable for areas prone to flooding. In this study, high-resolution Ikonos satellite images of the Muscat area recorded on March 2, 2006 and June 12, 2007 are used to map and study some of the most severely affected areas in Muscat. The entire built-up area in Muscat was studied, but only selected areas are discussed in this paper. Tropical cyclone and other natural disasters are rare in Oman and the tendency may be for planners and decision-makers to forget the extent of damage after a couple of years. Satellite imagery in digital format provides data that could be used to map the extent of destruction in an area, and also the imagery could be kept as reference for the future. During a natural disaster, accessibility and other infrastructure may not be in place to acquire valuable information from some of the affected sites. Consequently, the effective utilization of medium-to-high resolution satellite imagery is a prerequisite for the mapping and evaluation of major natural disasters.

Study Area

Muscat and surrounding areas are physiographically part of the Al Batinah coastal plain, which is composed of alluvial fans derived from the north-east side of the Northern Oman Mountains. The area can be divided into two, namely the alluvial plain and the coastal zone. The gently sloping alluvial plain is composed mainly of a group of recent and ancient alluvial fans which dominate the surface features. The surface consists of coarse sand and gravel along with alluvial terraces that stand about 600 m above sea level near the foothills. The surface has been dissected by numerous wadis descending from the mountains and meandering to drain into the Gulf of Oman. The coastal zone is not more than 20 m above sea level, and is composed of coarse-to-fine terrestrial and marine sands. Fields of coastal sand dunes and sabkha exist in this zone.

The city of Muscat, like most part of Oman, is located in an arid environment where rainfall is highly variable in space, time, quantity, and duration. The average

yearly rainfall recorded for all the Sultanate of Oman is 117.0 mm. However, the average rainfall in the Al Batinah plain is 100.8 mm per year (Kwarteng et al. 2008). In the event of heavy rains, surface runoff in the wadis lasts for a few hours to a few days primarily due to the relief – high topographical slope – and the very coarse top-soils and their absolutely dry conditions. During cyclone Gonu, Muscat International Airport recorded 50 mm of rainfall on June 6. Rainfall recorded by the monitoring stations of Ministry of Water Resources on June 5 and 6 in Northern Oman Mountains ranged from 97 to 943 mm. The volume of water cascading down the mountain slopes into the sea was enormous and perhaps more that the total rainfall recorded over a year. The main cause of the overflooding was due to the massive amounts of rain over a short period and the blocking of wadi access to the low-lying areas and the sea. It was quite obvious from the destruction that the city of Muscat and its infrastructure were completely overwhelmed by the volume and speed of rainwater from the mountains to the sea.

Methodology

Ikonos satellite images of Muscat and surrounding areas recorded on March 2, 2006 and June 12, 2007 were used in this study. Ideally, high-resolution images recorded on June 6, 2007, during the peak of cyclone Gonu in Oman would have been most suitable to capture the climax of the flooding episode. However, the closest high-resolution data recorded for the Muscat area were on July 12. QuickBird satellite acquired data of the flooded and other affected areas in Sur on June 7, 2007, but the data analysis is beyond the scope of this report. Table 1 shows the characteristics of images from Ikonos satellite, which was first launched on September 24, 1999. The revisit time of Ikonos satellite is 3–5 days in the off-nadir position and 144 days in true nadir position. Panchromatic and multi-spectral images can be merged to produce a pan-sharpened image with a resolution of 1 m. The three visible pan-sharpened bands were used in this study.

The images were rectified to the UTM zone 40 and WGS84 to facilitate their comparisons and to map changes between the two dates. In addition, the 2007 image was used as a geocoded image to geometrically correct the 2006 image. Color composite images (bands 3, 2, 1 in RGB) were generated for all the study sites. Change detection method was used to map the temporal difference between the 2006 and 2007 images.

Table 1 Characteristics of Ikonos spectral bands

Sensor	Spectral bands	Wavelength (μm)
Ikonos-2	Panchromatic	0.526–0.929
	Band 1 (blue)	0.445–0.516
	Band 2 (green)	0.506–0.595
	Band 3 (red)	0.632–0.698
	Band 4 (near-infrared)	0.757–0.853

Several change detection techniques applied to satellite digital images have been used successfully. Some of these include image difference, ratioing, principal component analysis (PCA), and selective principal component analysis (Jensen and Toll 1982; Singh 1989, Chavez and Kwarteng 1989, Chavez and Mackinnon 1994, Kwarteng and Chavez 1998). In this study, selective principal component was used to map changes between the two dates. The technique uses either two bands from the same image or one band from each of the two images as input to principal component analysis – a statistical technique that rotates the axes of a multidimensional image space in the direction of maximum variance. Two bands recorded on different dates were used as input to the PCA. The first component (PC1) maps information that is common to both images (topography and surface reflectance) whereas the second component (PC2) maps the temporal contrast between the input images (Chavez and Kwarteng 1989; Kwarteng and Chavez 1998). Color change images were generated from the color composite of the second principal components (PC2) of bands 3, 2, and 1.

Results

In general, the locations of the major wadis in Muscat area are known. Due to the paucity of rain, some of the areas near to the wadis have been built up resulting in the blocking of water flow toward the sea. In the event of a major rainfall, the path of water toward the sea is therefore unpredictable. The Ikonos images recorded on June 12, 2007, show the area approximately 6 days after cyclone Gonu. During the peak, most parts of the city were inundated as mentioned previously (see Fig. 1). Ikonos high-resolution imagery recorded on March 2, 2006 and June 12, 2007 show conditions before and after Gonu in the affected areas.

Figures 2A and 2B show Ikonos band 3, 2, and 1 color composite images of the Qurum National Park recorded on March 2, 2007 and June 12, 2007, respectively. The sea and lagoon with green algae show up in shades of green. Swimming pools and other water bodies show up in blue. The destroyed beach road and new water course to the sea is clearly evident in the 2007 image. The most significant surface/spectral changes between the two dates are shown in shades of white to brown in the change image (Fig. 2C). These are primarily the course of the new water flow toward the sea and the destroyed road.

Other changes between the two images are also shown in white to brown colors. In the change detection image each of the three bands detects many of the same temporal changes; however, there are some changes seen best in one of the three spectral bands versus the others, depending on the nature of the change.

Ikonos color composite images of the Sultan Qaboos Grand Mosque (domed building in central part of image) and its environs in Ghubrah recorded in 2006 and 2007, respectively are depicted in Fig. 3. During the peak of cyclone Gonu, that area was inundated and the damage to buildings, roads, and other infrastructure was high. The Grand Mosque building was affected by rushing waters to the east and west. The blue-green color shows pockets of water still remaining in the south–north-trending

Fig. 1 Ground photos showing some of the devastation from cyclone Gonu in Muscat on June 6, 2007

wadi Azaiba when the image was recorded on June 12, 2007. Comparison of the two images shows several destroyed trees to the west of the Grand Mosque building. In the change detection image (Fig. 3C), areas with the most dramatic changes are shown in shades of white to pink. These areas are primarily the remaining stagnant waters in the wadis. Gray areas did not show any significant changes between the images.

Toyota Automatic Garage in Ghala and the surrounding areas were completed devastated by the gushing brown water from the wadi slopes. The Ikonos color composite images acquired in 2006 and 2007 and the change images are depicted in Fig. 4. Figure 4A shows the orderly parked cars and vehicles in the garage, which are hardly recognizable after the event (Fig. 4B). Comparison of the 2006 and 2007 images show that more than 90% of the trees in the wadi (east of the white car packed roof) was destroyed by the rainfall due to cyclone Gonu. The uprooted trees are indicated by dark circular features in the change image (Fig. 4C). The white color in the change image maps areas that were seriously damaged or were present in the 2006 image but absent in the 2007. Note the number of cars that were in the 2006 but absent from the 2007 image. Figure 5 shows ground pictures of some of the destruction at Toyota Automotive Garage in Ghala taken on June 19, 2007.

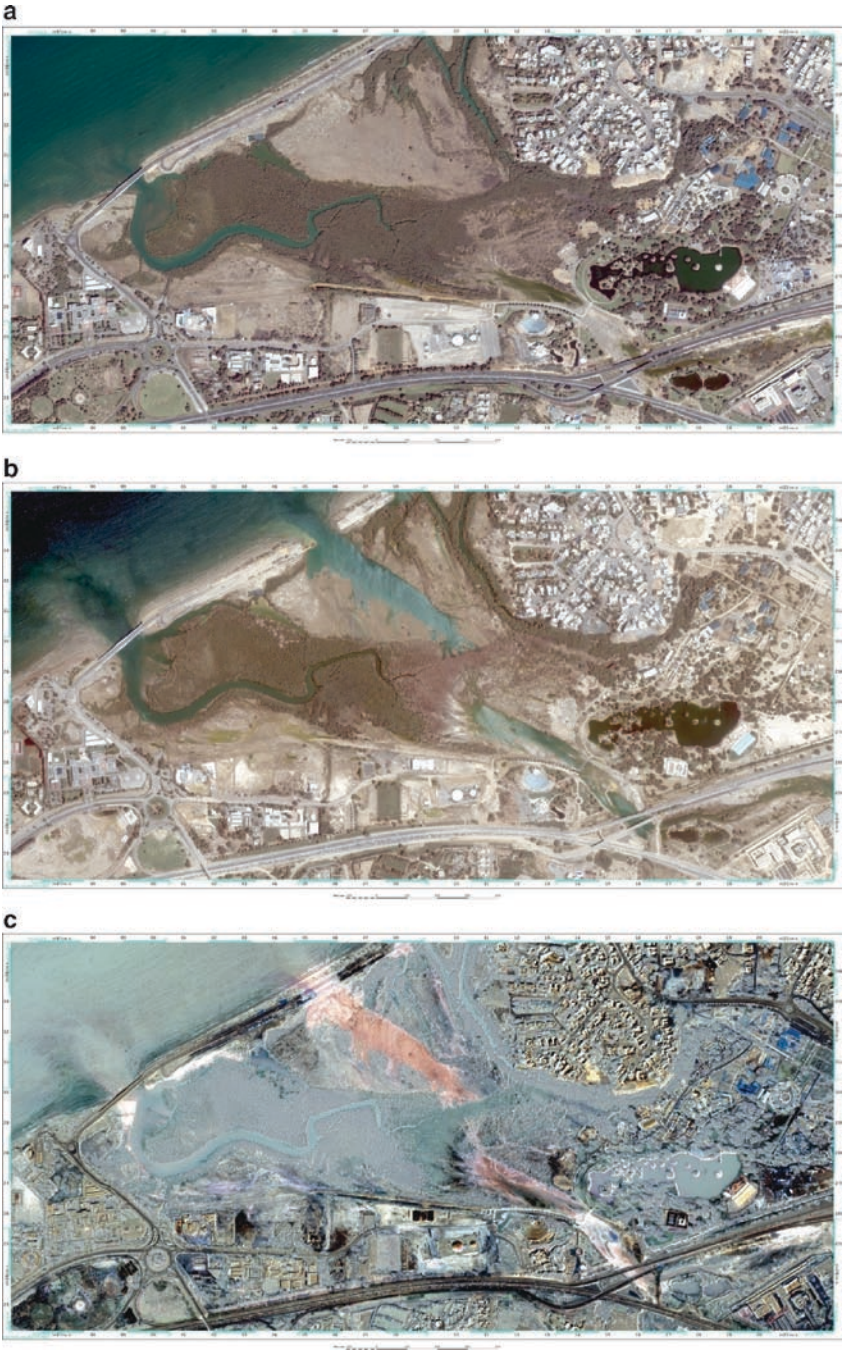

Fig. 2 Ikonos bands 3, 2, and 1 color composite image showing Qurum National Park area recorded on March 2, 2006 (**a**) and June 12, 2007 (**b**). The change detection image (**c**) maps the temporal difference between the 2006 and 2007 Ikonos images

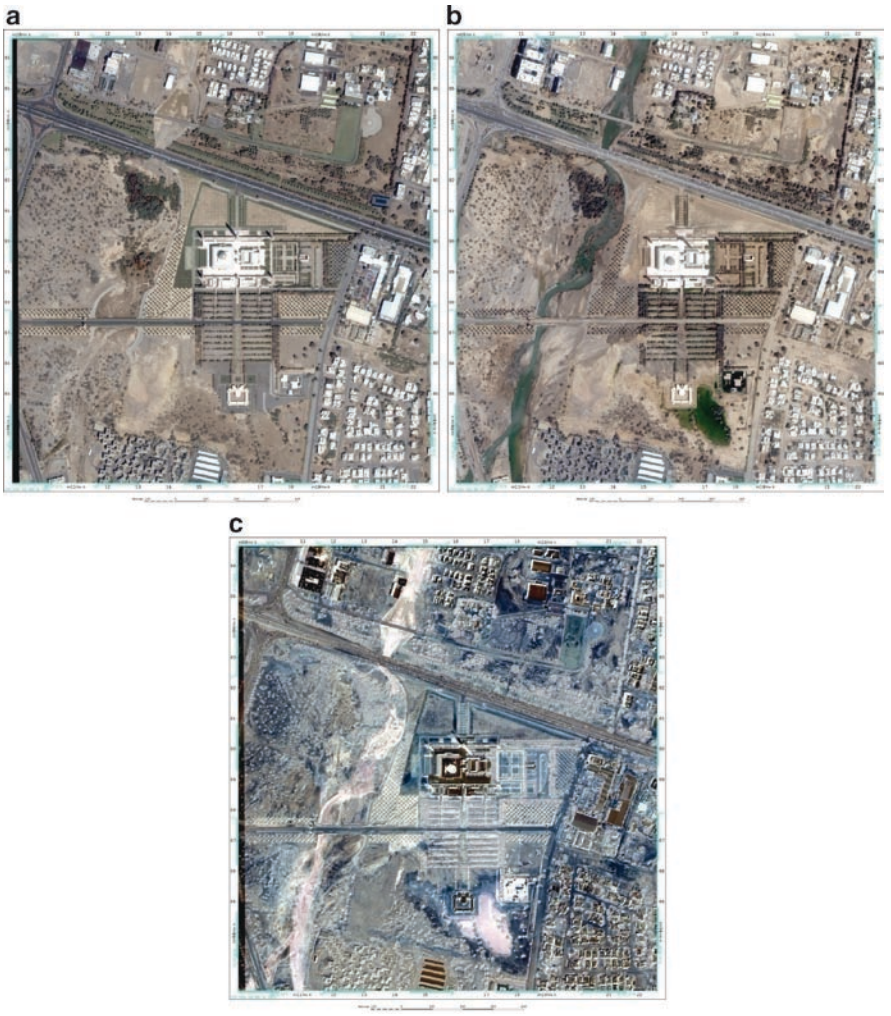

Fig. 3 Ikonos bands 3, 2, and 1 color composite image showing the National Mosque area, Ghubrah, recorded on March 2, 2006 (**a**) and June 12, 2007 (**b**). The change detection image (**c**) maps the temporal differences between the 2006 and 2007 images

Conclusion

High-resolution satellite imagery provides an unmatched technique to map areas affected by natural disasters. Invariably, such data are the only means for a reliable assessment in areas where infrastructure is destroyed and accessibility is limited. Cyclone Gonu affected the eastern part of the Sultanate of Oman on June 4, 2007, and brought along strong and torrential rains, high waves, and strong winds. The city of Muscat and its infrastructure were completely overwhelmed by the volume and speed of rainwater from the high areas to the sea.

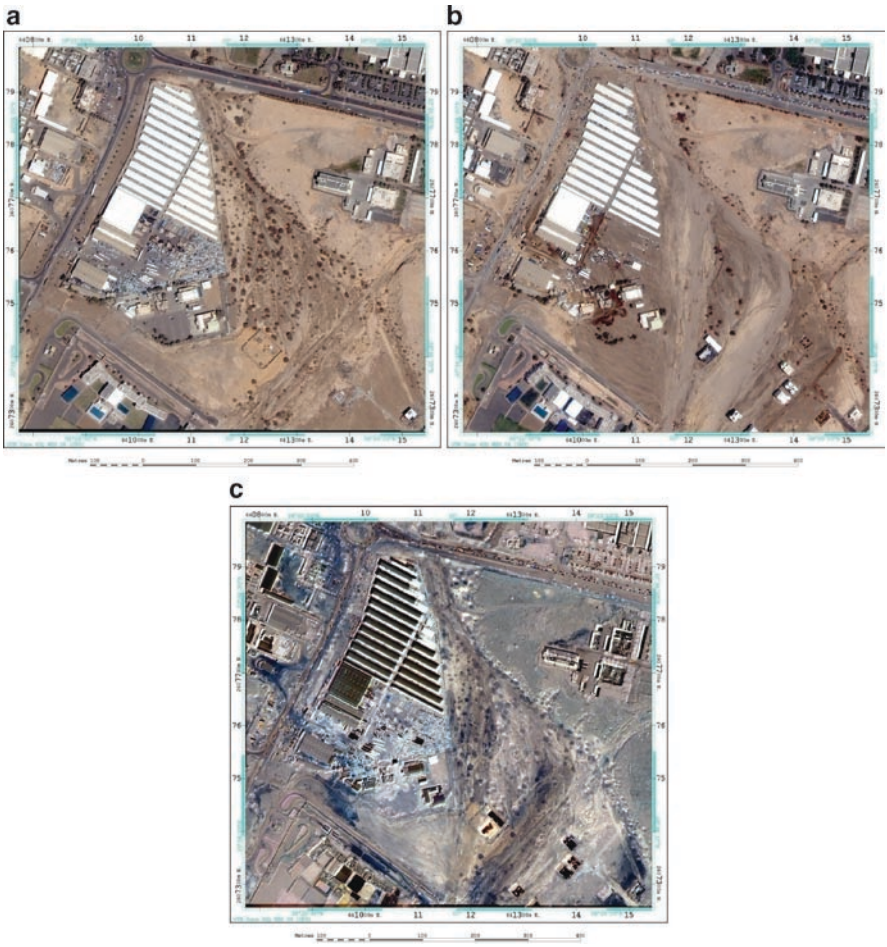

Fig. 4 Ikonos bands 3, 2, and 1 color composite image showing Toyota Automatic Garage, Ghala, recorded on (**a**) March 2, 2006 (**a**) and (**b**) June 12, 2007 (**b**). The change detection image (**c**) maps the temporal difference between the 2006 and 2007 images

In this study, Ikonos satellite images recorded on March 2, 2006 and June 12, 2007, respectively were used to map the extent of damage in the Muscat. The 2006 image recorded the pre-cyclone and 2007 image the post-cyclone conditions. The images were rectified to the UTM zone 40 and WGS84 to facilitate their comparisons and to map changes between images recorded on the two dates. Selective principal component analysis was used to map changes that had occurred between the image data recorded of the two different dates. The principal component two (PC2) three band color combination allows changes detected by different spectral windows to be combined in one product. The change images mapped the temporal

Fig. 5 Ground photos of some of the destruction at Toyota Automotive Garage, Ghala, taken on June 19, 2007

changes between Ikonos images recorded in March 2006 and June 2007, which was principally the devastation brought along by cyclone Gonu.

The changes recorded by the Ikonos images included areas prone to flooding, damaged roads, and other infrastructure. In the Qurum National park area, the data show a new water course to the sea and a damaged coastal road. The Sultan Qaboos National Mosque and surrounding areas in Ghala were inundated from wadis to the east and west. Toyota Automotive Garage in Ghala was completed destroyed by the wadi waters. More than 90% of the trees in the near-by wadis were uprooted. Information extracted from such high-resolution satellite images are invaluable and could help managers and city planners to make critical decisions regarding the extent of wadi flooding and the type of buildings and infrastructures suitable for areas prone to flooding in Muscat.

References

Chavez PS Jr, Kwarteng AY (1989) Extracting spectral contrast in Landsat Thematic Mapper image data using selective principal component analysis. Photogramm Eng Remote Sens 55:339–348

Chavez PS Jr, Mackinnon D (1994) Automatic detection of vegetation changes in the southwestern United States using remotely sensed images. Photogramm Eng Remote Sens 60:571–583

Jensen JR, Toll DL (1982) Detecting residential land-use development at the urban fringe. Photogramm Eng Remote Sens 48:629–643

Kwarteng AY, Chavez PS Jr (1998) Change detection study of Kuwait City and environs using multitemporal Landsat Thematic Mapper data. Int J Remote Sens 19(9):1651–1662

Kwarteng AY, Dorvlo ASS, Vijaya Kumar GT (2008) Analysis of a 27- year rainfall data (1977-2003) in the Sultanate of Oman. Int J Climatol. Published online in Wiley InterScience. (www.interscience.wiley.com), doi: 10.1002/joc.1727

Singh A (1989) Review article: digital change detection techniques using remotely-sensed data. Int J Remote Sens 10:989–1003

Urban Sprawl and City Vulnerability: Where Does Muscat Stand?

Mokhtar Belqacem

Keywords Muscat • Physical setting

Introduction

The past decades witnessed the birth of sustainable urban development as a focal research theme and a potent planning approach. Not only academics, but also planners, administrators, and politicians began to see in sustainable development an effective tool to address the pending economic, social, and environmental issues and problems in an integrated manner. Elements, choices, and patterns of sustainable city planning and management are varied. They build mainly on physical site characteristics (topography, surface hydrological system, land cover, natural buffers, etc.) and population's social and cultural attributes. However, as far as climate is concerned, the design of urban plans is customarily built on the assumption that weather conditions are normal and, hence, they seldom take into account the disastrous impacts of anomalous weather conditions. The human and capital damages caused by cyclone Gonu, which of late hit Muscat, have undoubtedly demonstrated that Muscat, being a coastal city facing the neighboring Indian Ocean, is extremely vulnerable to impacts of severe weather conditions, which may lead to devastating floods. However, vulnerability of Muscat is not only related to its maritime location. The population growth, which the city has experienced in the past decades, led to a very wide sprawl along the coastal fringe as well as across hill slopes and wadi valleys and, hence, made the population settlements therein more exposed to the disastrous impacts of any sudden severe weather event. With the expectation of increasingly severe weather events in the forthcoming years, planning for the management

M. Belqacem (✉)
Department of Geography, Sultan Qaboos University, Oman
e-mail: mokhtar@squ.edu.om

Y. Charabi (ed.), *Indian Ocean Tropical Cyclones and Climate Change*,
DOI 10.1007/978-90-481-3109-9_28,

of associated risks raises a serious challenge for planners. Therefore, there is a dire need to understand the processes, correlations, and probable expectations in case weather events like Gonu were to take place.

The nuances between urban growth and urban sprawl are very subtle and the distinction between these two spatial facets is a problematical question. Sometimes, the difference is no more than the connotation lying in each of these terms. At the time that urban growth points to the city expansion consequent to its demographic increase and economic feat, urban sprawl connotes a negative statement about the expanding built-up area in the suburbs and city fringes. Moreover, it should be recognized, that the criteria of definition and the standards of measurement differ enormously between thosethat are for and those that are against the urban sprawl. The same term varies in use from one scientist to another. However, for most researchers, urban sprawl is a potent clue for a healthy economy and for a welfare level of social life, at least for an important part of the urban population. In fact, this worldwide phenomenon is closely related to the citizens' capability to live in a single-family suburban vast house, and to their ability to commute daily to work, services, and entertainment spaces. This economic factor is closely related to the cultural customs and inherited practices as well. Thus, urban sprawl is understood as a specific pattern of spatial urban growth. It is characterized by an accelerated expansion of human constructions and covered surfaces outside the city, a low density of population and buildings in the suburbs, an intense commuting daily rhythm between residence and work places, an increasing reliability on vehicles, and noticeable spatial discontinuities.

Furthermore, because of the implications of urban sprawl on the environmental resources and ecosystems, and on the safety of city dwellers, in case of natural disasters, many researches, especially in the USA, focus on the threat related to this type of spatial expansion and emphasize that such territorial impact constitutes a dangerous challenge to a sustainable urban development. In the sense of this ecological trend, a city should be compact, dense, safe, and in harmony with the environmental components. The pros of this standpoint focus on the encroachment of sprawl on the site and on natural land cover. They claim that built-up area could harm the geomorphological features and weaken the site potentiality to lessen the severe natural blows such as landslides and floods. Nevertheless, the relationship between sprawl and site is reciprocal because the topography can orient and constraint human settlements and planners' projects. Sprawl is not often a choice; it could be an enforced fact because each city has its own physical and social reality. This statement is one of the major reasons behind the divergence between scholars in this matter. Outlining the causes and attributes of the current urban sprawl in Muscat could help to assess to what extent urban sprawl is related to human and physical factors and constraints. This paper attempts to analyze the urbanization process in Muscat district during the last 3 decades and to estimate the probable impacts of built-up-area spread and its repercussions. Within the framework of this conference, the analysis centers the attention especially on flood risks.

Study Area

The study area is the coastal part of Muscat governorate that currently constitutes the capital district of Oman, also known as Greater Muscat. This area was made, until 1970, of two principal cores and 19 small distant localities, strewn and isolated in a very narrow coastal band. This very difficult site ranging between the imposing mountainous chain of Hajar Acharqui (Eastern) in the south and the coast of the gulf of Oman in the north, took the shape of a discontinuous band dislocated by hills, waterways (wadis), and sand dunes. These physical elements subdivided the area in a series of inaccessible small hydrologic basins and a multitude of watersheds (Fig. 1).

In this space, Muscat constituted the center of the political power. It was like a walled enclave of approximately 1 km in diameter and made up of almost 300 residences. Out of the ramparts, there were nearly 16 different, poor and spatially disjoined hamlets. The other principal core is Mutrah. Twin of Muscat, but a little larger and more socially diversified, this locality constituted at that time the trade center radiating on a great part of Oman by its port and souk (traditional market). Around these two centers, and where the least quantity of drinking water appeared, very

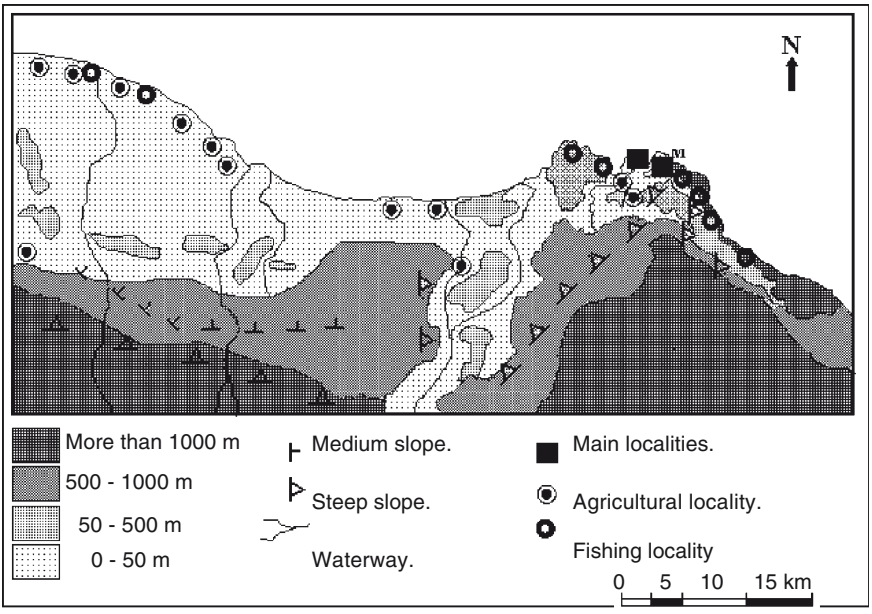

Fig. 1 Simplified physical setting of Muscat area and human settlements before 1970 (From the Author)

small localities were grafted living on agriculture and/or fishing. Moreover, in the absence of any road infrastructure, these localities did not maintain practically any space relation, except by coastal traffic. They appeared completely isolated one from the other as well as from the two principal centers. At the dawn of 1970, all these localities counted nearly 56,000 inhabitants composed of six or seven different ethnic groups with unequal social statuses. Suddenly, following the political change of 1970, a landmark in the contemporary Oman, and the substantial increase in oil revenue, everything changed. The opening of the new political era and its determination to rebuild Oman on modern bases were expressed by the adoption of plans of development in which Muscat had the lion's share during more than 2 decades. In the framework of the construction, the equipment, and the promotion of an appropriate national capital, the fast metamorphosis of about 20 distant and isolated traditional localities into a metropolis of more than 60 km length, launched an intense sustained urban development. The city has, since, the highest population and economic growth rates in the country. This area, as well as almost all the country, has an unstable and unreliable rainfall system in spite of the prevalence of winter rain in the north (of Oman) and summer monsoon in the south. The annual rainfall mean of about 110 mm does not mean that greater quantities could not occur. Indeed, thunderstorms, orographic heavy rain, and tropical cyclones could arouse, at times, vast deluges. Gonu cyclone, for example, carried more than 600 mm within 36 h (Fig. 2).

Methodology

The purpose is to put forward the factors and forms of urban growth in Muscat and to bring out the latent character of sprawl in the actual shape of the urbanized area. Thus, it will be possible to highlight the interconnection between the development of covered surfaces and the increase of the city vulnerability toward flood risks.

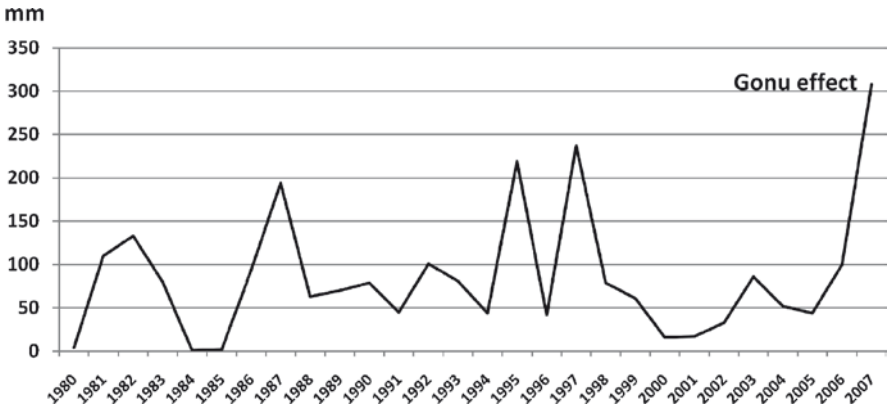

Fig. 2 The rainfall regime in Muscat, 1980–2007 (From the author)

Data Analysis

In order to put the studied phenomenon in its political and socioeconomic context, data related to the population and economic changes were analyzed. The consideration of the main orientations of the Five-year Development Plans in Oman helps to deduce the effect of policy options on the socioeconomic growth and urban expansion. The phases of urban growth and the rhythm of spreading were scrutinized. The various operations of land allotment and the official statistics related to construction permits, and to road network development were used to depict these patterns.

Mapping

Two maps were produced. The first (Fig. 1) is a simplified sketch of the physical setting. It was drawn from the topographic 1:100,000 map of the studied area. The second (Fig. 5), concerns the pattern of urban expansion during the last 3 decades. It is a compilation of two Landsat Satellite Imageries TM for the years 1980 and 2003 on which the watershed limits were superposed in order to compare between the urban proliferation and the catchments areas. This map attempts to demonstrate the relationship between the spatial spreading of the town and areas prone to flood risk. In spite of the development of new digital and quantitative methods, the classic field investigation remains an essential tool to assess the dimension of the urban complicated reality. From this standpoint, direct observation and photographing were used to augment the main statements deduced from data and sketches.

Results

The Physical Constraints

The Mountains and hills of the eastern Hajar chain strangle the city from the south and west and, sometimes they join the sea in the form of rough slopes and coarse cliffs particularly alongside the eastern coastal fringe. Indeed, along the urbanized area between Al Jissah, in the south-east, and Al Qurm heights in the middle northern coast the site is very desiccated and uneven. Thus, human settlements are inevitably hemmed into very small and narrow basins which are often watersheds (Fig. 3). In the central sector of the city is Bawshar chain, lying 700 m high and less than 5 km away from the coast. In the north-west, Bawshar chain ends suddenly in steep and medium slopes overhanging a very narrow coastal plain hardly 1–6 km in width. This plain is elsewhere sprinkled by a large number of hills 40–150 m above sea level. However, in the north-east vast sedimentary alluvial land is found. Its uniform and more open character has offered suitable extension space near the

Fig. 3 The hemming effect of relief. Al Hamriyah, Muscat (Photo of the author)

formerly agricultural localities of As Seeb and Al Khawd. Moreover, the area is dissected by at least nine big and small waterways (wadis), which cross the city from south to north on their way to the sea. The largest of these are from east to west, Wadi Alkabir, Wadi Aday, Wadi Al Ansub, and Wadi Al Khawd.

A Context of Growth

Urban growth is the direct result of growth in a city's population size, the urban functions it exercises and spatial extent it occupies. This fact reflects at the same time the city's dynamism and modernization. The state was from the start interested in building an appropriate new capital in the country to serve as a supreme urban center and a leading locomotive of development. The ad-hoc Plan 1970–1975 mobilized almost all the development funds for the construction of the primary national infrastructural network such as the first segments of roads, the airport, the commercial port, the refinery of Al Fahl, the public buildings and the social amenities, etc. The First and Second Five-year Plans 1976–1980 and 1981–1985 granted Muscat, respectively "42.4% and 56.1% of the public funds for development"

(Al Arifi 2000, T1). The share of Muscat in the Third Plan 1986–1990 rose to 48.9% of public expenditure assigned for national development. However, and since the Fourth Plan, this share started to decrease (20.4%). However, Muscat did not lose priority because the funds were not directed toward other areas or cities but invested into the national infrastructural projects (MoNE 2006) from which Muscat area profited. Thus, since 1970, Muscat is witnessing a steady expansion, and the most significant changes at the socioeconomic level are:

- The increasing polarization of the city quickly created many new urban functions: administrative, economic, financial, industrial, cultural, etc. The policy of centralization has accentuated the primacy of Muscat on the detriment of the other cities and areas. At the end of the twentieth century, the city monopolized the head offices of almost all the economic actors present in the country: 41.4% of bank headquarters, all high-standing hotels, 45% of tourist establishments, 74.2% of the industrial production units, and nearly all higher education institutions, etc.
- The primacy given to the capital triggered an unprecedented demographic rush from everywhere: intense exodus from the other regions, massive homecoming of the Omani of Zanzibar, immigration of a large work force from Asia and the Arab world, etc. Furthermore, the setting up of a modern health service and the improvement in the standard of living reduced the general death rate fourfold in less than 2 decades. Infant mortality, in particular, regressed from 64 ‰ per year at the beginning of the 1970s to 24 ‰ in 1993 and to 10.1‰ in 2007 (MoNE 2008), whilst the birth rate still remained very high. The annual natural increase reached the record rate of 3.8% and "the society shifted from the primitive stage of the demographic transition to the first phase" (Radhwan 1995).
- The new developments led to the growth of population size from 56,000 to 236,000 in 1 decade (1970–1980) with an enormous annual growth rate of 12.3%. This sustained growth raised the population of Muscat to more than 549,000 in 1993, 632,000 in 2003 and 742,000 in 2008 constituting, thus, 27% of the total population in Oman. Compared to a national demographic growth rate of 4% per year during the last 33 years (1970–2003) the population of the district of Muscat grew at the annual rate of 7.6% (Fig. 4).
- Under the conditions mentioned above, the city witnessed a spectacular increase in standard of living. Nevertheless, because of the lack of proper indicators for Muscat, the national data can be used as reference. The official statistics show that during the last 32 years the Omani GDP climbed from 651.5 million Rials in 1975 to 16010.3 million Rials in 2007 at current prices (10017.4 at 2000 constant price) (MoNE 2008). Thus, the annual per capita income rose in 2007 to about US$14,600 (5702.3 Omani Riyals) (MoNE 2008). This rise in individual and household incomes had an immediate impact on the residents' capability to improve their life conditions. The purchasing power triggered an enormous demand for real estate, cars, and services. Until the end of 2007, 142,916 plots were distributed in the capital district (30.4% of total countrywide distributed plots) and 103,873 were planned. 88.2% of the distributed plots were

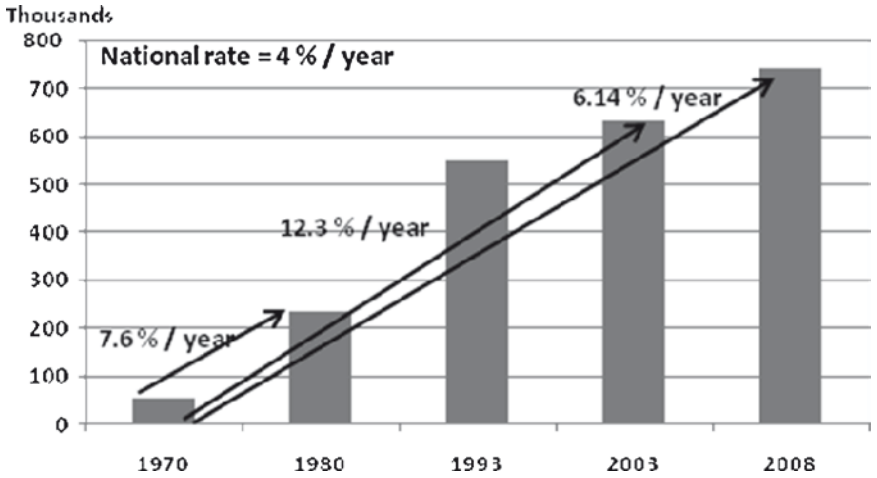

Fig. 4 The increase of the population size in Muscat, 1970–2008 (From the author)

residential, 4% were for mixed uses (commercial and residential), 2.8% for commerce, 2% for industrial activities, 0.5% for public utilities (mosques, schools and government uses), and 0.3% for agriculture (Statistical Year Book 2008, T 3.1 to 3.6). Furthermore, the government granted for free 2,783 housing units to the social security families. The older urban cores were, of course, not in a position to be part of these scenarios.

- Planning and production of plots in new spaces demands the opening of new roads. in this respect, the traffic network in Greater Muscat grew spectacularly from 50 km length in 1975 to more than 1,500 in 2003 (MoNE 2006). Most of the new paved roads were constructed in the new expansion areas such as As Seeb (34.4% of the total length), Bawshar (33.6%), and Al Amrat (12%). Thus, the paved road–individual ratio grew from 0.18 m in 1970 to 2.37 m per person in 2003.
- In the light of the natural and socioeconomic conditions mentioned above, the city continued to extend more and more toward the south-west and north-west directions. The built-up area of about 200 km² looks currently like a ribbon meandering throughout the narrow coastal prone areas as well as across hill slopes and wadi valleys. The old village localities, formerly distant and distinct, were completely included in the metropolis-urbanized zone (Fig. 5).

From Growth to Sprawl Scar

The natural attributes of the site of Muscat systematically influenced the direction and forms of the urban extension giving the city its linear plan of 60 km length and of 1–12 km width (Fig. 5). Throughout this topographically varied coastal band, the

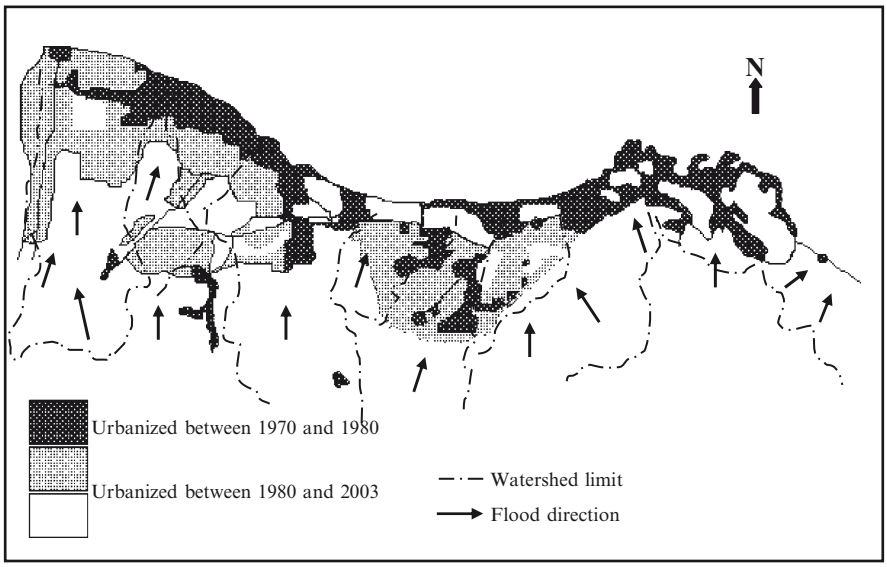

Fig. 5 Simplified sketch of the physical setting of Muscat (From the Author)

urban space seems paradoxically to have the profile of a continuous area and the structure of a fragmented body. Wherever natural buffers or vast public amenities exist they form discontinuities scratching the space. This leapfrog pattern of urban development leads to a very low density of buildings. Therefore, vacant fields appear all along the city coastal fringe. In the suburbs, the residential batches are likewise dispersed and individual housing plots show a patchy suburban landscape. Indeed, the building permits issued in Muscat area during 2007 indicate that the median size of the plots is about 649 m^2 and the percentage of lots bigger than 600 m^2 is 74.3% (Statistical Year Book 2008, T 3.9). Considering the part reserved for amenities, these facts mean that the number of buildings per hectare is supposed to be less than 13 units (12.4 units/ha in the assumption that the services land share is 20%) which is one of the lowest among the worldwide urbanized areas. The Parisian Master Plan, for example, requires, even in suburban zones, at least 35 housing units per hectare.

Moreover, because employment moves less swiftly from the city center to the periphery than population does, the population of Muscat witnessed a very intense intra-mobility because people shift from the center to the periphery following their social ascension. This spatial behavior reflects their financial ability to acquire a new suburban house and to bear the cost of the daily commuting between their residence and their work places. Old Muscat village inhabitants, for example, fell from 7.2% of the total population in 1993 to 3.5% in 2003. At the same time, the shares of Bawshar and As Seeb grew respectively from 18.2% and 24.3% to 25% and 29% (Omancensus.net 2008). Hence, the built-up area is spreading more and more.

Discussion

"The city is a part of our lives". It is a system seeking for the optimization of social life, residents' relationships, and for the satisfaction of the present and forthcoming dwellers' needs. Security is one of the most important requirements. From this statement, the adverse impacts of sprawl should be defined and highlighted. Considering that urban sprawl shapes out in the intersection of natural settings and institutional bases and socioeconomic facts, it is undoubtedly a complicated assignment to evaluate its miscellaneous spatial outgrowth. However, in its relationship with increasing flood risks in Muscat area it could be plausible to indicate the following:

- The impact of natural hazards depends both on the geographical setting and on the human actions on the environment.
- Urban sprawl, whatever its causes, encroaches on land cover. This may ultimately alter the hydrological system. So long the built-up area continues to extend, pressure on drainage channels is inevitable, something which will ultimately lead to imbalances in the watersheds. At the same time, the intensity of flood and solid load carried by water are highly determined by the proportion of covered land. This can be measured by the U-index.
- Over the last 38 years, Muscat has extended into many risky neighborhoods especially into or near waterways, prone basins, and hillsides.
- The urban development standards, the leapfrog pattern, and the conventional size of residential plots led to low density and a diffuse settlement. In the case of an extreme weather event like Gonu, the concerned authorities, especially Civil Defense, will find themselves facing a large populated area so that their efforts will be significantly dispersed.
- The vulnerability of Muscat is not an issue generated by urban sprawl only because natural settings and unforeseeable weather events are closely related to it. However, the management of unexpected hazards will be more knotty if sprawling is not contained. In the context of climate change and increase in cyclones' frequency, urban planning is facing a major challenge.

After this, the most paradoxical truth is that people believe that there is too much land to urbanize, but geographers and planners know that it is too difficult to find land to urbanize in Muscat area.

Recommendations

Certainly, we cannot avoid natural events, but we can moderate their impacts. So what can we suggest?

1. Fix an urban perimeter to the city as a first step to avoid unlimited extension.
2. Improve runoff drain system (Municipality and other authorities are already doing so)

3. Construct adequate artificial buffers to maintain water or to reduce flood speed and solid loading near to the origin.
4. Reduce the housing plot surface produced actually with an average of more than 600 m². For example, if we reduce it to the average of 400 m², we will save a third of every related component: a third of roads length, covered land, distances, and other infrastructures. And it will be possible to produce three housing units instead of two.
5. Think about new medium satellite cities in the neighborhood.
6. Densify the existing built-up area by:
   - Allowing bigger vertical constructions
   - Filling the vacant available terrains
7. Cultural approach: convince people that:
   - A flat is also a house.
   - A 400 m^2 residential plot is enough to build an adequate house with a garden and a domestic car parking.
8. There is an urgent need to carry out an exhaustive study using innovative research tools, such as GIS and remote sensing techniques, to examine and quantify the linkages between urban sprawl and flood risks.

References

Al-Arifi S (2000) The concentration of development: greater Muscat versus the other regions. Conference on development and regional planning, SQU, Muscat (unpublished)

Le Cour Grandmaison B (2000) The Sultanate of Oman. Karthala, Paris (French)

Radhwan TA (1995) The population of Muscat in the 20th century between estimation and census. Revue of the Geographic Association of Kuwait

Scholz F (1980) Sultanate of Oman. Geographical introduction, Part 1. Stuttgart, Germany

Sultanate of Oman, Ministry of National Economy (2004) Census Administration, selected data and indicators from 1993 and 2003 Censuses, Muscat

Sultanate of Oman, Ministry of National Economy (MoNE) (2006)

Sultanate of Oman, Ministry of National Economy (MoNE) (2008)

Sultanate of Oman, Ministry of National Economy (MoNE) (2009)

Sultanate of Oman, Ministry of National Economy Census Administration, Statistical year book 2006 and 2008. http://www.moneoman.gov.om/book/syb2008/syb2008.htm. Accessed January 25, 2009

Sultanate of Oman, Ministry of National Economy http://www.omancensus.net/selected_data_population_muscat.asp. Accessed January 25, 2009

Sultanate of Oman, Ministry of National Economy Major economic and social indicators. http://www.moneoman.gov.om/book/nub/dec2008/T1.PDF. Accessed January 25, 2009

Sultanate of Oman, Ministry of National Economy Major economic and social indicators. http://www.moneoman.gov.om/book/nub/dec2008/T3.-T3-6. PDF. Accessed January 25, 2009

Sultanate of Oman, Ministry of National Economy Major economic and social indicators. http://www.moneoman.gov.om/book/nub/dec2008/T3.-T6. PDF. Accessed January 25, 2009

Sultanate of Oman, Municipality of Muscat (1997) Muscat evolution and development. First English edition, Muscat

UNFPA, State of world population (2007) Chapter 5, Urbanization and sustainability in the 21st century. http://www.unfpa.org/swp/2007/english/chapter_5/print/chapter_5.html. Accessed August 10, 2008

Ministry of Defense (2008) National Survey Authority, topographic map 1:100,000. Sheet, Muscat

Flood Studies in Oman and the Difficulties in Using Rainfall-Runoff Analysis

Aisha Mufti Al-Qurashi

Keywords Rainfall-runoff analysis

Introduction

The hydrological characteristics in arid areas are different from that of humid areas. The high temporal and spatial variability of the rainfall, flash floods, absence of base flow, sparsity of plant cover, high transmission losses, high amounts of evaporation, and evapotranspiration and the general climatology are examples of such differences in hydrological features between arid and humid areas. Hence, these differences lead to different flood characteristics. However, as most studies were carried out in humid areas, the arid areas received less attention except recently. These lead to less understanding of some of these characteristics and their effects on the obtained results when using some known methods for rainfall-runoff analysis. The floods in arid areas are very rare but when it occurs they can cause severe damages. Very high flood peaks have been recorded in different parts of arid areas. The recorded flood peaks in Oman were greater than 10% of the wards maximum. Hence, flood studies and controls became very important in all the areas that are subjected to flood risk.

However, the rapid development in Oman made it important to carry out flood studies. Many studies have been carried out regarding rainfall and runoff and their frequency analysis. Those studies have aided in project designs and town planning and flood management. Flood risk maps that delineate the high-risk, medium-risk, and low-risk zones have also prepared to aid in locating properties in risky areas. This chapter overviews the flood studies and the rainfall and runoff analyses that are important in city planning and flood management.

A.M. Al-Qurashi
Ministry of Regional Municipalities and Water Resources, Directorate General of Water Resources Assessment, Oman
Al-Qurashi@yahoo.uk

Y. Charabi (ed.), *Indian Ocean Tropical Cyclones and Climate Change*,
DOI 10.1007/978-90-481-3109-9_29,

Hydrological Analysis

Hydrological analysis of rainfall and runoff are very important for understanding the hydrological characteristics of the study area. Hence, many studies have been carried out to improve this understanding and assess the water resources in the study areas. However, the short period of records, the quality, and the special hydrological characteristics of the arid areas, which are not fully understood yet, made it a difficult task sometimes. An overview on the different studies that have been carried out by the hydrologists in the Ministry of Regional Municipalities and Water Resources (MRMWR) is shown below.

Rainfall Analysis

There are many studies that have been carried out in the rainfall analysis. These include the rainfall intensity analyses as they are a very important input for the design computations for hydraulic structures, in particular for urban drainage, bridges, culverts, and dam spillways. As the rainfall characteristics could be different from one part to another, using local data is essential to get the proper results and provide the appropriate understanding of rainfall intensities and the probable frequency with which they occur. Table 1 shows the maximum recorded rainfall in Oman for durations of 15 min to 24 h.

However, much higher values have been experienced during some cyclones. The greatest storm and flood known to Muscat occurred in June1890, just over 100 years ago. It was a full-blown cyclone, which dumped huge rainfall totals and greatly raised sea levels all the way from Muscat to Sohar 200 km up the coast. The resulting land and sea floods had a devastating effect on lives and properties over a wide area, and almost wiped out Muscat. The greatest 1-day rainfall ever recorded in Muscat, at the time, 286 mm, occurred during that event. In the recent years, the highest was experienced during the Guno storm, Jun 2007, where up to 943 mm was recorded in 1 day in Wadi Dayqah and 438 mm at Wadi Aday, with similar damage effects to the 1890 cyclone.

The approach adopted in the rainfall frequency analysis has been log-normal frequency analysis of partial series of data, using a lumped station-year approach. It was noted from the analysis that there are apparent rainfall intensity differences in characteristics relating to terrain. Hence, to account for these differences, the stations with enough data for analysis have been divided into the three categories: plains (those within relatively flat areas with no significant nearby hills likely to induce orographic rainfall effects), mountains (those at elevations above 800 m above mean sea level), and the remainder have been categorized as representing hill areas. Table 2 shows the frequency of rainfall intensities for plains, hills, and mountains.

Table 1 Maximum recorded rainfall in North Oman for Durations 15 min to 24 h

Rank	1	2	3	4	5
15 min					
Rainfall (mm)	48	43	39	37	37
Location	Darsait	Ibra	Sayh Khatum	Nizwa	J Harim
Date	3.5.81	10–11.4.90	5.12.91	7–8.7.82	20.7.88
30 min					
Rainfall (mm)	74	69	52	52	52
Location	Darsait	Ibra	Nizwa	Nuway	J Hayl
Date	3.5.81	10–11.4.90	7–8.7.82	27.7.95	25–27.7.95
1 h					
Rainfall (mm)	84	76	74	72	70
Location	Darsait	Ibra	J Shams	Nuway	Al khadrah
Date	3.5.81	10–11.4.90	27–28.7.88	27.7.95	21–22.7.90
2 h					
Rainfall (mm)	90	88	81	77	77
Location	Darsait	J Shams	Ibra	Nuway	Madruj
Date	3.5.81	7–9.7.94	10–11.4.90	27.7.95	27.7.88
3 h					
Rainfall (mm)	98	96	95	83	79
Location	Ibra	Darsait	J Shams	Izki	Madruj
Date	10–11.4.90	3.5.81	7–9.7.94	24–26.2.90	27.7.88
6 h					
Rainfall (mm)	109	106	101	99	97
Location	Ibra	Al Muqayfah	J Bani Jabir	Darsait	Izki
Date	10–11.4.90	30.3.97	7.6.96	3.5.81	24–26.2.90
12 h					
Rainfall (mm)	129	119	118	115	112
Location	Dahiyah	Izki	J Shams	Al Muqayfah	Qahlah
Date	23–26.2.82	24–26.2.90	21–25.7.95	30.3.97	25–27.2.90
24 h					
Rainfall (mm)	152	137	135	133	131
Location	J Shams	Dahiyah	Yanbu	As Sabakh	Al Khan
Date	21–25.7.95	23–26.2.82	16–19.2.88	16–21.2.88	16–19.2.88

Runoff Analysis

Estimation of runoff is an essential component in the management of water resources.

MRMWR has been collecting flood peak data through its wadi gauging station network, and also general flood information. This program included initially the identification of flood debris marks for major historic floods and the levels and

Table 2 Frequency of Rainfall intensities for plains, hills, and mountains

	Rainfall (mm) for the following return periods						
Duration hours	Av	5-year	10-year	20-year	50-year	100-year	200 year
Plains areas (287 station-years, 21 stations)							
0.25	13	16	20	23	27	31	34
0.5	17	21	26	30	36	41	45
1	20	25	31	36	44	50	55
2	22	28	35	41	49	56	62
3	24	31	38	45	54	62	69
6	28	35	43	51	61	69	77
12	31	39	48	57	69	78	87
24	35	44	56	68	83	94	106
Hill areas (504 station-years, 41 stations)							
0.25	15	18	21	24	28	31	35
0.5	21	26	31	36	43	48	53
1	25	32	38	45	54	61	67
2	28	36	43	50	60	67	74
3	31	39	47	55	65	73	81
6	35	44	53	63	76	86	96
12	39	50	62	75	91	104	116
24	44	57	71	86	105	120	135
Mountain areas (221 station-years, 22 stations)							
0.25	18	21	24	27	31	34	37
0.5	24	29	34	39	45	50	55
1	31	38	44	51	59	66	72
2	35	43	50	58	67	75	82
3	37	45	53	61	71	78	86
6	42	51	59	68	79	88	97
12	48	59	70	80	94	104	114
24	56	70	83	96	113	125	138

slopes of these debris marks were used together with wadi cross-sectional dimensions and assessments of channel roughness to derive estimates wherever possible of the historic flood peaks using slope-area measurement method. Because of its aridity, Oman has many years when wadi flow is zero or very small. Consequently annual series (AS) trends may be dominated by zero or low flows which do not in any way reflect flood peak characteristics. The peak-over-threshold (POT) series is better at reflecting the real flood characteristics, but even this series tends to consist of low or zero flows in its lower half. For this reason, standard flood frequency methods that rely in fitting a distribution to all points are not appropriate. Hence, a comparison of methodology using various standard methods (HDA, 1996) resulted in the adoption of semi-log analysis of the POT series (Pilgrim, 1987), but with best-fit trend lines for the range 50% upwards only. The 50% upwards fitting avoided the

nonfloods or zeros which taper off at the bottom of the range, and still seem to be generally satisfactory.

Table 3 shows the maximum flood peaks that were reported in the different parts of Oman. It should be noted that the floods of Wadi Andur and Ghudun were most probably the result of the cyclone. Fig. 1 shows the greatest recorded flood peaks in Oman compared with the world maximum. However, much higher flood peak values must been experienced in Guno storm but, unfortunately, no flood peak data were found available, currently, except on flood volumes. Fig. 2 shows the flood frequency curves for Oman (MWR, 1991) which was constructed based on the slope area measurements using the historical events. These curves related flood peaks to catchment area only, and they were used to develop flood risk maps for a number of major towns and key flood risk areas as shown in Fig. 3.

Table 3 Maximum flood peaks reported in Oman

Wadi name	Catchment area (km^2)	Flood peak (m^3/s)	Flood date
Wadi Dayqah at Mazara	1,711	9,500	1927
		7,750	1965
		5,190	1982
Wadi Ibra	687	5,140	1927
Wadi Halfayn Izki	270	4,130	1951
Wadi Muaydin at Birkat al-Mauz	197	3,580	1951
Wadi Andur	884	8,250	1977
Wadi Ghudun	1,937	10,600	1977
		10,400	1983

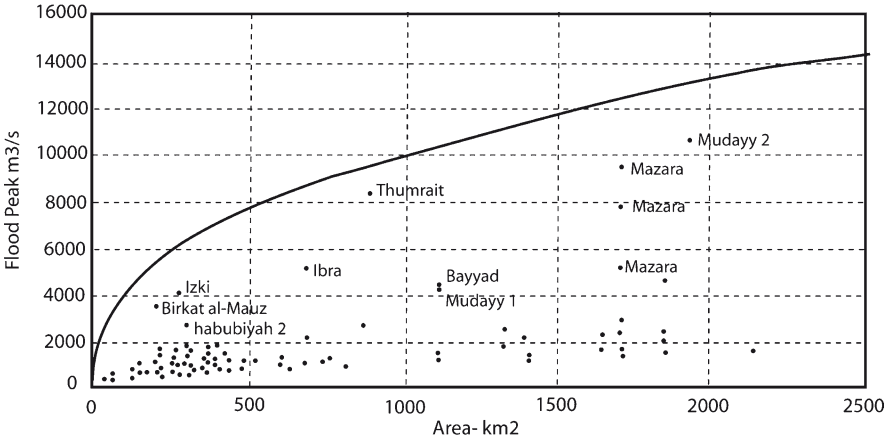

Fig. 1 Greatest recorded flood peaks in Oman compared with World Maximum (From Rodier, 1984)

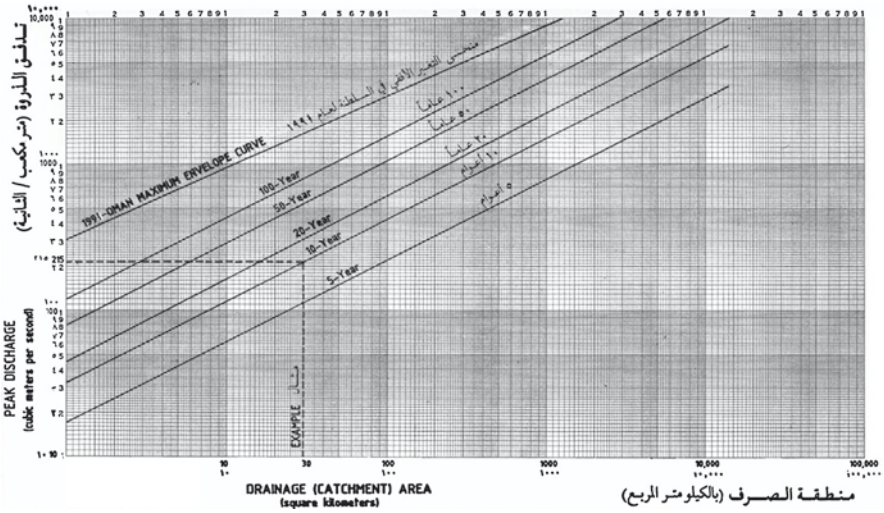

Fig. 2 Flood frequency curve of 1991 (From MWR, 1991)

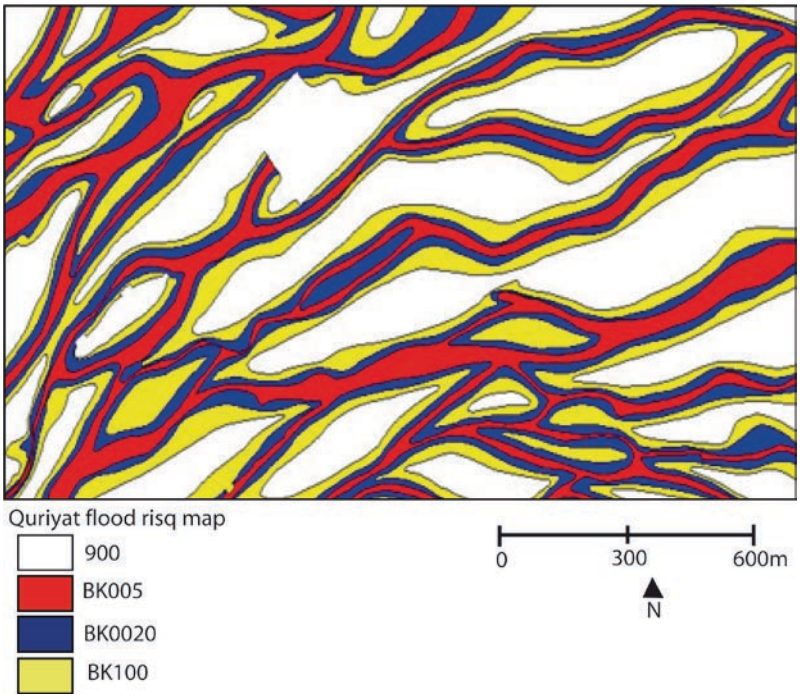

Fig. 3 Flood risk map showing different risk area zones

Flood Guideline Manual

Floods in Oman are notoriously dangerous despite being rare. A proper understanding of flood characteristics is essential for the development of Oman, so that houses, highways, factories, and offices will not be suddenly engulfed. The main analysis required to achieve such guideline manual can be briefed in the following points:

- Flood frequency analysis using the available wadi-gauge-recorded data, using Peak-over-threshold (POT) series with station-year approach and semi-log analysis with best fit line.
- Growth factors, which are used for the purposes of enabling flood frequencies to be predicted for ungauged wadis. This procedure has entailed developing flood growth factors for Oman, i.e., factors by which to multiply estimates of the mean annual flood (MAF) to derive flood peaks for any return period. The method also involved correlation of observed MAFs with catchment parameters to enable MAFs for any wadi to be predicted.
- Correlation of MAF to catchment parameter, which is an essential step in deriving the methodology for enabling flood frequencies to be estimated for any ungauged wadi. There are many parameters which could be correlated, but the area (A), wadi length (L), wadi slope (S), and percentage of the catchment which is non-mountain/hill or alluvial plain (NM) were found to be the most important and affecting parameters, and hence were used in this method.
- Design flood approach, which includes flood peak frequencies, flood volume analysis, and flood hydrograph analysis**.** Design flood requirements may relate to flood peaks or flood volumes or both, in which case full-design flood hydrographs (or probably a range of them) are needed. In most of the studies, the requirement is for the wadi flood peak frequencies for town developments, highway bridges, and culverts, and the flood volumes are not normally required. However, in the case of dam spillway design, when flood storage is a key issue, flood volumes and full hydrographs are needed.

Conclusions

Oman is one of the arid countries with no frequent rainfall or continuous flow. The floods in arid areas are very rare, but when it occurs, they can cause severe damages. The rapid development in Oman made it important to carry out flood studies. Many studies have been carried out regarding rainfall and runoff and their frequency analysis and flood guideline manual. Those studies have aided project designs, town planning, and flood management. Flood risk maps that delineate the high-risk, medium-risk, and low-risk zones have also been prepared to aid in locating properties in risky areas. However, the short period of records, the quality, and the special hydrological characteristics of the arid areas, which is not fully understood yet, made it a difficult task some time. Hence, these studies need to be updated as new data become available

or new information. Guno cyclone is evident of such data. Such new storms can change many results and needs to be considered in any study or project.

References

MWR (2001) Daily rainfall frequency analysis
MRMWR (2002) Design flood estimation guide for Oman
Pilgrim DH, et al. (1987) Australian rainfall and runoff. A guide to flood estimation Vol 1.The Institution of Engineers, Australia
HDA, MWR (1996) Updating of flood frequency curves for Oman. Initial frequency analysis and results and section of best method, Intrim Report
Rodier JA (1985) Aspects of arid zone hydrology. In: Rodda JC (ed) Facets of hydrology, Vol. II. Wiley, Chichester, UK

Part V
Disaster Preparedness, Management and Reduction

Cyclone Gonu Storm Surge in the Gulf of Oman

Hermann M. Fritz, Chris Blount, Fawzi B. Albusaidi, and Ahmed Hamoud Mohammed Al-Harthy

Keywords Coastal flooding

Introduction

Tropical cyclones develop in the north Indian Ocean from 55°E to 90°E and 5°N to 20°N (Webster et al. 2005). There are two cyclone seasons in the north Indian Ocean, namely, the pre-monsoon (May) and post-monsoon (October and November). Some cyclones form in the transitional months June and September. The socioeconomic impact of tropical cyclones based on damage and loss of life is enormous in the Bay of Bengal with cyclone Nargis in Myanmar as the most recent example (Fritz et al. 2009). More cyclones form in the Bay of Bengal than in the Arabian Sea based on a respective frequency ratio of approximately 4:1 (Singh et al. 2001). The Joint Typhoon Warning Center (JTWC) maintains a "best-track" database for cyclones in the Indian Ocean with time span 1945–2007. The Arabian Sea tropical

H.M. Fritz (✉)
Associate Professor, Civil and Environmental Engineering, Georgia Institute of Technology, Savannah, GA, 31407, USA
e-mail: fritz@gatech.edu

C. Blount
Graduate Research Assistant, Civil and Environmental Engineering, Georgia Institute of Technology, Savannah, GA, 31407, USA
e-mail: chris.blount@gatech.edu

F.B. Albusaidi
Department of Meteorology, Directorate General of Civil Aviation and Meteorology, Muscat, Sultanate of Oman
e-mail: f.albusaidi@met.gov.om

A. Hamoud Mohammed Al-Harthy
Director of Meteorology, Department of Meteorology, Directorate General of Civil Aviation and Meteorology, Muscat, Sultanate of Oman
e-mail: a.alharthy@met.gov.om

Y. Charabi (ed.), *Indian Ocean Tropical Cyclones and Climate Change*,
DOI 10.1007/978-90-481-3109-9_30,

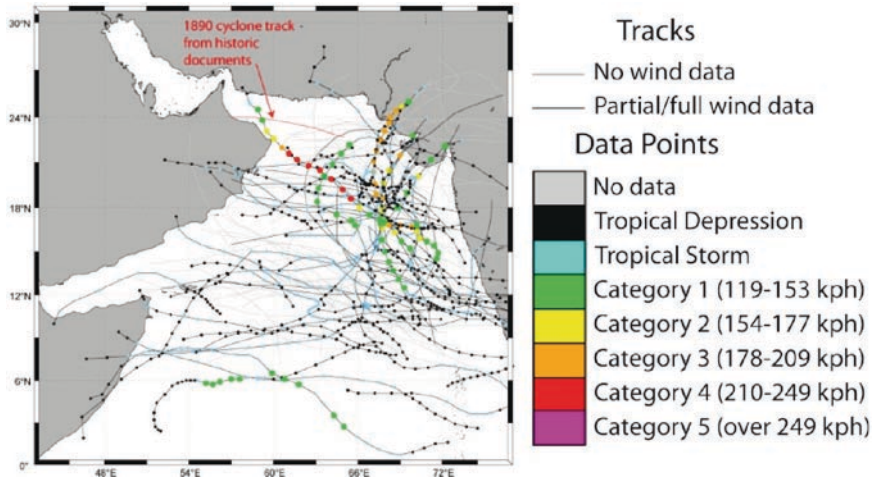

Fig. 1 Storm track data for the Arabian Sea from 1945 to 2007 according to Joint Typhoon Warning Center (JTWC). The additional track of the 1890 cyclone is based on historical documents. Note the 2007 cyclone Gonu track is the only confirmed category 4 storm

cyclone center tracks in the data are shown in Fig. 1. Prior to 1975, only track information was available. From 1975 to 1979, maximum wind velocity was not available for all cyclones or was only available for partial cyclone tracks. Since 1979, maximum wind velocity is available for all storms.

Intense cyclones like Gonu have been extremely rare over the Arabian Sea, as most storms in this area tend to be small and dissipate quickly. Prior to cyclone Gonu, at least two similarly destructive storms have struck Oman in 1890 and 1895 (Bailey 1988). The 1890 storm remains the deadliest natural disaster in Oman's history with a reported 727 fatalities. Blount et al. 2009 numerically modeled the storm surges created by these historic storms and inversely optimized the best track to match the coastal flooding documented in the historic records.

Cyclone Gonu

Gonu is the strongest tropical cyclone on record in the Arabian Sea. Gonu was the second named tropical cyclone of the 2007 north Indian Ocean pre-monsoon cyclone season and developed from a persistent area of convection in the eastern Arabian Sea. On 2 June, the India Meteorological Department (IMD) classified the system as cyclonic storm Gonu about 760 km southwest of Mumbai, India. Late on 3 June, the IMD classified the storm as very severe cyclonic storm Gonu. The cyclone strengthened further to attain peak 1 min sustained winds of 270 km/h and gusts to 315 km/h about 285 km east-southeast of Masirah Island off the coast of Oman. The IMD upgraded it to super cyclonic storm Gonu late on 4 June, with

sustained winds reaching 240 km/h and an estimated pressure of 920 mbar. This corresponds to a category 4 hurricane on the Saffir–Simpson Hurricane Scale (SSHS). The cyclone gradually weakened due to cooler water temperatures and drier air as it approached the Arabian Peninsula. Cyclone Gonu crossed the easternmost tip of Oman at Ras al-Hadd with winds of 150 km/h late on 5 June, making it the strongest tropical cyclone on record to strike the Arabian Peninsula. On 6 June, the cyclone turned to the north-northwest and the IMD downgraded Gonu to cyclonic storm status early on 7 June. Gonu made final landfall on the Makran coast in Iran. Gonu caused about $4 billion in damage and at least 49 deaths in the Sultanate of Oman, where the cyclone was considered the worst natural disaster. Gonu dropped heavy rainfall near the eastern coastline, reaching up to 610 mm, which caused wadi flooding and heavy damage. The shore parallel cyclone track resulted in coastal damage due to storm surge and storm wave impact along a 300 km stretch of Omani coastline. In Iran, the cyclone caused 23 deaths and $215 million in damage.

Post-Cyclone Field Observations

Coastal Flooding

The widespread failure of tide gauges along the Gulf of Oman called upon a field survey crew to collect high water marks based on established protocol (Fritz et al. 2007). The team surveyed the impacted Omani coastline within less than 2 months of Gonu's landfall from 1 to 4 August 2007. The off-road vehicle-based survey extended from Ras al-Hadd to Abu-Abali encompassing 270 km of Omani coastline and several mountainous wadis. The team measured coastal high water marks (the elevation of the water level), wadi and overland flow depth (depth of the water above the ground), inundation distance (the straight-line distance between the coastline and the maximum extent of saltwater intrusion), and areas of inundation. Further coastal erosion and deposition was documented. Ephemeral infrastructure damage was recorded at various scales. The elevations of water marks on buildings, scars on trees, and rafted debris were measured as indicators of the maximum water surface elevation composed of storm surge and superimposed storm waves. High water marks were photographed and located using GPS. Transects from the beach to the high water marks were recorded with a laser range finder. Fig. 2 shows the measured Gonu high water marks at 27 locations and three superimposed 2004 Indian Ocean tsunami run-up points surveyed simultaneously. The high water marks peaked 180 km southeast of Muscat at the eastern most tip of the Arabian Peninsula at Ras al-Hadd with 5 m (Fig. 3a, b). Multiple compound walls built in rows parallel to the shoreline were destroyed 200 m inland at Ras al-Hadd. The steep coastline in the landfall area increased the contributions of storm waves superimposed on the storm surge contained in the high water marks. The shore parallel cyclone track limited the high water marks to half of those measured after

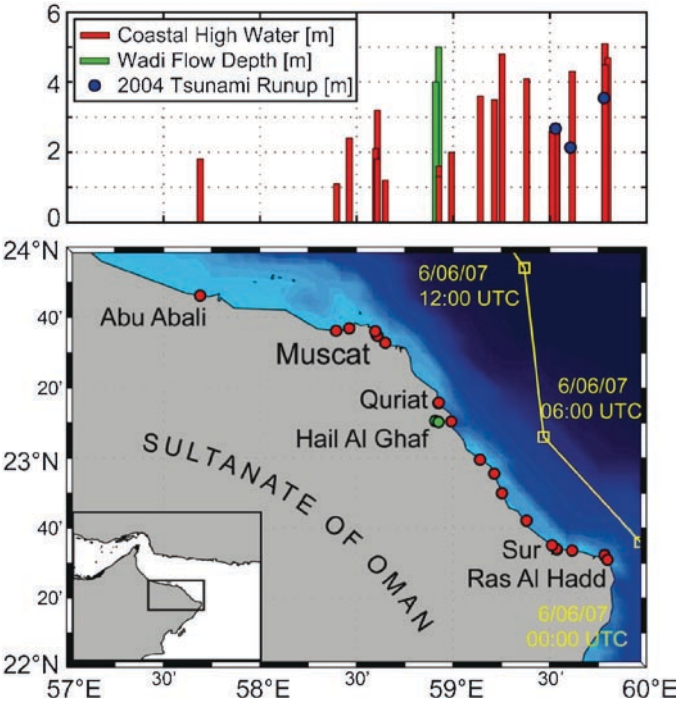

Fig. 2 High water marks measured in the aftermath of cyclone Gonu and run-up heights of the 2004 Indian Ocean tsunami collected in 2007

Hurricane Katrina with a higher impact landfall track perpendicular to the coastline (Fritz et al. 2008).

The high water marks continuously decreased with distance from the landfall area to 3 m at Muscat where the coastline was characterized by massive beach erosion and collapsed coastal roads (Fig. 3c). High water marks of 2 m elevation with collapsed compound walls 200 m inland across the coastal road were observed 90 km northwest of Muscat at Abu Abali, although cyclone Gonu had already turned northward toward Iran prior to this longitude (Fig. 3d). This highlights the potential for large storm surge and the vulnerability of the shallow coastline between Muscat, Sultanate of Oman, and Al Fujayrah, United Arab Emirates, in the rare event of a direct cyclone landfall such as in 1890. The convergence of the Gulf of Oman toward the Strait of Hormuz would further amplify cyclone-induced storm surge.

Wadi Flooding

The mountainous and arid terrain near the coasts of Oman and Iran pose an additional hazard to coastal regions along the Gulf of Oman. Heavy rain falling on the steep mountains sends torrents of fast-moving floodwater down to the coastal areas.

Fig. 3 Coastal damage: (**a**) Ras al-Hadd with survey locations and GPS-track (image credit: Google Earth); (**b**) multiple shore parallel compound walls destroyed at Ras al-Hadd; (**c**) massive beach erosion at Muscat; (**d**) compound wall destroyed 200 m inland at Abu Abali

The storm surge combined with mountainous wadi runoff flooded valleys and plains several kilometers inland at various locations. Pure wadi flow depths of 5 m were measured at Hail al Ghaf along a 1 km wide wadi bed based on rafted debris in trees and mud lines on houses (Fig. 4a). Hail al Ghaf is located at 50 m elevation and 7 km west of the coastline at Al Hajir. Many larger settlements such as Sur and Quriat along the mountainous stretch of coastline between Muscat and Ras al-Hadd are located at wadi mouths or on wadi deltas. Some of the largest cyclone impact and associated damage were observed on low-lying wadi deltas due to the combined effects of wadi discharge from the mountainside and coastal storm surge flooding. Parts of the wadi delta were engulfed at Quriat and numerous engineered structures within the flood plain collapsed due to the scouring at the foundations (Fig. 4b). Even highway bridges along wadis collapsed due to buoyancy and uplift from floodwater as shown in Fig. 4c in the mountains, south of Muscat. The bridge collapse mechanism is identical to the highway bridge collapses along the Louisiana and Mississippi Gulf Coast during Hurricane Katrina (Padgett et al. 2008). An eyewitness photo of the flooding at Muscat due to the combined wadi discharge and storm-surge-induced backwater is shown in Fig. 4d.

Fig. 4 Wadi runoff: (**a**) high water marks in the form of rafted debris in a tree at Hail al Ghaf located 7 km inland and at 50 m elevation; (**b**) pancake collapse of a building due to foundation scour at Quriat (**c**) highway bridge collapse due to uplift forces in the mountains south of Muscat; (**d**) Wadi flooding due to discharge and storm-surge-induced backwater at Muscat (Photo credit: Department of Meteorology, Sultanate of Oman)

Comparison with Indian Ocean Tsunami

The measured high water marks, overland flow depths, and inundation distances surpassed the 2004 Indian Ocean tsunami run-up at every corresponding location (Fig. 2). Similar 2004 Indian Ocean tsunami run-up heights were only observed in southern Oman (Okal et al. 2006) and Yemen (Fritz and Okal 2008). However, even in southern Oman and Yemen, tsunami inundation distances were limited to a few hundred meters. In sharp contrast, cyclones typically flood several kilometers inland along low-lying coastal plains because of significantly longer storm surge periods compared to typical tsunami wave periods (Fritz et al. 2008, 2009). Eyewitnesses were interviewed to document the time history of the event, survival strategies, cyclone awareness, and evacuation plans. Besides cyclone Gonu, most fishermen and residents mentioned the 1977 tropical storm or cyclone, which impacted primarily Masirah Island. Some residents recalled the 1890 super cyclone, whereas no one spontaneously mentioned any tsunami events. The 2004 Indian Ocean tsunami was observed inside the Gulf of Oman mostly flooding beaches, but

fishermen only interpreted the observations as a tsunami after they heard it in the news. Several elders were interviewed, but no account was unambiguously attributed to the 1945 Makran tsunami. Various historical tropical storms and cyclones have produced high water records of a few meters along the coastline in eastern Oman. The cyclone history must be considered when analyzing tsunami deposits in the Gulf of Oman. Deposits in Sur Lagoon were attributed to the 1945 Makran tsunami by Donato et al. 2008.

Numerical Storm Surge Modeling

A high-resolution numerical storm surge model was created of the Arabian Sea (Blount et al. 2009) using the ADCIRC code (Luettich et al. 1992) to simulate the storm surge distribution of Gonu (Fig. 5a). The grid consists of 125,511 nodes and 231,770 elements with grid size ranging approximately from 1 km to 80 km. Best track data were adopted from the JTWC Automated Tropical Cyclone Forecasting database and were used to force the wind model within ADCIRC. The modeling results show a peak storm surge distribution trend that is similar to the observed high water mark distribution with decreasing storm surge from Ras al-Hadd to Muscat (Fig. 5b). Model results indicate more than 1 m storm surge along the coast between Ras al-Hadd and Quriat. The discrepancy between high water marks and model results may mainly be attributed to wave action and overland flow. A short-wave model remains to be coupled to the storm surge model, which will also increase modeled storm surge. Independently run storm wave models indicated significant storm waves in the landfall area (Golshani and Taebi 2008). At present inland inundation is not included in the model and wadi runoff not considered.

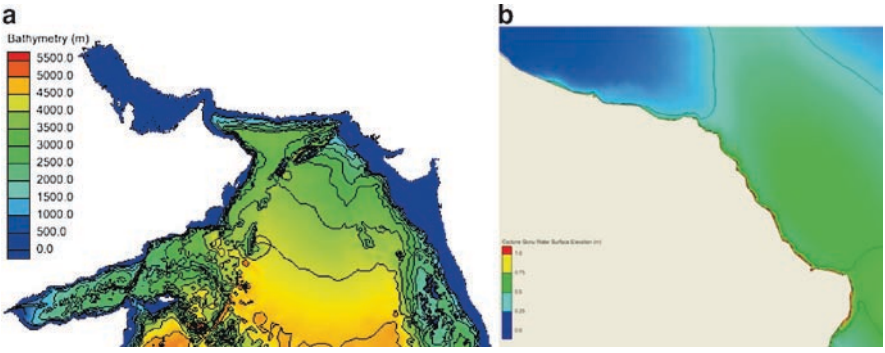

Fig. 5 Storm surge modeling with ADCIRC: (**a**) Arabian Sea modeling domain and corresponding ETOPO1 bathymetry; (**b**) peak storm surge distribution computed for Gonu

Conclusions

A high water mark survey was performed along 270 km of Omani coastline in the aftermath of Cyclone Gonu, which is the strongest cyclone on record for the Arabian Sea. High water marks peaked with 5 m at Ras Al Hadd. The steep bathymetry between Ras al Hadd to Muscat limits the relative contribution of storm surge, but increases storm wave impact. Cyclone Gonu's fatalities and damage were mostly attributed to wadi flooding as well as coastal storm surge and storm waves. A high resolution storm surge model was used to estimate Gonu's storm surge. Future work requires the coupling of storm surge and storm wave modeling to reveal the relative importance of storm surge and storm waves to the coastal vulnerability of Oman. The storm surge flooding hazard is expected to increase in the rare event of a cyclone landfall along the shallow shelf between Muscat, Oman, and Al Fujayrah, United Arab Emirates, or near the Island of Masirah, Oman. Coastal protection in the Gulf of Oman must be approached from a multihazard perspective given the combined tropical cyclone and tsunami hazards. The importance of raising tropical cyclone and tsunami public awareness is highlighted.

Acknowledgments The authors would like to thank the Meteorological Department of the Sultanate of Oman for supporting the field survey and the ADCIRC Development Group for their modeling support.

References

Bailey RW (ed) (1988) Records of Oman: 1867–1947. 8 Vols. Archive Editions, Buckinghamshire, England

Blount C, Fritz HM, Al-Harthy AHM (2010) Coastal vulnerability assessment based on historic tropical cyclones in the Arabian Sea. Proceedings of the First International Conference on Indian Ocean Tropical Cyclones and Climatic Change (in this volume)

Donato SV, Reinhardt EG, Boyce JI, Rothaus R, Vosmer T (2008) Identifying tsunami deposits using bivalve shell taphonomy. Geology 36(3):199–202

Fritz HM, Okal EA (2008) Socotra Island, Yemen: field survey of the 2004 Indian Ocean tsunami. Nat Hazards 46(1):107–117. doi:10.1007/s11069-007-9185-3

Fritz HM, Blount C, Sokoloski R, Singleton J, Fuggle A, McAdoo BG, Moore A, Grass C, Tate B (2007) Hurricane Katrina storm surge distribution and field observations on the Mississippi Barrier Islands, *Estuarine*. Coastal and Shelf Sciences 74(1–2):12–20. doi:10.1016/j.ecss.2007.03.015

Fritz HM, Blount C, Sokoloski R, Singleton J, Fuggle A, McAdoo BG, Moore A, Grass C, Tate B (2008) Hurricane Katrina storm surge reconnaissance, J Geotechnical and Geoenvironmental Eng ASCE, 134(5):644–656, doi:10.1061/(ASCE)1090-0241(2008)134:5(644).

Fritz HM, Blount C, Thwin S, Thu MK, Chan N (2010) Cyclone Nargis storm surge flooding in Myanmar's Ayeyarwady River delta. Proceedings of the First International Conference on Indian Ocean Tropical Cyclones and Climatic Change (in this volume).

Golshani A, Taebi S (2008) Numerical modeling and warning procedures for Gonu super cyclone along Iranian Coastlines. In: Wallendorf L, et al. (Eds) Proceedings of the 3rd COPRI Solutions to Coastal Disasters Conference, ASCE, Oahu, HI, 13–16 April, 2008.

Luettich RA Jr, Westerink JJ, Scheffner NW (1992) ADCIRC: an advanced three-dimensional circulation model for shelves, coasts and estuaries, Report 1: theory and methodology of

ADCIRC-2DDI and ADCIRC-3DL, Dredging Research Program Technical Report DRP-92–6. USACE WES, Vicksburg, MS 137p

Okal EA, Fritz HM, Synolakis CE, Raad PE, Al-Shijbi Y, Al-Saifi M (2006) Field survey of the 2004 Indonesian Tsunami in Oman. Earthquake Spectra 22(S3):S203–S218

Padgett J, DesRoches R, Nielson B, Yashinsky M, Kwon OS, Burdette N, Tavera E (2008) Bridge damage and repair costs from Hurricane Katrina. J. Waterway, Port, Coastal, and Ocean Eng, ASCE, 13(1):6–14, 10.1061/(ASCE)1084-0702(2008)13:1(6).

Singh OP, Khan TMA, Rahman MS (2001) Has the frequency of intense tropical cyclones increased in the north Indian Ocean? Current Science 80(4):575–580

Webster PJ, Holland GJ, Curry JA, Chang HR (2005) Changes in tropical cyclone number, duration, and intensity in a warming environment. Science 309(5742):1844–1846

How the National Forecasting Centre in Oman Dealt with Tropical Cyclone Gonu

Juma Al-Maskari

Keywords Hourly surface pressure

Introduction

Tropical storms and cyclones over the Arabian Sea are almost entirely confined to two cyclone seasons (Fig. 1), namely, the pre-monsoonal period (May–June) and the post-monsoonal period (October–November) (Membery, 1985). Most storms originate over the southeastern Arabian Sea in the vicinity of the Laccadive Islands, but some late season storms start over the southeastern Bay of Bengal and move westwards across southern India regenerating as they cross over the warm waters of the Arabian Sea. Once a storm/cyclone has formed over the southeastern Arabian Sea, it moves in the northwest direction toward the Arabian Peninsula, sometimes curving northeastwards toward Gujarat and Pakistan and sometimes curving westwards toward the Gulf of Aden (see Fig. 1 in Pedgley 1969). Pedgley (1969) has discussed the characteristics of these coastal storms, and more recently Galvin (2008).

Tropical cyclone Gonu affected the coastal areas of Oman, UAE, and Iran in June 2007; leaving at least 49 people dead and 27 missing in Oman, 20 dead in Iran and at least ten reported missing when a boat sank by the port of Fujairah in the UAE. Gonu caused lots of damage to the infrastructure of Muscat, the modern capital city of Oman. The estimated damage was over 1.5 billion Omani Rials (approximately US$4 billion). This makes Gonu the most expensive weather event ever to have affected the Sultanate of Oman. However, as mentioned above, tropical cyclones have affected Muscat and the rest of the Gulf of Oman coast in the past. This chapter will highlight the history of tropical storms that have affected the Omani coasts with special emphasis on the tropical cyclone Gonu, especially, on

J. Al-Maskari (✉)
DGMAN, Civil Aviation Affairs, Muscat International Airport, Oman
e-mail: j.almaskari@met.gov.om

Y. Charabi (ed.), *Indian Ocean Tropical Cyclones and Climate Change*,
DOI 10.1007/978-90-481-3109-9_31,

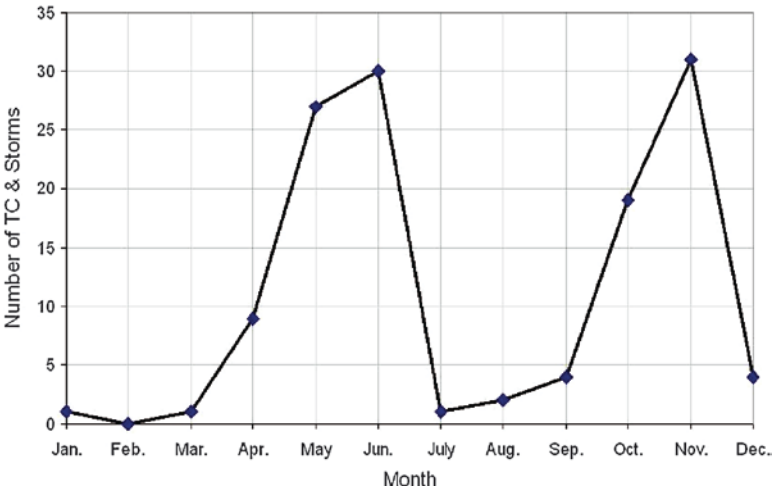

Fig. 1 Frequency of tropical storms and cyclones affecting the Arabian Sea, 1801–2007

how the Oman National Forecasting Centre (ONFC) and its management dealt with a first-hand experience in forecasting and managing the storm. Lessons learned by the ONFC and its management from this severe weather event will be discussed and future plans will be highlighted. The chapter will end with a conclusion and recommendations.

History of Tropical Cyclones that Affected Omani Coasts

Cyclones have been known to enter the Gulf of Aden and more rarely the Gulf of Oman. According to unpublished notes by the Department of Meteorology in Oman (see also Membery 2001, 2002), on 4 June 1890, a tropical cyclone brought 24 h of torrential rain to Batinah and Muscat regions, with severe flooding and widespread damage to property. Close to 300 mm of rain fell on Muscat city and the destruction that followed led directly to the death of 727 people. More recently, severe cyclones have occurred in the Salalah area in May 1959, May 1963, and November 1966. In June 1977, a severe cyclone crossed Masirah Island with a central pressure of about 976 hPa; maximum sustained winds in the region were 90 knots with gusts upto 120 knots. The 24 h rainfall was 430.6 mm. In June 1996, a tropical storm crossed the Omani coast near Ras Madraka (south of Masirah Island) and brought more than 200 mm of rain to the eastern Hajar Mountains with more than 150 mm to the mountain of Dhofar in the south. In May 2002, a tropical storm affected Salalah city. Rain of 58.6 mm was reported at the Salalah plain and 250.6 mm over the adjoining mountains. According to Membery (2001), the Hajar Mountains received up to 300 mm of rainfall in July 1995 due to a monsoon depression.

Table 1 Some tropical storms/cyclones that affected coastal areas of Oman in the past

	Year – month	Cyclone/storm
1	1889	Tropical storm struck Oman
2	1890 – Jun	Tropical cyclone affected Muscat killing ~727 (~285 mm)
3	1948 – Oct	Tropical cyclone struck Oman (Salalah)
4	1959 –May	Tropical cyclone struck Oman (Salalah) killing ~141 (~117 mm)
5	1963 – May	Tropical cyclone struck Oman (Salalah)
6	1966 – Nov	Tropical cyclone struck Oman (Salalah)
7	1977 – Jun	Tropical cyclone struck Oman (Masirah) (~430 mm)
8	1983	Tropical storm struck Oman.
9	1992 – Oct	Tropical storm 06A struck Oman.
10	1993 – Nov	Tropical storm affected coastal areas of Oman
11	1996 – Jun	Tropical storm 02A struck Oman
12	1998 – Dec	Tropical storm affected coastal areas of Oman (near Ras Madraka)
13	2002 – May	Tropical storm struck Oman (Salalah)
14	2007 – Jun	Tropical cyclone Gonu struck parts of Oman (Muscat) killing ~49 (~943 mm)

Table 1 lists the most tropical cyclones/storms that directly affected the coastal areas of Oman.

Tropical Cyclone Gonu (02A)

Track

Tropical cyclone Gonu started as a low pressure system on 1 June 2007. The system first developed southwest of India and moved slowly in west-northwest direction toward the coastal areas of Oman (Fig. 2)

Storm History

The following points give an account of the system as it developed from the beginning when it was first observed over the southeastern part of the Arabian Sea.

- 27 May, a widespread area of convection persisted over the southeastern Arabian Sea.
- 31 May, an organized tropical disturbance developed about 645 km south of Mumbai, with cyclonic convection and a well-defined mid-level circulation. There was still no distinct low-level circulation.
- 1 June, a low-level circulation formed; in the day the system developed further and Indian Meteorological Department (IMD) classified it as a depression.
- 2 June, convection continued to organize and tracked westward. Early on 2 June, the Joint Typhoon Warning Center (JTWC) classified it tropical cyclone 02A (685 km southwest of Mumbai).

Fig. 2 Track of tropical cyclone Gonu (3–7 June 2007)

- Early 2 June, IMD upgraded the system to deep depression, and later in the day the IMD classified the system as cyclonic storm Gonu (760 km southwest of Mumbai).
- Early 3 June, JTWC upgraded the system to CAT 1 tropical cyclone.
- Late 3 June, IMD classified the storm as very severe cyclonic storm Gonu.
- While the system was located 285 km east-southeast of Masirah Island, the IMD upgraded it to super cyclonic storm Gonu late on 4 June.
- Early 5 June, after maintaining peak winds for about 9 h, the IMD downgraded Gonu to very severe cyclonic storm.
- The eye of the storm became cloud-filled and ragged and the cyclone gradually weakened as it continued tracking northwestward over cooler water temperatures and through drier air. Then due to land interaction with Oman, the inner core of the deep convection rapidly weakened. According to IMD, cyclone Gonu crossed the eastern-most tip of Oman. However, according to the ONFC, the closest point of the center of the cyclone Gonu to the coast of Oman was approximately 50 km to the north of Quriat before turning north into the Gulf of Oman and the Republic of Iran.

Preparations

- The Chairman of the internal committee on natural hazards of DGMAN officially called the Director of the Executive Office of the National Committee for Civil Defence (NCCD) on 2 June to brief him about the situation.
- 3 June, the first advisory was issued to the public.

- 3 June, NCCD called for urgent meeting to be held on 4 June.
- 4 June, NCCD met with all its members and was briefed by the representatives of the DGMAN about the TC.
- 4 June, a state of emergency was declared by the Chairman of NCCD.
- The contingency plan was activated which included the activation of army and police personnel well in advance of the storm's arrival.
- 4 June, the first warning was issued.
- 4 June, direct satellite broadcast was established with national TV and other press.
- 5 June, Masirah Island was evacuated completely and shelters were set at government schools.
- 20,000 were evacuated and over all 67,000 people were sheltered.
- Port of Sohar evacuated 11,000 workers (according to port spokesman Dirk Jan De Vink).
- Oman Liquefied Natural Gas Company (LNG), and Mina Al Fahal Oil terminal were closed for over 3 days.
- A 5-day long national holiday was declared that commenced from Tuesday 5 June.
- All flights after 2000 UTC on 5 June from Muscat International Airport were delayed.
- DGMAN and NCCD issued several warnings through text messages (SMS) in both Arabic and English languages.

Observations

Qalhat station observed 982 hPa (Fig. 3) surface pressure before the station stopped transmitting due to power failure at approximately 01 UTC on 6 June 2007. Qalhat is the closest station to the cyclone track and recorded the lowest pressure. This is approximately 20 hPa higher than what was observed by satellite (CIMSS AMSU) for the center of the storm for the same time. Similarly, Qalhat reported the strongest winds (95 Knots) for the same time (Fig. 4). Winds observed by CIMSS AMSU are comparable to those observed at Qalhat for the same time. Highest rainfall recorded during Gonu was 943 mm (Table 2) by a mountainous rain gage (1390 m above mean sea level). Higher precipitation over high and steep mountains led to flash floods in the low-lying areas. More damage was caused by flash floods during cyclone Gonu compared to storm surges and high winds.

Coordination with the National Committee for Civil Defence (NCCD)

During the period 27–30 May 2007, forecasters at Oman National Forecasting Centre (ONFC) analyzed carefully the various products from the several NWP models available to them where there was an indication for the possibility of the development

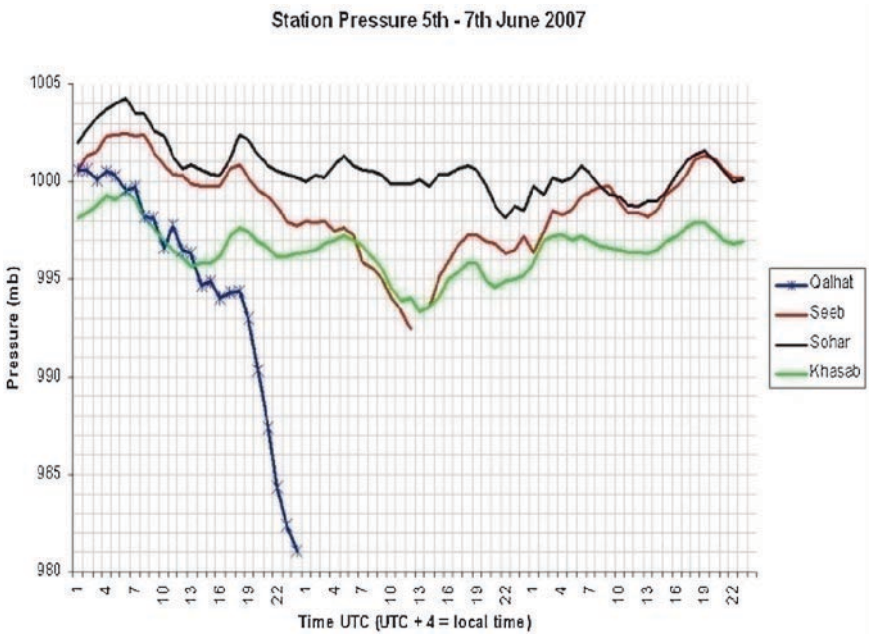

Fig. 3 Hourly surface pressure, 5–7 June 2007

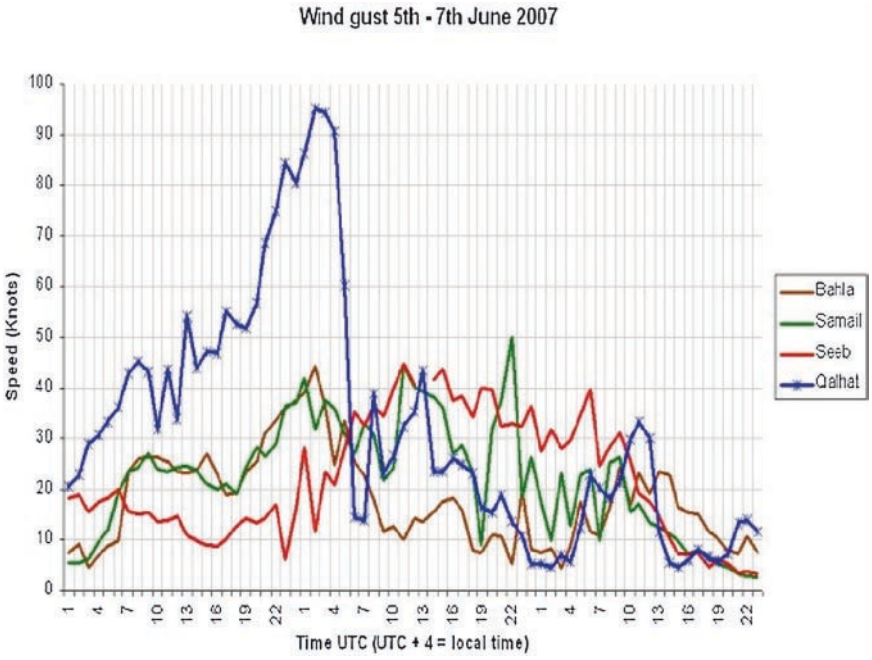

Fig. 4 Hourly wind gust, 5–7 June 2007

Table 2 Total accumulated rainfall for cyclone Gonu (5 and 6 June 2007)

Rainfall (mm)	Location
401	Qalhat
230	Sur
257	Seeb
60	Ibra
2.2	Masirah
78	Rustaq
83.2	Samail
4.8	Nizwa
253	Taiin Mountain
592	Abiadh Mountain
943	Asfar Mountain

of a low pressure system during the first week of June. On 31 May, the convective clouds southwest of India started to organize developing into a low pressure system by 1 June 2007. Later on that day, the system developed further and the Indian Meteorological Department (IMD) classified it as a depression. The system continued to develop further and was classified as a deep depression on Saturday 2 June, the system was moving in a northwesterly direction toward the Omani coasts. On this day, members of the Executive Office for NCCD were asked to attend a briefing at the Department of Meteorology. During the briefing, the possibility of a severe tropical cyclone to affect Oman coastal areas within days was noted.

Early on 2 June 2007, the Joint Typhoon Warning Centre (JTWC) classified the system as tropical cyclone 02A, and later on that day IMD upgraded the system and classified it as cyclonic storm Gonu, the system was approximately 760 km southwest of Mumbai. On 3 June 2007, NCCD called all its members for an urgent meeting to be held on 4 June. The meeting was chaired by His Excellency the Chief Inspector of Oman Police, the Chair of NCCD. During the meeting, a presentation was given by a representative from DGMAN. The presentation gave details of the current location, severity, expected wind, rainfall, and track. In addition, expected damage associated with the system was highlighted. Based on this meeting, His Excellency the Chair of NCCD declared a state of emergency. The meeting was then followed by a press conference. Staff at the Department of Meteorology worked around the clock to monitor the situation and continuously briefed NCCD. This early coordination between the Department of Meteorology and NCCD which started on Saturday 2 June 2007 allowed NCCD enough time to make all the necessary coordination and arrangements with its 16 members from various government agencies. Moreover, a forecaster was made available with a mobile satellite receiving station at NCCD operation room to work closely with NCCD to answer questions and clarify doubts. A series of emergency crisis meetings were called for right from 2 June till 6 June which involved the high authorities of DGMAN and representatives of NCCD. They were briefed on the latest intensity and forecast of track of the cyclone and the expected impact to be caused so as to take the necessary preventive and mitigation measures by the relevant agencies.

Coordination with Press and Media

DGMAN learned well in advance the importance and urgent need to coordinate closely with the press and media in order to deliver the warnings on time to the public. This coordination played a vital role in delivering not only warnings but various live interviews with officials from DGMAN to provide latest information to the public about the progress of the cyclone. On 3 June 2007, the first weather advisory was issued at 0800 local standard time. A direct TV satellite link was put into place on 4 June between DGMAN and Oman TV. Simultaneously, warnings were broadcast on local radio stations with several live telephone interviews. On the same day, the weather advisory was upgraded to a tropical cyclone and a warning was issued at 2000 local time with updates every 3 h. A total of 16 tropical cyclone warnings were issued. On 7 June DGMAN declared the end of the warnings as the cyclone moved away from the coastal areas and was downgraded to a tropical storm. All warnings and advisories were issued in Arabic and English to cater to both Arabic and nonArabic-speaking residents.

This coordination helped the general public to receive warnings well in advance of the approach of the tropical cyclone which continued till the end of the weather event. However, the amount of load put on DGMAN to provide and answer queries and deliver interviews to the many press and media agencies was huge. Several press and media agencies (both local and International) were seeking information simultaneously. Better organization on how to handle press and media queries was seen to be essential and was taken into consideration in the lessons learned.

Lessons Learned and Future Directions

Immediately after Gonu, the management team at DGMAN started to evaluate the performance of its staff (level of confidence, adequacy of staff, and training needs), equipments (hardware, software, and models), and coordination with relevant agencies. Despite the very successful management by DGMAN which included early warnings both to the decision makers and to the general public; some shortcomings appeared and measures have been taken to overcome these shortcomings. Measures taken were divided into five categories:

The Need to Strengthen the Coordination with NCCD and the Need for Better Organization on How to Handle the Various Press and Media

Two meetings with NCCD, Oman TV, and Oman Radio were organized to highlight the measures to strengthen coordination. Outcomes from these meetings included:

the need to establish direct broadcast links with NCCD, Oman TV, and Oman Radio so that these links are ready to be activated as and when ONFC sees necessary to broadcast weather warnings to the public.

In addition, a seminar was organized by DGMAN to highlight the role of ONFC. The seminar was aimed at personnel from local press and media agencies

The Need to Re-Organize the Organization Structure and Increase the Number of Staff and Provide Necessary Training

Before Gonu, there was only one department for meteorology with four sections; ONFC was one of these four sections. However, after Gonu, the Civil Aviation Affairs was reorganized and expanded to have two separate directorate generals. One of these two directorate generals is the Directorate General of Meteorology and Air Navigation (DGMAN). Meteorology is part of DGMAN and it consists of two departments with four sections each. The new organization structure allowed specialization. In addition, 89 new additional staffs were requested to overcome the shortage and allow for the expansion as per the new organization. Continuous training is essential for meteorologists working at DGMAN. Three staffs were sent after Gonu to complete master studies in the UK in various meteorological specializations. They completed their studies successfully and resumed duty. One other member of staff is currently completing his Ph.D. studies in the UK. In addition, a comprehensive yearly training plan is being implemented.

The Need to Upgrade the Current Tools Used to Observe and Forecast Weather in ONFC

In addition to the planed TV/radio studio (with a direct broadcast link from ONFC), plans were put forward to further improve the equipment, programs, and forecasting tools used to provide weather information. These included:

1. Establish five new automatic weather observing stations (in progress)
2. Sign an agreement with EUMETSAT to continue to receive half hourly data from Meteosat satellite centered over the Indian Ocean
3. Improve and upgrade NWP models (and clusters) used at ONFC including high resolution nonhydrostatic models, and specialized NWP model for tropical cyclone intensity and tracking (in progress)
4. Network of weather radars (in progress)
5. Wave radars (in progress)
6. Special wind sensors with masts that withstand strong winds (in progress)

A national multihazard early warning center is also planned in coordination with other government agencies.

Increase Public Awareness

DGMAN continues to work closely with the ministry of education to include meteorology in schools syllabus. ONFC receives short visits from schools throughout the academic year to give more insight on what is taught about meteorology in school books. After Gonu, ONFC continued to receive a overwhelming number of phone calls almost on a daily basis and especially when any low pressure develops over the Arabian Sea regardless of its distance and/or relevance to the weather in Oman. This Gonuphobia is fueled occasionally by what people write/read on chat rooms on the Internet. Unfortunately, the situation sometimes becomes unbearable especially when some local newspapers publish what is written in these chat rooms without consultation with ONFC.

A short book about tropical cyclones is in preparation in Arabic by DGMAN. The aim of the book is to educate both students and the general public and raise general awareness on the impact of tropical cyclones.

Broadcasting in Several Languages

Although Arabic and English were used to broadcast warnings during Gonu, it became evident that other languages like Hindi, Urdu, etc. should also be used in the future in order to make the warnings more effective and reach a wider range of different communities living in Oman.

Conclusion

Tropical cyclones are not uncommon over the Arabian Sea. However, many of these storms rarely reach the coastal areas of Oman with tropical cyclone intensity, and from historical data, they very rarely enter the Gulf of Oman. Tropical cyclone Gonu was the first destructive tropical cyclone to affect Muscat after the 1890 cyclone. In order for DGMAN to be ready to deal with severe weather events in the future, it must be equipped with tropical cyclone intensity and track forecast models. Continuous training should be provided for meteorologists dealing with severe weather. In addition, coordination between DGMAN, NCCD, and press and media should be strengthened and further improved. A need for video conferencing between DGMAN and India's Regional Specialized Meteorological Centre (RSMC) on tropical cyclones is highly desirable in order for both centers to discuss on the arising situation on a real-time basis. Further coordination and effort is required to educate the general public and increase their awareness about tropical cyclones and other natural disasters. The importance of various satellite data which helped in monitoring and tracking cyclone Gonu, in particular Meteosat-7, must be noted.

The importance of various outputs and warnings from the Regional Specialized Meteorological Centre (RSMC – New Delhi, India) and the Joint Typhoon Warning Centre (JTWC), which helped the forecasters at DGMAN make the right decisions, is also to be noted.

Acknowledgments Thanks to the staff at DGMAN and Water Resources Department who helped in providing the data. Further thanks to Mr. Ahmed Al-Harthy for his valuable comments and proofreading.

References

Galvin JFP (2008) The weather and climate of the tropics, Part 7 – tropical revolving storms. Weather 63:327–338
Membery DA (1985) A unique August cyclonic storm crosses Arabia. Weather 40:108–115
Membery D (2001) Monsoon tropical cyclone: Part 1. Weather 56:431–438
Membery D (2002) Monsoon tropical cyclone: Part 2. Weather 57:246–255
Pedgley D (1969) Cyclones along the Arabian coast. Weather 24:456–469

Cyclone Disaster Management: A Case Study of MODES Experience with Cyclone Gonu

Al-Maani Saif Suliman and Al-Zaabi Mohammed Nasser

Keywords MODES

Introduction

Natural disasters and their consequent damages are considered to be the biggest challenges facing countries, organizations, and human beings on the Earth. Natural disasters, cyclones, earthquakes, floods, etc., normally lead to a great loss of lives, destruction to the infrastructure, and subsequently an unexpected financial burden on the governments to restore things to their original status. Cyclone Gonu was the strongest tropical cyclone on record in the Arabian Sea, and it was one of the most devastating cyclones that hit Oman in recent history. The way by which the disaster was managed by the government authorities, private sector organizations, and the people of Oman played a vital role in reducing the effects of the disaster.

The Armed Forces were at the forefront providing the necessary support to the Omani people during the incident of the cyclone Gonu. They undertook a commendable role to restore things to the status they were in before the cyclone. The Ministry of Defence Engineering Services (MODES) provided many engineering support activities during the crises; especially after the cyclone had hit the country. These were not only limited to the reopening of the main roads to the public, but extended to providing drinking water and electricity to many governmental and public organizations in addition to many other support services. The aim of this chapter is to present a case study on MODES' experience during the cyclone Gonu. The chapter evaluates the disaster preparedness and management system at MODES throughout the stages of preparedness, during (response), and after the cyclone (recovery). The roles it played, its contingency plan, and the efforts exerted

A-M.S. Suliman and A.-Z.M. Nasser
Ministry of Defense, Oman
e-mail: Al-maani@hotmail.com

Y. Charabi (ed.), *Indian Ocean Tropical Cyclones and Climate Change*,
DOI 10.1007/978-90-481-3109-9_32,

to manage the effects of the disaster after the cyclone are discussed. The lessons learnt from the experience are also presented. The concentration of this chapter is on natural disasters and cyclone-specific type of natural disasters. This case study is related to the cyclone "Gonu" that hit the areas of Oman in June 2007.

Background on MODES

The Ministry of Defence Engineering Services (MODES) is a department of the Ministry of Defence responsible for the general engineering and maintenance support for the Ministry and the Armed Forces. Its role involves the provision of essential services of power, water, and sewage treatment to all camps belonging to the Ministry. It is also responsible for the design and management of construction projects and service contracts on behalf of the Ministry and the Armed Forces. In addition, MODES is also responsible for the maintenance of the existing buildings, infrastructure, roads, etc. MODES also provide nontactical support to the Armed Forces' operations and exercises. MODES exist in more than 100 locations around the country to provide engineering support to the Armed Forces.[1]

Definitions and Terminologies

A disaster is a sudden, catastrophic event that brings great damage, loss, and destruction and devastation to life and property. The damage caused by a disaster is not easily measured and may vary from place to place depending on the vulnerability of the affected area and the extent of the disaster. Disaster management system is a system that deals with, and avoids, risks. It involves preparing for a disaster before it happens. Disaster management is concerned with putting in place necessary plans to reduce the effects of disasters. It entails carrying out an assessment of the likely risks of a particular type of disaster and putting in place necessary measures to reduce their effects. Good preparedness and disaster management systems are concerned with disaster effects mitigation not avoidance. It entails risk management as opposed to crisis management.

Experts in disaster relief, like Fred Cuny, note that the process of disaster management involves four phases: mitigation, preparedness, response, and recovery (Cuny 1983). However, for the purpose of this chapter, the disaster management system is addressed only under three headings excluding mitigation. Mitigation in this context is considered to be a part of the recovery process as has been applied in Oman after the cyclone has taken place.

[1]More information on MODES can be found on www.modes.gov.om

The three phases of the disaster management system can be defined as follows.

Preparedness phase: this takes place before the disaster happens. This phase normally involves preparation of the plans of action, communication of the same, setting up response teams and operation centers, etc. It involves preparing equipment and procedures for use when disaster occurs. It can take many forms including construction of shelters or even creating a backup of essential services of power, water, and sewage.

Response phase: this takes place during or immediately after the disaster. It covers the mobilization of necessary services and the first respondents in the disaster area. During this phase, an immediate practical assistance is provided, e.g., first aid people rescue efforts, etc., i.e., it starts with search and rescue.

Recovery phase: this phase starts after the immediate threat to human life is subsidized. It aims at restoring the affected area, services, etc. to its previous state.

The MODES Experience

Preparedness Phase

Having realized the importance of prior planning and preparation to encounter the effects of the cyclone, MODES endeavored from the outset to plan the efficient use of its available resources in the areas where the cyclone was expected to hit. Despite the fact that this was the first experience of its kind, the preparation that has taken place has helped to deal effectively with the aftermath effects of the cyclone.

It has proved to be very important to pull together in a centralized manner the following plant and equipment, which we anticipated would be required in the areas that were expected to be affected by the cyclone:

- Earthmoving plant
- Drilling equipments
- Welding equipments
- Cranes
- Power generation sets
- Water and sewage tankers

These plants and equipment were distributed around the areas where the cyclone was expected to hit based on the original weather forecast: Sur, Ibra, Shafa, the MOD main camp MAM in Muscat, and Wudam Navel Base. This was considered necessary so that the rescue teams can provide the necessary support in the respective sites as it would be difficult to maneuver them during or even post the cyclone.

At the preparedness phase MODES undertook the following activities/action:

a) It set up an executive steering committee chaired by the Head of Engineering services represented by all Directors. The committee was responsible for overseeing the execution phase of the internal action plan. The committee affected daily meetings and when necessary meetings were held more than once.
b) It established effective communication with the sub-disaster management committees, based on the requirements of the Armed Force Disaster Management plan.
c) It prepared and communicated a response and recovery plan to encounter the effects of the cyclone.
d) It activated its emergency operation centers in Muscat and other major cities in areas where the cyclone was supposed to hit.
e) It prepared and put on call all necessary resources of manpower, plant, equipment, etc. in preparation to what may be required by MODES.
f) It identified shelter centers for families of its married staff on MAM camp, providing them with food and other requirements for at least 2 days.
g) It was prepared to provide the necessary help to establish shelter centers, provide them with power, water, toilets, gas, etc. as may be required.
h) It undertook necessary steps to maintain a continuous power supply to the Armed Forces, and at the same time support government organizations and civil community such as:

   - Armed Forces hospitals (including the mobile hospital)
   - Concentrate on the areas that were likely to be affected by the cyclone (Sur, Ibra, Shafa, MAM, and Wudam)
   - Carry out necessary inspection and keep ready all standby power generators at all locations
   - Keep ready all mobile power-generating sets

i) It undertook the necessary precautions to ensure the availability of water through the following:

   - Identify water sources in the vicinity of the affected areas, carryout the necessary inspections and maintenance to ensure its preparedness including its readiness for operation during the cyclone
   - Enhance the potable water reserves by topping up all overhead and underground water tanks to encounter problems with water supply during and after the crises
   - Keep mobile water treatment plants and their associated pumping facilities ready for use as and when required

j) It undertook necessary precautions to top-up all diesel fuel tanks of main power stations to have an alternative fuel supply in case of disconnection of external gas supply, so that sufficient quantity of diesel was there for at least 3 days for all sensitive areas, especially on MAM camp. This measure proved important toward the support MODES provided later on.
k) It undertook necessary precautions to mobilize mobile toilets as and when necessary.

Response Phase

Although the situation was dangerous when the cyclone hit the different areas, MODES provided what they could in response to the emergency works. MODES efforts at this stage were limited to the following:

a) Restoring power supply to sensitive locations
b) Reopening some of the affected roads
c) Supplying water to some of the affected people, hospitals, other government departments, and other MOD camps
d) Supplying diesel to some government departments and MOD camps
e) Pumping out water from flooded offices
f) Rescue efforts in some areas

Recovery Phase

The morning of 6 June was a different day in the capital city Muscat; some of the roads were severely affected as a result of the destruction of the cyclone. Gonu caused major damages to the infrastructure and assets due to which the traffic flow was disabled. The essential services of water and power were out of order.

After the cyclone had subsided, MODES recovery efforts were in the areas of water supply, reopening of roads, and in the restoration of power supply.

Water

As the water network in some areas of Muscat was damaged, water supply was disconnected to many areas in Muscat, and MODES played a vital role in assisting in the supply of drinking water to affected people and some government organizations by virtue of providing water sources and distributing water as explained below.

(1) Water Sources

This was done through the operation of existing bore wells by means of installing necessary pumping facilities, including some power generators, so that these bore wells were ready for usage. The drilling of additional bore wells also took place in some places like Al Khoudh, Bawshar, and Qurayat, This was in addition to the full operation of MODES MAM camp Water treatment Plants (RO Plants) to their maximum operation capacity to cater for the high demand of water then. One can imagine then the nature of the problem if there was no power in the main MOD camp at Muasker Al Murtafaa to run its RO Plants, or the inability to use the existing bore wells.

One issue that came to the surface was the effects of pollution on drinking water during the disaster. In providing the sources of water, the MOD ensured that the water from these sources was saved to drink. This was done by testing samples of the water at MODES Public Health Laboratory.

(2) Water Distribution

In this area, MODES distributed and supplied water of more than 1.5 million gallons using its large-size water bowsers (Al Maani and Al Zaabi 2007). This was provided to affected areas of Seeb, Mawaleh, Al-Khoud, Mabella, Al-Hail, Bait Al-Falaj, Al-Ameerat, and Qurait. The water supply was extended to many hospitals in the capital area and some other government departments.

Power

After the cyclone hit Muscat and other places, the national power network was disabled but power was not affected on the MOD main camp (MAM). This was mainly due to MODES' own dedicated power facilities on the MAM camp which were not affected.

The recovery efforts in this area covered the following:

(1) While it maintained a continuous power supply to MOD camps, logistical and technical support was provided to the National Grid Power Company to restore power in some areas of Muscat.
(2) It provided power generation sets to various government departments until power was restored.
(3) It provided power generation sets and technical support team to the Armed Forces mobile hospital at both Watayah and Quriat.

Roads

MODES took utmost efforts to reopen essential main and internal roads so that both people and recovery aids could be transported easily to the affected areas. MODES' efforts in this field were highly appreciated by everybody, and brought life back to the areas that were isolated for quite some time after the cyclone.

Main road reinstatement works included, but were not limited to, the following:

(1) Reopening of Wadi Eday – Al-amrat road (19 km) in a very short period of time.
(2) Reopening of Nizwa road at the junction of Al-Jafnaan village (500 m).
(3) Reopening of the road leading to Sultan Qaboos University from Armed Forces hospital (50 m)
(4) Reopening of Mabella – Al Khoud road (200m)
(5) Reopening of Northern al-hail road (75 m)
(6) Reopening of the road leading to Sayyidah Mazoun Mosque (300 m)
(7) Reopening of various internal roads at Seeb

The work in this area also included clearing wadi debris from internal roads in many places in Al-khoud, Seeb, Al-hail, Mawaleh, Ghobrah, and Uthaiba.

Lessons Learnt

It goes without saying that the Armed Forces have played a commendable role during the cyclone. The same has certainly brought to surface many lessons that are useful for other organizations and are also crucial to improve the present preparedness and disaster management systems. These are detailed in the following paragraphs.

(1) Contingency plans should have clear definition of responsibilities for all parties' involvement. Responsibilities should be transmitted clearly to the different parties involved in the response and recovery works. Limitations of responsibilities and areas of operation on the ground should also be clearly spelt out, in order to avoid overlapping. Responsibilities should be allocated to the different parties based on their specialization, expertise, and available resources, i.e., should be given to the party capable of undertaking.
(2) The line of communication should also be clearly spelt out in the plan to avoid delays during recovery execution phase as a result of gaps in communication.
(3) If the contingency plan calls for an external coordination with other government departments then this should be clearly detailed including the parties responsible for such coordination.
(4) In order to avoid duplications and overlapping leading to delays and ineffective recovery phase, changes in the originally intended roles and responsibilities should not happen during the execution phase.
(5) An important ingredient for success in disaster management systems is an effective coordination and cooperation between the different parties and the provision of necessary resources so that best recovery services can be provided. As recovery efforts require close cooperation and coordination, organizations with identical resources (i.e., similarity in resources) should foster coordination to avoid duplication and overlapping of responsibilities which result in abortive work and waste of time.
(6) Effective preparation and prior planning are necessary ingredients for effective response and recovery activities during disasters. Planning phase should take on board utmost potential risks and consequential damages so that response and recovery teams are prepared for the worst, and would be able to execute their roles swiftly and expeditiously with minimum management interference.
(7) Efficient utilization plan of the resources in the areas expected to be affected by the disaster leads to avoidance of unexpected surprises and uncalculated risks.
(8) Dealing with events as they happen (i.e., centralized planning and resourcing-coupled decentralized execution) is an important requirement in disaster management. Any delay in response would lead to life losses and more difficult recovery phase (link it to para 6 (Arabic version 1) already typed under preparedness).
(9) The option of using bore well water in emergencies has proved to be a viable alternative when it becomes impossible to use desalinated water. Hence, the upkeeping of such water sources readily available for use is far important.

(10) It proved right, that the major parts of the response and recovery efforts during this type of disaster would rely on the presence of an effective fleet of earth-moving plant and reliable sources of water and electricity. The working teams were given clear terms of reference and were asked to have their internal action plan to enhance flexibility into decision making and working methods.
(11) If MODES is required to provide similar support in the future, then it is important to enhance its current capabilities in the following areas:

- To enhance better mobility, there is a need to procure small- and medium-size water tankers.
- Four- and six-wheel drive heavy vehicles to transport recovery aids through difficult and rough terrains are required.
- Mobile pumping equipments (wheeled) to pump water out of flooded offices, buildings, and roads are required.
- Certain types of earthmoving equipments, e.g., rock breakers, excavators, etc., are required.

(12) Having alternative power and other services sources have proved to a viable option during emergencies, especially in the event of the disconnection of the main services. The problem with slow response once these main services are disconnected may affect the response and recovery efforts. Hence, the availability of standby power generation sets, water treatment plants, and water bore wells readily available proved to be highly useful.
(13) The response time for privatized water and electricity services was slow in comparison to the in-house capabilities. This calls for a review of the contractual terms for effective response at times of emergencies to be clearly spelt out in the agreements between the government departments and the private sector companies.
(14) Top management involvement in any commitment is an important ingredient for a successful and timely recovery phase. As an example, the specially formulated executive committee under the chairmanship of the Head of Engineering Services played a major role in the successful response and recovery efforts through the following:

- Follow-up and monitoring of execution stage
- Ensuring smooth execution of the action plan
- Revise priorities based on actual ground conditions
- Timely decisions for mobilization of major works

Recommendations

The lessons learnt have highlighted the need to enhance certain areas of the preparedness and disaster management system and hence the following recommendations are provided:

(1) Disaster management plans should have a clear definition of responsibilities that all parties should adhere to and if these are to be changed then that should be done before the implementation stage. Effective plans should detail the following:

   - Clear aims of the plan
   - Clear roles and responsibilities
   - Communication and representation agents
   - Clear execution guidelines for preparedness, response, and recover phases

(2) When disasters take place money would be the last thing to think about; therefore, it would be important to set special funds for disasters to be activated once the disaster takes place.
(3) Organizations participating in the response and recovery efforts should enhance their capabilities by procuring the necessary plant and equipment that are important to improve their mobility and be able to provide efficient services.
(4) Organizations should carry out training programs for their staff on response and recovery activities (disaster management).
(5) Carry out joint drills in the field of recovery to foster better coordination and cooperation between the different parties involved. This should be with the aim of achieving optimal output with limited resources.
(6) Upkeeping of up-to-date records of water and power sources available with the MOD and around the country.

Conclusions

The role MODES has undertaken during the cyclone was major and very evident as a contribution toward the recovery efforts as a result of the cyclone. These efforts were not limited to the provision of water and electricity services but extended to the reopening of main and internal roads and rescue efforts.

The support provided during the disaster has provided MODES with very valuable experience and lessons that can be used to improve the present disaster management system.

MODES experience has shown the importance of proper planning of activities, clear definitions of responsibilities, and the need for high-standard coordination between the different parties responsible for the support. The lessons learnt should be effectively used to revise contingency plans at the time of crises, which can lead to improved disaster management systems.

References

Al Maani S, Al Zaabi M (2007) A date with Gonu. Oman Establishment for press, publishing and advertisement, Muscat

Cuny FC (1983) Disaster and development. Oxford University Press, Oxford

Part VI
Recent High Impact Tropical Cyclone Events in the Indian Ocean: Nargis, SIDR, Gonu and Other Events

The Impact of Cyclone Gonu on Selected Coral Rich Areas of the Gulf of Oman Including Indications of Recovery at the Daymanyiat Islands

Oliver Taylor

Keywords Gonu cyclone • Coral • Golf of Oman

Introduction

The Gulf of Oman is located at the northwest end of the Indian Ocean, separating the Arabian Gulf from the Arabian Sea (Fig. 1), bordered by India, Oman, Pakistan, and Iran. This study summarizes the impacts of cyclone Gonu on coral communities within the Gulf of Oman and specifically those associated with the coast of the Sultanate of Oman (Fig. 2).

Upwelling and associated oceanographic features within the Gulf of Oman dominate marine ecosystems, preventing oligotrophic conditions favorable for true reef development by reducing water temperature, light attenuation, and bringing nutrients into the euphotic zone (Wilson 2007). The net result is the absence of the true coral reefs as defined in most tropical oceanic zones from much of the coastline (Wilson 2007). Instead, coral colonies grow on exposed rocky substrates or other dead coral colonies (e.g., *Porites*) and do not lay down a limestone-based reef matrix, subsequently forming incipient reefs. Very few true reefs have been identified in the Gulf of Oman, and where they do occur, they are limited in extent. True reefs are restricted to small areas, typically in shallow water embayments where light attenuation is high and the effects of upwelling events are limited (Wilson 2007). Examples of true reefs within the Gulf of Oman have been recorded at Barr Al Hikman (a large monospecific *Montipora* reef), Ras Sawadi, and Goat Island in Musandum (Sheppard and Salm 1988; Sheppard and Sheppard 1991; Salm 1992; Wilson 2007). However, coral communities of one form or another are widespread throughout the region typically comprising mixed hard and soft coral assemblages in surface waters at depths above 18 m. Hard coral cover is typically low in most areas ranging from 5–30% in mixed assemblages. Monospecific stands of *Acropora*

O. Taylor
Five Oceans Environmental Services LLC, Muscat, Oman
e-mail: oli.taylor@fiveoceansenvironmental.com

Y. Charabi (ed.), *Indian Ocean Tropical Cyclones and Climate Change*,
DOI 10.1007/978-90-481-3109-9_33,

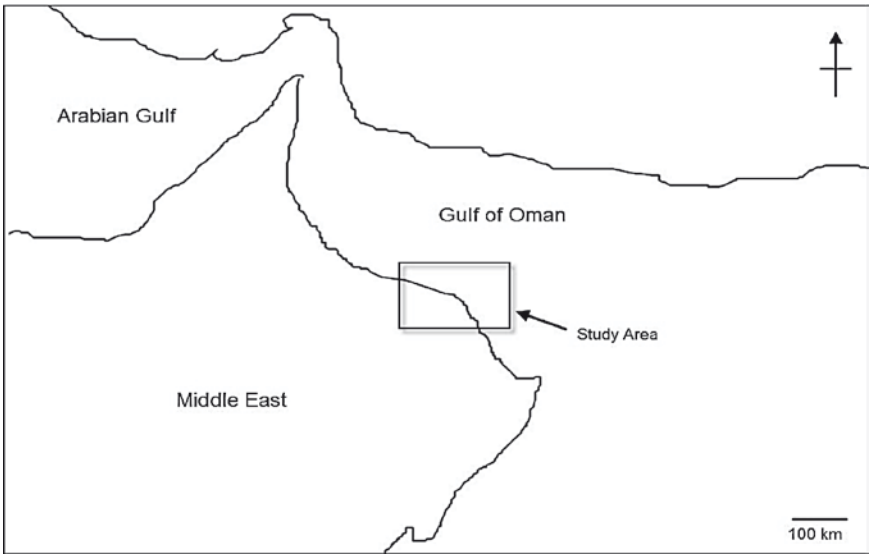

Fig. 1 The location of the Gulf of Oman indicating the boundary of the current study

and *Pocillopora*, however, can exceed 90% of the total coral cover over areas of 50 m^2 or more (personal observation).

The life-history traits and physical structuring of coral communities within this marginal environment may be strongly affected by rare catastrophic events and may exhibit resilience and recovery unlike more widespread and well-studied coral communities throughout the Indo-Pacific and the wider Caribbean. The information presented here forms the basis of a Ph.D. study.

Data

Coral communities within the Gulf of Oman have only been subjected to limited study. However, significant effort has been applied within the wider Muscat capital area, extending to the Islands at Ras Sawadi and particularly the Daymanyiat Islands. Between 2005 and the occurrence of the cyclone Gonu in June 2007, data were collected at 141 known islands and coastal locations utilizing a variety of assessment techniques (e.g., manta tow, area-based visual appraisal, line intercept transects, and quadrats). Since June 2007, coral communities have been resurveyed at 101 locations of the same locations, providing useful data for determining the immediate impact of the cyclone on a wide range of coral habitats, as well as for monitoring subsequent recovery.

Cyclone Gonu (June 2007) was the strongest cyclone on record in the Arabian Sea, and a tie for the strongest on record for the northern Indian Ocean. Cyclone

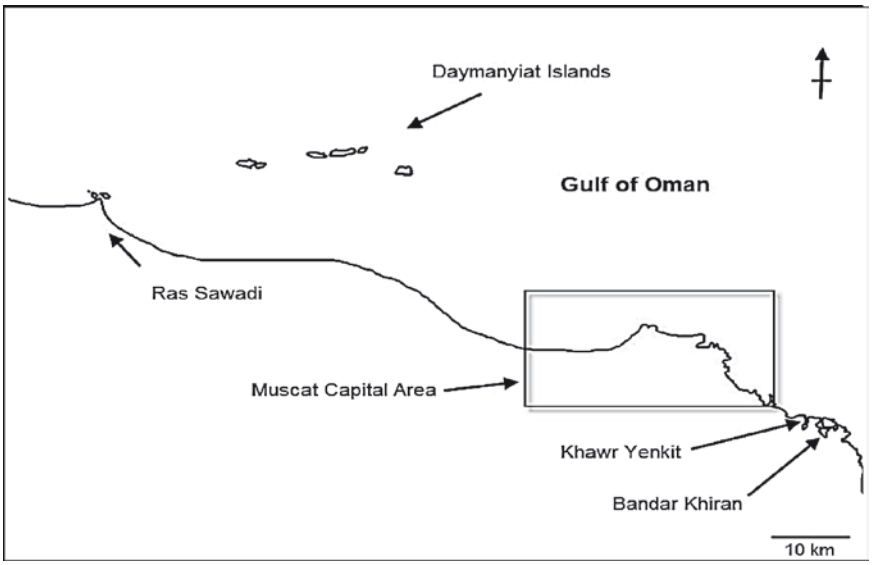

Fig. 2 Detailed map of the study area including the extent of the Muscat capital area and other areas supporting coral communities

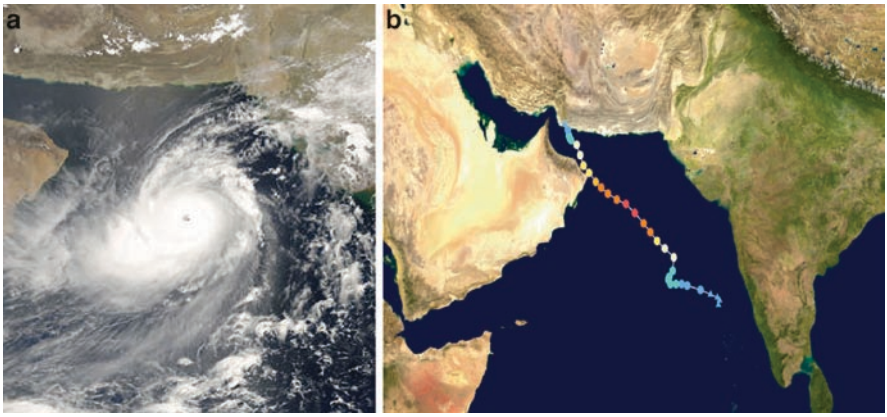

Fig. 3 Images depicting cyclone Gonu (June 2007). Image (A) depicts the eye of the storm as formed over the Gulf of Oman. Image B indicates the storm track from off the coast of India traveling to Iran

Gonu began to form in the eastern Arabian Sea on 1 June 2007, rapidly intensified to peak wind speeds of 240 km/h on 3 June (information courtesy of the Indian Meteorological Department), which declined to 150 km/h prior to landfall on 5 June on the eastern most tip of Oman, making it the strongest tropical cyclone to hit the Arabian Peninsula. The storm track before dissipating over Iran is shown in Fig. 3.

Results and Discussion

The cyclone resulted in significant destruction of coral communities primarily associated with the intense wave action and storm water runoff; the extent of the impacts was largely dependent on the location, coral morphology, depth, and exposure. Shallow water sites above 8 m bore the brunt of the high-energy waves, and suffered very significant coral mortality resulting from abrasive and attritional forces. Exposed (and even semi-exposed) landward and island sites have shown reductions in coral cover of 30–99%, particularly in areas dominated by monospecific stands of *Pocillopora damicornis* and mixed *Acropora* (Fig. 4). These same stands showed very large declines in structural heterogeneity (3-D complexity). More resistant and resilient growth forms (e.g., those of *Porites*, *Symphyllia*, Favites, and *Platygyra*) were also affected in the most exposed locations, physically moved by wave action, or suffered large declines in live coral cover due to "sand blasting".

In intermediate areas, the nature of the impact was largely predictable with fast-growing branching and tabular species suffering considerably higher mortality than boulder corals (e.g., *Platgyra*, *Favites*, and small *Poritids*). Over 1 year, the coral communities have now entered a period of recovery, which shows significant variation according to biotic and abiotic characteristics encountered at particular locations. Semi-exposed and sheltered sites exhibit the most obvious regrowth of existing coral communities with branching *Acropora* and *Pocillopora*, which are

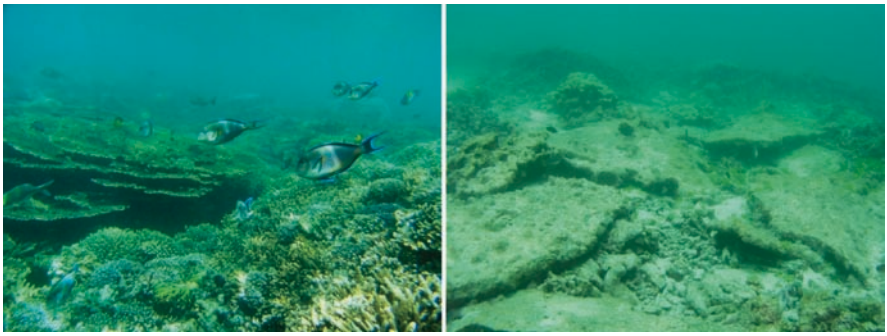

Fig. 4 Two photographs depicting the same *Acropora*-dominated coral community at the Daymanyiat Islands in February 2007 (left) and again in March 2008 (right) following the cyclone. Coral mortality exceeded 80%. In the months since considerable new recruitment has been observed directly onto dead coral rubble. More sheltered coral communities suffered less direct physical damage (i.e., those in the entrances to khawrs, within small semisheltered embayments, or sheltered island locations); however, freshwater lens effects and sedimentation associated with wadi discharges also resulted in significant mortality. The former affected at least shallow water coral communities within Bandar Khiran and Khawr Yenkit, where mortality rates of up to 100% have been recorded above 1.5 m depth, with mortality unrelated to genera. Sedimentation effects have been less well-documented, but are thought to have less severe impacts based on observations to date

very evident particularly in island locations. This regrowth is not, however, obvious in most mainland locations where oceanographic conditions are thought to be less suitable and standing stock (sources of fragments) are generally low. More exposed locations currently show less signs of recovery, and in a handful of instances, no sign, although recent recruitment is apparent in a number of areas and from a number of genera (particularly in those areas with a good proportion of communities still intact, inferring the importance of localized recruitment).

The outlook for long-term recovery for these dynamic communities is largely positive even after only 1 year. Recovery of habitats to their approximate condition prior to the cyclone may take decades. It is important to note, however, the dynamic nature of reef systems. Storms, cyclones, and the history of these events are important determinants of the coral community status and structure (Treml et al. 1997). To all intents and purposes, the coral communities surveyed over the past few years have most likely been in a state of "recovery" since the last major structuring event, interspersed with factors operating over less-punctuated time frames (e.g., competition, predation, as well as other periodic climate-related events), which in combination drive these dynamic coral ecosystems.

References

Salm RV (1992) Coral reefs of the Sultanate of Oman. Atoll Res Bull 380:1–85

Sheppard CRC, Salm RV (1988) Reef and coral communities of Oman, with a description of a new species (Order Scleractinia, genus *Acanthastrea*). J Natural History 22:263–279

Sheppard CRC, Sheppard, ALS (1991) Corals and Coral Communities of Arabia. Fauna of Saudi Arabia, 12(170):190–120

Treml E, Colgan M, Keevican M (1997) Hurricane disturbance and coral reef development: A geographic information system (GIS) analysis of 501 years of hurricane data from the Lesser Antilles. Proceedings of the 8th International Coral Reef Symposium 1:54 –546

Wilson SC (2007) Ecology of coral communities in a marginal environment: Southern Arabia. PhD Thesis. University of Warwick, Department of Biological Sciences.

Cyclone Nargis Storm Surge Flooding in Myanmar's Ayeyarwady River Delta

Hermann M. Fritz, Chris Blount, Swe Thwin, Moe Kyaw Thu, and Nyein Chan

Keywords Coastal erosion

Introduction

Tropical cyclones develop in the north Indian Ocean from 55 to 90°E and 5 to 20°N (Webster et al. 2005). The Joint Typhoon Warning Center (JTWC) maintains a "best-track" database for cyclones in the Indian Ocean in the time span of 1945–2007. The Bay of Bengal tropical cyclone center tracks in the database are shown in Fig. 1. Only track information is available prior to 1975. From 1975 to 1979, maximum wind velocity is not available for all cyclones or is only available for partial cyclone tracks. Since 1979, maximum wind velocity is available for all storms.

There are two cyclone seasons in the north Indian Ocean, namely, the pre-monsoon (May) and post-monsoon (October and November). Some cyclones form in the transitional months of June and September. More cyclones form in the Bay of Bengal than in the Arabian Sea based on a respective frequency ratio of approximately 4:1 (Singh et al. 2001). Intense cyclones have been extremely rare over the Arabian Sea with the exception of Gonu in 2007 (Blount et al. 2009; Fritz et al. 2009).

H.M. Fritz (✉) and C. Blount
Associate Professor, Civil and Environmental Engineering, Georgia Institute of Technology, Savannah, GA, 31407, USA
e-mail: fritz@gatech.edu

S. Thwin
Chairman, Myanmar Coastal Conservation Society, Yangon, Union of Myanmar

S. Thwin, M.K. Thu, and N. Chan
Mingalar Myanmar NGO, Yangon, Union of Myanmar
e-mail: chair.mccs@gmail.com

Y. Charabi (ed.), *Indian Ocean Tropical Cyclones and Climate Change*,
DOI 10.1007/978-90-481-3109-9_34,

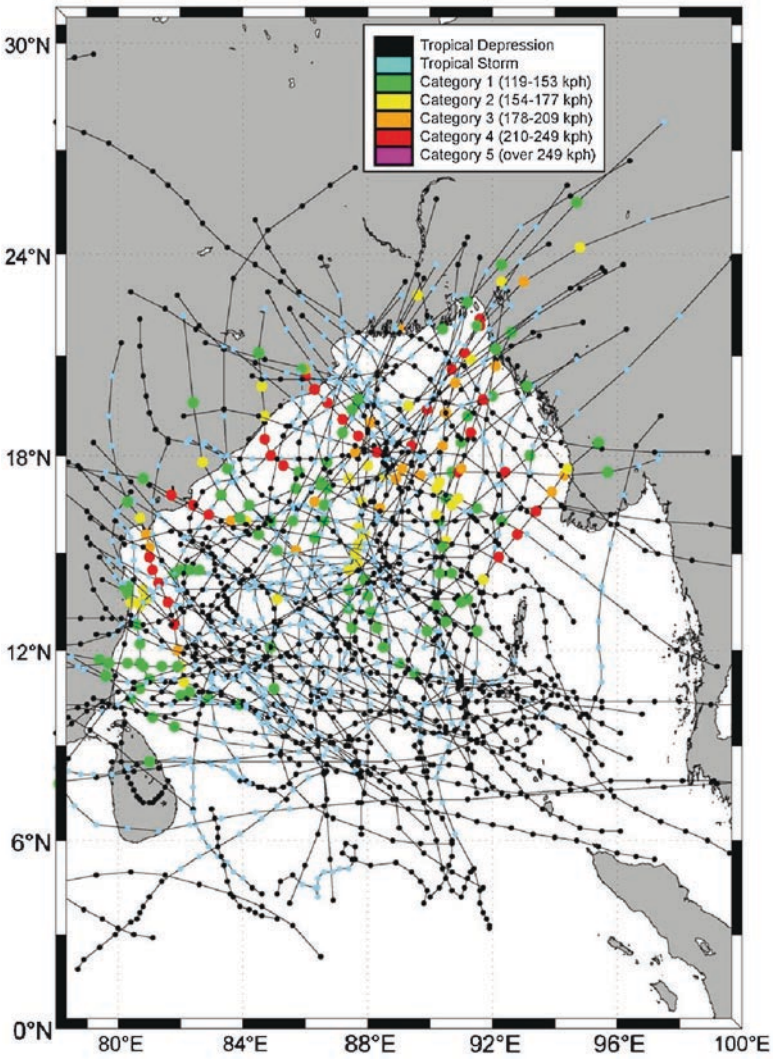

Fig. 1 Storm track data for the Bay of Bengal from 1945 to 2007 according to Joint Typhoon Warning Center (JTWC). Note the 2006 category 4 cyclone Mala track impacting Myanmar

Similarly, there is no tropical cyclone track in the JTWC database making a direct landfall at the Ayeyarwady River delta in the Union of Myanmar. In 2006, category 4 cyclone Mala impacted the Gwa coastline roughly 150 km north of the Nargis track.

Cyclone Nargis

On 28 April, Nargis was upgraded to cyclone status (category 1, SSHS) by the JTWC (Joint Typhoon Warning Center) while it was nearly stationary and located near the center of the Bay of Bengal (Fig. 1). While initially forecasted to follow a common track to Bangladesh, on 1 May Nargis rapidly intensified and took a rare nearly eastern track. The tropical cyclone developed sustained winds over 210 km/h with gusts up to 260 km/h, hours prior to landfall in Myanmar at untypically low latitude near 16°N on 2 May as a category 4 storm on the Saffir–Simpson Hurricane Scale (SSHS). Proximity to the Andaman Sea prevented rapid weakening as it traveled northeast and reached Yangon approximately 12 h later as a category 1 storm. Official death toll estimates exceed 146,000 fatalities making it the seventh deadliest cyclone ever recorded worldwide. Damage estimates at over $10 billion made it the most damaging cyclone ever recorded in the Indian Ocean. Controversially, Myanmar's coast was impacted in 2006 by a slightly stronger tropical cyclone Mala (category 4) causing only 22 deaths after a well-executed evacuation effort. Similarly, the 2004 Indian Ocean tsunami impacted coastal villages in the Ayeyarwady delta resulting in 71 fatalities. Why did cyclone Nargis, 2 years later, become a humanitarian disaster?

Post-Cyclone Field Observations

The widespread lack and failure of tide gauges in Myanmar called upon a field survey crew to collect high water marks based on established protocol (Fritz et al. 2007). Finally, after 3 months of diplomatic activities unconditional escorted access to the hardest hit Ayeyarwady River delta was granted to the first independent storm surge reconnaissance team from 9 to 23 August 2008. The team surveyed coastal and inland villages encompassing the Bogale and Ayeyarwady River mouths. The boat and helicopter survey spanned more than 150 km parallel to the cyclone track between Pyapon and Pyinkhayan encompassing the 20 hardest hit settlements such as Pyinsalu. The team measured coastal high water marks (the elevation of the water level), overland flow depth (depth of the water above the ground), inundation distance (the straight-line distance between the coastline and the maximum extent of saltwater intrusion), and areas of inundation. Further coastal erosion and deposition were documented. Ephemeral infrastructure damage was recorded at various scales. The elevations of water marks on buildings, scars on trees, and rafted debris were measured as indicators of the maximum water surface elevation composed of storm surge and superimposed storm waves. High water marks were photographed and located using GPS. Transects from the beach to the high water marks were recorded with a laser range finder.

Figure 2 shows the measured Nargis high water marks and three superimposed 2004 Indian Ocean tsunami run-up points surveyed simultaneously as well as tsunami run-up surveyed by Satake et al. 2006. The measured high water marks,

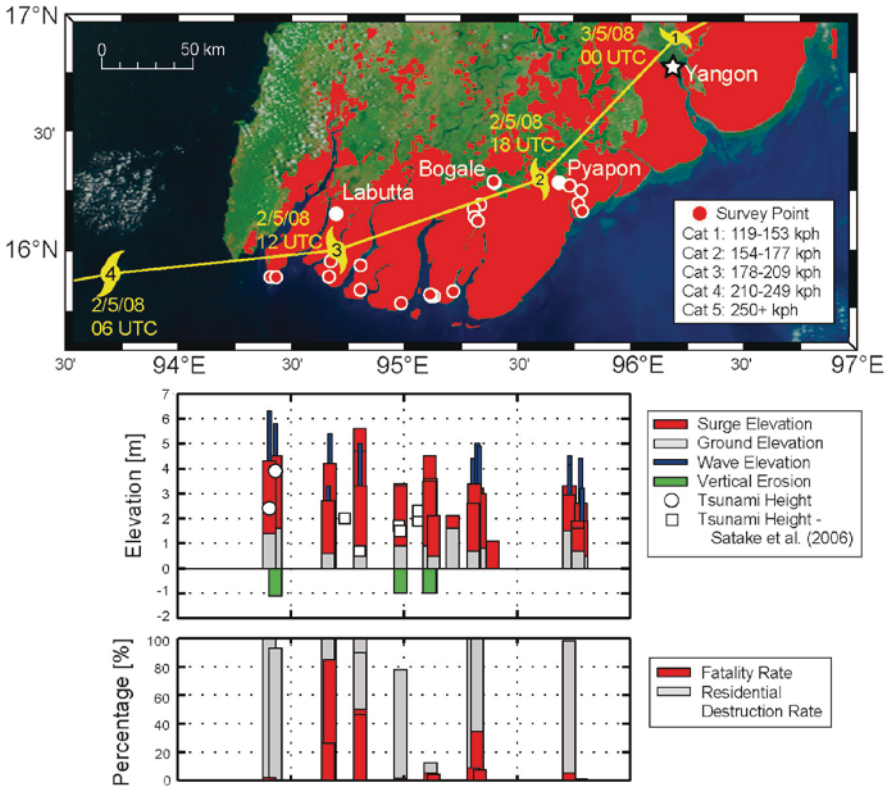

Fig. 2 Field observations superimposed on NASA MODIS rapid response imagery; measured storm surge and storm wave heights in comparison to the 2004 Indian Ocean tsunami; recorded mortality and residential destruction rates

overland flow depths, and inundation distances surpassed the 2004 Indian Ocean tsunami run-up at every corresponding location. The storm surge peaked in the landfall area exceeding 5 m. Measurements of storm surge elevations and overland flow depths at Pyinsalu based on scars on trees and rafted debris are shown in Fig. 3. The Nargis storm surge compared to Hurricane Katrina's surge in Louisiana's Mississippi delta was only half of the 10 m measured along Mississippi Gulf coast (Fritz et al. 2008). Inundation distances reached beyond 50 km inland. Storm waves more than 2 m high were superimposed on the storm surge level in most areas. More than 1 m vertical erosion and 100 m land loss were measured at various coastal locations from the landfall area at Kyauk Ka Latt to the Ayeyarwady river mouth at Aung Hlaing and Aya (Fig. 4). Drinking water wells were flooded with saltwater, scoured, and left stranded in the surf zone at the coastal villages of Aung Hlaing and Aya located to the east and west of the Ayeyarwady river mouth, respectively (Fig. 4c). At Aya, three rows of houses and their land eroded away leaving the centuries old golden Buddhist Stupa, originally built on dry land, piercing the water surface 150 m offshore (Fig. 4d).

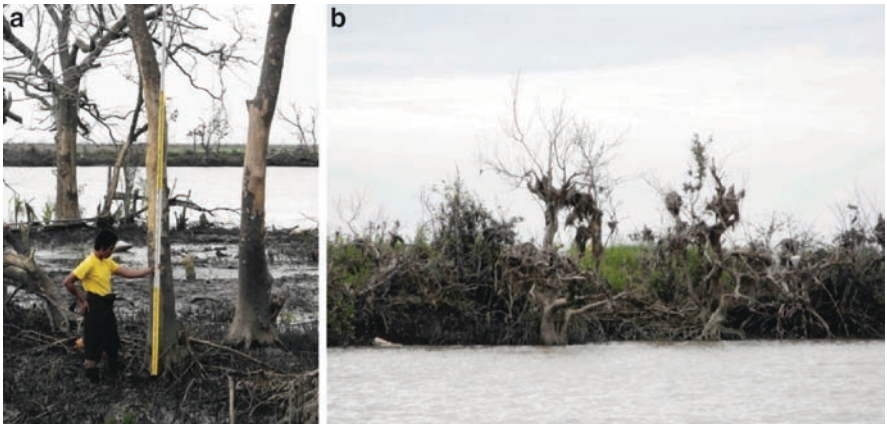

Fig. 3 High water mark survey at Pyinsalu: (**a**) bark damage on trees; (**b**) rafted debris in trees

Fig. 4 Coastal erosion: (**a**) survey of vertical erosion on palm tree roots at Aung Hlaing; (**b**) beach erosion at Kyauk Ka Latt; (**c**) drinking water wells scoured in surf zone at Aya; (**d**) Golden Buddhist Stupa built on land piercing the water surface offshore highlighting 150 m land loss

Coastal Vulnerability and Land Use

Catastrophic peak fatality rates exceeded 80% in the hardest hit villages with the majority being children and women. Accurate fatality rates were difficult to estimate due to many displaced or relocated survivors. Fortunately, in the initial landfall area, fatality rates were extremely low provided the nearby high ground with well-built structures, which enabled a successful spontaneous self-evacuation. The fatality rates, high water marks, and inundation distances significantly exceeded 2004 Indian Ocean tsunami values at every corresponding location (Satake et al. 2006). Tropical cyclones remain the most significant coastal hazard in the Bay of Bengal given the discrepancy in cyclone and tsunami frequencies in the Bay of Bengal (Emanuel 2005; Webster et al. 2005; Okal and Synolakis 2008; Jankaew et al. 2008; Monecke et al. 2008). This is of key importance to focus properly on the efforts of coastal protection and planning, as well as education, warning, and evacuation. Unfortunately, most mangroves, which can provide wave attenuation, had been cut and there was secondary growth with little primary growth found within 30 km of the coast, even in forestry reserves (Fig. 5). Rice paddies are the main land use and the primary reason for the deforestation besides charcoal.

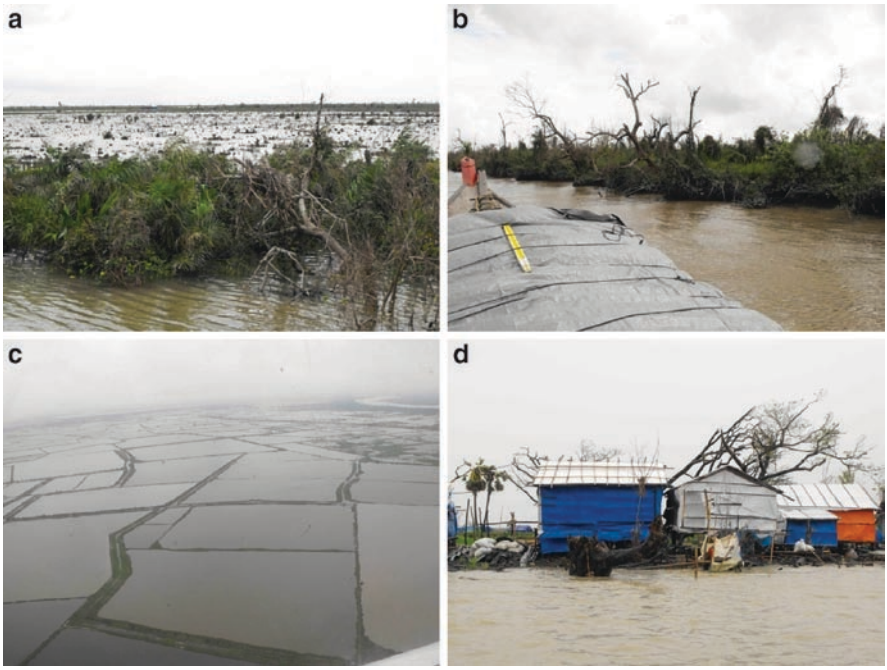

Fig. 5 Land use: (**a**) deforestation of mangroves for use as charcoal and rice paddies; (**b**) secondary growth mangroves with cyclone damage in a forestry reserve; (**c**) rice paddies as seen from the helicopter; and (**d**) residential reconstruction and coastal vulnerability

Eyewitnesses were interviewed to document the time history of the event, survival strategies, cyclone awareness, and evacuation. Survivors reported initial terrain flooding in the afternoon, a peak storm tide around midnight (1800 UTC), and dry land surfacing early next morning. Residents were surprised by the storm surge resulting in a deadly struggle with capsizing small boats and canoes. Amazingly the "floaters," who literally tied themselves to a tree and bounced in the storm waves all night, accounted for the majority of the survivors. All interviewed eyewitnesses including elders ignored warnings due to a total lack of cyclone awareness and evacuation plans, absence of high ground or shelters, and no indigenous knowledge of comparable prior storm surge flooding in the Ayeyarwady River delta. In sharp contrast, the residents of the Gwa coastline in western Myanmar who are frequently struck by cyclones such as Mala are aware of cyclone hazards and have evacuation plans. The storm surge of cyclone Nargis when compared to Hurricane Katrina's surge in Louisiana's Mississippi delta is roughly 100 times the fatality rates. At the end of the initial relief operations, survivors were left drinking from rice paddies with contaminated wells and no source of safe drinking water besides rain water.

Numerical Storm Surge Modeling

Practical limits reduce the spatial resolution of the high water mark surveys and little temporal information is available. Currently, a numerical model is under development for the Bay of Bengal and the Ayeyarwady delta to compare computed values against the field measurements. A preliminary mesh consisting of 231,772 elements and 127,617 nodes (Fig. 6) has been created for use with ADCIRC (Luettich et al. 1992), the most advanced storm surge model currently available. The mesh size ranges from approximately 300 m to 86 km. The storm surge model will be coupled with a wave model to provide a high-resolution estimate of the Cyclone Nargis water elevations which will be benchmarked against measurements. The resulting model can then be used to estimate the coastal vulnerability due to storm surge and waves and provide forecasts of approaching storms.

Conclusions

A high water mark survey was performed along 150 km of Myannar coastline in the aftermath of Cyclone Nargis. High water marks peaked with more than 5 m at Pyinsalu. The inundation penetrated 50 km inland inhibiting last minute evacuations due to the lack of high ground at most locations. Unfortunately, the widely deforested, low lying, and densely populated Ayeyarwady delta with its poor housing construction remains extremely vulnerable to future storm surge flooding or potential sea-level rise (Fig.5d). Coastal protection in the Bay of Bengal must be approached from a multihazard perspective given the combined tropical cyclone

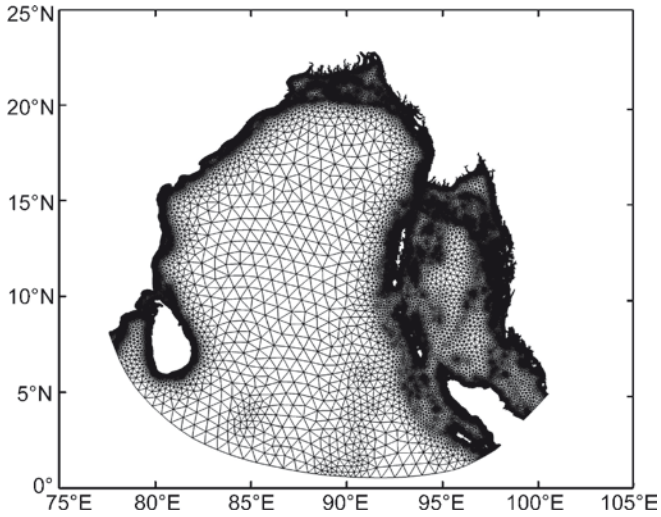

Fig. 6 Finite element mesh of the Bay of Bengal consisting of 231,772 elements and 127.617 nodes

and tsunami hazards. Community-based education and awareness programs are particularly essential to help save lives in locales at risk from multiple coastal hazards.

Acknowledgments The disaster zone access and survey was enabled by Dr. Phone Win (Mingalar Myanmar), Yuza Maw Htoon (Myanmar Development Foundation), Dr. Jeremy Broadhead (United Nations Food and Agricultural Organization, FAO), Brigadier General Aye Myint Kyu (National Committee for Environmental Affairs), and Director General U Soe Kyi (Ministry of Social Welfare, Relief and Resettlement). The World Food Program (WFP) for providing a helicopter exit flight.

References

Blount C, Fritz HM, Al-Harthy AHM (2010) Coastal vulnerability assessment based on historic tropical cyclones in the Arabian Sea. Proceedings of the First International Conference on Indian Ocean Tropical Cyclones and Climatic Change (in this volume)

Emanuel K (2005) Increasing destructiveness of tropical cyclones over the past 30 years. Nature 436:686–688

Fritz HM, Blount C, Sokoloski R, Singleton J, Fuggle A, McAdoo BG, Moore A, Grass C, Tate B (2007) Hurricane Katrina storm surge distribution and field observations on the Mississippi barrier islands, *Estuarine*. Coastal Shelf Sci 74(1–2):12–20. doi:10.1016/j.ecss.2007.03.015

Fritz HM, Blount C, Sokoloski R, Singleton J, Fuggle A, McAdoo BG, Moore A, Grass C, Tate B (2008) Hurricane Katrina storm surge reconnaissance. J Geotech Geoenviron Eng, ASCE 134(5):644–656. doi:doi:10.1061/(ASCE)1090-0241(2008)134:5(644)

Fritz HM, Blount C, Albusaidi FB, and Al-Harthy AHM (2010) Cyclone Gonu storm surge in the Gulf of Oman. Proceedings of the First International Conference on Indian Ocean Tropical Cyclones and Climatic Change (in this volume)

Jankaew K, Atwater BF, Sawai Y, Choowong M, Charoentitirat T, Martin ME, Prendergast A (2008) Medieval forewarning of the 2004 Indian Ocean tsunami in Thailand. Nature 455:1228–1231

Luettich RA Jr, Westerink JJ, Scheffner NW (1992) ADCIRC: An Advanced Three-dimensional Circulation Model for Shelves, Coasts and Estuaries, Report 1: Theory and Methodology of ADCIRC-2DDI and ADCIRC-3DL, Dredging Research Program Technical Report DRP-92–6. USACE WES, Vicksburg, MS 137p

Monecke K, Finger W, Klarer D, Kongko W, McAdoo BG, Moore AL, Sudrajat SU (2008) 1,000-year sediment record of tsunami recurrence in northern Sumatra. Nature 455:1232–1234

Okal EA, Synolakis CE (2008) Far-field tsunami hazard from mega-thrust earthquakes in the Indian Ocean. Geophys J Int 172:995–1015

Satake K, Aung TT, Sawai Y, Okamura Y, Win KS, Swe W, Swe C, Swe TL, Tun ST, Soe MM, Oo TZ, Zaw SH (2006) Tsunami heights and damage along the Myanmar coast from the December 2004 Sumatra–Andaman earthquake. Earth Planets Space 58:243–252

Singh OP, Khan TMA, Rahman MS (2001) Has the frequency of intense tropical cyclones increased in the north Indian Ocean? Current Sci 80(4):575–580

Webster PJ, Holland GJ, Curry JA, Chang HR (2005) Changes in tropical cyclone number, duration, and intensity in a warming environment. Science 309(5742):1844–1846

The First Ever Super Cyclonic Storm "GONU" over the Arabian Sea During 1–7 June 2007: A Case Study

Ajit Tyagi, M. Mohapatra, B.K. Bandyopadhyay, Charan Singh, and Naresh Kumar

Keywords Cyclonic storm GONU

Introduction

Four cyclonic storms including a super cyclonic storm (Gonu) formed over the north Indian Ocean during 2007. The first ever super cyclonic storm Gonu developed over the Arabian Sea as per the history recorded by IMD since 1877. It made its first landfall over Oman as a very severe cyclonic storm, and then emerged into the Gulf of Oman and made a second landfall over Iran as a cyclonic storm. Heavy to very heavy rainfall occurred over the eastern coast of Oman, causing flood and heavy damage. Gale winds with a speed of 100 km/h were recorded at Muscat at the time of landfall. About 50 persons died and estimated damage to property was about $4.2 billion in Oman. The number of human deaths was 28 and loss of property was $215 million over Iran. The special features of "Gonu" are as follows.

- It was the first ever super cyclonic storm developed over the Arabian Sea as per recorded history of IMD (1979, 1996, 2008)
- The super cyclonic storm, GONU made two landfalls over Oman and Iran. This was the second landfalling cyclonic storm over Iran after 4 June 1898 (IMD 1979, 2008).

Considering the formation of such an intense system over the Arabian Sea, a study has been undertaken to analyze the long-term trends in the genesis of intense systems. Further, the possible causes leading to genesis, intensification, and movement

A. Tyagi (✉), M. Mohapatra, B.K. Bandyopadhyay, C. Singh, and N. Kumar
India Meteorological Department, Mausam Bhavan, Lodi Road, New Delhi, 110003
e-mail: ajit.tyagi@gmail.com

Y. Charabi (ed.), *Indian Ocean Tropical Cyclones and Climate Change*,
DOI 10.1007/978-90-481-3109-9_35,

have been analyzed along with the characteristics of double landfall. The weather realized, the damage due to the system, and the causes thereof are analyzed and presented. The performance of the forecasts issued by Regional Specialized Meteorological Centre (RSMC), New Delhi, and Numerical Weather Prediction (NWP) model predictions in association with "Gonu" have been evaluated and presented. The limitations of early warning system vis-à-vis "GONU" and future scopes are also discussed.

Data and Methodology

To analyze the various characteristics of Gonu, the best track data of RSMC, New Delhi, (RSMC, New Delhi 2008) have been considered. The system was tracked by INSAT and hence all the INSAT observations and derived satellite products have been considered to analyze the characteristics of the system. In addition, the synoptic analyses and NWP model analyses available from different centers have been considered. To study the climate change aspect, the data on frequency, intensity, and the track of the cyclone over the Arabian Sea have been collected from cyclone e-Atlas developed by IMD (2008). For the purpose of analysis, depression and deep depression have been considered as a single category. Similarly, severe cyclonic storm, very severe cyclonic storm, and super cyclonic storm have been considered as a single category. Hence, the frequencies of cyclonic disturbances have been analyzed in three categories: (1) depression/deep depression (D), (2) cyclonic storm (C), and (3) severe cyclonic storm and above (S). The annual and decadal average, coefficient of variation (CV), and linear trend coefficients of the frequencies of the above categories of cyclonic disturbances have been calculated and analyzed. Also, the annual average and linear trend coefficients of the total frequencies of cyclonic storms (C + S) and total cyclonic disturbances (D + C + S) have been analyzed. The results and discussions are presented in the Section "Results and Discussion." The broad conclusions along with the limitations and future scope of the study are presented in the Section "Conclusions."

Results and Discussion

The genesis, intensification, movement, and landfall of the cyclone are analyzed and discussed in the Section "Genesis, Intensification, and Movement of Cyclone, Gonu." The performance of forecasts issued by RSMC, New Delhi, and the performance of NWP models on the track and intensity prediction of *Gonu* are presented and analyzed in the Section "Performance of NWP Models." The trends and periodicities in the frequency of cyclones crossing Oman coast are presented in the Section "Trends in Frequencies of Cyclonic Disturbances."

Genesis, Intensification, and Movement of Cyclone, Gonu

A low pressure area developed over the east-central Arabian Sea in association with the prevailing surge in the onset phase of monsoon over the Indian region. During this period, there was favorable upper-level environment and warm sea with sea surface temperature of the order of 27–29°C over the Arabian Sea. As a result, the system concentrated into a depression and lay centered at 1800 UTC of 1 June over east-central Arabian Sea near latitude 15.0°N and longitude 68.5°E (Figs. 1 and 2). Initially, the system moved in a westerly direction and concentrated into a deep depression at 0300 UTC of 2 June and into a cyclonic storm *Gonu* at 0900 UTC and lay centered near latitude 15.0°N and longitude 67.0°E. Moving in a northwesterly direction, it further intensified into a severe cyclonic storm near 0000 UTC of 3 June and lay centered at 15.5°N and longitude 66.5°. The eye of the system was first visible at 0600 UTC of 4 June according to INSAT Kalpana-1 imagery. At this time, the ridge in upper air was located at about 16.0°N over the storm region.

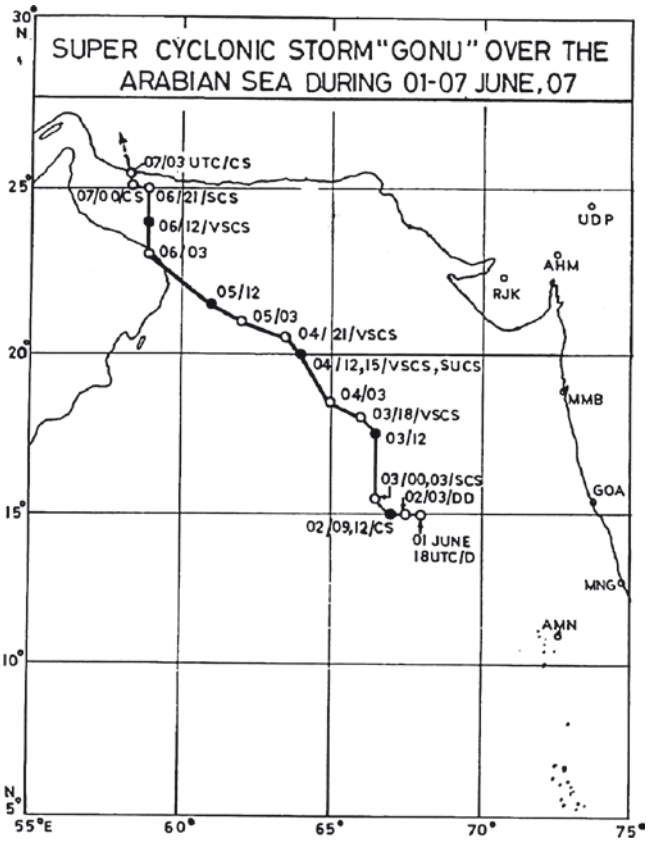

Fig. 1 Track of super cyclonic storm "GONU"

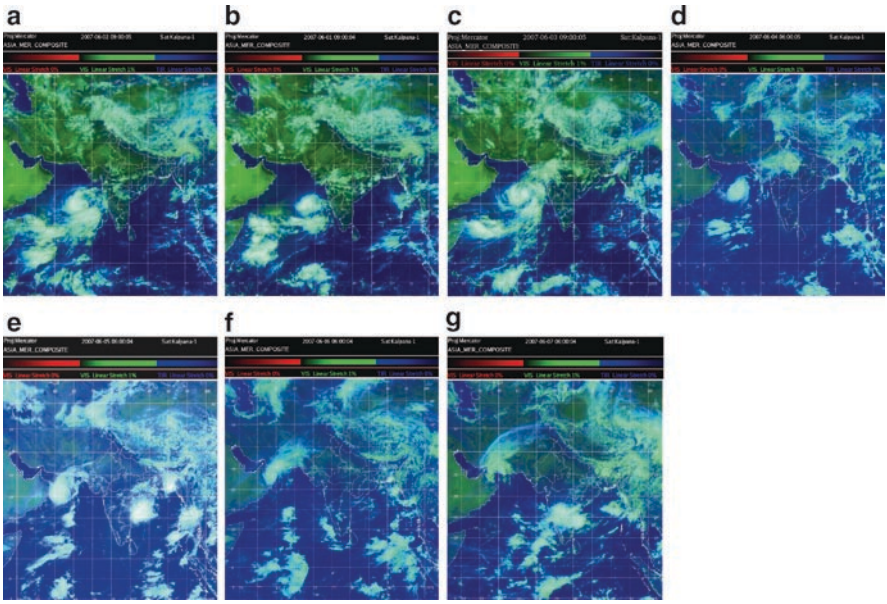

Fig. 2 Satellite Kalpana-1imagery at (**a**) 0900 UTC of 1 June 2007 showing development of two convective cloud clusters, (**b**) 0900 UTC of 2 June showing organization of convective cloud clusters over the same area, leading to the genesis of cyclonic storm, (**c**) 0900 UTC of 3 June showing well-organized convection with band features in association with severe cyclonic storm, (**d**) 0600 UTC of 4 June showing well-organized CDO in association with the very severe cyclonic storm, (**e**) 0600 UTC of 5 June showing "eye" of the system with the intensity of T 6.0, (**f**) 0600 UTC of 6 June showing the system entering into the Gulf of Oman and spiral clouds oriented toward northeast of the system, and (**g**) 0600 UTC of 7 June showing rapid dissipation over Iran and the adjoining Gulf of Oman after the landfall over Iran coast

Moving in a northwesterly direction it again intensified into a very severe cyclonic storm at 1800 UTC of 3 June. The eye was raged (Kalsi, 2002 and IMD 2003,) within the central dense overcast (CDO) cloud. The system further intensified into a super cyclonic storm and lay centered at 1500 UTC of 4 June near latitude 20.0°N and longitude 64.0°E, with the lowest estimated central pressure 920 hPa and pressure drop of 80 hPa. The maximum wind was estimated to be 127 knots during 1500–1800 UTC of 4 June 2007. The detailed classification of the low pressure system into depression and different stages of cyclones are discussed in IMD (2003).

The system maintained super cyclonic storm intensity for a short period and weakened into a very severe cyclonic storm at 2100 UTC of 4 June due to the entrainment of dry and cold air and colder seawater over the region. Moving in a west-northwesterly direction, it crossed Oman coast near 22.5°N as a very severe cyclonic storm between 0200 and 0300 UTC of 6 June. The system emerged then into the Gulf of Oman, moved in a northerly direction, and made second landfall over Iran coast near longitude 58.5°E between 0300 and 0400 UTC of 7 June 2007

as a cyclonic storm. Moving in the same direction, it weakened gradually and it was seen as a well-marked low pressure area over Iran and the neighborhood on 8 June 2007. Throughout its life span, the upper air ridge line remained to the north of the system (not shown). As the system moved northward, simultaneously the ridge line also shifted toward the north. The track of the system along with a few Kalpana-1 cloud imageries of the system showing genesis, intensification, and decay of the system are shown in Fig. 3 (a–g). The sustained maximum wind speed at the time of landfall over Oman and Iran was estimated to be 77 and 45 knots, respectively.

METEOSAT-7 InfraRed (IR) imagery showed very cold brightness temperature values (−80º to −88º C) in the eyewall region during its maximum intensity stage. As observed from Figs. 3 and 4, the dynamical parameters like lower-level convergence, relative vorticity, vertical wind shear, and upper-level divergence were favorable for intensification of the system. Further, the SST, specific humidity at mid-tropospheric level, (not shown) was favorable (Gray 1992). The water-vapour-derived wind vector (WVWV) based on METEOSAT satellite over the data-sparse Arabian Sea region was very helpful in estimating the location of the upper tropospheric ridge, anti-cyclonic circulation, and hence to find out

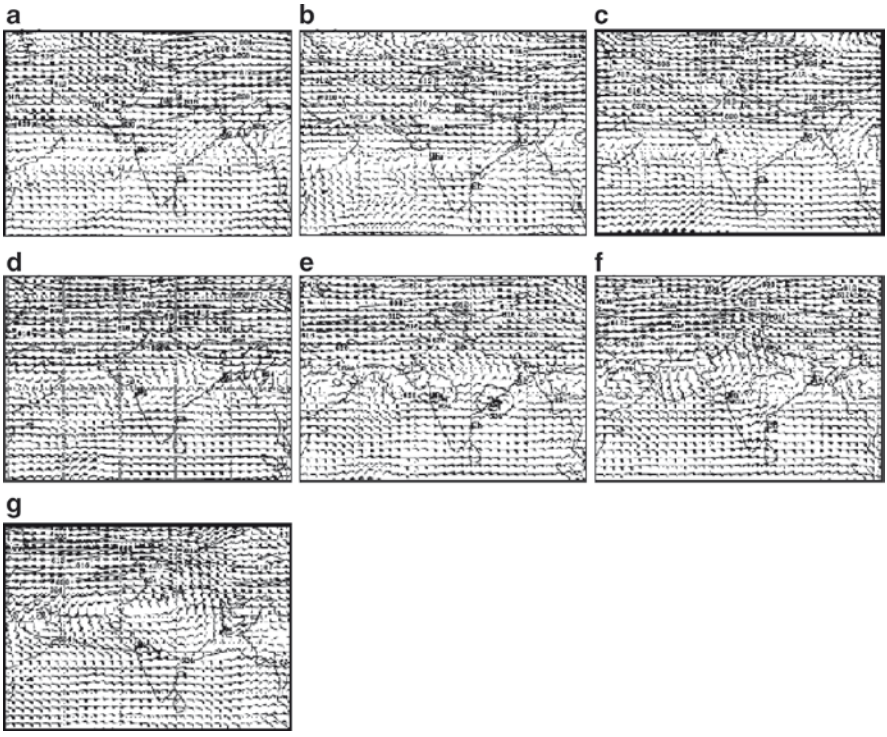

Fig. 3 (**a**–**g**). 200 hPa analysis at 0000 UTC of 1–7 June 2007 according to MM5 model analysis of IMD

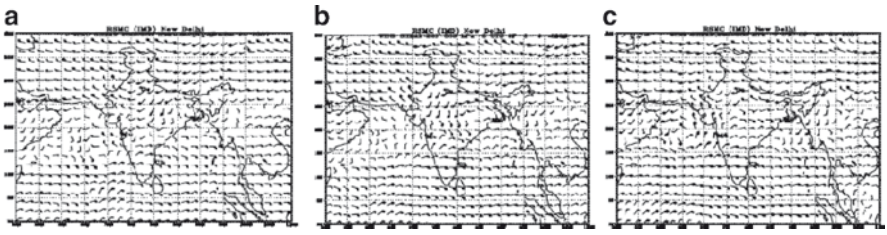

Fig. 4 Vertical wind shear (kts) of horizontal winds (knots) at 00 UTC of (**a**) 2, (**b**) 3, and (**c**) 4 June 2007 according to Limited Area Model (LAM) analysis of IMD

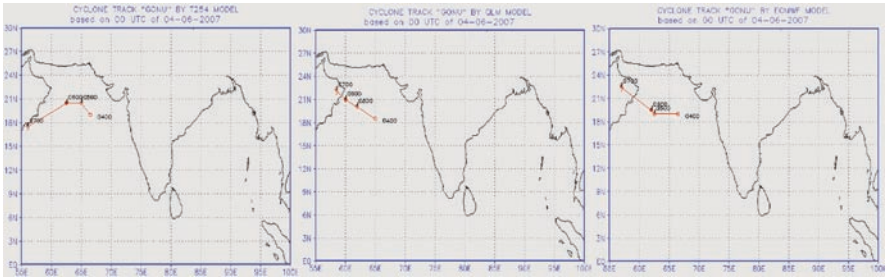

Fig. 5 NWP models predicted tracks of Arabian Sea super cyclone GONU of June 2007

the role of upper tropospheric stearing current and predict the movement of the system in short range (not shown).

Performance of NWP Models

Figure 5 presents the forecast tracks of the system based on initial condition of 00 UTC of 4 June by operational NWP models**.** In this case, the NCMRWF (T254) model forecast track showed southwesterly movement when the system moved north-northwestwards. QLM and ECMWF model could capture the northwesterly movement of the system relatively better than T-254. However, the 48 h landfall forecast errors for first landfall over Oman were very large for QLM and ECMWF models.

No model could predict the intensity of the system. Rama Rao et al. (2007) have also shown that the NWP models at present are not capable of capturing the intensity of the system.

Trends in Frequencies of Cyclonic Disturbances

The tracks of the cyclones which landfall over the Arabian-African coast adjacent to the Arabian Sea are shown in Fig. 6. Only two cyclonic storms have crossed Iran in the recorded history of IMD including one each in 1898 and 2007. Both the cyclones have first landfall over Oman. As the average annual frequencies of cyclonic disturbances crossing Oman coast are very less, only the results of decadal frequencies are presented and discussed. Twenty cyclonic disturbances (depression and above) including 13 systems with cyclonic storm and higher intensity have crossed Oman coast during 1891–2007 (Table 1). Hence, on an average, one cyclonic storm has crossed Oman coast per decade (Table 1) with the coefficient of variation of 83%. It suggests that the landfalling cyclones are very rare for Oman coast and they exhibit large interannual and interdecadal variabilities.

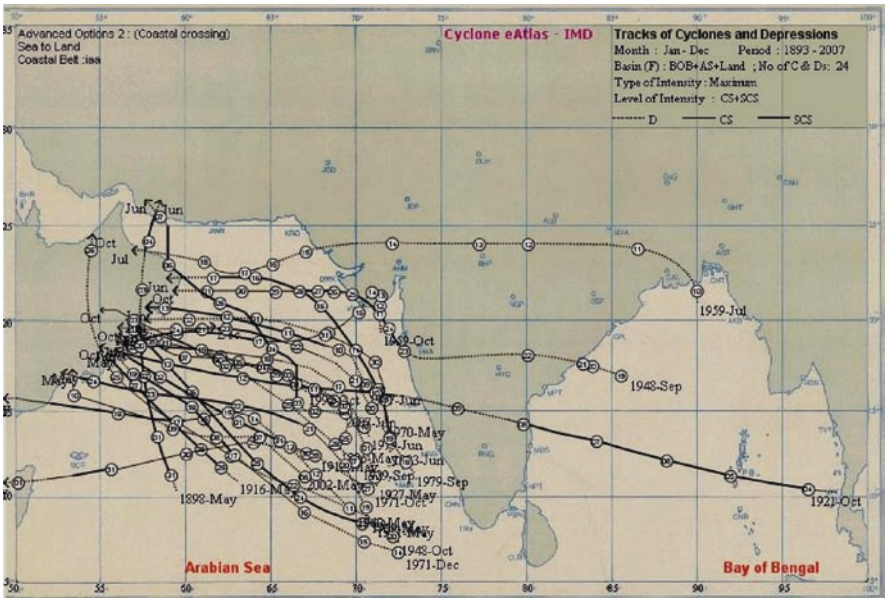

Fig. 6 Tracks of cyclones landfalling over Arabian-African coast adjacent to Arabian Sea

Table 1 Mean and coefficient of variability (CV) of decadal frequencies of cyclonic disturbances crossing Oman coast

Cyclonic disturbances	Mean	CV (%)
Depression (D)	0.58	136
Cyclonic storm (C)	0.83	69
Severe cyclonic storm(S)	0.25	181
Total cyclonic storm (C + S)	1.08	83
Total cyclonic disturbances (D + C + S)	1.67	74

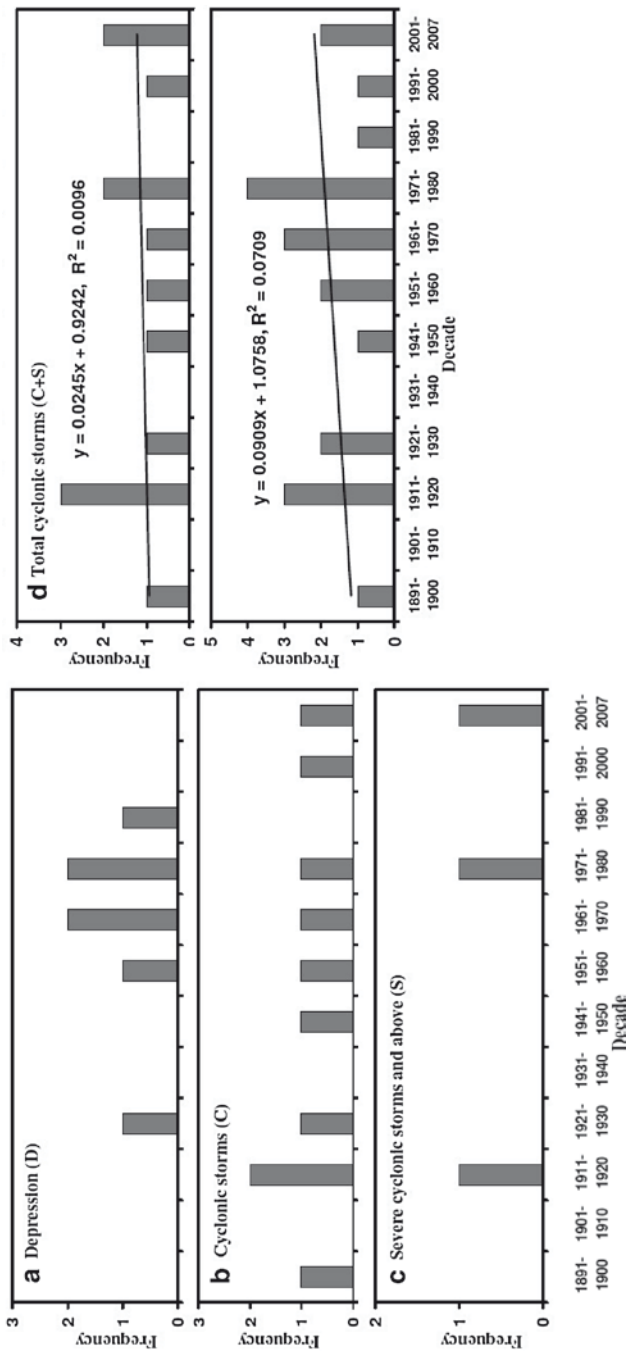

Fig. 7 Decadal frequencies of (**a**) depressions (D), (**b**) cyclonic storms (C), (**c**) severe cyclonic storms and above (S), (**d**) total cyclonic storms (C + S), and (**e**) total cyclonic disturbances (D + C + S) crossing Oman coast

The decadal frequencies of different categories of cyclonic disturbances crossing Oman coast and the results of the linear trend analysis on the decadal frequencies of total cyclonic storms and total cyclonic disturbances are also shown in the Fig. 7. It is found that there is no significant trend at 1% level in the decadal frequencies of different categories of cyclonic disturbances crossing Oman coast during 1891–2007. On the other hand, the decadal frequencies of the total cyclonic disturbances show epochal nature with three epochs during 1891–1930, 1941–1980, and 1991–2007.

Conclusions

1. Under the favorable dynamical and thermodynamic factors as suggested by Gray (1992), the cyclone "Gonu" attained this maximum intensity of super cyclonic storm. The NWP models are limited in predicting the intensity of the system
2. METEOSAT-based WVWV is very useful to monitor the location of the upper tropospheric anticyclone and ridge and hence the role of steering current. It is also useful to predict the movement of the system in short range based on the principle of the steering current.
3. The ECMWF model could predict the genesis, intensification, and movement of the system well in advance with better accuracy compared to other models.
4. The occurrence of severe cyclonic storm landfalling over Oman does not show any significant long-term trend. On the other hand, it shows local behavior in decadal frequency with current epoch commencing in the 1990s.

References

Gray WM (1992) Tropical cyclone formation and intensity change. In: Lighthill J, Holland G, Zhemin Z, Ommanuel K (eds) Tropical cyclone disasters. Peking University Press, Beijing, China

IMD (1979) Tracks of storms and depressions. IMD, New Delhi

IMD (1996) Tracks of storms and depressions. An addendum to the storm track atlas (1891–1970). IMD, New Delhi

IMD (2003) Cyclone manual. IMD, New Delhi

IMD (2008) Track of storm and depressions over the Indian Seas during 1891–2007, Cyclone e-Atlas of IMD. IMD, New Delhi

Kalsi SR (2002) Use of satellite imagery in tropical cyclone intensity analysis and forecasting. Meteorological monograph. IMD, New Delhi

Rama Rao YV, Hatwar HR, Salah AK, Sudhakar Y (2007) An experiment using high resolution ETA and WRF models for forecasting heavy precipitation over India. Pageoph 164:1593–1615

RSMC, New Delhi (2008) A report on cyclonic disturbances over the North Indian Ocean during 2007. IMD, New Delhi

Characteristics of Very Severe Cyclonic Storm "NARGIS" over the Bay of Bengal During 27 April to 3 May 2008

Ajit Tyagi, M. Mohapatra, B.K. Bandyopadhyay, Charan Singh, and Naresh Kumar

Keywords Cyclone Nargis

Introduction

A very severe cyclonic storm crossed southwest coast of Myanmar near latitude 16.0°N between 1200 and 1400 UTC of 2 May 2008. It caused loss of more than 22,000 human lives in Myanmar. The special features of "Nargis" are given below.

(i) The system continued to intensify even after the recurvature.
(ii) The system moved almost in the easterly direction from 0600 UTC of 1 May till 1500 UTC of 2 May.
(iii) The system maintained the intensity of very severe cyclonic storm for about 12 h after the landfall.
(iv) It was the most devastating cyclone over the Bay of Bengal after the 1991 Bangladesh cyclone in term of loss of life and property.

Considering all the above, a detailed study has been taken up to analyze the life history of "Nargis," including genesis, intensification, movement, and landfall. The realized weather and damage due to the system and the cause thereof are analyzed. The detailed performance of the forecasts issued by Regional Specialized Meteorological Centre (RSMC), New Delhi, and NWP model predictions in association with the cyclonic storm "Nargis" have been evaluated. The objective of the study is to find out the various synoptic, thermodynamical, and dynamical features associated with Nargis so that the same can be used as precursors to predict the intensity and track of such a high impact cyclone.

A. Tyagi (✉), M. Mohapatra, B. Bandyopadhyay, C. Singh, and N. Kumar
India Meteorological Department, Mausam Bhavan, Lodi Road, New Delhi, 110003
e-mail: ajit.tyagi@gmail.com

Y. Charabi (ed.), *Indian Ocean Tropical Cyclones and Climate Change*,
DOI 10.1007/978-90-481-3109-9_36,

Data and Methodology

To analyze the various characteristics of Nargis, the best track data of RSMC, New Delhi, have been considered. The system was tracked by INSAT and hence all the INSAT observations and derived satellite products have been considered to analyze the characteristics of Nargis. In addition, the synoptic analyzes and NWP model analyzes available from different centers have been considered. The results and discussions are presented in Section "Results and Discussion". The broad conclusions along with the limitations and future scope of the study are presented in Section "Conclusions".

Results and Discussion

The detailed life history of *Nargis*, describing genesis, intensification, movement, and landfall are discussed in the Section "Brief Life History of Nargis". The main features observed in Satellite imageries are described in the Section "Satellite Imageries". Various dynamical and thermodynamical features are analyzed and presented in the Section "Dynamical and Thermodynamical Parameters". The cause for severe adverse weather and damage thereof due to the system are given in the Section "Adverse Weather". The performance of forecasts issued by RSMC, New Delhi, and the performance of NWP models on track and intensity prediction of *Nargis* are presented and analyzed in the Section "Performance of Forecast Issued by RSMC, New Delhi, and NWP Predictions".

Brief Life History of Nargis

During the last week of April, Intertropical Convergence Zone (ITCZ) was very active. Under its influence a cyclonic circulation developed and the associated cloud clusters persisted for 3–4 days over the southeast Bay of Bengal. As a result of increasing convection under the influence of cyclonic circulation, a low-pressure area formed over southeast Bay of Bengal in the morning of 26 April. Under the favorable conditions like warmer sea surface temperature, low vertical wind shear, and polewards outflow, it concentrated into a depression over the same area and lay centered at 0300 UTC of 27 April near latitude 12.0°N and longitude 87.0°E. Initially, the depression moved westwards, intensified into a deep depression and lay centered at 1200 UTC of 27 April near latitude 12.0°N and longitude 86.5°E. At this time, upper air ridge was running roughly along 15.0°N over the region. There was an anticyclonic circulation, located to the east and centered near latitude

15°N and longitude 95°E. Due to this, strong steering flow from the southeast prevailed and the system started to move in a northwesterly direction. It intensified into a cyclonic storm and lay centered at 0000 UTC of 28 April near latitude 13.0°N and longitude 85.5°E. The upper tropospheric ridge over the storm region ran roughly along 14°N. However, anticyclonic circulation lay to the east-southeast of the system center and became the primary steering influence to cause nearly northerly but slow movement of the system. A trough in extra tropical westerlies roughly ran along 60°E to the north of 15°N. It provided the added upper air divergence to the system. The system intensified into a severe cyclonic storm at 0900 UTC of 28 April and into a very severe cyclonic storm at 0300 UTC of 29 April. As the system lay very close to the upper tropospheric ridge, its movement in the northerly direction slowed down till 29 April. Thereafter, the system lay to the north of the ridge and came under the joint influence of upper air anticyclone lying to the southeast and the mid-latitude upper tropospheric westerlies. Due to the above reason (IMD, 2003), the system started to move in a east northeasterly direction till 1200 UTC of 1 May. The system then moved in easterly direction while intensifying further and crossed southwest coast of Myanmar between 1200 and 1400 UTC of 2 May near latitude 16.0°N.

From 1500 UTC of 2 May, it took northeasterly course and started to move in a northeasterly direction. After crossing the coast, the system maintained the intensity of very severe cyclonic storm till 3 May early morning and gradually weakened thereafter. It laid a severe cyclonic storm centered at 0300 UTC of 3 May over Myanmar near latitude 17.0°N and longitude 96.0°E, close to Yangon. The system weakened into a low pressure area over northeast Myanmar and adjoining Thailand in the evening of 3 May, 2008. Hence the system maintained the intensity for above 24 h while moving slowly over Irrawaddy region of Myanmar. The best track position and other parameters are given in Table 1. The track of the system is shown in Fig. 1.

The maximum sustained wind speed of 90 knots prevailed around the system center during 0600 UTC of 2 May to 0000 UTC of 3 May. As the system moved eastwards close to the coast, the system maintained its intensity even upto 24 h after landfall comparing with past cases, the Orissa super cyclone, 1999 (Mohapatra et al. 2002), which maintained the intensity of the cyclone upto 30 h after landfall causing large-scale devastation. The lowest estimated central pressure (ECP) of the system was 962 hPa recorded at 0600 UTC of 2 May with a pressure drop of about 40 hPa. Throughout the life of cyclone, the sea surface temperature over the Bay of Bengal was 29–32°C, which was favorable for both cyclogenesis and intensification. The vertical wind shear of horizontal winds between 200 and 850 hPa levels was also favorable as it was less than 20 knots around the system center throughout the period except a few hours on 29 April, when satellite imagery showed slight weakening of the system. The upper-level divergence, lower-level convergence, and lower-level relative vorticity were also favorable for intensification of the system (Gray, 1992).

Table 1 Best track positions and other parameters for cyclone, Nargis

Date	Time (UTC)	Centre latitude °N/ longitude °E	C.I. No.	Estimated central pressure (hPa)	Estimated max. sustained wind (kt)	Estimated Pressure drop at center (hPa)	Intensity
27-04-2008	0300	12.0/87.0	1.5	1000	25	–	D
	0600	12.0/87.0	1.5	998	25	–	D
	0900	12.0/87.0	1.5	998	25	–	D
	1200	12.0/86.5	2.0	998	30	4	DD
	1500	12.0/86.5	2.0	994	30	4	DD
	1800	12.5/86.0	2.0	994	30	4	DD
	2100	13.0/85.5	2.0	994	30	4	DD
28-04-2008	0000	13.0/85.5	2.5	994	35	6	CS
	0300	13.0/85.5	2.5	994	35	6	CS
	0600	13.0/85.5	2.5	994	35	6	CS
	0900	13.0/85.5	3.5	986	55	14	SCS
	1200	13.0/85.5	3.5	986	55	14	SCS
	1500	13.0/85.5	3.5	986	55	14	SCS
	1800	13.0/85.5	3.5	986	55	14	SCS
	2100	13.0/85.5	3.5	986	55	14	SCS
29-04-2008	0000	13.0/85.5	3.5	986	55	14	SCS
	0300	13.5/85.5	4.0	980	65	20	VSCS
	0600	13.5/85.5	4.0	980	65	20	VSCS
	0900	13.5/85.5	4.0	980	65	20	VSCS
	1200	14.0/85.5	4.0	980	65	20	VSCS
	1500	14.0/85.5	4.0	980	65	20	VSCS
	1800	14.0/85.5	4.0	980	65	20	VSCS
	2100	14.0/86.0	4.0	980	65	20	VSCS
30-04-2008	0000	14.0/86.0	4.0	980	65	20	VSCS
	0300	14.5/86.5	4.0	980	65	20	VSCS
	0600	14.5/86.5	4.0	980	65	20	VSCS
	0900	14.5/87.0	4.0	980	65	20	VSCS
	1200	14.5/87.0	4.0	980	65	20	VSCS
	1500	15.0/87.5	4.0	980	65	20	VSCS
	1800	15.0/87.5	4.0	980	65	20	VSCS
	2100	15.0/87.5	4.0	980	65	20	VSCS
01-05-2008	0000	15.0/88.0	4.0	980	65	20	VSCS
	0300	15.5/89.0	4.0	980	65	20	VSCS
	0600	16.0/89.5	4.0	980	65	20	VSCS
	0900	16.0/90.0	4.0	980	65	20	VSCS
	1200	16.0/90.5	4.0	980	65	20	VSCS
	1500	16.0/91.0	4.0	980	65	20	VSCS
	1800	16.0/91.5	4.0	980	65	20	VSCS
	2100	16.0/91.5	4.0	980	65	20	VSCS

(continued)

Table 1 (continued)

Date	Time (UTC)	Centre latitude °N/ longitude °E	C.I. No.	Estimated central pressure (hPa)	Estimated max. sustained wind (kt)	Estimated Pressure drop at center (hPa)	Intensity
02-05-2008	0000	16.0/92.5	4.5	972	77	28	VSCS
	0300	16.0/93.0	4.5	972	77	28	VSCS
	0600	16.0/93.5	5.0	962	90	40	VSCS
	0900	16.0/94.0	5.0	962	90	40	VSCS
	1200	16.0/94.0	5.0	962	90	40	VSCS
	1500	16.0/95.0	Nargis crossed southwest coast of Myanmar between 1730 and 1930 h IST on May 2, 2008				
	1800	16.5/95.5	–	–	90		VSCS
	2100	16.5/95.5	–	–	90		VSCS
03-05-2008	0000	16.5/95.5	–	–	90		VSCS
	0300	17.0/96.0	–	–	55		SCS
	0600	17.5/96.5	–	–	45		SCS
	0900	18.0/97.0	–	–	35		CS
	1200	Weakened into a well marked low pressure area over east-central Myanmar					

Satellite Imageries

The very severe cyclonic storm *Nargis* was mostly tracked by satellite. A few satellite imageries of the system taken by INSAT are shown in Figs. 2 and 3. Satellite imageries showed banding features with arc length of 0.5° and intensity T 2.5 (cyclonic storm) at 0000 UTC of 28 April. It showed CDO pattern (Dvorak 1984) with banding features at 0200 UTC of 29 April with T 4.0. In the evening of same day, due to the increase in shearing, the system showed slight disorganization. However, the system again intensified and the eye of the cyclone was visible around 0500 UTC of 2 May. The eye temperature was −57°C. The intensity of the system increased to T 5.0 at 0500 UTC of 2 May and the same intensity continued till the landfall of the system.

Dynamical and Thermodynamical Parameters

The favorable dynamics and thermodynamics parameters for intensification of system includes low to moderate vertical wind shear, warmer SST, high relative humidity, higher upper-level divergence, and lower-level relative vorticity as presented by Gray (1992). The factors, which were favorable for eastwards movement of the system included location of upper tropospheric westerly trough to the west of the system center, upper-level tropospheric westerly steering current, and fall in

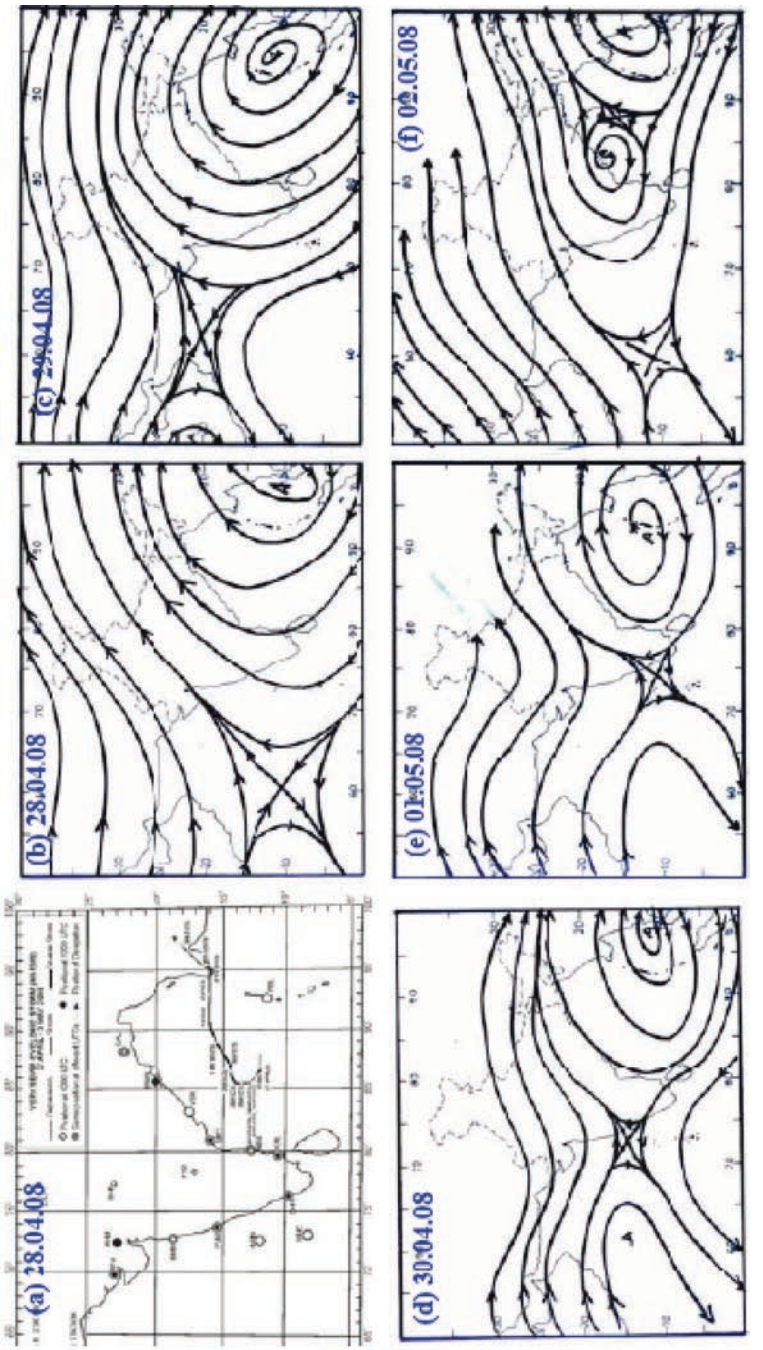

Fig. 1 (**a**) Track of cyclone, Nargis, and (**b–f**) stream line analysis at 200 hPa level based on observations at 0000 UTC during 28 April to 2 May 2008

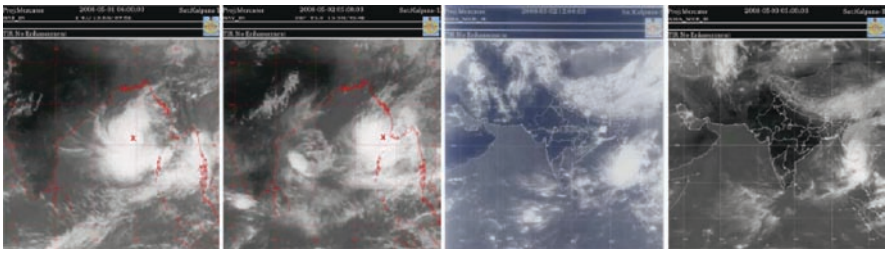

Fig. 2 INSAT imageries of Nargis

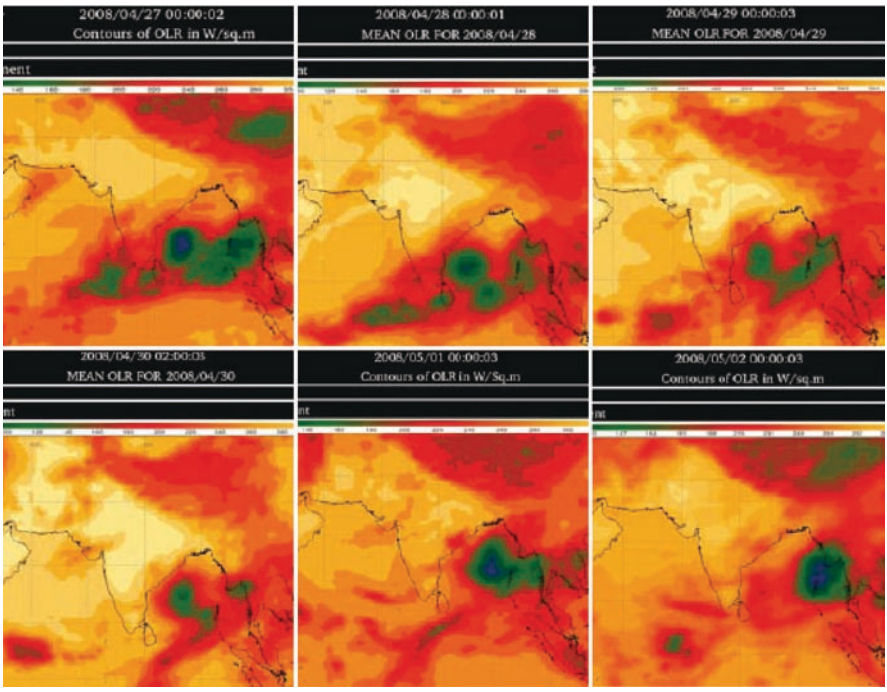

Fig. 3 Mean daily OLR during 27 April to 2 May 2008

pressure along Myanmar coast (IMD, 2003). The factors favoring adverse impact of Nargis include the maintenance of the cyclone intensity as the system lay close to the coast in the delta region, apart from all the above-mentioned factors which were favorable for intensification.

Adverse Weather

As per news paper report, widespread rainfall caused flood over Irrawaddy river delta and Yangon city. As per the newspaper reports, the maximum wind speed of 190 km/h prevailed over the delta region. The storm surge of about 3.6 m over the Irrawaddy delta region of Myanmar has been reported in the media. More than 22,500 people have died and still 41, 000 missing as per media reports.

Performance of Forecast Issued by RSMC, New Delhi, and NWP Predictions

Performance of Forecast Issued by RSMC, New Delhi

The first tropical cyclone advisory indicating landfall over Myanmar coast was issued about 36 h in advance of landfall; this bulletin was at 0600 UTC of 1 May based on observations of 0300 UTC. It was indicated in the bulletin that the system would cross Myanmar coast between latitude 16°N and 18°N around the night of 2 May 2008. On 2 May morning, it was indicated in the bulletin that the system would cross Myanmar coast near 16°N around the evening of the same day. The forecast for maximum intensity (T 5.0) corresponding to maximum sustained wind speed of 90 knots was predicted and maintained in the tropical cyclone advisories for WMO/ESCAP panel member countries from 2100 UTC of 1 May based on the observations of 1800 UTC. Considering 24 h intensity forecast error of RSMC, New Delhi, the average error was about T 0.5. The landfall forecast errors of RSMC, New Delhi, are given in Table 2. Comparing with the average error of RSMC, New Delhi, based on long-period data, the 24 h forecast error was above 40 km less than normal.

NWP Model Prediction

Figure 4 displays the forecast track positions of the system by various NWP models with the initial condition of 30 April 2008 (about 60 h before landfall). The Quasi Lagrangian Model (QLM) of IMD showed northerly movement initially, but during

Table 2 Landfall forecast errors of Nargis as per operational forecast of RSMC, New Delhi

Landfall forecast error	Point error	Time error
(i) 12 h landfall forecast error	55 km	1.5 h
(ii) 24 h landfall forecast error	110 km	2 h
(iii) 36 h landfall forecast error	110 km 3.5 h	

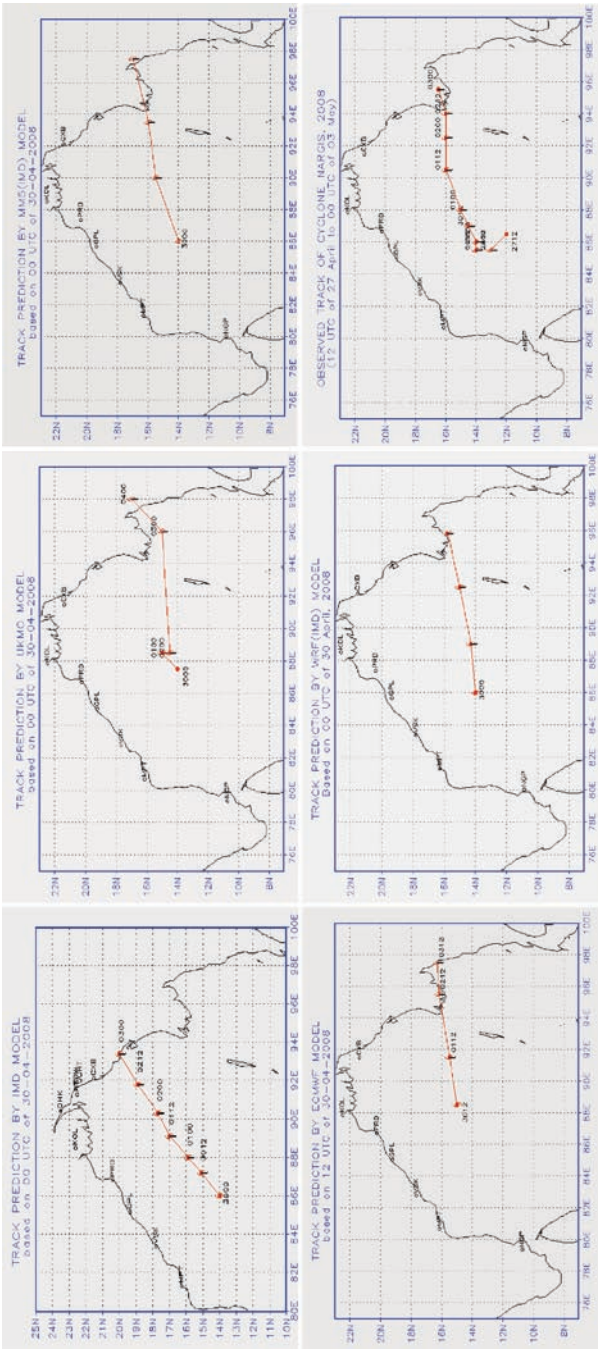

Fig. 4 Track predictions of various models based on April 30 observations

Table 3 Landfall error of cyclone, Nargis, based on NWP models

Models	Hours of forecast	Initial date/time	Landfall Latitude/ Longitude (°)	Landfall position error (km)	Landfall time error (IST)
QLM	72 h	2904/00	No landfall	–430	–12 h early
(IMD)	48 h	3004/00	20.0/93.5	300	5 h late
	24 h	0105/00	18.5/94.5		
MM5	72h	2904/00	No landfall	–10	–8 h early
(IMD)	48 h	3004/00	Close to obs.	110	1 h early
	24 h	0104/00	17.0/94.7		
ECMWF	72 h	2904/00	No landfall	–10	–8 h early
	48 h	3004/12	Close to obs.	50	7 h early
	24 h	0104/00	15.8/95.2		
UKMO	72 h	2904/00	No landfall	–150	5 h delay
	48 h	3004/00	15.0/94.8	110	4 h early
	24 h	0104/00	15.3/94.8		
WRF	72 h	2904/00	No landfall	–85	–11 h delay
(IMD)	48 h	3004/00	15.8/95.8	50	1 h delay
	24 h	0104/00	16.2/94.4		
T254	72 h	NA	NA	NA	NA
	48 h	3004/00	15.4/95.5	120	11 h delay
	24 h	NA	NA	NA	NA

subsequent forecast hours it showed northeast to easterly movement. MM5 of IMD showed northeasterly to easterly movement. ECMWF showed northeasterly movement initially and during subsequent forecast hours it showed easterly movement. UKMO showed easterly movement persistently. WRF model of IMD showed easterly movement. Numerical products were also available from other centers like IIT Delhi and SAC, Ahmedabad, and these products were found quite useful. The QLM showed mean forecast error of 10–285 km for the forecast range 12–48 h. MM5 of IMD showed mean forecast error of 150–160 km for the 72 h forecast range. ECMWF showed mean forecast error of 140–170 km for the forecast range up to 72 h. WRF of IMD showed mean forecast error of 95–225 km for the forecast range of 24–72 h. UKMO model showed mean forecast error of 90–310 km for 24–72 h forecast range. In Table 3, the landfall errors of different models are presented. The landfall errors in the 24–48 h forecasts by MM5 of IMD, WRF of IMD, ECMWF, and UKMO are found to be between 10 and 110 km.

Conclusions

The high adverse impact of the cyclone Nargis was mainly due to the maintenance of cyclone intensity even 24 h after the landfall. The system intensified into very severe cyclonic storms even after the recurvature due to favorable dynamic and thermodynamic factors including warmer SST (29–32°C), lower vertical wind shear (< 20 knots), and occurrence of westerly trough to the west providing

upper-level divergence. The rear eastwards movement of the system was mainly due to the fact that the system lay to the periphery of the upper tropospheric anti-cyclonic circulation located to the southwest of the system center. The ECMWF model could predict better the genesis, intensification, and movement of the system well in advance.

References

Dvorak VF (1984) Satellite observed upper level moisture pattern associated with tropical cyclone movement. Proceedings of the 15th American Met. Sec. Conf. on Hurricane and Tropical Meteorology, pp 163–168

Gray WM (1992) Tropical cyclone formation and intensity change. In: Lighthill J, Holland G, Zhemin Z, Ommanuel K (eds) Tropical cyclone disasters. Peking University Press, Beijing, China

IMD (2003) Cyclone manual. Indian Meteorological Department, New Delhi

Mohapatra M, Gupta DS, Chanchalani NK, Dastidar SK (2002) Orissa super cyclone, 1999 – a case study. J Ind Geophys Union 6:93–106

Characteristics of Very Severe Cyclonic Storm "SIDR" over the Bay of Bengal During 11–16 November 2007

Ajit Tyagi, M. Mohapatra, B.K. Bandyopadhyay, Charan Singh, and Naresh Kumar

Keywords Cyclone SIDR

Introduction

The year 2007 showed increased cyclonic activity over the Bay of Bengal, compared to recent years with the formation of nine cyclonic disturbances. Out of these disturbances, two cyclonic storms, including a very severe cyclonic storm "SIDR", formed over the Bay of Bengal. This system crossed Bangladesh coast around 1700 UTC of 15 November 2007. The system caused heavy to very heavy rainfall over Bangladesh and northeastern states of India. According to media report, the wind speed of about 200 km/h prevailed over Bangladesh coast at the time of landfall and tidal wave of about 6 m inundated low lying areas of Bangladesh. It caused a loss of about 3,400 human lives and huge loss of property. The special features of "SIDR" are as follows.

- It was the first ever very severe cyclonic storm crossing Bangladesh after 1991 and first severe cyclonic storm after 1998 (Table 1).
- The system moved in a near northerly direction till a few hours before landfall and recurved northeastwards during landfall. It moved faster during 12 h before landfall.
- The size of the storm was less, though it had severe damage potential.
- The very severe cyclonic storm was monitored by the latest technological tools like Doppler Weather Radar (DWR), Automatic Weather Stations (AWS), and satellite derived products including atmospheric motion vectors (AMV).

A. Tyagi (✉), M. Mohapatra, B.K. Bandyopadhyay, C. Singh, and N. Kumar
India Meteorological Department, Mausam Bhavan, Lodi Road, New Delhi, 110003
e-mail: ajit.tyagi@gmail.com

Y. Charabi (ed.), *Indian Ocean Tropical Cyclones and Climate Change*,
DOI 10.1007/978-90-481-3109-9_37,

Table 1 Severe cyclonic storms which crossed Bangladesh during 1891–2007

S. No.	Date of landfall	S. No.	Date of landfall	S. No.	Date of landfall
1	22-10-1893	10	30-05-1961	19	09-12-1973
2	12-12-1895	11	30-10-1962	20	28-11-1974
3	24-10-1897	12	29-05-1963	21	15-10-1983
4	07-05-1898	13	12-05-1965	22	25-05-1985
5	06-12-1909	14	01-06-1965	23	30-04-1991
6	23-04-1922	15	15-12-1965	24	25-11-1995
7	26-05-1941	16	24-10-1967	25	22-11-1998
8.	11-10-1960	17	13-11-1970	26	15-11-2007
9	09-05-1961	18	06-11-1971	–	–

Considering all the above, a detailed study has been taken up to analyze the life history of "SIDR", including genesis, intensification, movement, and landfall. The weather realized, the damage due to the system, and the cause thereof are analyzed. The track and intensity of the system could be well predicted with the support of various observational tools and Numerical Weather Prediction (NWP) models. The utilities of the modern observational tools like DWR, AWS, and AMVs have been demonstrated. The detailed performance of the forecasts issued by Regional Specialized Meteorological Centre (RSMC), New Delhi, and the NWP model predictions in association with the cyclone "SIDR" have been evaluated and presented. The objective of the study is to find out the various synoptic, thermodynamical, and dynamical features associated with "SIDR" so that the same can be used as precursors to predict the intensity and track of such high impact cyclone.

Data and Methodology

To analyze various characteristics of SIDR, the best track data of RSMC, New Delhi (2008), has been considered. The system was tracked by INSAT and hence all the INSAT observations and derived satellite products have been considered to analyze the characteristics of SIDR. The water-vapor-derived wind vectors (WVWV) at upper levels (100–250 hPa) during the life period of this system have been analyzed and discussed as they can provide the measure of steering wind for the system (Bhatia et al. 2006; Kelkar 1997; Krishna Rao 1997). Hourly AWS data of coastal stations of West Bengal and Orissa have been collected from IMD and analyzed for the cyclone period. In addition, the synoptic analyses and NWP model analyses available from different centers have been considered. The results and discussions are presented in Section "Results and Discussion". The broad conclusions are presented in Section "Conclusion".

Results and Discussion

The genesis, intensification, movement, and landfall of cyclone *SIDR* are discussed in Section "Genesis, Intensification, Movement, and Landfall of 'SIDR'". The main features observed in satellite imageries are described in Section "Monitoring of 'SIDR' by Satellite". The utility of DWR products and AWS data are presented in Sections "DWR Imageries" and "Utilities of AWS Data", respectively. The performance of forecasts issued by RSMC, New Delhi, and performance of NWP models on track and intensity prediction of "SIDR" are presented and analyzed in Section "Performance of Forecast Issued by RSMC, New Delhi, and NWP Predictions."

Genesis, Intensification, Movement, and Landfall of "SIDR"

An upper air cyclonic circulation lay over southeast Bay of Bengal and the adjoining area of south Andaman Sea during 8–10 November 2007. Initially, moderate to high vertical wind shear inhibited organization, while strong diffluence aloft aided in developing convection. During this period, intertropical convergence zone (ITCZ) was also active. The vertical wind shear over the region decreased gradually and the circulation became more defined. Under the influence of these scenarios, a low pressure area formed at 0300 UTC of 11 November over southeast Bay of Bengal and neighborhood. It concentrated into a depression and lay centered at 0900 UTC of the same day over southeast Bay of Bengal near latitude 10.0°N and longitude 92°E, about 200 km south-southwest of Port Blair. Moving slightly northwestwards, it intensified into a deep depression and lay centered at 1800 UTC of 11 November near latitude 10.5°N and 91.5°E. It intensified into a cyclonic storm, *SIDR*, and lay centered at 0300 UTC of 12 November near latitude 10.5°N and 91.0°E, about 220 km southwest of Port Blair. With favorable upper-level divergence, lower-level convergence, lower-level relative vorticity, and south easterly upper tropospheric flow (Gray 1992), the system moved in the northwesterly direction, further intensified into severe cyclonic storm, and lay centered at 1200 UTC of the same day near latitude 11.5°N and longitude 90.0°E. It remained practically stationary then and intensified into a very severe cyclonic storm at 1800 UTC of 12 November. The system moved slightly northwestwards thereafter till 0000 UTC of 13 November. Afterwards, the system moved in a near northerly direction upto 1200 UTC of 15 November as the system lay close to the upper tropospheric ridge. The upper tropospheric ridge moved gradually northward with northward movement of the system. From 1200 UTC of 15 November, the system recurved and moved in a north-northeasterly direction, under the influence of the upper tropospheric trough to the west of the system center as the system lay to the north of the upper tropospheric ridge. It crossed west Bangladesh coast around 1700 UTC near longitude 89.8°E as a very severe cyclonic storm and lay centered at 1800

UTC near latitude 22.5°N and long 90.5°E, about 100 km south of Dhaka (Bangladesh). The system then weakened rapidly into a cyclonic storm while moving northeastwards and lay centered at 2100 UTC of 15 November near latitude 23.5°N and longitude 91.0°E, about 70 km southwest of Agartala (India). It further weakened into a depression and lay centered at 0300 UTC of 16 November near latitude 24.5°N and longitude 91.5°E, about 50 km north of Agartala. It lay as a well-marked low pressure area over northeastern states of India at 1200 UTC of 16 November. The track of the system is shown in Fig. 1.

Monitoring of "SIDR" by Satellite

The very severe cyclonic storm *SIDR* was mostly tracked by satellite till 14 November 2007. A few satellite imageries of the system taken by INSAT are shown in Fig. 2. Satellite imageries showed the envelopment of convective clouds over southeast Andaman Sea in association with the low pressure area at 0600 UTC of 11 November 2007. It showed well-organized convective clouds over east central and adjoining southeast Bay of Bengal in association with the cyclonic storm over southeast Bay of Bengal at 0600 UTC of 12 November 2007, with T 3.0. It showed CDO (Dvorak 1984; Kalsi 2002) pattern over east central Bay of Bengal at 0600 UTC of 13 November 2007, with T 5.0 and CDO pattern with banding features over

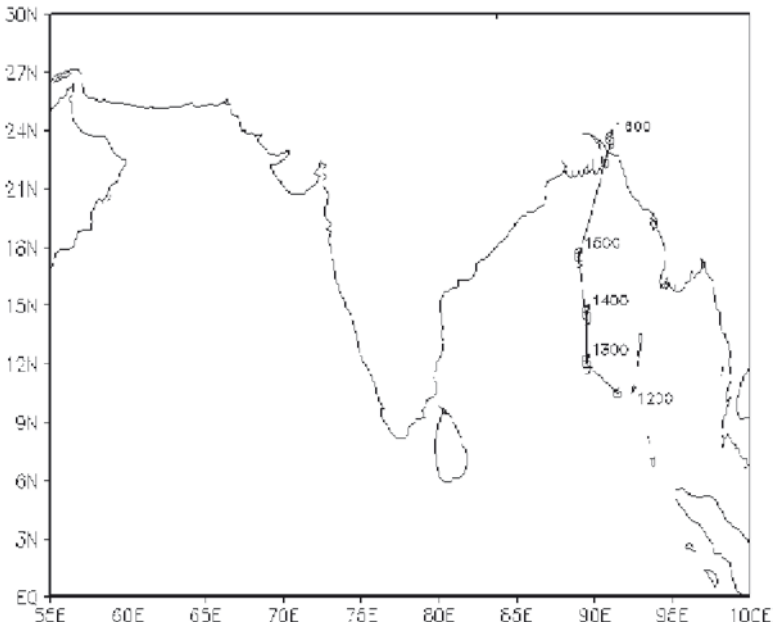

Fig. 1 Track of very severe cyclonic storm "SIDR"

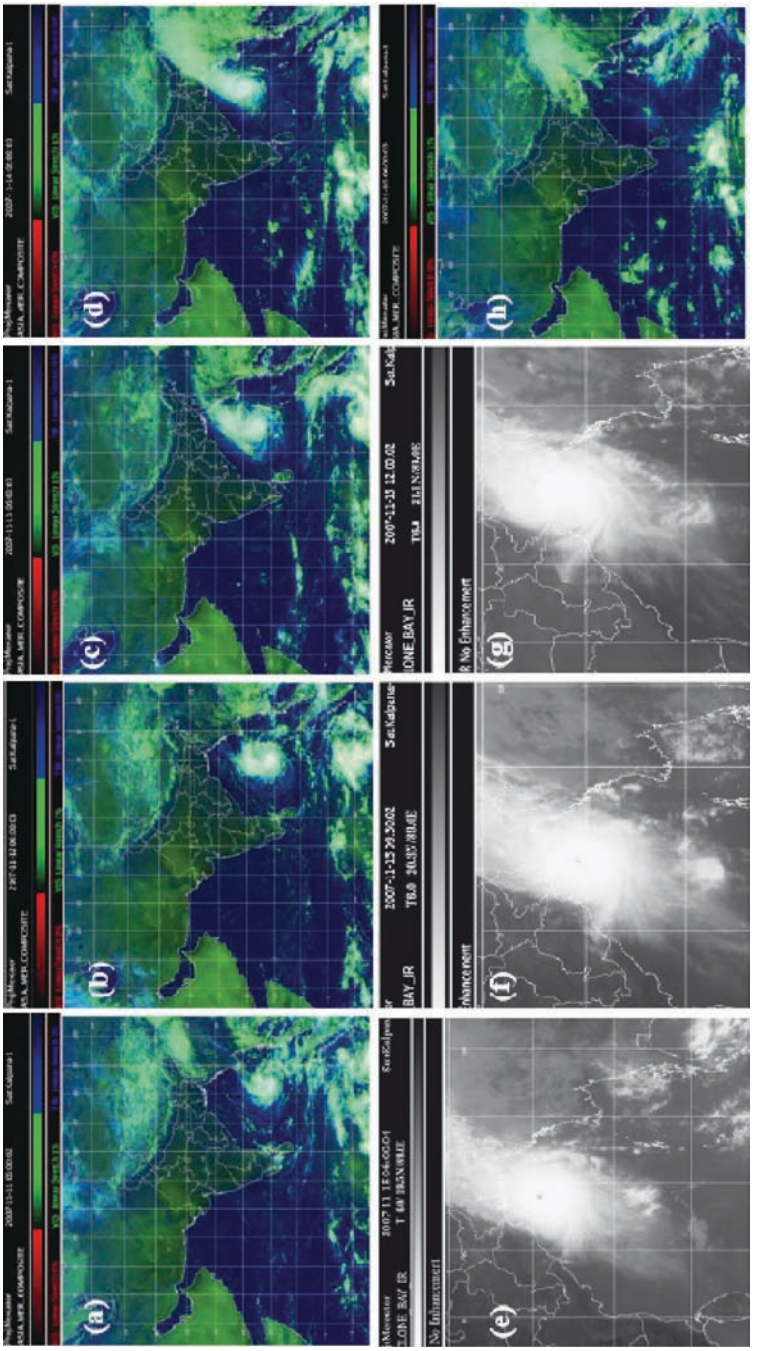

Fig. 2 Satellite KALPANA-1 imagery (**a**) at 0600 UTC of 11 November 2007 (**b**) at 0600 UTC of 12 November Bay (**c**) at 0600 UTC of 13 November (**d**) at 0600 UTC of 14 November (**e**) at 0600 UTC of 15 November (**f**) at 0900 UTC of 15 November (**g**) at 1200 UTC of 15 November, and (**h**) at 0600 UTC of 16 November

east-central and adjoining west-central Bay of Bengal at 0600 UTC of 14 November. Satellite imagery at 0600 and 0900 UTC of 15 November showed the open eye of a very severe cyclonic storm, and feeding bands with T 6.0. Satellite imagery of 15 November at 1200 UTC showed system center over the sea and half of the convective cloud mass lying over the land areas and hence the interaction of the system with land surface.

The outflow from the system was directed north-northeastwards from 13 November onwards. The WVWV at the upper level (100–250 hPa) during 0000 UTC to 1500 UTC of 15 November 2007 are shown in Fig. 3. The WVWV product clearly indicated the system to move initially in a northerly direction and then in a north-northeasterly direction before landfall according to 0000 UTC to 0600 UTC observations of 15 November. However, the WVWV products based on 1200 UTC observations suggested north-northeasterly movement of the system. The similar movement was also suggested at 1500 UTC of 15 November 2007. Considering the likely landfall point of the system according to stream line analysis of WVWV and the assumption that the movement of the system is mainly governed by the wind at 250–100 hPa levels, all the observations on 15 November during 0000 UTC to 1500 UTC suggested that the system would cross Bangladesh coast near 90.0°E. The WVWV products at 0300 UTC and 1200 UTC of 13 and 14 November 2007 also suggested initial northward movement and north-northeastward movement of the system (north of 20°) before landfall.

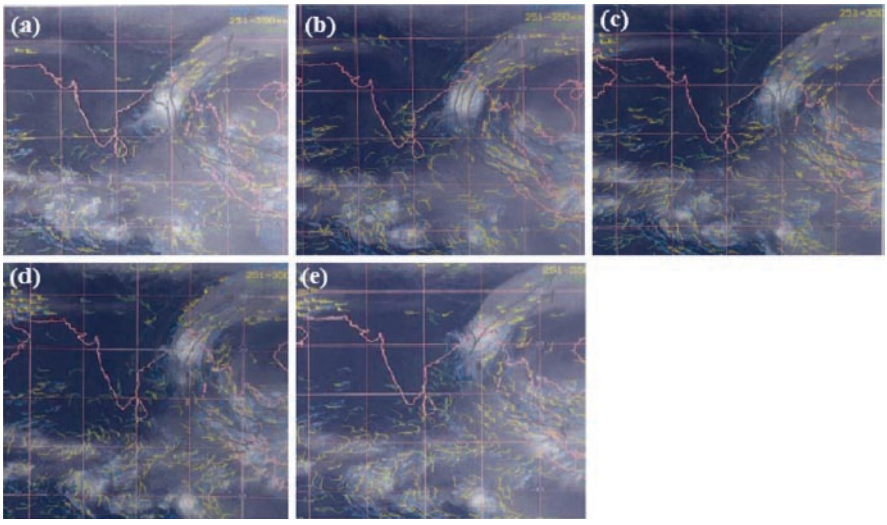

Fig. 3 WVWV analysis over Indian region at (**a**) 0000 UTC, (**b**) 0300 UTC , (**c**) 0600 UTC, (**d**) 1200 UTC, and (**e**) 1500 UTC observations of METEOSAT of 15 November 2007.

DWR Imageries

The system has been tracked by Doppler weather radar at Kolkata from 0500 UTC of 15 November 2007, onwards. The DWR Kolkata observations of the system are shown in Fig. 4. The DWR imageries suggested north-northeastward movement of the system. The eye of the system along with spiral bands could be observed. The pre-cyclone squall lines over Bangladesh suggested movement of the system toward Bangladesh (Raghavan 1997).

Utilities of AWS Data

The mean sea level pressure, 24 h pressure changes, and surface wind observations from coastal AWS stations in West Bengal and north Orissa suggested north-northeastward movement of the system with effect from 1300 UTC of 15 November 2007. However, the actual track of the system based on AWS data could not be derived quantitatively due to nonavailability of similar stations in Bangladesh. Hence, AWS data if available on real time basis can be utilized for monitoring the system and predicting the sudden changes in the track and hence the landfall point.

Performance of Forecast Issued by RSMC, New Delhi, and NWP Predictions

Performance of Forecast Issued by RSMC, New Delhi

Considering 24 h intensity forecast error of RSMC, New Delhi, the average error was about T 0.5. The landfall forecast errors of 12, 24, and 36 h forecast were 46, 121, and 180 km, respectively. The time forecast errors of 12, 24, and 36 h are 1.5, 5.5, and 5.5 h, respectively. Comparing with long-term average error over the north Indian Ocean of RSMC, New Delhi, based on long-period data, the 30 h forecast error was above 20 km less than normal.

NWP Model Prediction

Fig. 5 displays the forecast track positions of *SIDR* by the operational models at 72, 48, and 24 h time scale. The corresponding landfall errors are summarized in Table 2. The 72 h forecasts based on 00 UTC initial conditions of 13 November depicted large landfall error by all the models except the ECMWF. Similar error with less magnitude persisted in the 48 h forecasts based on 00 UTC initial

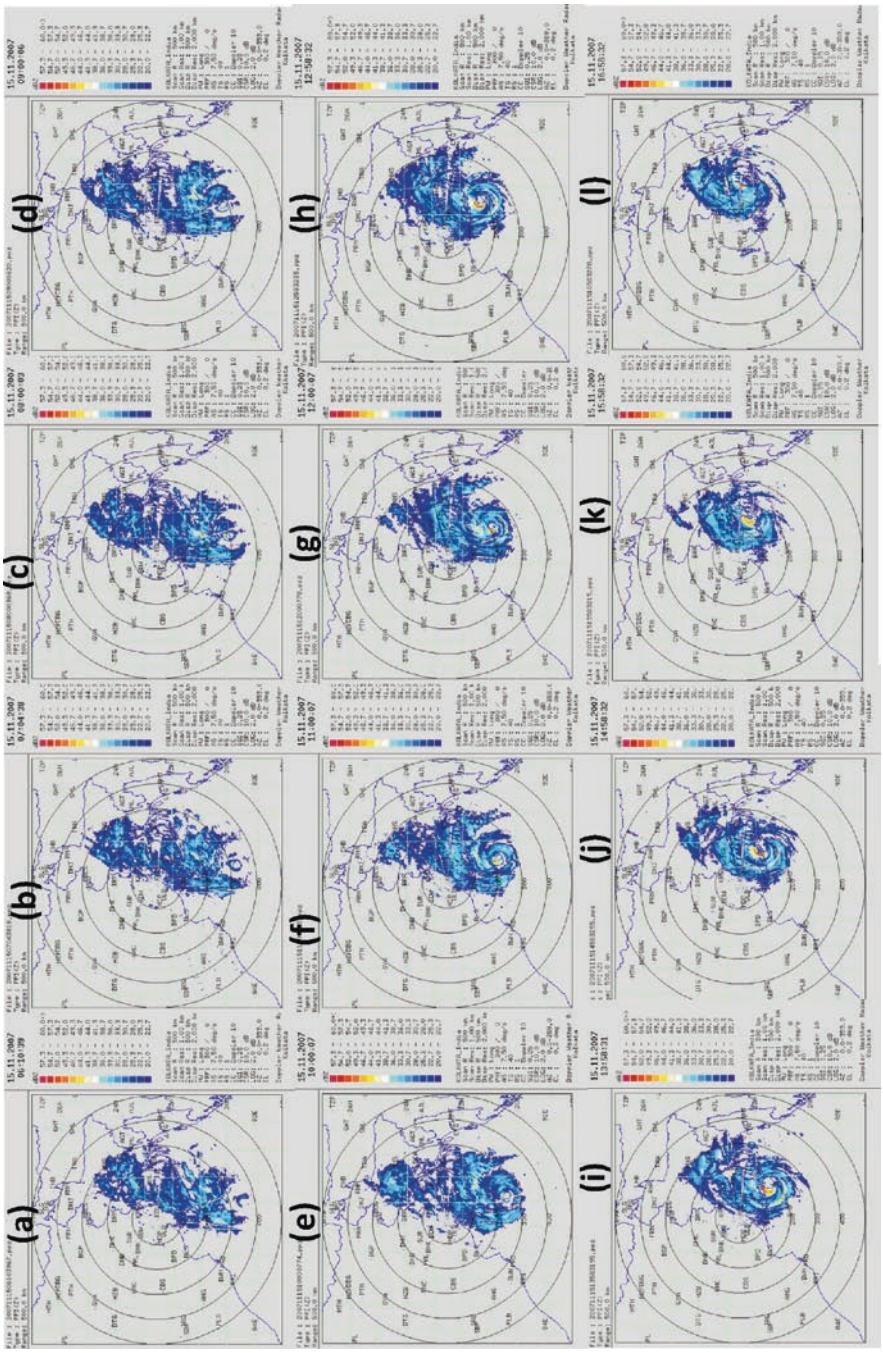

Fig. 4 Kolkata doppler weather radar imageries during (**a–l**) 0600 UTC to 1700 UTC of 15 November 2007

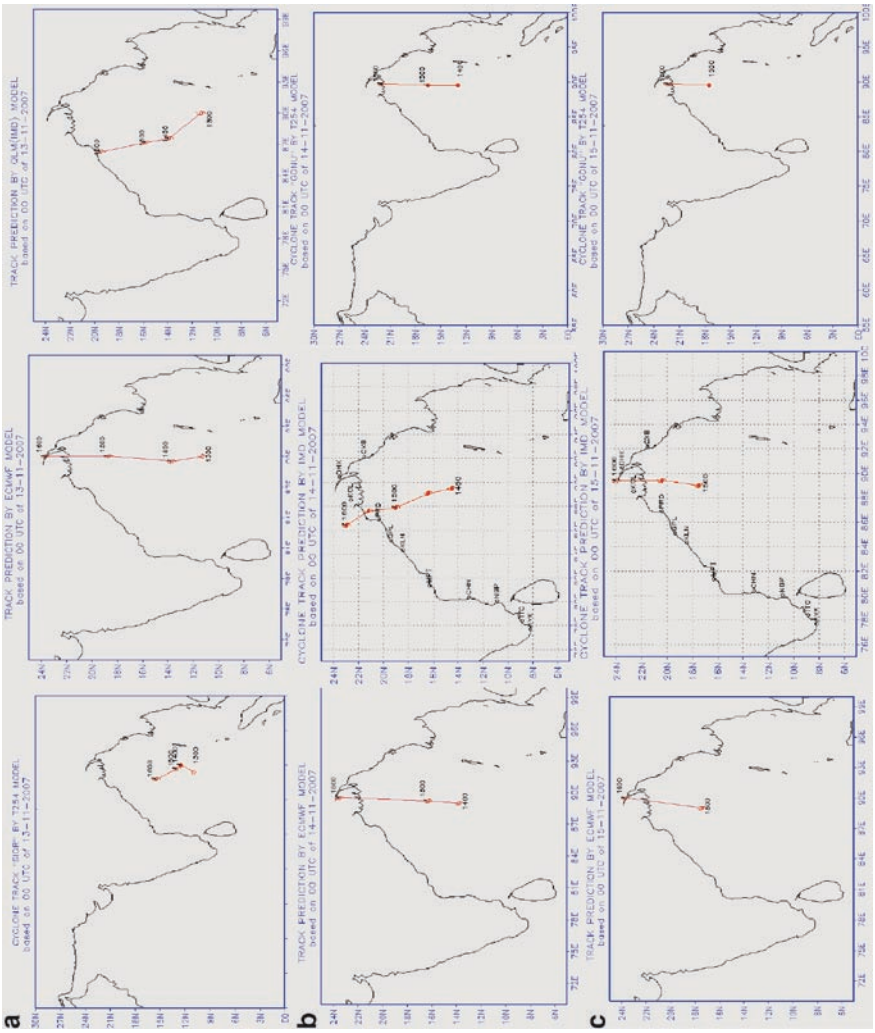

Fig. 5 Very severe cyclonic storm SIDR of November 2007 (**a**) 72 h forecasts (**b**) 48 h forecasts (**c**) 24 h forecasts

Table 2 Landfall error of the very severe cyclonic storm SIDR of November 2007

Models	Initial date/ time	Landfall/ Forecast point (^{0}N/^{0}E)	Landfall Forecast date/ time (UTC)	Landfall error (km)	Landfall time error
T254	13/0000	18.2/84.0	17/1900	720	25 h delay
	14/0000	21.8/88.7	16/0600	115	12 h delay
	15/0000	22.0/88.7	15/1800	120	1 h delay
ECMWF	13/0000	22.4/89.4	16/1900	55	2 h delay
	14/0000	22.1/89.5	15/1600	55	7 h delay
	15/0000	21.9/89.7	15/1500	25	2 h early
QLM	13/0000	19.5/86.3	–15/1300	650	No landfall
	14/0000	21.4/87.2	15/1600	270	4 h early
	15/0000	21.9/89.4		45	1 h early

conditions of 14 November. All the models showed reasonably good performance in the 24 h forecasts based on the initial conditions of 00 UTC of 15 November, when some convergence in the forecasts by these models is noted. Forecasts produced by ECMWF model are found to be superior both in terms of landfall point and landfall time. All the forecasts (72, 48, and 24 h) by ECMWF were found to be consistent. Landfall position errors were around 55 to 25 km at the 72 to 24 h forecast period (Table 2). The landfall time error was within 2 h of observed landfall time.

Conclusions

The system recurved just a few hours before the landfall and moved fast in a north-northeasterly direction as the system lay to the north of the upper tropospheric ridge and comes under the influence of the upper tropospheric trough to the west of the system center at 1200 UTC of 15 November 2007. Prior to that the system moved in a near northerly direction during 0000 UTC of 13 November, as the system lay close to the upper tropospheric ridge and the ridge shifted northward with the northward movement of the system. The satellite based WVWV and AWS data and DWR products can be utilized for monitoring the system and predicting the landfall point of the system in short range. The ECMWF model could predict the genesis, intensification, and movement of the system well in advance with better accuracy compared to other models.

References

Bhatia RC, Singh D, Giri RK (2006) Use of METEOSAT-5 derived winds for operational weather forecasting. Eighth International Winds Workshop, Beijing, China, April 24–28, 2006.

Dvorak VF (1984) Satellite observed upper level moisture pattern associated with tropical cyclone movement. Proceedings of the 15th American Met. Sec. Conf. on Hurricane and Tropical Meteorology, pp 163–168.

Gray WM (1992) Tropical cyclone formation and intensity change. In: Lighthill J, Holland G, Zhemin Z, Ommanuel K (eds) Tropical cyclone disasters. Peking University Press, Beijing, China

Kalsi SR (2002) Use of satellite imagery in tropical cyclone intensity analysis and forecasting. Meteorological Monograph. IMD, New Delhi

Kelkar RR (1997) Satellite based monitoring and prediction of tropical cyclone intensity and movement. Mausam 48:157–168

Krishna Rao AVRK (1997) Tropical cyclone – synoptic methods of forecasting. Mausam 48:239–256

Raghavan S (1997) Radar observation of tropical cyclones over the Indian sea. Mausam 48:169–188

RSMC, New Delhi (2008) Report on cyclonic disturbances over the north Indian Ocean during 2007. RSMC, New Delhi

Influence of a Tropical Cyclone Gonu on Phytoplankton Biomass (Chlorophyll a) in the Arabian Sea

Sergey Piontkovski and Adnan Al-Azri

Keywords Phytoplankton biomass

Introduction

Tropical cyclones could gradually affect the physical, chemical, and biological processes in the upper layer of the ocean. In terms of biological consequences, the cyclone wind field causes local mixing which results in the injection of nutrients into the upper layer of the ocean and triggering phytoplankton bloom (Subrahmanyam et al. 2002). In some cases, the magnitude of the hurricane-induced bloom could reach a gradual (30-fold) increase in the surface chlorophyll a concentration, as well as an increase in the primary production (Lin et al. 2003; Smitha et al. 2006). In the regions where cyclones often occur, their propagation could chiefly influence the annual productivity of the ocean. For example, an average of 14 cyclones pass over the South China Sea annually, which suggests the contribution of cyclones to annual production to be as much as 20–30% (Lin et al. 2003).

About 13% of the world's tropical cyclones were reported in the northern part of the Indian Ocean (Gray 1968). Cyclone Gonu (which made a landfall in the coast of Oman on 5 June 2007) was documented as the strongest cyclone ever recorded in the northern part of the Indian Ocean over the past 60 years. Two days prior to the landfall, Gonu had intensified to a super storm with maximum wind speed of about 260 km/h becoming the first documented category 4 status cyclone in the Arabian Sea, as well as the first cyclone to traverse this basin. Our aim is to analyze the response of chlorophyll a to the passage of Gonu.

S. Piontkovski (✉) and A. Al-Azri
College of Agricultural and Marine Sciences, Sultan Qaboos University,
P.O. Box 34, Al-Khod 123, Sultanate of Oman
e-mail: spiontkovski@gmail.com

Y. Charabi (ed.), *Indian Ocean Tropical Cyclones and Climate Change*,
DOI 10.1007/978-90-481-3109-9_38,

Methods

The QuikSCAT scatterometer data (available on the PO-DAAC ftp site- ftp://podaac.jpl.nasa.gov/ocean_wind/quikscat/NRT/) were used to determine the scale, location, and wind field characteristics of a cyclone over time. Satellite-derived (9 km spatial resolution MODIS Aqua) weekly and monthly Level-2 and Level-3 binned data for sea surface temperature, sea surface heights, and chlorophyll a concentration were used to analyze the response of these fields to the passage of Gonu. Maps for the sea surface height anomaly were produced from Jason, TOPEX/Poseidon, and Geostat altimeter data processed in near real time. A product analysis (developed by the Colorado Center for Astrodynamic Research) was based on the latest 10 days of Jason and T/P, and 17 days of Geostat sampling. Mapping the chlorophyll field along the cyclone track, the three $2^{o} \times 2^{o}$ quadrates have been used to analyze changes of chlorophyll a concentration in June 2007 compared to that throughout the annual cycle. From June 4 through June 6, Gonu had passed through the following three quadrates ending with landfall in the coast of Oman:

1. (20–18°N, 63–65°E)
2. (22–20°N, 61–63°E)
3. (22–24°N, 60–62°E)

In order to compare the chlorophyll a concentration presumably induced by Gonu with the reported coastal upwelling of Oman, monthly averaged MODIS Aqua maps of the Arabian Sea for the years from 2002 through 2008 were used. This enabled us to compare the amplitudes of the seasonal and interannual variability with a special reference to the Gonu-induced amplitude. Monthly time series used in this study were acquired using the GES-DISC Interactive Online Visualization and Analysis Infrastructure software as part of NASA's Goddard Earth Sciences Data and Information Services Center.

Results

The first warnings on a tropical cyclone 02A, which emerged 370 nautical miles southwest of Mumbai (India) and moved westward at a speed of seven knots, were issued by JTWC on June 2, although the beginning of the track was attributed to June 1, near 14.2°N/70.6°E (https://metocph.nmci.navy.mil/jtwc.php). The end of the track was reported on June 7, near southern coast of Iran (25.5°N/58.1°E). During its peak intensity on 4 June, Gonu (moving at a speed of 19 km/h) was located about 650 km east-southeast of Masirah Island off the coast of Oman. The cyclone maintained its peak intensity for 12 h, and on 6 June, the wind had dropped from a peak of 240 km/h (Fig. 1) to 157 km/h, with the center of the cyclone located 185 km southeast of Muscat. In terms of size, the cyclone was slightly smaller at its peak than an average tropical cyclone in which the gale used to extend outward from the center for about 240 km (Padgett 2008).

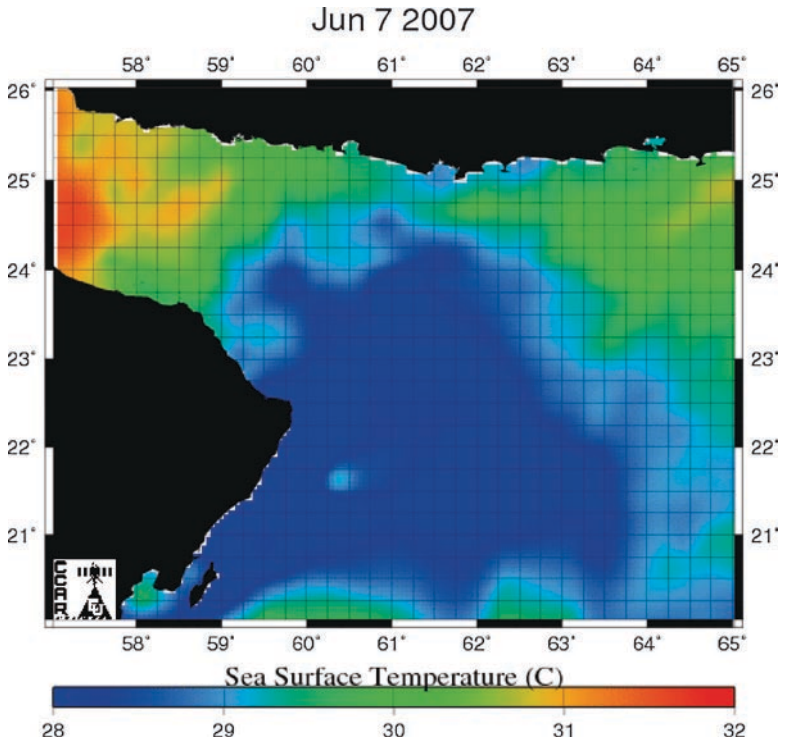

Fig. 1 Sea surface temperature after the passage of a cyclone Gonu (7 June; http://argo.colorado.edu)

The sea surface temperature 5-day composite (centered on June 7) exhibited that a wide area of the northwestern Arabian Sea was occupied by waters with minimal temperature within the range observed (Fig. 1). Compared to the end of May (featuring the pre-cyclone mode), the area with a temperature of about 28°C had expanded tenfold, after the passage of the cyclone. In May, that level of minimal sea surface temperature had been observed only in the coastal upwelling region (Fig. 2). The issue of huge cloud field had gradually complicated remote sensing of the chlorophyll concentration in the region. Few cloud windows in the images resembling the chlorophyll field on June 7 have enabled a sensor to detect the concentration range of about 8–10 mg/m^3 for the region featuring the northeast periphery of the passage of the cyclone (23.4°N/61.3°E). However, the reliability of these windows available for analysis was low in general. The 5-day composite of the chlorophyll a distribution (centered on June 4) exhibited two major zones of enhanced concentration – the coastal one stretched along the Omani and Iranian coasts and the oceanic one stretched longitudinally between 61 and 62°E (Fig. 3). The mean chlorophyll concentration observed in the coastal zone exceeded 1.2 times that in the oceanic zone.

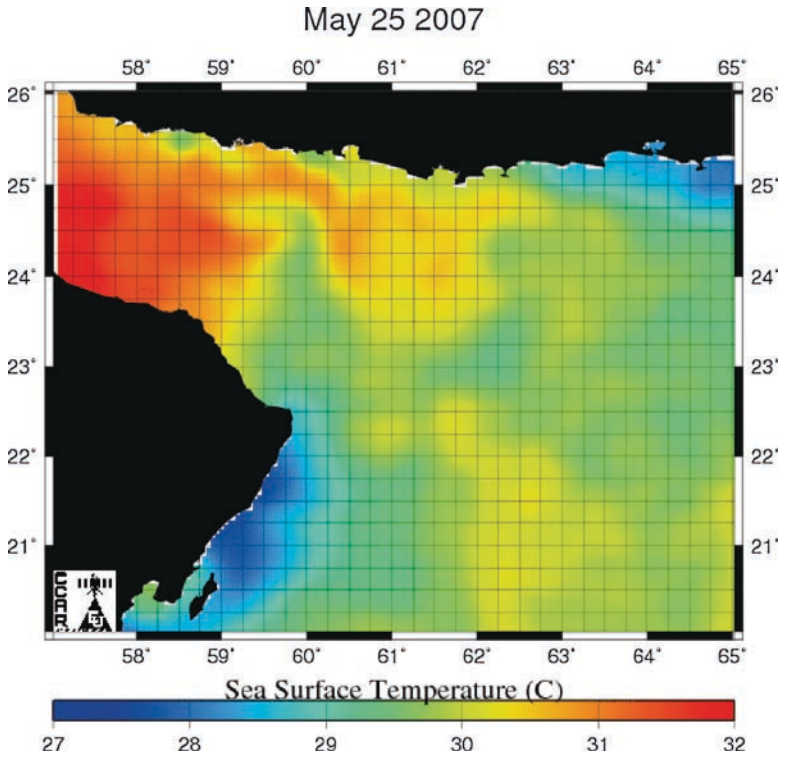

Fig. 2 Sea surface temperature before the passage of a cyclone Gonu (25 May; http://argo.colorado.edu)

The MODIS database enables one to come up with monthly changes of chlorophyll over regions. In terms of our goal, this means that the concentration observed in June (influenced by cyclone passage) could be compared to the range of concentration observed throughout the seasonal cycle. We retrieved monthly time series for the three $2^{o} \times 2^{o}$ quadrates covering the track of Gonu (Fig. 4). All three time series showed well-pronounced seasonal cycle of chlorophyll a, with peak concentration in August and February due to summer and winter monsoons. In the northwestern quadrate (22–24°N/60–62°E) corresponding to the end of the track, the third well-developed peak was observed. It matched the month of June – the time of cyclone passage. The chlorophyll a concentration in June 2007 in this region was 1.2 times less the concentration featuring the summer monsoon of the same year. The seasonal changes observed in the cyclone-affected region (northwestern quadrate, 22–24°N/60–62°E) in 2007 were compared to the seasonal changes for the previous years – in 2005 and 2003 (Fig. 5). However, none of these changes has exhibited peaks in June. The two most developed peaks were during the time of summer and winter monsoons.

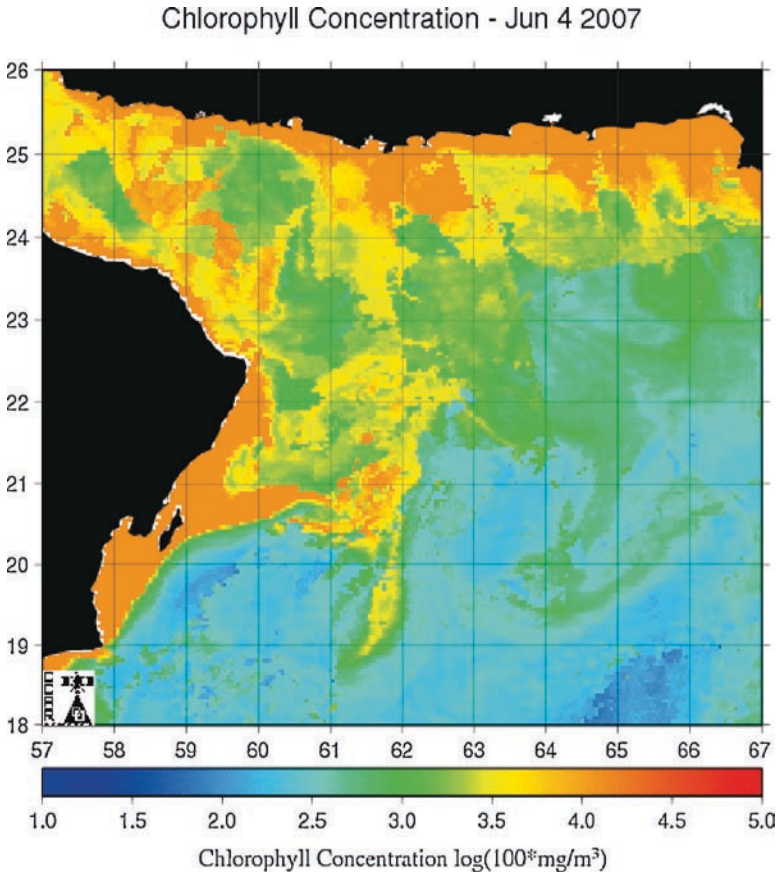

Fig. 3 Distribution of chlorophyll a on 4 June 2007 (5-day composite; http://argo.colorado.edu)

Discussion

The winds of the tropical cyclones lead to localized mixing of the upper layers causing depleted temperature (Sriver and Huber 2007). In our case (which was the case of super cyclone activity), sea surface temperature images showed that an entire northwestern part of the Arabian Sea was occupied by waters with depleted temperature usually observed over the coastal upwelling area of Oman. The scale of this event has corresponded to the scale of the cyclone – as it has been seen in the field of wind from the QuikScat satellite data (http://www.nasa.gov/multimedia/imagegallery/image_feature_841.html). The temperature drop observed over the region was about 1.5–2°C, which is close to that reported for the case of cyclone passage in the southwestern Bay of Bengal in 2000 (Ali et al. 2006). Mixing of the upper layer leads to the injection of nutrients into this layer and subsequent enhancement of the chlorophyll a concentration – the indicator of phytoplankton

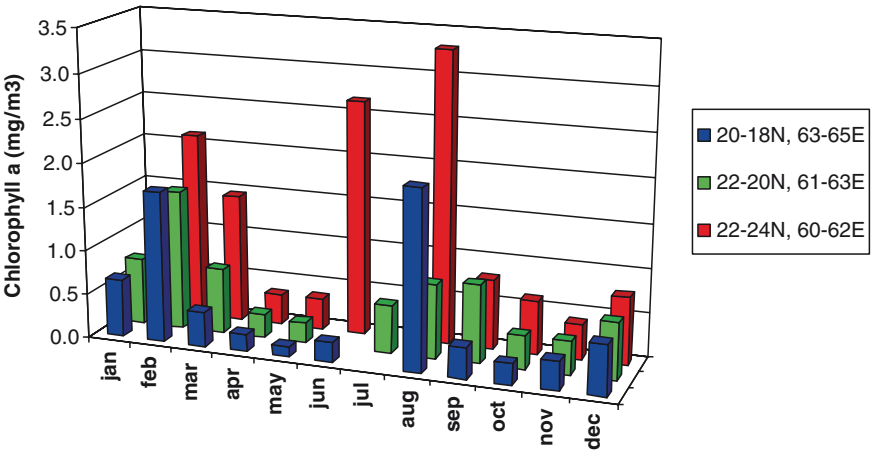

Fig. 4 Monthly changes of chlorophyll a (mg/m^3) in the three regions (2° × 2° quadrates) along the track of a cyclone Gonu

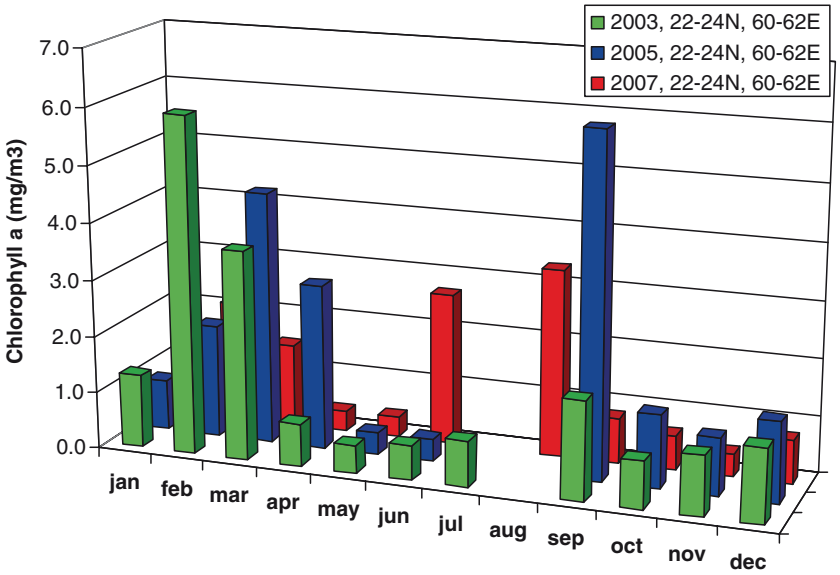

Fig. 5 Monthly changes of chlorophyll a (mg/m^3) in 2007 compared to 2005 and 2003 (22–24°N, 60–62°E)

bloom. However, huge clouds in the cyclone region usually do not allow one to come up with daily resolution in the chlorophyll imagery. The 5-day composite used in our study showed an enhanced concentration of chlorophyll a in the final part of the cyclone track only. This zone of enhanced concentration had a form of the local filament, i.e., it did not match the scale of the depleted temperature zone.

Being much less in size, the phytoplankton bloom was stretched longitudinally, between 61–62°E, hence appearing mainly to the right of a cyclone. Similar location of the cyclone-induced phytoplankton bloom was reported for the typhoon Damrey in the South China Sea (Zheng and Tang 2007) and a cyclone 01A in the eastern Arabian Sea (Subrahmanyam et al. 2002). Overall, interpretation of the influence of Gonu on phytoplankton productivity is fairly difficult, due to the passage of this cyclone through the region affected by Omani and Iran coastal upwelling. The chlorophyll field image (Fig. 2) showed a filament of enhanced concentration (of about 2.7 mg/m) stretched out from the coastal regions towards the ocean. However, the analysis of the seasonal changes revealed the value of the month of June 2007 as the only anomaly in the seasonal cycle, compared to the other years. Plus, this anomaly coincided spatially with the track of Gonu, when it picked up the strength of the super cyclone. Due to the monthly resolution in the time series derived, we could notice that the persistence of the peak concentration induced by the passage of Gonu did not exceed 1 month. Compared to the other regions and cases, local increase of the chlorophyll a concentration attributed to the passage of tropical cyclones fits the time range from several days to 1 month (Babin et al. 2004; Lin et al. 2003; Subrahmanyam et al. 2002). The development of a cyclone-induced chlorophyll peaks was reported to lag the passage of the cyclone from 3 to 6 days (Lin et al. 2003; Subrahmanyam et al. 2002; Zheng and Tang 2007; Walker et al. 2005). Patterns of physical stratification of water masses under cyclone track affect parameters of phytoplankton bloom. Following the passage of a tropical cyclone in the Bay of Bengal in October by the SeaWiFS records, Patra et al. (2007) have noticed that due to strong stratification, enhanced production occurred only in small patches even under the influence of the Orissa Super Cyclone, which exhibited wind speed up to 140 knots. As far as the Gonu track is concerned, the cyclone motion toward the Omani coast has been in fact the motion from highly stratified oligotrphic waters toward the high productive ones. This might be one of the reasons why an actual response of chlorophyll concentration (i.e. the June peak) was observed in the most western part of the track.

Comparing the magnitude of the chlorophyll a concentration presumably induced by Gonu with the maximal concentration observed over the seasonal cycle (Fig. 4 and 5), one could notice that "the Gonu-induced concentration" was less than that observed in August 2007 during summer upwelling. On the other hand, "the Gonu-induced concentration" has exceeded the concentration observed during the 2007 winter upwelling (with its peak in February). With a remark to the interannual variability (Fig. 4), one could treat the Gonu-induced bloom to be less pronounced (by the magnitude of chlorophyll a concentration) when compared to the blooms induced by Omani seasonal upwelling in summer. Among the other reasons for moderate chlorophyll concentration induced by Gonu, its high translation speed should be taken into account. Upwelling-induced injection of nutrients and enhanced vertical mixing could take place at a certain (low) translation speed of tropical cyclones (Price 1981). For instance, typhoons "Kai-Tak" and "Damrey", which had induced intensive (over tenfold increase) phytoplankton blooms in the South China Sea, had a translation speed of 0–1.4 and 3.7 m/s, respectively

(Zheng and Tang 2007). Cyclone Gonu had a much higher translation speed (about 5 m/s), which did not allow a huge phytoplankton bloom to develop, under the most part of the cyclone track. A survey of the chemical and biological parameters in the continental shelf of the south East China Sea, northwest of Taiwan, conducted shortly after the passage of the tropical cyclone, Herb, during summer 1996 has indicated typical oligotrophic waters in the study region. After the cyclone passage, all values of the chemical and biological parameters were much greater than those derived from normal summer periods (Shiah et al. 2000). This study has demonstrated that the whole shelf ecosystem could become more productive after the cyclone event. Checking out for the same event with regard to Gonu, we compared (over the years) the summer concentration of chlorophyll a (from July through September) averaged within a rectangle (21–23°N/59–60°E) covering the major part of the Omani coastal upwelling. No differences were found. Over the 5 consecutive years (from 2004 through 2007), the average concentration in 2006 and 2007 could be attributed to the lowest ones.

Conclusion

The concentration of the chlorophyll a (detected for some "color windows" in the atmospheric cloud mask) along the track of the tropical cyclone, Gonu, exceeded the background concentration in the adjacent regions. The enhanced concentration was observed over the final (western) part of a track, corresponding to a super cyclone phase. The persistence of the enhanced concentration induced by the passage of Gonu did not exceed 1 month and did not reach the concentration range typical for the Omani coastal upwelling in summer, which is the season of the highest concentration of chlorophyll a due to the southwest monsoon.

References

Ali MM, Smitha A, Rao KH (2006) A study on cyclone induced productivity in south-western Bay of Bengal during November-December 2000 using MODIS (SST and chlorophyll-a) and altimeter sea surface height observations. Ind J Mar Sci 35:153–160

Babin S, Carton JA, Dickey TD et al (2004) Satellite evidence of hurricane-induced phytoplankton blooms in an oceanic desert. J Geophys Res . doi:10.1029/2003JC001938

Gray WM (1968) Global view of the origin of tropical disturbances and storms. Mon Weath Rev 96:669–700

Lin I, Liu WT, Wu CC et al (2003) New evidence for enhanced ocean primary production triggered by tropical cyclone. Geophys Res Let . doi:10.1029/2003GL017141

Padgett G (2008) Monthly global tropical cyclone summary. http://www.typhoon2000.ph/garyp_mgtcs/jun07sum.txt. Accessed 16 September 2008

Patra PK, Kumar MD, Mahowald N et al (2007) Atmospheric deposition and surface stratification as controls of contrasting chlorophyll abundance in the North Indian Ocean. J Geophys Res C: Oceans 112(5):Article C05029

Price JF (1981) Upper ocean response to a hurricane. J Phys Oceanogr 11:153–175
Shiah FK, Chung SW, Kao SJ et al (2000) Biological and hydrographical responses to tropical cyclones (typhoons) in the continental shelf of the Taiwan Strait. Cont Shelf Res 20:2029–2044
Smitha A, Rao KH, Sengupta D (2006) Effect of May 2003 tropical cyclone on physical and biological processes in the Bay of Bengal. Intern J Remote Sen 27:5301–5314
Sriver RL, Huber M (2007) Observational evidence for an ocean heat pump induced by tropical cyclones. Nature 447:577–580
Subrahmanyam B, Rao KH, Srinivasa Rao N et al (2002) Influence of a tropical cyclone on chlorophyll-a concentration in the Arabian Sea. Geophys Res Let 29:1–22
Walker ND, Leben RR, Balasubramanian S (2005) Hurricane-forced upwelling and chlorophyll a enhancement within cold-core cyclones in the Gulf of Mexico. Geophys Res Lett . doi:10.1029/2005GL023716
Zheng GM, Tang D (2007) Offshore and nearshore chlorophyll increases induced by typhoon winds and subsequent terrestrial rainwater runoff. Mar Ecol Progr Ser 333:61–74

Recent Outbreaks of Harmful Algal Blooms Along the Coast of Oman: Possible Response to Climate Change?

Adnan R. Al-Azri, Sergey A. Piontkovski, Khalid A. Al-Hashmi, Joaquim I. Goes, and Helga do R. Gomes

Keywords Harmful algal blooms

Introduction

The Sultanate of Oman has an extensive coastline of 3,615 km, which includes the Gulf of Oman (GOO) in the north and the Arabian Sea (NAS) in the south (Fig. 1). In comparison to the extensive research on phytoplankton productivity processes carried out in the offshore oceanic waters of the Arabian Sea during the International Joint Global Fluxes program (Wiggert et al. 2000; Smith 2001; Barber et al. 2001), phytoplankton variability in the coastal waters of Oman is poorly known. One of the limitations has been the lack of a dedicated program with systematic sampling along the coast at regular time intervals. Consequently, no information is available on plankton variability on an annual cycle. Based on the extensive array of investigations designed to observe the physical and biochemical processes in the Arabian sea, we can infer that physical-biological coupling in the coastal ecosystem of the GOO and NAS is largely driven by meteorological forcing, termed the monsoon, which manifests itself as strong, seasonally reversing winds (Wiggert et al. 2000). The two components of this annual cycle are referred to as the northeast monsoon (NEM) and the southwest monsoon (SWM).

The NEM winter season extends from November–February, during which sea surface winds over the GOO are predominantly northeasterly (Shankar et al. 2002) and the SWM season extends from June–mid-September when sea surface winds over the region are predominantly from the southwest and stronger than during the NEM (Brock and McClain 1992). During SWM coastal upwelling persists along

A.R. Al-Azri (✉), S.A. Piontkovski, and K.A. Al-Hashmi
Sultan Qaboos University, College of Agricultural and Marine Sciences, Muscat, Sultanate of Oman

J.I. Goes and H.d.R. Gomes
Bigelow Laboratory for Ocean Sciences, West Boothbay Harbor, ME, 04575, USA

Y. Charabi (ed.), *Indian Ocean Tropical Cyclones and Climate Change*,
DOI 10.1007/978-90-481-3109-9_39,

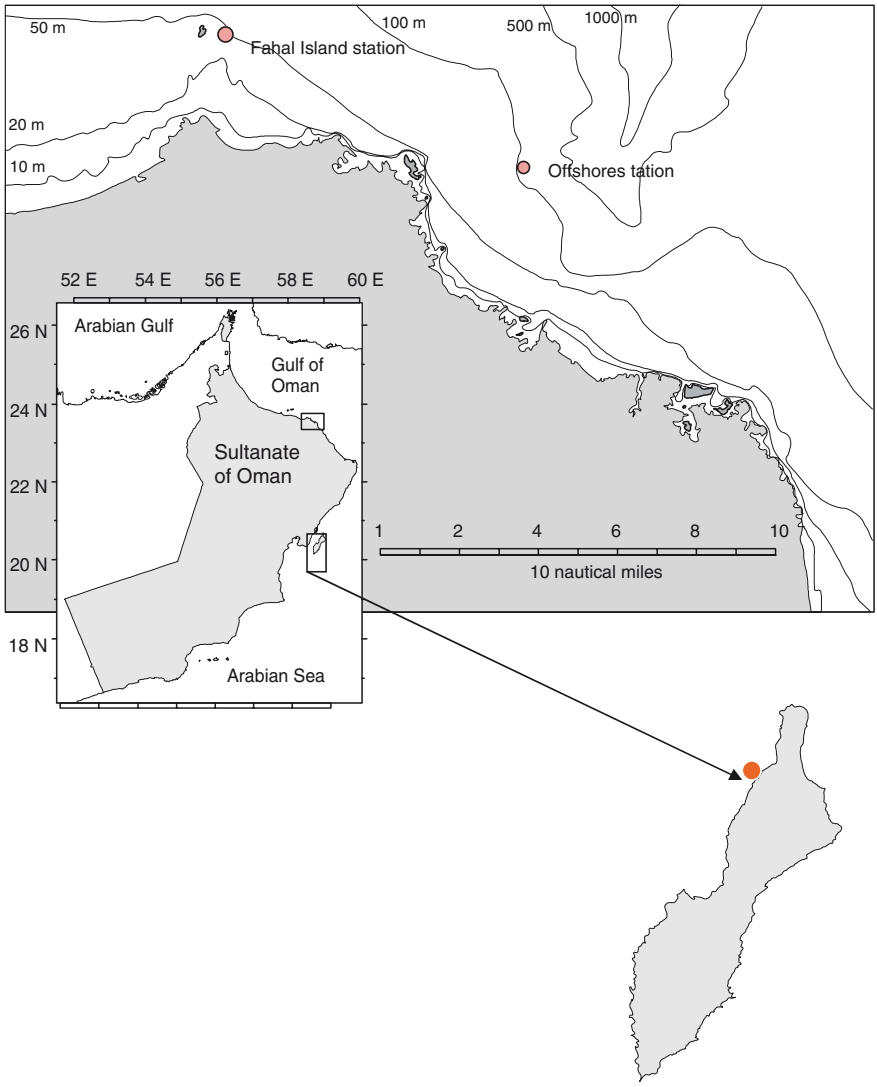

Fig. 1 A map showing the study area

the coast of Oman with stronger impacts in the southern part of the coast (Dhofar region) (Savidge et al. 1990; Coles SL, Seapy DG (1997).

The effects of upwelling can extend to about 750 km offshore of Oman and can also be seen in the GOO through the injection of cool water which strongly affects the temperature profiles during summer in the form of eddies Coles SL, Seapy DG (1997). The influence of southern upwelling on phytoplankton productivity was reported by Barber et al. (2001); their study has shown that high productivity was

influenced by SWM. These authors attributed the enhancement of the productivity to the processes of coastal upwelling, wind-driven mixing, and eddies, which provide new nutrients necessary for phytoplankton productivity. Furthermore, their study showed that the measured rates in primary productivity in 1995 were significantly higher than those recorded in the 1960s. It is worth noting that a recent paper by Goes et al. (2005) reported an increase of year-by-year of phytoplankton biomass in the Arabian Sea over 7 years (1997–2004). This increase was estimated to reach threefold from 1997 to 2004. These authors attributed this increase of phytoplankton biomass to climate change and predicted that the western as well as the central regions of the Arabian Sea could witness more widespread blooms of phytoplankton due to climate change. It is therefore the aim of this study to use the available environmental and phytoplankton data from our time series along the coast of Oman to investigate the response of phytoplankton biomass and composition to monsoonal winds.

Materials and Methods

Water samples were collected from a depth of 1 m twice a month, from February 2004–February 2008, at two stations: Fahal (F, 23.67°N, 58.5°E) and Bandar Al-Khyran (BK, 23.51°N, 58.72°E) (Fig. 1). The latter is the largest semi-enclosed bay on the southern end of the Gulf of Oman, with an approximate surface area of 4 km^2 and an average depth of 10 m. The bay has two inlets and is surrounded by steep rocky hills and cliffs of Permian limestones and shales lined with shallow coral communities. Fahal is located 25 km to the north, with an average depth of 20 m in the sampling region, while the southern station at Masira Island is located west of the Island, and is sampled once a month whenever possible. The southern station is under the influence of the southern coastal upwelling during the SWM.

Temperature and conductivity profiles were measured with an Idronaut-Ocean Seven 316 CTD© probe fitted with additional sensors for measuring chlorophyll *a* (Chl *a)* by fluorescence and dissolved oxygen (DO). Subsurface water samples representative of the mixed layer were collected at 1 m with 5 L Niskin bottles for analyses of nitrate, ammonia, and phosphorus. After collection samples were immediately frozen for analysis in the laboratory. Water samples were later thawed and analyzed for nutrients using a 5–channel SKALAR© FlowAccess auto-analyzer according to the procedures described in and modified by the manufacturer (Skalar analytical, 1996). Subsamples for phytoplankton abundance were collected in dark glass bottles (50–100 ml) into which ten drops of acid Lugol's solution (Throndsen 1978) were added and stored at 4°C. Wind speed (knot) and direction were obtained from the Meteorological Department at Muscat international airport. Values used in this study represent monthly mean throughout the study period.

Results and Discussions

The seasonal variation of wind speed (Fig. 2) exhibited the usual trend of the region, northeast blowing from the north during winter and reversing to southwest during summer. Over the study period (2004–2008), the wind pattern exhibited an unusual drop in October 2007 in the Arabian Sea along the Island of Masira following the tropical cyclone Gonu. Average wind speed reached a minimum of two knots. During the same year, the average wind speed reached the highest speed (seven knots) over the study period in the Gulf of Oman (Muscat area). Water temperatures (Fig. 3) revealed a distinct seasonal pattern in the evolution of the thermal structure. At all three stations the water column was warmest during the spring inter-monsoon (SIM) months of April and May. The transition into the southwest monsoon (SWM) saw a steep upward shoaling of isotherms and cooling of the surface waters due to wind-driven upwelling. Significant drops (8°C) of water temperature were recorded at stations F and BK in GOM during August over the study period with a maximum drop of temperature (10°C) in August 2008. Water temperatures at BK and F were colder in 2008 in comparison to previous years. However, sea surface temperatures were at their lowest during the NEM due to winter convective mixing, which led to a colder and well-mixed water column. Water temperature at M station ranged between 22 and 30°C. The coldest water temperature was observed during the NEM in 2008 and the highest during SWM in 2007. In 2008, water temperature at station M exhibited the coldest temperature during the SWM compared to 2007. Although the surface dissolved oxygen concentration (Fig. 4) does not show a significant drop in the level of dissolved oxygen, in general, the coastal water of Oman is characterized with the presence of a shallow oxygen minimum layer. The onset of the SWM clearly contributed to the upliftment of these oxygen-poor

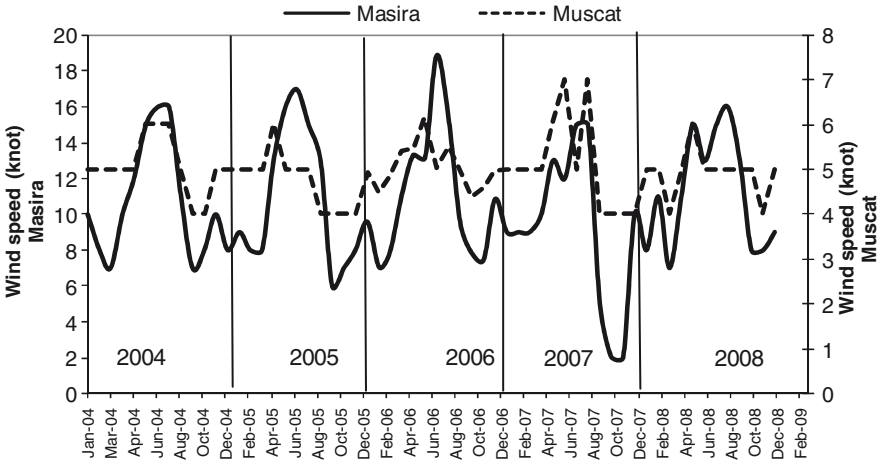

Fig. 2 Average monthly wind speed at stations F, BK, and M

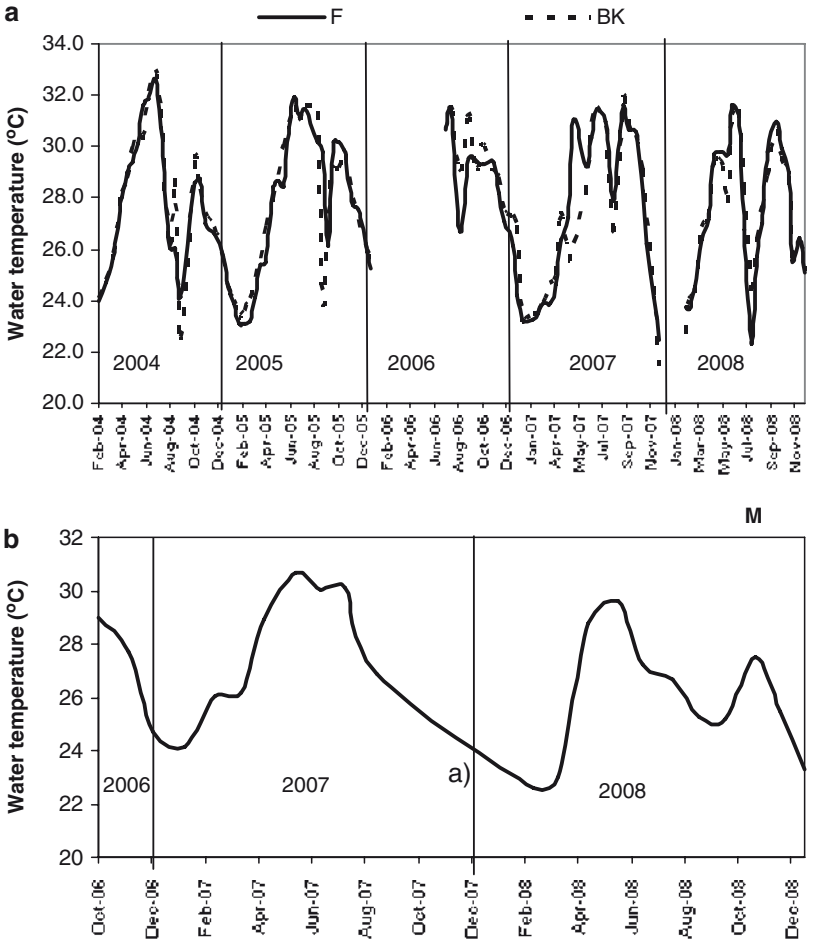

Fig. 3 Water temperature at stations: (**a**) F and BK (**b**) M

waters to depths as shallow as 10 m (A.R. Al-Azri Adnan unpublished data) at BK and F. Both stations F and BK showed the lowest dissolved oxygen during the SIM and NEM. The lowest dissolved oxygen concentration at M was recorded during the onset of the SWM in 2007. A number of fish kill events in the coastal water of Oman are associated with oxygen depletion. Nutrient (nitrate, phosphate, and ammonia) concentrations (Fig. 5) were always above detection limits throughout the year and followed a distinct pattern of seasonality at all three stations. The trends especially in the shallow stations (F and BK) were slightly different from station M. At these stations, the transition to the NEM saw the largest influx of nutrients into the euphotic layer. At station BK in 2005, a prominent influx of nutrients was also observed during fall. High values of nutrients during winter, followed by a decrease during spring, and the minimal values during summer influenced the

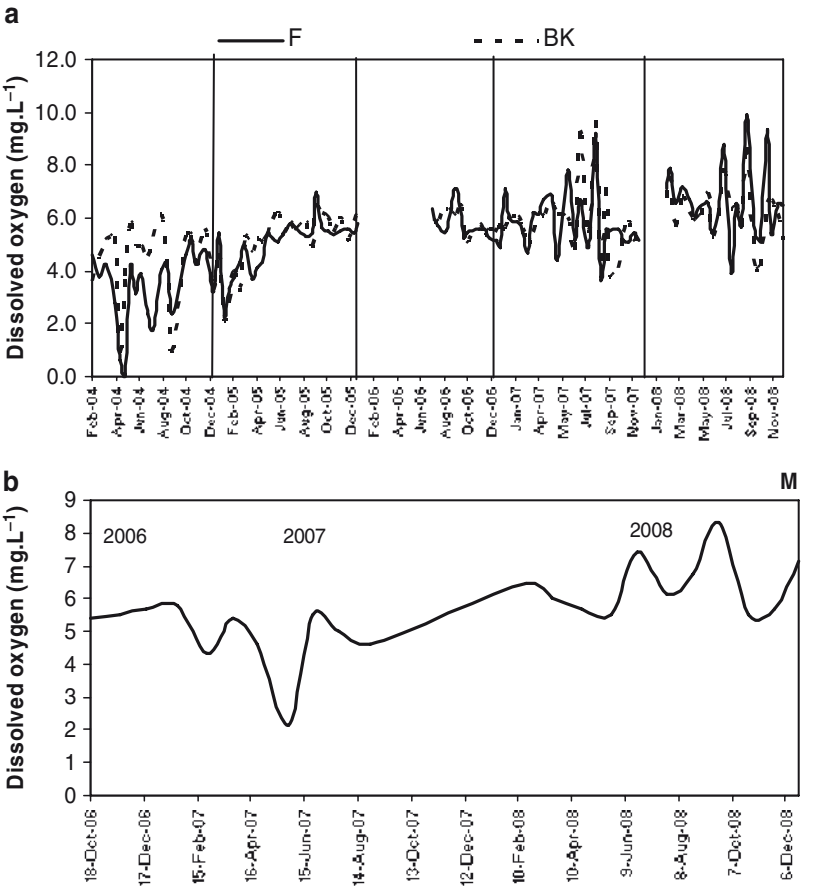

Fig. 4 Dissolved oxygen concentration at stations: (**a**) F and BK (**b**) M

phytoplankton component. The yearly variation in nutrient (nitrate and ammonia) concentrations correlated positively (p = 0.042, p = 0.049, consecutively) with chlorophyll a.

Seasonality of chlorophyll a at all stations (Fig. 6) was characterized with high concentrations during NEM and fall inter-monsoon. The seasonal variation of chlorophyll a at F and BK ranged between concentrations below 1 μg/L and highest of 3.5 μg/L. Distinct winter, summer, and fall time increases in chlorophyll provide clear indication of the existence of clear seasonal cycles of phytoplankton biomass distribution in the Gulf of Oman. At least at F and BK, increases in phytoplankton biomass were clearly tied to the influx of nutrients. Chlorophyll trends at the shallower stations were identical, but in 2005, the NEM increase in chlorophyll was delayed until February indicating interannual variability in the seasonal trends. Dinoflagellates were the most dominant species at all stations in GOO in 2004 and 2005, except for August at station F (93% *Leptocylindrus* sp.). *Cyanobacteria*

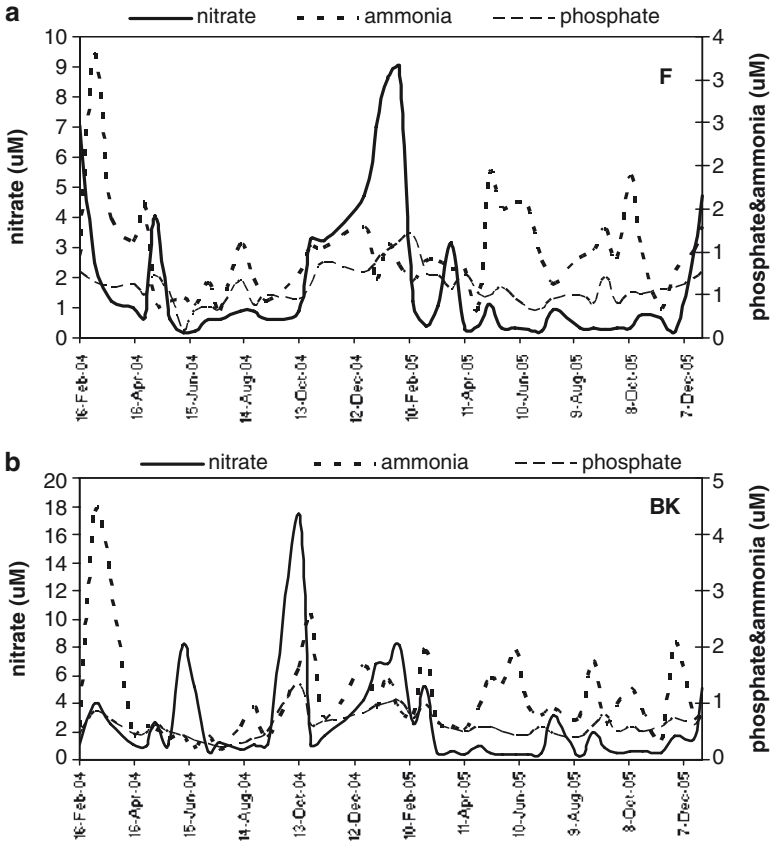

Fig. 5 Nutrients concentrations at stations F and BK

accounted for a much lower percentage and occurred during summer at both stations when nitrate concentrations were below 1 μm. Dinoflagellates were present throughout the year, but it was from March to August at station F and May, June, August, and November at station BK when their relative contribution in the number of cells was most important. In addition, *Noctiluca scintillans* seemed to contribute significantly to total phytoplankton abundance during winter and spring at all stations in 2004 and 2005. Preliminary results of seasonal variation of chlorophyll a from 2004 to 2008 indicate the interannual changes associated with monsoonal forcing. Phytoplankton standing stocks were much larger in the Arabian Sea than in the Gulf of Oman. Note that the coastal waters along the southeast coast of Oman come under the direct influence of the SWM. Diatoms were by far the dominant phytoplankton east of the island, whereas the GOO comprised largely of dinoflagellates. The monsoon winds not only contributed to the seasonal and interannual variations in the phytoplankton biomass and composition, but also to the increase of harmful algal blooms (HABs) outbreak. The fish kill associated with oxygen

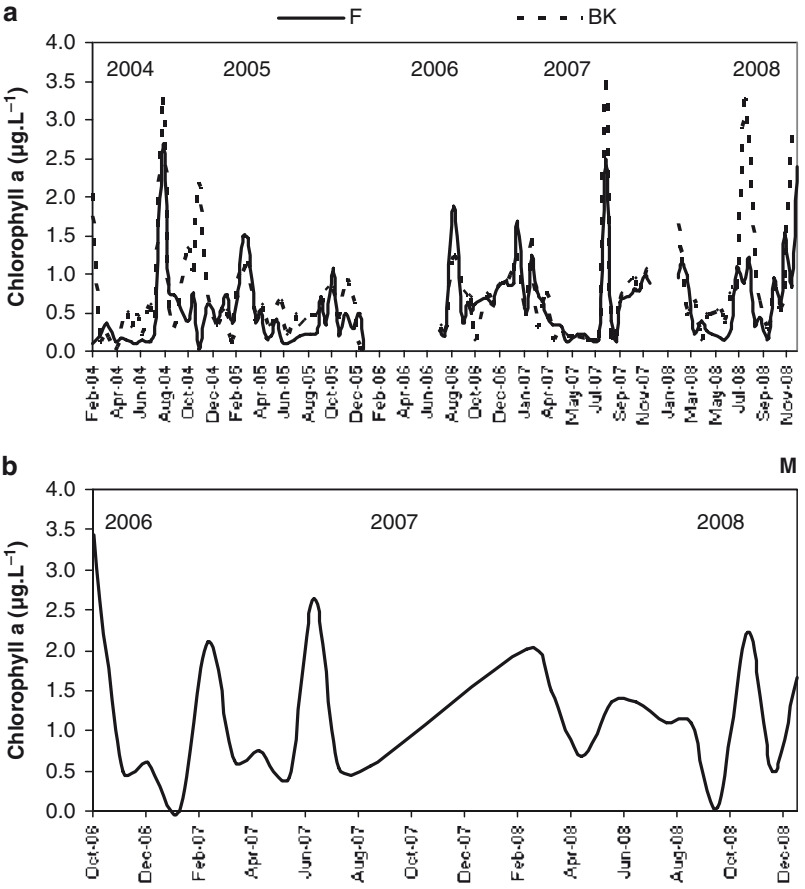

Fig. 6 Chlorophyll a concentrations at stations: (**a**) F and BK (**b**) M

depletion and HABs has increased in the last decade (Thangaraja 1995; Adnan et al. 2007). The highest chlorophyll a observed during the NEM at F and BK was the result of the outbreak of the dinoflagellates *Cochlodinium polykrikoides* which was recorded for the first time in the Oman waters and persisted for almost 6 months causing massive loss in fisheries and tourisms sectors.

Conclusion

Observations of phytoplankton communities in the coastal region of Oman indicate that prominent temporal and spatial variability associated with changes in environmental conditions is brought about by the reversal of the monsoonal cycle. The close relationship between environmental conditions and phytoplankton community

structure suggests that any alterations in the monsoon periodicity or its intensity could have a large influence on phytoplankton communities, with potentially large impacts on the fisheries resources of Oman in-turn. In the light of the evidence by Goes et al. (2005), coastal upwelling along the coasts of Somalia, Oman, and Yemen is intensifying as a result of climate change; our observations assume tremendous significance impact of climate change in the coastal water of Oman. The role of cyclonic and anticyclonic eddies in the spatial and temporal abundance of phytoplankton communities and the changes in dissolved oxygen in the coastal water of Oman are yet to be investigated.

References

Adnan AR, Al-Hashmi K, Goes J, Gomes H, Rushdi AI, Al-Habsi H, Al-Khusaibi S, Al-Kindi R, Al-Azri N (2007) Seasonality of the bloom-forming dinoflagellate *Noctiluca scintillans* in the Gulf of Oman in relation to environmental conditions. Int J Ocean Oceanogr 2(1):51–60

Barber RT, Marra J, Bidigare RC, Codispoti LA, Halpen D, Johnson Z, Latasa M, Goericke R, Smith SL (2001) Primary productivity and its regulation in the Arabian Sea during 1995. Deep-Sea Res II 48:1127–1172

Brock JC, McClain CR (1992) Interannual variability in phytoplankton blooms observe in the northwestern Arabian Sea during the southwestern monsoon. J Mar Res 97(C1):733–750

Coles SL, Seapy DG (1997) Ultra-violet absorbing compounds and tumorous growths on acroporid corals from Bandar Khayran, Gulf of Oman, Indian Ocean. Coral Reefs 17:195–198

Goes JI, Thoppil PG, Gomes H do R, Fasullo JT (2005) Warming of the Eurasian landmass is making the Arabian Sea more productive. Science 308:545–547

Parson TR, Maita Y, Lalli CM (1984) A manual of chemical and biological methods for seawater analysis. Pergamon Press, Oxford, New York, Toronto

Savidge G, Lemon J, Matthews AJ (1990) A shore-based survey of upwelling along the coast of Dhofar region, southern Oman. Cont Shelf Res 10:259–275

Shankar D, Vinayachandran PN, Unnikrishnan AS (2002) The monsoon currents in the north Indian Ocean. Prog Oceanogr 52:63–120

Smith SL (2001) Understanding the Arabian Sea: reflections on the 1994–1996 Arabian sea expedition. Deep-Sea Res 48(II):1385–1402

Thangaraja M (1995) Hydro-biology of Oman. MSFC Research Report No. 95-1. Ministry of Agriculture and Fisheries. Muscat, 153pp

Throndsen J (1978) Preservation and storage. In: Sournia A (ed) Monographs on oceanographic Methodology 6: Phytoplankton manual. United Nations Educational, Scientific and Cultural Organisation (UNESCO), Paris

Wiggert JD, Jones BH, Dickey TD, Brink KH, Weller RA, Marra J, Cadispoti LA (2000) The northeast monsoon's impact on mixing, phytoplankton biomass and nutrient cycling in the Arabian Sea. Deep-Sea Res 47:1353–1386

Understanding the Tropical Cyclone Gonu

Khalid Ahmad Al Najar and P.S. Salvekar

Keywords Cyclone Gonu, Model MM5

Introduction

Tropical cyclones are non-frontal synoptic-scale warm-core low-pressure systems that originate over the tropical or subtropical oceans and contain organized deep convection and a well-defined cyclonic surface wind circulation. Tropical cyclones form over warm ocean waters, which supply energy to the atmosphere in the form of latent and sensible heat. Under favorable atmospheric thermodynamical conditions associated with low-level convergence a surface low develops into a cyclonic storm. The movement of the tropical cyclone is generally known by the knowledge of the upper atmospheric conditions and the prevailing circulations. Based on intensity, tropical cyclones in the Atlantic, Eastern, and Western Pacific are classified as a tropical depression for a weaker system with $V_{max} \leq$ 17 m/s ($\approx$ 62 km/h), a tropical storm for a moderate system with 18 m/s $\leq V_{max} \leq$ 32 m/s, and a hurricane or typhoon for a strong system with $V_{max} \geq$ 33 m/s. Hurricanes are called major hurricanes when $V_{max} \leq$ 50 m/s and typhoons are classified as super typhoons when $V_{max} \leq$ 67 m/s. The maximum wind speed of a strong tropical cyclone may exceed 100 m/s, which may produce storm surge by driving an ocean rise of several meters along the coast. On the average about five tropical cyclones occur annually over the Bay of Bengal (Bhaskar Rao DV, Ashok K (1999) in the north Indian Ocean, which contributes 6% of the global annual frequency. Based on the maximum sustained winds associated with the system and geographical location of their occurrences,

K.A.A. Najar (✉)
Directorate General of Navigation and Meteorology, Salalah Airport, Oman
e-mail: khalid_najjar@yahoo.com

P. S. Salvekar
Indian Institute of Tropical meteorology, Pune, 411008, India

Y. Charabi (ed.), *Indian Ocean Tropical Cyclones and Climate Change*,
DOI 10.1007/978-90-481-3109-9_40,

they are classified as depression, tropical storm, severe cyclone, or hurricane (Asnani 1993). *There are two cyclone seasons in the north Indian Ocean, viz., pre-monsoon (especially May) and post-monsoon (October and November). A few cyclones can also form in the transitional monsoon months, June and September (i.e., arrival and withdrawl phase of the Indian summer monsoon).*

Tropical Cyclones at Oman Coast

Oman suffers the danger of the tropical cyclones in the transitional seasons. The tracks of tropical cyclones affected Oman since 1948 are shown in Fig. 1.

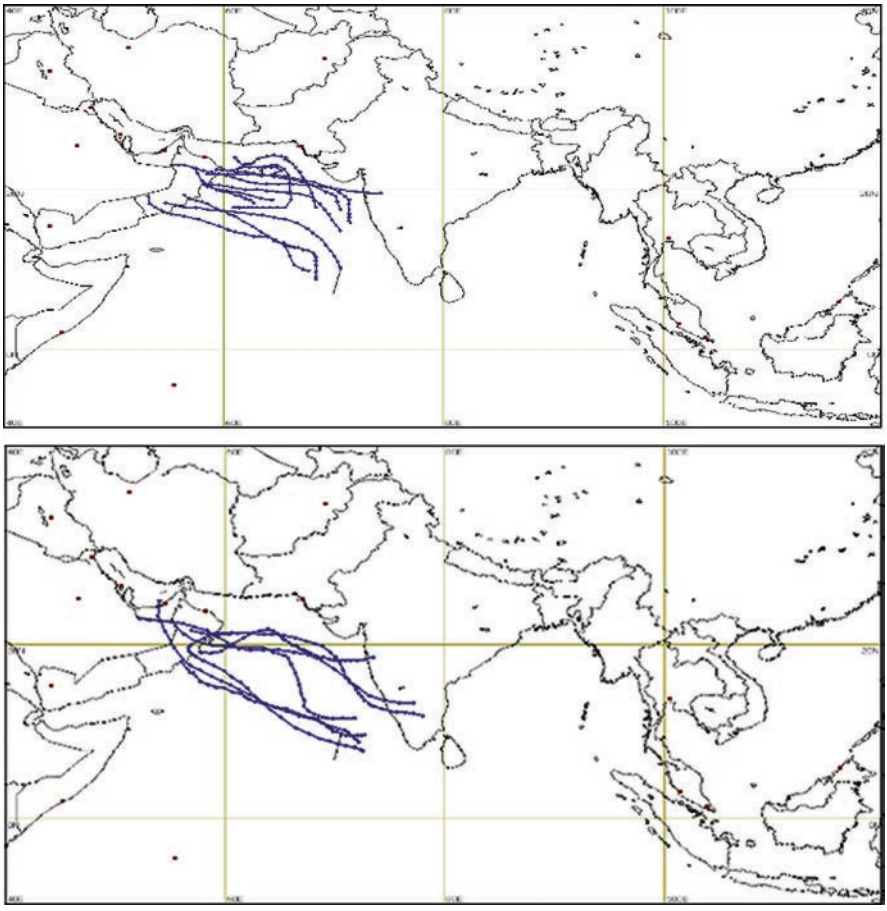

Fig. 1 Tracks of the tropical cyclones over the Arabian Sea and affected Oman in first transitional period (*left*) and second transitional period (*right*) since 1948 till now (the tracks are based on data taken from http://weather.unisys.com)

Recently in June 2007, the super cyclone Gonu reached Oman coast. This cyclone is considered as the strongest in last 100 years. Observations contain phenomenal record such as 900 mm of rain during 5 June, very high wind about 130 km/h and sea level rising to 12 m during the passage of the cyclone. About 7 h before passing near the northeastern Oman coastline, Cyclone Gonu began affecting the country with rough winds and heavy precipitation, with rainfall total reaching 610 mm near the coast. Gonu produced strong waves along much of the coastline, leaving many coastal roads flooded. The cyclone caused extensive damage along the coastline, including in the city of Sur and the village of Ras al Hadd at the eastern most point of the Omani mainland. Around 20,000 people were affected, and damage in the country was estimated at around US$4 billion, ranking it as the worst natural disaster on record in Oman. Due to this disastrous event, the understanding and prediction of tropical cyclones along the Oman coast has got importance. In the literature numerical simulations of many other cyclones are available (e.g., Trivedi PM, Vaidya SS (2006). Hence, the present study is attempted to simulate the Gonu cyclone track using mesoscale numerical model.

Gonu Cyclone Case Description

On May 27, a widespread area of convection persisted over the southeastern Arabian Sea. By May 31, an organized tropical disturbance developed about 645 km south of Mumbai, India with cyclonic convection and a well-defined midlevel circulation. On June 1, the system it developed to the extent that the Indian meteorological department (IMD) classified it a depression. On June 2, the joint Typhoon warning Center (JTWC) classified it a tropical cyclone 02A, while it was located about 685 km southwest of Mumbai, India. Gonu turned to the north and northeast, though resumed a westward track. It rapidly intensified to attain a severe cyclonic status early on June 3. Gonu rapidly deepened and developed a well-defined eye. Late on June 3, the storm was classified as Very Severe Cyclonic Storm Gonu, upon which it became the most intense cyclone on record in the Arabian Sea. Gonu strengthened further to attain peak 1-min sustained winds of 260 km/h and gusts to 315 km/h while located about 285 km east–southeast of Masirah Island on the coast of Oman. The IMD upgraded it to Super Cyclonic Storm Gonu late on June 4, with 10-min sustained winds reaching 240 km/h and an estimated pressure of 920 mbar (Table 1).

After maintaining peak winds for about 9 h, the IMD downgraded Gonu to very severe cyclonic storm status early on June 5. Due to land interaction with Oman, the inner core of deep convection rapidly weakened, and over a period of 24 h the intensity decreased by 95 km/h. That day evening Gonu reached Jabal Ras Al Had bringing torrential rains, high waves, and very strong winds, Kalhat recorded 131 km/h at 2.50 A.M and rainfall was 235 mm. Also on the same day, during the passage of the cyclone Al Jabal Al Asfar station had an accumulated rainfall in 24 h of 934 mm. As Gonu crossed the eastern-most tip the winds continued to gradually decrease due to interaction with land. After emerging into the Gulf of Oman, the

Table 1 The total number of cyclones in the Bay of Bengal and the Arabian Sea during May and June (The data in the table are taken from Singh et al. 2001)

	Month				
	May	June	September	October	November
Bay of Bengal					
Cyclonic storms	59	35	40	89	114
Severe cyclonic storms	42	5	16	38	63
Arabian Sea					
Cyclonic storms	24	25	4	24	20
Severe cyclonic storms	19	17	2	11	15

cyclone intensified slightly, becoming the first recorded tropical cyclone in the Gulf of Oman. On June 6, the cyclone turned to the north–northwest and downgraded to tropical storm status. The IMD downgraded Gonu to severe cyclonic storm status and later to cyclonic storm status early on June 7. Gonu crossed the Makran coast in Iran 6 h later and the IMD stopped issuing advisories on the cyclone.

Model Description and Data

The present study utilizes the MM5 version 3.7. Grell et al. (1994) give the model description. The sensitivity of high-resolution simulations in hurricane case is discussed by Braun and Tao (2000). Here the model is configured with 23 vertical layers and two nested domains as shown in Fig. 2 (outer domain: 45 km grid spacing with 150 × 110 grid cells in the east–west direction and north–south directions; and inner domain: 15 km grid spacing with 193 ×151 grid cells in the east–west and north–south direction). The options used are the Medium Range Forecast (MRF) PBL scheme, the Kain Fritsch 2 (KF2) for cumulus, a mixed-phase for explicit moisture, a cloud radiation scheme, and multilevel soil model. The NCEP FNL reanalysis data available at 1° × 1° was used two develop the initial and lateral boundary conditions corresponding to 00 UTC of 4 June 2007. In fact, the model was also run for different times using the same sources of data at 00 UTC June 3, 5, 12 UTC June 3 and 5. The input data was not able to give a suitable position of the cyclone when they were analyzed, so the results were discarded. Other convection schemes such as Grell and KF in combination with different PBL schemes such as Blackadar (BL) and Eta Mellor-Yamada (MY) were used in the simulations. The combination of MARF PBL and KF2 for convection yielded the best results with regard to track of the cyclone and its evolution. The data and position of the Gonu cyclone is taken from the IMD for comparison with model results. The station data are obtained from Omani Directorate General of Aviation and Meteorology (Fig. 3).

The Kain-Fritisch scheme considers a Lagrangian parcel method along with vertical momentum dynamics to estimate properties of cumulus convection. It incorporates a trigger function, a mass flux formulation, and closure assumption.

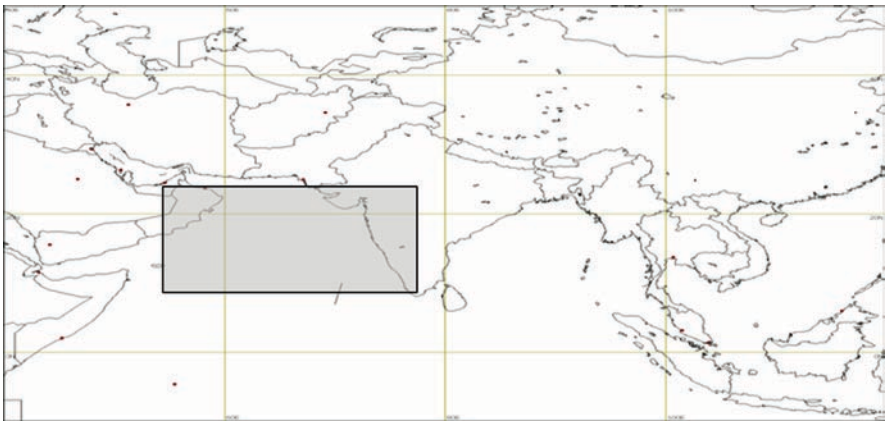

Fig. 2 The two domains used for simulation of the cyclone Gonu. The inner domain is indicated by a white rectangle

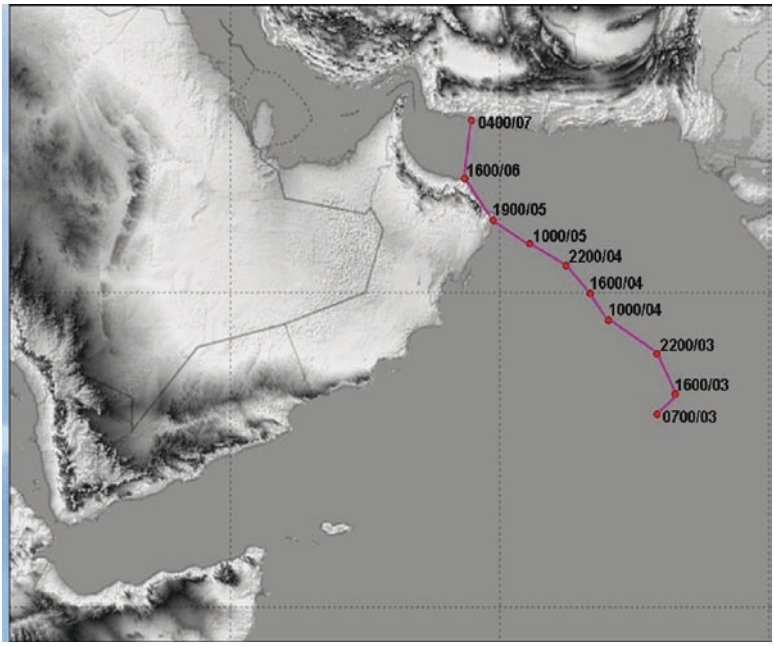

Fig. 3 The red curved line shows the actual track of Gonu starting 07 UTC 3 June till 04 UTC 7 June 2007

The trigger function identifies the potential updraft source layers associated with convection, whereas the mass flux formulation calculates the updraft, downdraft, and the environment mass flux associated with that. The closure assumption for the scheme is that the convective effects removes convective available potential energy

(CAPE) in a grid element with an advective time period by rearranging mass in a column using updrafts, downdrafts, and environment mass flux until at least 90% of the CAPE is removed. The CAPE is calculated based on the path of an entrained diluted parcel. The cloud radius, which controls the maximum possible entrainment rate is specified as a function of sub-cloud layer convergence. A minimum cloud depth required for activation of deep convection is allowed to vary as a function cloud base temperature. The scheme assumes conservation of mass, thermal energy, total moisture, and momentum, and since it represents different processes associated with convection, is used for this study.

Results

The prediction of the track is of prime interest since any mistakes in the track cannot be compensated by knowledge of any other quantities. The MRF and KF2 combination was able to detect the track of the cyclone with least error (Fig. 4). For 72 h of model integration and a time step of 1 h the results were generally in agreement with the actual track except when the low retreats a little or meanders on its way.

The values of the pressure at the center show the deepening of the cyclone to 993 mb when it hits the Omani coast. The size of the cyclone changes during its motion with the smallest size at the beginning of 5 June and growing in size as it enters Oman, and later gaining a smaller size as it enters the Gulf of Oman. The pressure values of the cyclones are in the range 996–990, which is underestimated in the model results. Sometimes the cyclone meanders in its way for few hours before following the track, which approximates the actual track. At time 18 UTC the chart shows the cyclone inside the Arabian Peninsula; actually the greater part, but not all of it. The change in size is not accompanied with change in pressure at the center of the cyclone before entering Oman. Model-simulated wind speed and vorticity at different levels are shown in Fig. 5. High cloud cover and the precipitable amount of water during the track of the cyclone are shown in Figs. 6 and 7, respectively.

The wind speed at level 925 hPa is about 25 m/s. Winds are as high as could be seen at level 500 hPa and when we go up to level 200 hPa, very high winds 55 m/s are encountered in the region of the cyclone. The vorticity field at 925, 500, and 200 hPa shows positive cyclonic vorticity exceeding 25×10^{-5}/s and maintaining the same value in the region of the storm up to 500 hPa level. At 200 hPa, the cyclonic vorticity diminishes greatly to become nearly 1×10^{-5}/s and then at a level higher than 200 hPa, it is replaced by negative anticyclonic vorticity.

Conclusion

Oman suffered the danger of the tropical cyclone Gonu, which is considered as the strongest in 100 years. Observations contain phenomenal record such as 900 mm of rain during 5 June, very high wind about 130 km/h, and sea level rising to 12 m

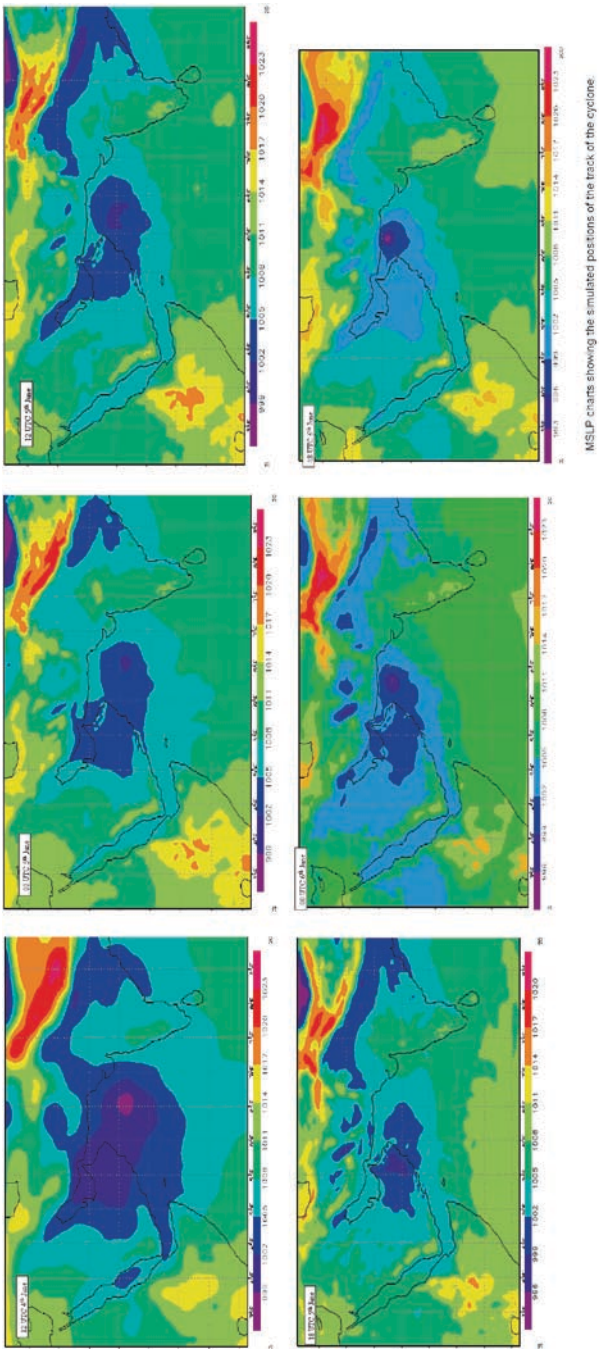

Fig. 4 MSLP charts showing the simulated positions of the track of the cyclone

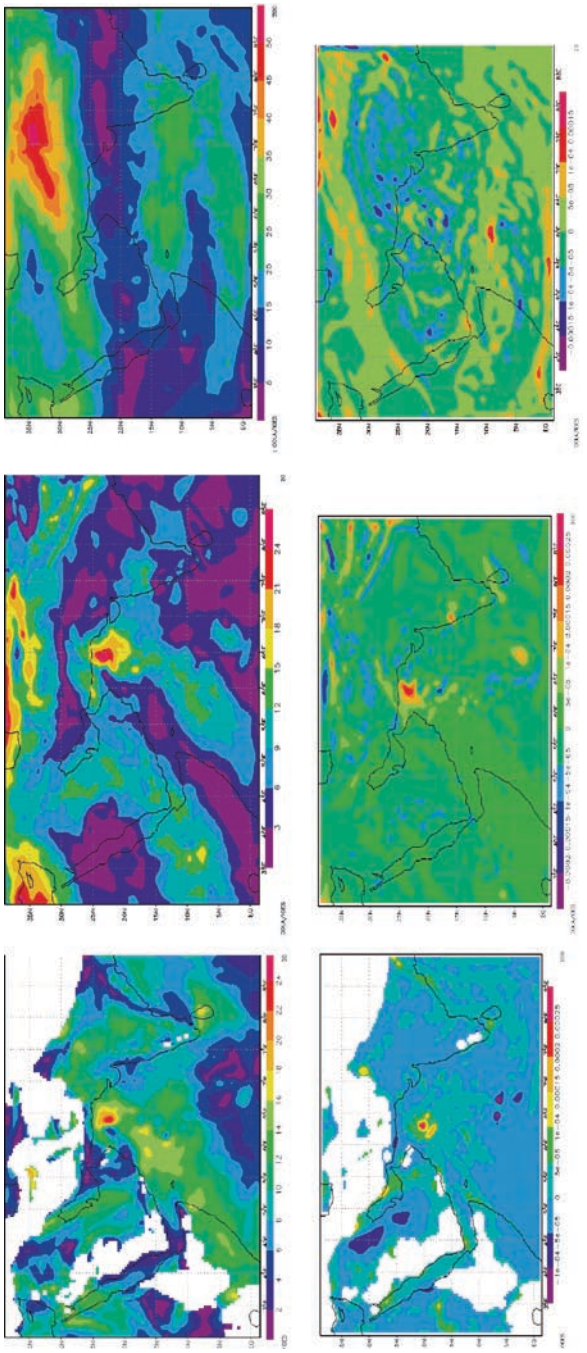

Fig. 5 The wind speed and vorticity at levels 925, 500, and 200 hPa for 12 UTC 6 June (from *right* to *left*; the upper charts are the wind speed in m/s and the lower charts are the vorticity in units of per second

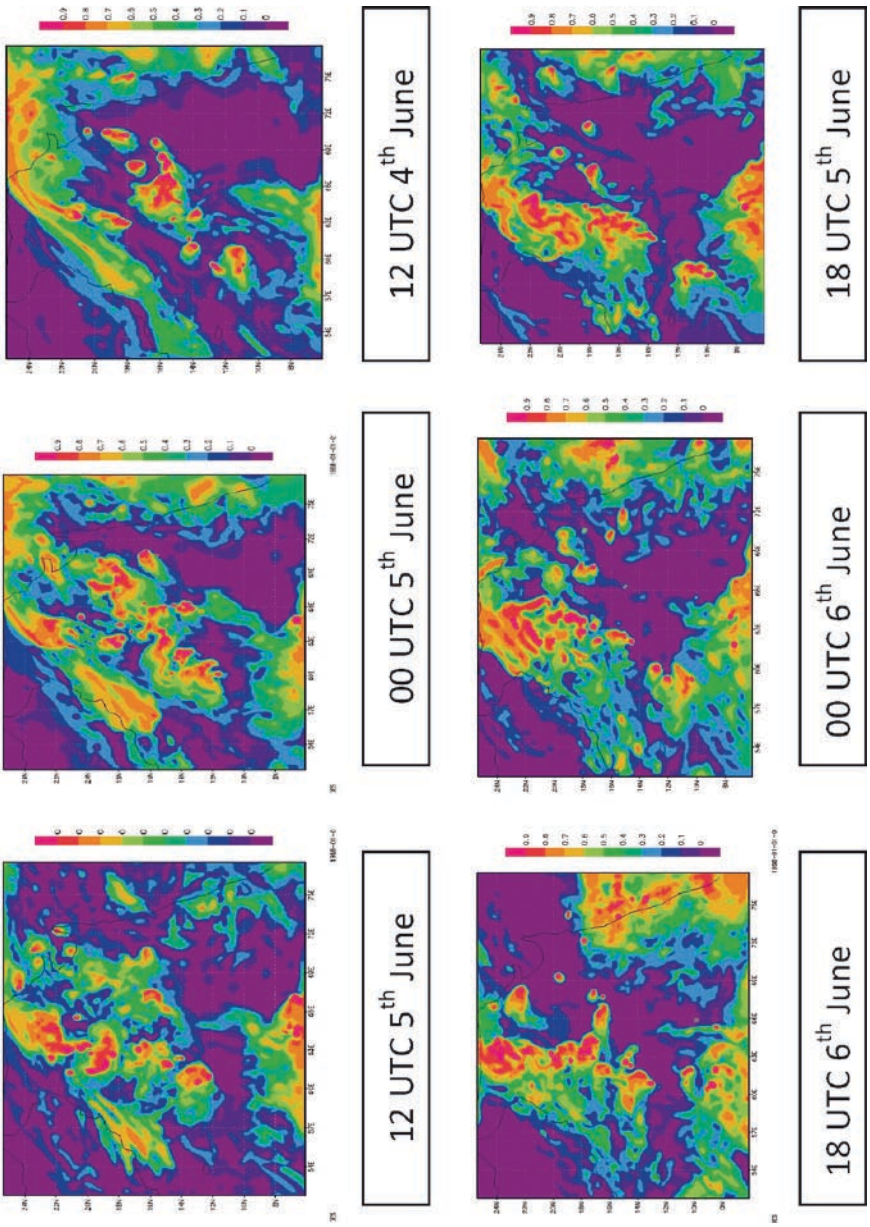

Fig. 6 High cloud cover during the track of the cyclone

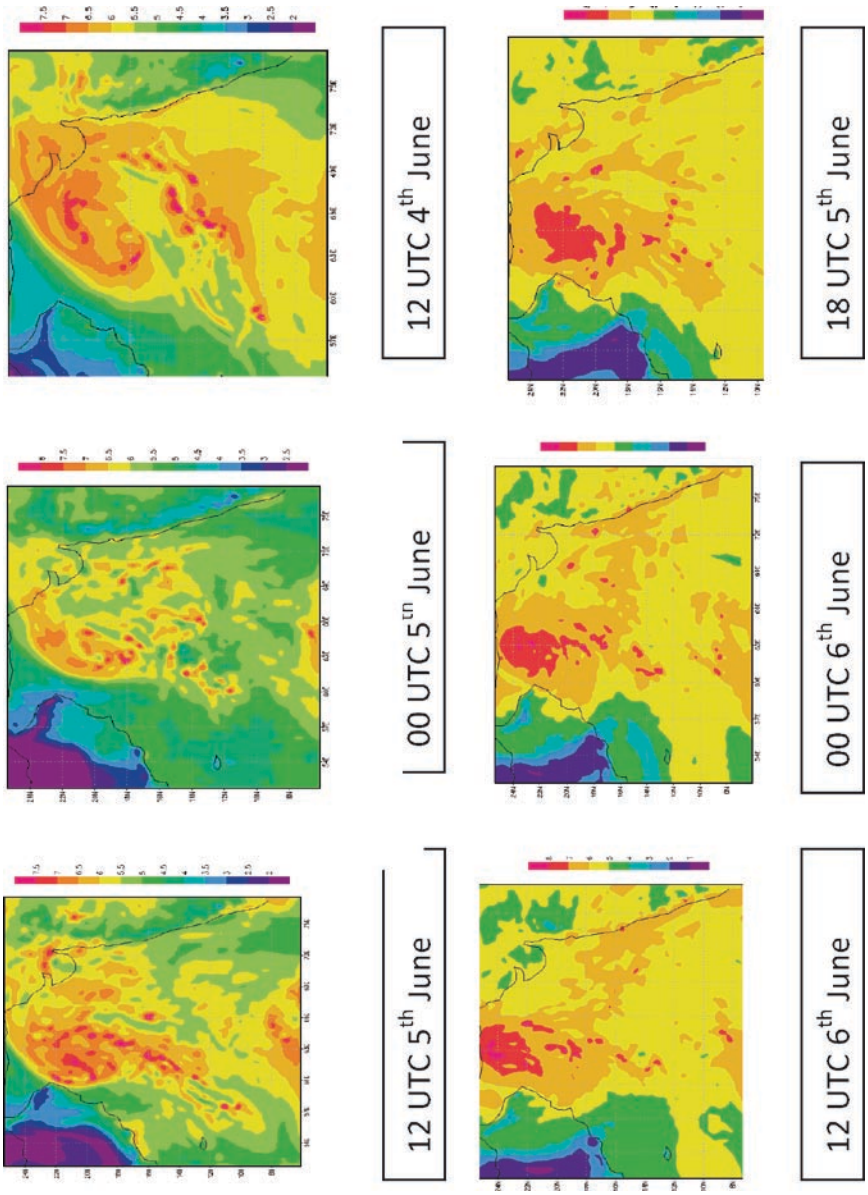

Fig. 7 Precipitable amount of water during the track of Gonu cyclone

during the passage of the cyclone. The MM5 model was used to simulate the case of Gonu. A combination of MRT PBL and KF2 for convection was used and proved suitable in the prediction of the nearest track to the actual one. The model was run on two nested domains at resolutions of 45 and 15 km. The model rendered lowest MSL pressure of about 990 mb when it reached Oman coast and was able to describe the intensity of the wind speeds at three levels in the atmosphere, i.e., 925, 500, and 200 hPa. Severe cyclonic winds were observed at lower levels up to 500 hPa and positive vorticity was as high as 25×10^{-5}/s. Beyond 200 hPa anticyclonic circulation is seen by an area of high pressure. The model was not able to simulate the location and quantity of rainfall exactly. Precipitable amount of water distribution was given and it followed the locations of the cyclone. The cloud cover is also found to follow the track of the cyclone.

Acknowledgments Authors are grateful to the Directorate General of Navigation and Meteorology, Oman and Director of forecasting and observing at Muscat airport. Authors are thankful to Director of Salalah Airport, Oman and Director of Indian Institute of Tropical Meteorology, Pune, India for supporting the collaborative work and extending the necessary facilities.

References

Anthes RA (1977) Hurricane model experiments with a new cumulus parametrization scheme. Mon Wea Rev 105:287–300

Asnani GC (1993) Tropical meteorology vols 1, 2. Published by Prof. G. C. Asnani, c/o Indian Institute of Tropical Meteorology, Dr. Homi Bhabha Road, Pashan, Pune-411008, India

Bhaskar Rao DV, Ashok K (1999) Simulations of tropical cyclone circulations over the Bay of Bengal. Part 1, description of the model, initial data and results of the control experiment. Pure Appl Geophys 156(3):525–542

Braun SA, Tao WK (2000) Sensitivity of high resolution simulations of hurricane Bob (1991) to planetary boundary layer parameterization. Mon Wea Rev 128:3941–3961

Grell GA, Dudhia J, Stauffer DR (1994) A description of the fifth generations Penn State/NCAR Mesoscale Model (MM5)/NCAR Technical Note NCAR/Tn 398 TSR, p 117

Singh OP et al (2001) Has the frequency of the intense tropical cyclones increased in the Indian Ocean. Curr Sci 80(4):575–580

Trivedi PM, Vaidya SS (2006) Impact of physical parameterization scheme on numerical simulation of Orissa Super cyclone (1999). Mausam 57(1):97–110

Index